From the University Hospital of the Heinrich-Heine-University Düsseldorf
Center for Pediatric and Adolescent Medicine
Clinic for Pediatric Hematology, Oncology and Clinical Immunology
(Director: Univ.-Prof. Dr. med. Arndt Borkhardt)

Novel immunological mechanisms of targeting tumors and their micro-environment

Habilitation thesis
for the conferral of the Venia legendi for the subject of
Molecular Medicine of the Faculty of Medicine of the Heinrich-Heine-University Düsseldorf

presented by
Dr. phil. Aleksandra Pandyra
Düsseldorf

2021

1. Abbreviations

ADAM17	Protease A disintegrin and metalloproteinase 17
APC	Antigen presenting cells
Akt	Protein kinase B
BCR	B cell receptor
cAMP	Cyclic adenosine monophosphate
CAR	Chimeric antigen receptors
CCL22	C-C motif chemokine 22
CCR4	C-C chemokine receptor type 4
CCR5	C-C chemokine receptor type 5
CCR8	C-C chemokine receptor type 8
CCR10	C-C chemokine receptor type 10
CD80	Cluster of differentiation 80
CD86	Cluster of differentiation 86
CLL	Chronic lymphocytic leukemia
CTL-4	Cytotoxic T-lymphocyte-associated protein 4
DCs	Dendritic cells
EGFR	Epidermal growth factor receptor
Eomes	Eomesodermin
EPAC	Exchange protein directly activated by cAMP
FAST	Fas-activated serine/threonine kinase
FOXP3	Forkhead box P3
GzmB	Granzyme B
HIF-1α	Hypoxia-inducible factor-1α

HMGCR	3-hydroxy-3-methyl-glutaryl-coenzyme A reductase
IBS	Irritable bowel syndrome
iDCs	Inflammatory dendritic cells
IFN-I	Type I interferon
IL-2	Interleukin 2
IL-10	Interleukin 10
IL-35	Interleukin 35
IgM	Immunoglobulin M
IPP	Isopentenyl-diphosphate
LCMV	Lymphocytic choriomeningitis virus
LPS	Lipopolysaccharide
MDSC	Myeloid-derived suppressor cells
MHC	Major histocompatibility comple
MVA	Mevalonate
mTOR	Mechanistic target of rapamycin
NFAT	Nuclear factor of activated T cell
NSCLC	Non-small cell lung cancer
OV	Oncolytic viruses
PD-1	Programmed cell death 1
PDE	Phosphodiesterase
PD-L1	Programmed death-ligand 1
PI3K	Phosphoinositide 3-kinases
PKA	Proteinkinase A
ROR-γt	Retinoic acid–related orphan receptor
SASP	Senescence-associated secretory phenotype

TACE	TNFα converting enzyme
TAM	Tumor-associated macrophages
Tc	Cytotoxic antigen-activated $CD8^+$ T
TCA	Tricarboxylic acid
TCR	T cell receptor
TGF-β	Transforming growth factor beta
Th17	T helper 17
TIGIT	Tyrosine-based inhibitory motif (ITIM) domain
TME	Tumor micro-environment
TNFα	Tumor necrosis factor alpha
TNFR	Tumor necrosis factor receptor
TLR	Toll-like receptor
TOC	Tylosis with esophageal cancer
Toso	Fas apoptotic inhibitory molecule 3
TOX	Thymocyte selection-associated HMG box
Treg	Regulatory T cells
Tsp1	Thrombospondin-1

2. Introduction

Cancer is a major cause or mortality world-wide and understanding the processes influencing tumor growth will help to uncover novel therapeutic options and preventative strategies. Tumor-defining characteristics, the so-called 'Hallmarks of Cancer' have been described decades earlier by Hanahan and Weinberg in their seminal paper[1]. These characteristics, mainly attributable to the tumor cells themselves such as the ability to sustain proliferative signaling and evade apoptosis have now been re-worked into a more complex model involving the tumor micro-environment (TME) and the inflammatory, metabolic and immune processes shaping and remodeling it[2]. Specifically, tumor-promoting inflammation has been recognized as an enabling characteristic of tumor growth and the ability to evade the immune system as an emerging hallmark. Both tumor-promoting inflammation and the ability to evade the immune system support the development of the core hallmarks namely sustaining proliferative signaling, resisting cell-death, inducing angiogenesis, enabling replicative immortality, activating invasion and metastasis and evading growth suppressors[2]. Although it is debatable whether tumor-promoting inflammation should be considered a separate enabling characteristic or a natural consequence of the immune components within the TME[3], it is clear that inflammation and immune evasion are intimately linked and a deeper understanding of both is required in order to identify targetable therapeutic vulnerabilities. The over-arching topics presented in this thesis are illustrated in Figure 1 and are centered on the themes novel-anti cancer therapeutics particularly in the context of combinatorial and immunotherapeutic approaches. The themes of immune responses following infection, viral immunotherapy and non-infectious inflammatory stimuli are explored from the perspective of specific immune subsets differentially regulated by these processes using murine knock-out and transgenic models.

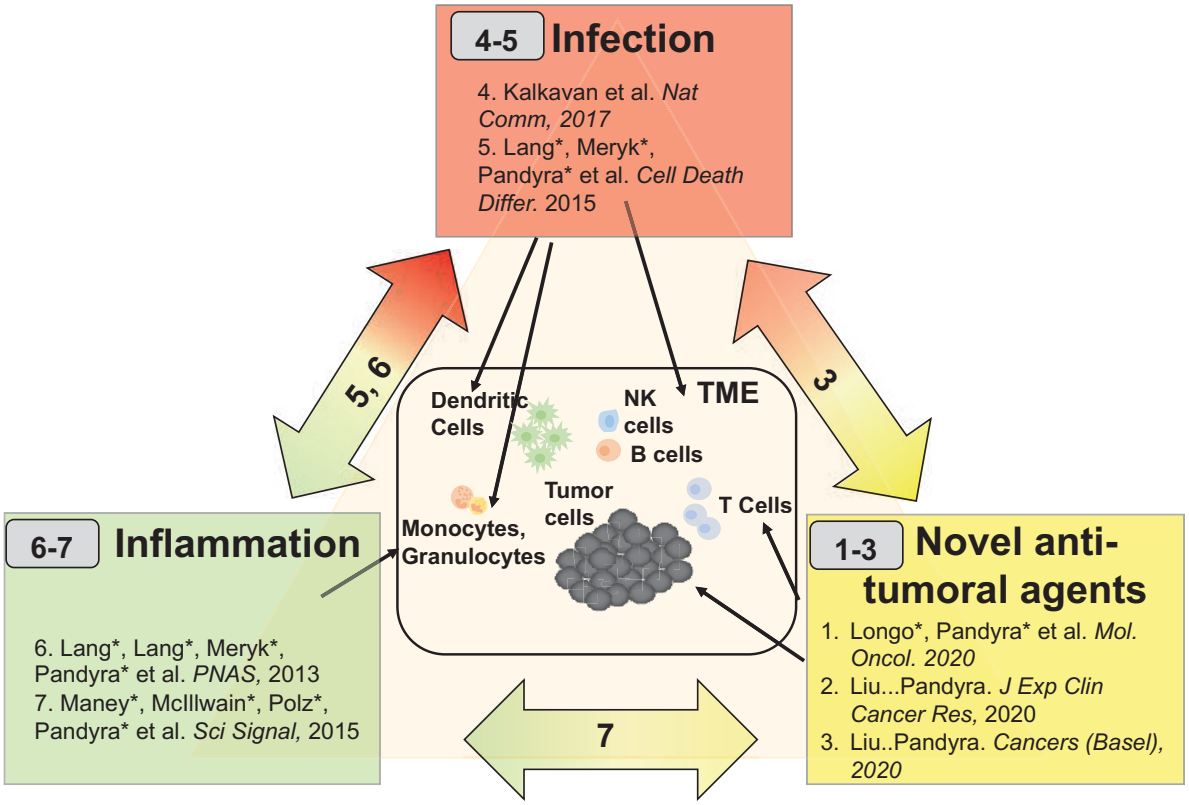

TME = Tumor Micro-environment

Figure 1: Schematic overview of the over-arching topics (Novel anti-tumoral agents, Infection and Inflammation) in this habilitation thesis. Publications are numbered from 1-7. Double sided arrows between the different areas indicate thematic overlap between the areas. Specifically, the publication whose theme overlaps with multiple areas is indicated inside the arrow. The illustration was created by A. Pandyra.

The publications comprising this this thesis focus on the following three areas:

(1) *Discovering novel anti-cancer treatment options, through drug repurposing strategies (Publication 1, Longo*, Pandyra* et al.) that influence the TME (Publication 2, Liu…Pandyra) or are novel viral immunotherapies (Publication 4, Kalkavan et al.). Publication 3 (Liu..Pandyra) summarizes the impediments to successful immunotherapies in the context of T cell exhaustion and senescence mechanisms within the TME.*

(2) *Identifying novel factors governing immunological responses in dendritic cells (DCs, Publication 5, Lang*, Meryk*, Pandyra* et al) and monocytic populations (monocytes, granulocytes and macrophages, Publication 6, Lang*, Lang*, Meryk*, Pandyra* et al.) following chronic viral infection and inflammatory innate stimuli respectively and*

(3) *Uncovering molecular inflammatory mechanisms governing shedding of the tumor necrosis factor (TNF) receptor (Publication 7, Maney*, McIlwain*, Polz*, Pandyra* et al.).*

I. A. Immune cells influencing anti-tumoral responses

Harnessing the immune system to treat solid tumors and hematological malignancies has ushered a novel therapeutic era. The tumor micro-environment (TME) is complex with many targeting opportunities due to the signaling networks and cross-talk between immune and tumor cells. The modulation of cytotoxic antigen-activated $CD8^+$ T (Tc) cells using checkpoint inhibitors has been at the forefront of this immunotherapy revolution[4]. The antigen-specific process requires the engagement of the TCR-CD3 complex on Tc cells with an MHC class I bound tumor antigen-derived peptide as well as co-stimulatory signals. Responsible for the direct tumor cell killing through granule exocytosis[5], Tc cells are integral in eradicating tumors and are currently targeted by many approved immunotherapies.

A tumor's ability to evade the immune system is dynamic, complex and dependent on the balance of immunosuppressive and/or activating activities of infiltrating immune cells. These include antigen presenting cells (APCs) such as dendritic cells (DCs), tumor-associated macrophages (TAMs), myeloid-derived suppressor cells (MDSC) and $CD4^+CD25^{hi}FoxP3^+$T regulatory T cells (Tregs) (Figure 2).

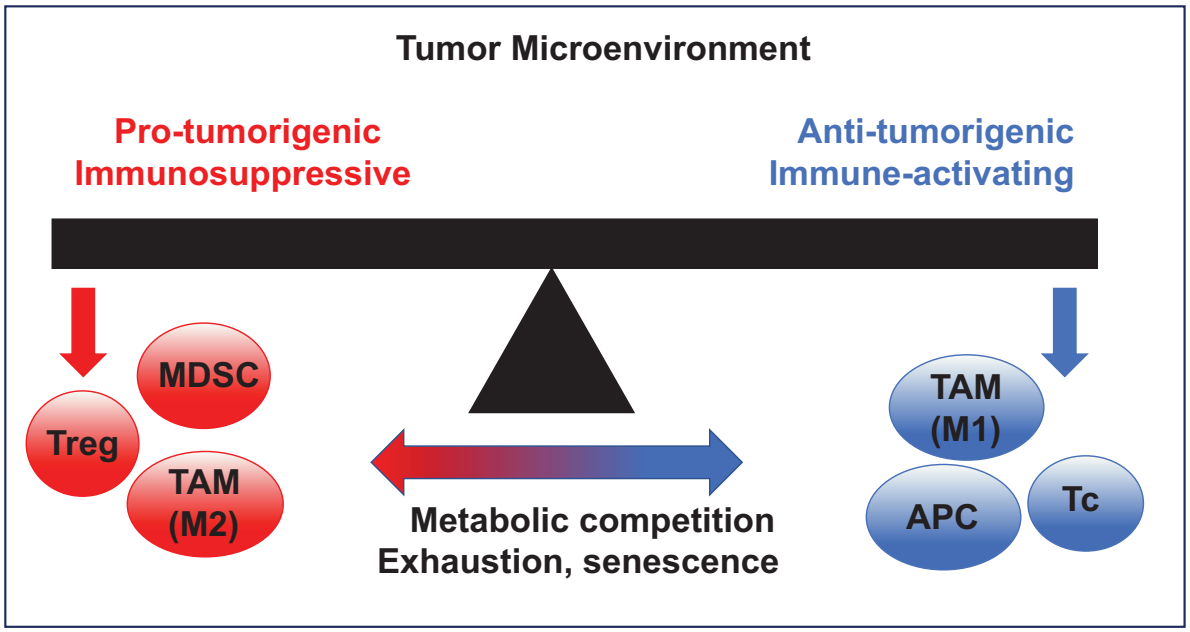

APC = Antigen presenting cells, MDSC = myeloid derived suppressor cells, TAM = tumor Associated macrophages, Treg = Regulatory T cells, Tc = $CD8^+$ Effector cells

Figure 2: Overview of the tumor microenvironment and the different immune infiltrates impacting the balance between immunosuppressive and immune-activating processes. Infiltrates which are generally immunosuppressive (Treg, MDSC and M2 TAMs are indicated in red circles. Infiltrates which are anti-tumorigenic (Tc, APC and M1 TAMs) are pictured in in blue circles. The illustration was created by A. Pandyra.

Tc effector function is complicated and shaped by the spatiotemporal distribution of APCs in the tumor milieu and tumor-draining lymph nodes, cytokines and the presence of other immune cells. Initial priming of naïve T cells occurs in the lymph node through direct interaction with antigen present on APCs such as DCs. DCs also co-express receptors such as CD80 necessary for binding to CD28 and inducing co-stimulatory signals. Upon migration of primed Tc cells into the TME, the tumor cells expressing the antigenic peptide become targets. The numbers of infiltrating $CD8^+$ T cells varies widely across tumor types. Some tumors, such as melanoma and non-small cell lung cancer (NSCLC), generally have a high degree Tc infiltration. Other tumors, such as pancreatic and neuroblastoma, typically have a low degree of Tc infiltrates, although within a specific tumor type, there is a lot of intra-tumoral heterogeneity[6]. Many factors during this process can impact the ability of Tc cells to target tumor cells.

Treg's are subsets of T cells which play a role in maintaining immune homeostasis and present a critical barrier for immunotherapies through their

suppressive effects on Tc cells. Tregs have been found in lymph nodes where they impact DC function through CCL22. CCL22, a chemokine produced by dendritic cells, enables cell-to-cell contact between DCs and Treg through Treg-expressed CCR4[7]. Tregs accumulate within the TME, and their ability to infiltrate into tumors has been linked to the expression of multiple chemokine receptors such as CCR4, CCR5, CCR8 and CCR10. Within the TME, Tregs usually express immunosuppressive molecules such as CTL-4, which binds to CD80 and CD86 on APCs thereby affecting Tc effector function[8]. Treg suppressive mediated-effects on APCs and Tc effector cells can also occur through cytokine secretion of IL-10, TGF-β, and IL-35. These inhibitory cytokines suppress antigen presentation in APCs. IL-35 and IL-10 promote T cell exhaustion. Metabolic competition for the consumption of IL-2 through the expression of CD25 on Tregs also suppresses Tc effector functions[9]. Tregs are also found in peripheral circulation, but their precise role in facilitating immune evasion are not as well characterized as with the TME-associated Tregs.

While myeloid-derived suppressor cells (MDSC) which can be of granulocytic or monocytic origin share phenotypic characteristics with monocytes and neutrophils, the markers that precisely define them are still poorly defined and their characterization as a separate immune population is controversial. Bone marrow derived myeloid cells are mainly composed of granulocytes and mononuclear cells such as monocytes, macrophages and DCs. Following signals from pathogens, toll-like receptor (TLR) ligands, damage-associated molecular patterns and pathogen-associated molecular pattern molecules, the mobilization of monocytes and granulocytes occurs from the bone marrow to the site of infection/stimulation and/or damage followed by short-term release proinflammatory cytokines and phagocytic activity[10]. However, during persistent albeit lower grade steady unresolved inflammatory signals such as during cancer of chronic infection, myeloid cells experience a different set of triggers that is thought to differentiate them into MDSCs. MDSCs suppress adaptive immunity, enhance tumor progression and metastasis, are considered pathologic and their accumulation in the peripheral blood been shown to correlate with response to therapy, clinical outcome, stage, metastasis in many tumors such as melanoma, breast, non-small-cell lung cancer and hematological malignancies[10]. Furthermore, monocyte infiltration into the TME is indicative of a poor clinical prognosis[11]. Monocytic MDSC (M-MDSCs) can differentiate into TAMs or

inflammatory DCs (iDCs) in tumor tissues[10]. TAMs are generally considered to be immunosuppressive and promote tumor progression but that is largely dependent on their polarization. Specifically, M1 macrophages are considered to be anti-tumorigenic, pro-inflammatory, capable of high antigen presentation and inhibiting cell proliferation. In contrast, M2 macrophages are generally anti-inflammatory, immunosuppressive and characterized by a low antigen presenting capacity[12]. iDCs have been shown to have a dual role within the TME. While some studies suggest that they can promote T cell responses[13], others have shown them to be immunosuppressive under specific contexts[14]. The immune subsets investigated in this cumulative body of work are shown in Table 1.

Table 1: Immune subsets investigated in this cumulative body of work

Immune Cells	Markers *	Publication	Stimuli
Treg's	CD4,CD25,FOXP3, RORγ	2	Tegaserod
Monocytes	CD11b, Ly6C, IFNβ	4,5,6	LCMV, Listeria, LPS
Granulocytes	CD11b, Ly6G, CD115	6	LCMV, Listeria, LPS
iDCs	CD11b, CD11c, Ly6C	5	LCMV, CpG
CD8 T cells	Tet-GP33, IFNγ	2,4, 5	LCMV, Tegaserod

*Murine markers, iDCs = inflammatory dendritic cells, LPS = Lipopolysaccharide

I. B. Challenges to effective checkpoint inhibition

Monoclonal antibody checkpoint inhibitors such as Nivolumab[15] are currently used to treat solid tumors and they target the inhibitory receptors such as the programmed cell death 1 (PD-1)[16] receptor which is expressed on T cells following activation of T cells as a mechanism of inhibitory immunoregulation. Expression of PD-1 or other inhibitory receptors on T cells, coupled with the corresponding ligands such as Programmed death-ligand 1 (PD-L1) often expressed by tumor cells, preclude lasting and effective anti-tumoral responses by infiltrating Tc's. Checkpoint inhibitors that are mainly monoclonal antibodies targeting inhibitory receptors de-repress these inhibitory networks. Examples include nivolumab, pembrolizumab and pidilizumab that target PD-1 and the anti-CTLA-4 antibody ipilimumab. CTLA-4 is expressed on Tregs and treatment with ipilimumab depletes Tregs from the TME[17]. PD-L1, which can be expressed by tumor cells in the TME as well as tumor and lymph node infiltrating DCs, limits the activation of Tc's. Several anti-PD-L1 monoclonal antibodies such as Durvalumab and Atezolizumab are approved for the treatment of various solid tumor moieties.

Many more T cell based therapies are currently in the experimental phase of pre-clinical or clinical testing[18]. While immunotherapies have made remarkable progress in increasing the survival of some patients, low response-rates, toxicities as well as lack of available bio-markers in predicting response, makes the successful implementation of these therapies challenging. Although the repertoire of suggested biomarkers including PD-L1 expression, genomic and transcriptomic signatures, profiling of tumor-infiltrates and presence of clonal neoantigens have been proposed, they are yet to be clinically validated and implemented[19, 20, 21, 22, 23]. A major obstacle is the inability to effectively target Tc's. This can occur through Tc intrinsic or acquired resistance helped by dysfunctional states present within the immunosuppressive networks[24] of the TME: exhaustion and senescence. While T cell exhaustion has been extensively studied and targeted, T cell senescence, especially within the context of anti-tumor immunity, is an emerging concept in the field of T cell dysfunction.

Both exhausted and senescent T cells accumulate during chronic viral infections[25] and cancers[26]. Exhaustion and senescence are both considered dysfunctional states. They are characterized by dampened granzyme B (GzmB)—mediated effector function and impaired proliferation[27]. However, they are defined by distinct surface marker, cytokine, transcriptional and metabolic profiles. When Tc cells are exhausted through excessive and continuous stimulation, they upregulate inhibitory cell surface receptors such as PD-1 and LAG-3 and possess a decreased capacity to secrete interleukin 2 (IL-2) and interferon gamma (IFN-γ)[28](Figure 3). The exhausted transcriptional Tc profile is very context dependent and is driven, during varying stages of exhaustion, by nuclear factor of activated T cell (NFAT), nuclear receptor Nr4a, thymocyte selection-associated HMG box (TOX), eomesodermin (Eomes) and T-Bet[29]. While exhausted and senescent Tc cells share characteristics such as the upregulation of surface markers Tim-3 and tyrosine-based inhibitory motif (ITIM) domain (TIGIT), senescent Tc cells also upregulate CD57 and CD45RA (Figure 3). The cytokine secretory profile of senescent Tc cells sharply contrasts that of exhausted T cells (Figure 3). Senescent Tc cells secrete high levels of inflammatory cytokines such as IL-2, IL-6, IL-8, TNF-α, IFN-γ and the immunosuppressive IL-10 and TGF-β (Figure 3), a program known as senescence-associated secretory phenotype (SASP). This in turn has critical consequences not

only for T cell themselves, but for other immune cells within the TME milieu, including APCs such as DCs, TAMs and MDSCs. Transcriptional programs in senescent Tc's have been shown to be mediated by T-bet[30] but otherwise are poorly characterized. Senescence-inducing stimuli include exposure to DNA damaging agents, stress signals and repetitive stimulation linked but not limited to the ageing process. It should be pointed out that dysfunctional T cell states other than exhaustion and senescence such as anergy have also been described. Anergic T cells are hypo-responsive, produce low levels of IL-2 and generally have little effector function. T cell anergy is caused by insufficient CD28 dependent co-stimulation of the TCR, but the surface markers of anergic T cells are poorly characterized[31]. Insufficient CD28 stimulation within the TME combined with tumor cell expressing factors, such as PD-L1 and CD95, is also closely linked to deletion of effector T cells through a process known as tolerance. Tolerance is exacerbated by TGF-β and IL-10[32]. Taken together, senescent, anergic and exhausted Tc cells often co-exist in the TME or circulation and simultaneously exert immunosuppressive effects. The current limitations of check-point inhibitors suggest that targeting multiple dysfunctional Tc cell states would be therapeutically beneficial. A deeper understanding of the mechanisms and functional consequences of T cell senescence are urgently needed

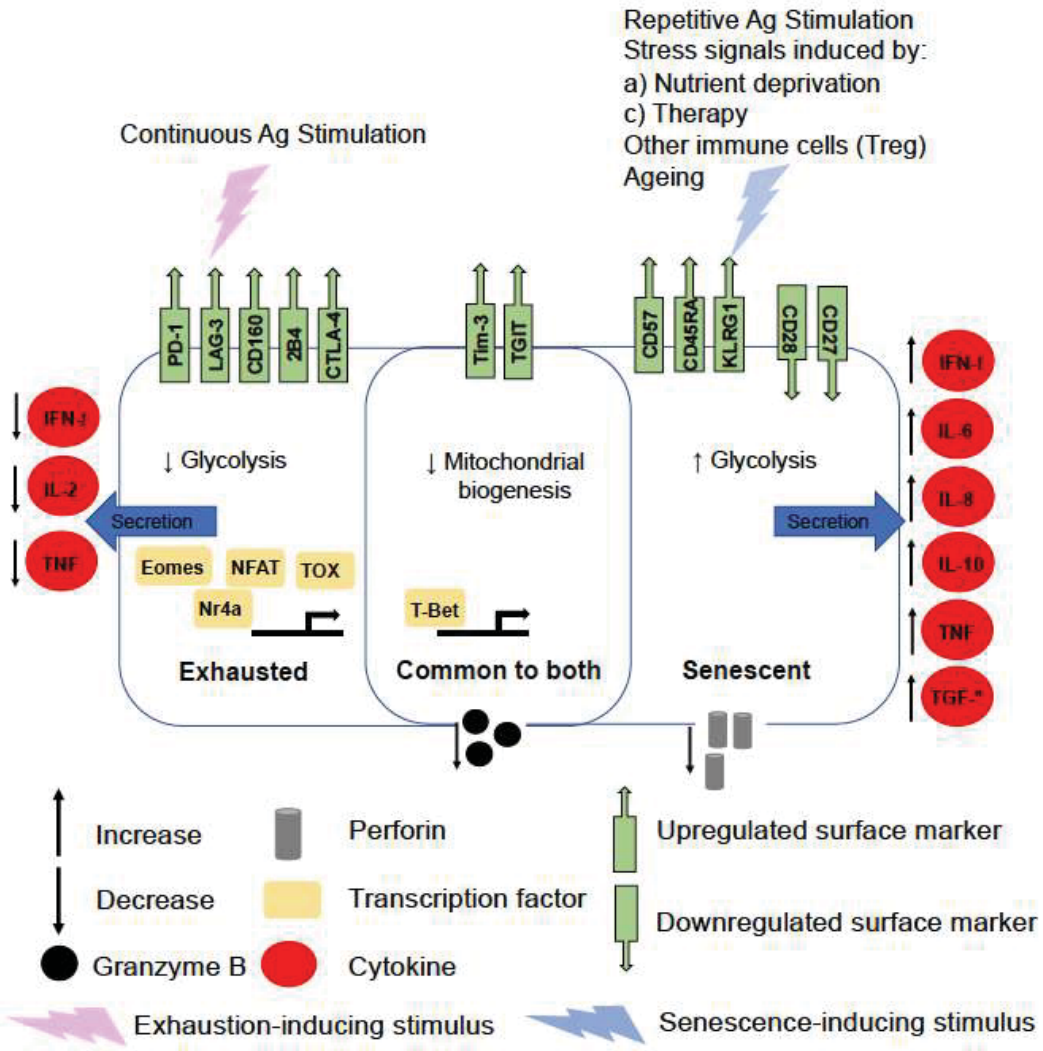

Figure 3: Surface phenotypic, metabolic and transcriptional differences between CD8$^+$ T cell dysfunctional senescent and exhaustive states. Characteristics common to both dysfunctional states are shown in the middle, overlapping section. While both T cell states exhibit decreased effector function, senescent T cells have a very distinct senescence-associated secretory phenotype (SASP). While some surface markers such as Tim-3 and TGIT are common to both dysfunctional T cell states, there is otherwise quite a distinct pattern of expression. Ag = antigen. Use of Illustration is permitted by MDPI (open access journal Creative Commons CC BY 4.0 license, authors retain copyrights)[33].

II. Metabolic rewiring of the TME

Metabolic re-programming within the TME is critical to many pro-tumorigenic processes[34, 35]. Cancer cells have a high rate of glucose consumption through aerobic glycolysis, resulting in low glucose and high lactate concentrations in the TME[36]. Antigen-activated effector T cells, once they become primed and activated in the lymph nodes, begin their clonal expansion and rapid

proliferation[34]. Therefore, they have metabolic requirements different to those of circulating naïve cells which rely on oxidative phosphorylation for their energy requirements. Rapidly proliferating T cells have higher glycolytic activity[37] and increased amino acid metabolism[38]. TCR-mediated T cell activation is followed by metabolic re-programming and biomass accumulation. Changes in metabolism include a switch to aerobic glycolysis despite there being enough oxygen present to generate glucose through the tricarboxylic acid (TCA) cycle[34]. Aerobic glycolysis provides important intermediates for cell growth, such as glucose-6-phosphate, 3-phosphoglycerate and citrate. Molecularly, this metabolic transition is supported by mTOR, PI3K activity, the transcription factor Myc and hypoxia-inducible factor-1α (HIF-1α)[34, 38].

Effector T cell activity is sensitive towards intracellular NAD depletion, often occurring in the TME. Tregs, however, have developed re-programming strategies mediated by the transcription factor FOXP3 to maintain their proliferative capabilities and suppressive functions, despite low glucose and high lactate levels[39]. It remains to be elucidated whether within the TME Treg numbers would be high enough to deplete glucose pools. However, in addition to Treg competing for glucose consumption, other immune cells within the TME also have distinct metabolic requirements which can affect glucose pools. MDSCs have high glucose uptake rates and can contribute to the dysfunction of other immune cells by limiting pools of available glucose[40]. MDSCs can also affect the T cell activation through depletion of amino acids such as cystine and cysteine[41]. Conditions of hypoxia within the TME compounded by increased tumor acidity can cause an accumulation of immunosuppressive M2 polarized TAMs, which are critical in maintaining a tolerogenic phenotype, expanding Tregs and suppressing $CD8^+$ T cell function[42].

III. A. Approaches to target the TME

Combining checkpoint inhibitors with other activators of the immune system such as innate activating toll-like receptor (TLR) 8 agonists could maximize the benefits of immunotherapy in hematological malignancies and solid tumors. TLR8 agonists have already been shown to reverse the T cell tumor-induced senescence in mouse models of cancer[43]. They have the added benefit of increasing immune infiltration and activating other anti-tumoral immune cells such as dendritic and NK cells. The TLR8 agonist motolimod (VTX-2337) has been evaluated in clinical trials,

is well tolerated and shows promise activating the immune system in cancer patients[44, 45]. Other approaches include combining immunotherapies with oncolytic viruses or other anti-cancer agents. The first clinical trial combining an oncolytic virus therapy (T-Vec) with the anti PD-1 Pembrolizumab demonstrated that T-Vec promoted tumoral T cell infiltration improving Pembrolizumab's efficacy[46]. Patients with advanced melanoma in a phase II randomized study receiving a combination of T-Vec with the anti-CTLA-4 antibody ipilimumab experienced significantly higher objective responses than patients receiving ipilimumab alone[47]. Virus based vaccines are also being evaluated in currently open clinical trials such as viagenpumatucel-L (gp96-Ig-secreting allogeneic tumor-cell vaccine HS110) in combination with the anti-PD-1 Nivolumab in patients with non-small cell lung adenocarcinoma.

As 40–85 percent of patients treated with checkpoint inhibitors fail to exhibit a sustained clinical response[48], combinatorial approaches that also reverse Tc cell senescence could be of therapeutic benefit. As induction of tumor cell senescence can be advantageous in the context of tumor clearance, strategies to reverse T cell senescence should be carefully considered. While induction of tumor cell senescence can initially stop uncontrolled proliferation, the SASP profile of senescent tumor cells can promote tumor relapse, inflammation and recruit immunosuppressive immune cells to the TME. Agents that induce apoptosis in senescent cells termed "senolytics" (e.g., dasatanib and quercetin), are currently being tested in pulmonary fibrosis and after radiotherapy to improve clinical symptoms[49]. Whether these agents can be used in neoplastic malignancies to clear senescent tumor cells and/ or senescent Tc cells is an area warranting further exploration.

Agents such as ralimetinib that target p38 MAPK, which are safe and have already been used in clinical trials[50], are an attractive option as they could dually target Tc senescence signaling and tumor proliferation. In addition to their direct anti-tumoral effects, other inhibitors of the MAPK pathway already approved for the treatment of metastatic melanoma are also promising. These include the B-Raf-targeting inhibitor vemurafenib or MEK1/2 targeting inhibitor trametinib. These drugs have already been shown to increase the number of $CD8^+$ TILs and enhance checkpoint inhibition in murine models[51]. Whether these inhibitors also reverse Tc senescence and enhance checkpoint inhibition in the clinical setting remains to be

elucidated. However, combinatorial therapy is paramount in achieving clinical success.

Combinatorial approaches of various targeted therapies together with immunotherapies are also being tested[52]. However, the high-costs[53] associated with immunotherapy highlights an urgent need for novel anti-cancer therapeutic options. The application of drugs used for alternate diseases as novel anti-cancer therapeutics, known as drug repositioning, has been successfully implemented in the clinical setting[54] and these compounds can be a rich potential source of novel, readily available anti-cancer therapeutics.

Statins, potent inhibitors of the rate-limiting enzyme in the essential metabolic mevalonate (MVA) pathway, HMGCR[55, 56], are used in the treatment of patients with hypercholesterolemia (Figure 4). The MVA pathway utilizes acetyl-CoA to generate sterols and isoprenoids which are essential to sustain tumor growth and progression and is highly integrated into other crucial pathways of cancer cells including PI3K–AKT, hedgehog and steroid hormone signaling[57].

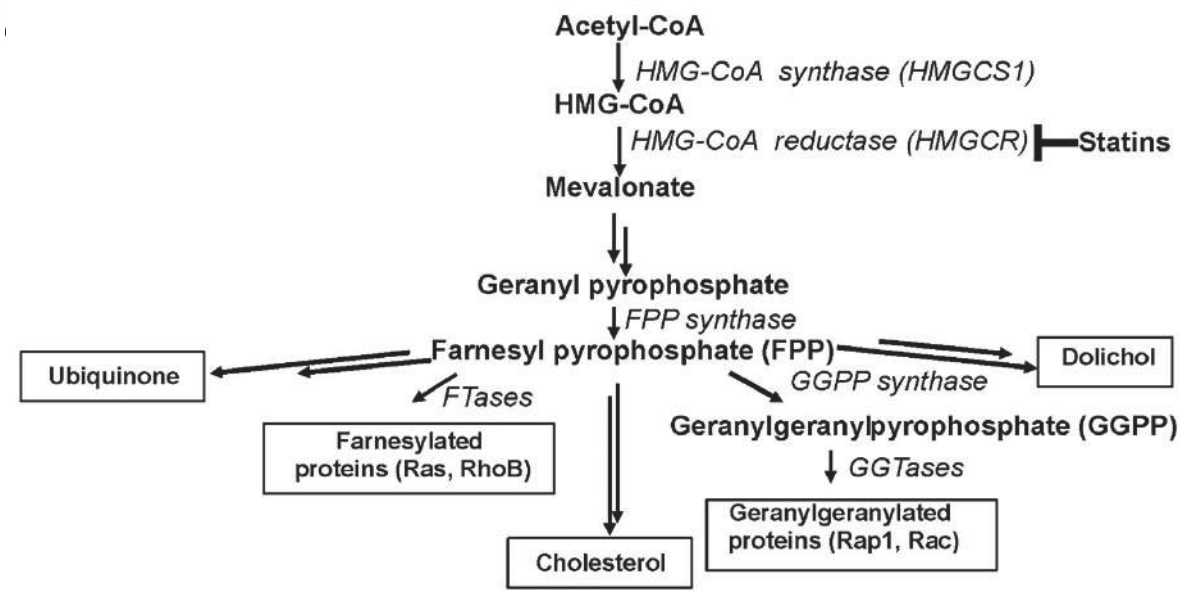

Figure 4: A schematic overview of the mevalonate (MVA) pathway and its downstream metabolites (pictured in black rectangles). These metabolites are affected by the inhibition of the MVA pathway's rate limiting enzyme HMG-CoA reductase by statins. Use of illustration is permitted under standard copyright in AACR journals[58].

The frequent use of statins in the prevention of adverse cardiovascular events has led to epidemiologic evidence suggesting that statin use may reduce cancer

incidence[59]. It has been shown that statins can trigger tumor-specific apoptosis[60, 61, 62]. These apoptotic effects have been attributed to direct inhibition of HMGCR in tumor cells followed by depletion of fundamental MVA-derived end products such as isoprenoids and cholesterol[63].

In tumor cells, dysregulation of the MVA pathway has been postulated to be responsible for the observed therapeutic index. Higher tumor expression levels of HMGCR and other MVA pathway enzymes are associated with poor prognosis and reduced survival in patients with cancer[64]. Statins have been shown to have anti-tumoral immunomodulatory roles[65, 66] and have been suggested to enhance the activity of other immunotherapies including oncolytic viruses (OVs)[67]. Interestingly, one of the metabolites of the MVA pathway, isopentenyl-diphosphate (IPP) tend to accumulate in tumor cells with aberrant activation of the MVA pathway. IPP activates the expansion of host γδ T cells which kill IPP-expressing cells in an MHC-I independent manner. Inducing accumulation of IPP in tumor cells is being investigated as an anti-cancer strategy in combination with IL-2 for the treatment of solid tumors such as breast and prostate cancer[57].

Publication 1 (Longo, J*, Pandyra, AA*, Stachura P, Minden MD, Schimmer AD, Penn LZ. Cyclic AMP-hydrolyzing phosphodiesterase inhibitors potentiate statin-induced cancer cell death. Mol Oncol; 2020, 14:2545, Published by FEBS Press and John Wiley & Sons Ltd.) explores the topic of repurposing statins in combination with phosphodiesterase inhibitors (PDE) to increase tumor-cell apoptosis in hematological malignancies Figure 5). **Publication 2 (Liu W, Stachura P, Xu HC, Umesh Ganesh N, Cox F, Wang R, Lang KS, Gopalakrishnan J, Haussinger D, Homey B, Lang PA, Pandyra AA. Repurposing the serotonin agonist Tegaserod as an anticancer agent in melanoma: molecular mechanisms and clinical implications. *J Exp Clin Cancer Res,* 2020, 39:38)** used a pharmacological screen to identify Tegaserod, a serotonin agonist used in the clinic to treat IBS, as having anti-tumor activity (Figure 5). Tegaserod's anti-melanoma activity was verified in *in vivo* syngeneic models of cancer where the compound decreased the infiltration of Treg's into the TME and synergized with the standard of care therapies. Taken together, the first portion of the thesis identified novel treatment combinatorial modalities with immunomodulatory properties.

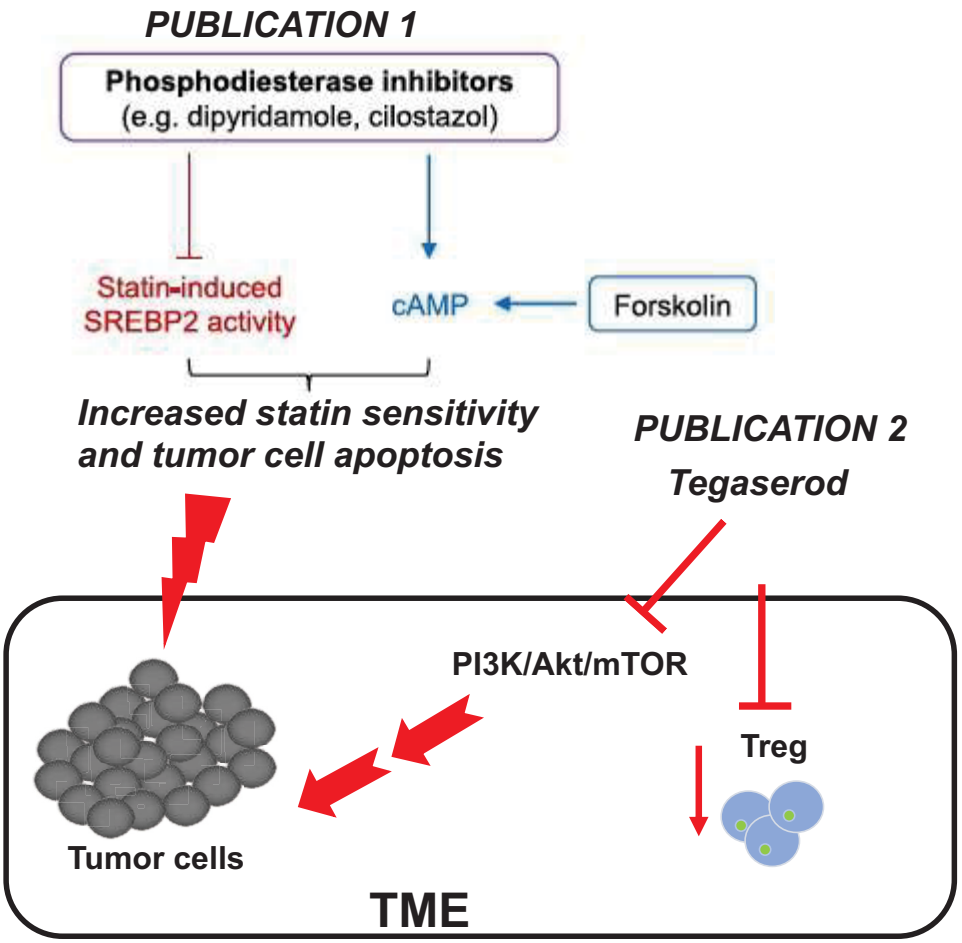

Figure 5: Graphical abstract summary of publications 1 and 2 is shown. In Publication 1 phosphodiesterase inhibitors were found to potentiate stain-induced tumor cell death through inhibition of SREBP2 (red) cleavage and cAMP accumulation (blue). In Publication 2, Tegaserod was identified as a novel anti-tumor agent decreasing the infiltration of T regulatory cells (Treg) and inhibiting the the PI3K/Akt/mTOR pathway. The illustration was created by A. Pandyra, with parts of the figure re-used with permission from FEBS PRESS (under the terms of the Creative Commons Attribution License (CC BY)[56]

III. B. *The Lymphocytic choriomeningitis virus (LCMV) as an immunotherapy and model to study viral infection*

The use of viruses to combat cancer presents many unique opportunities and advantages. This has been particularly relevant in recent decades as recognition of the importance of the immune system in tumor surveillance has revolutionized the therapeutic landscape. Viruses are ideal vectors for gene therapy approaches and have been successfully applied in virus-based therapeutic vaccines as well as cell-based vaccines[68]. Virus-based anti-tumor vaccines encode a combination of tumor-

specific antigens, co-stimulatory proteins and immunomodulating molecules which boost the immune system to elicit anti-tumor responses[68]. Promising examples in clinical development include the TG4010 modified vaccinia virus Ankara (MVA) vaccine encoding the prostate specific mucin 1 (MUC1) antigen and the interleukin 2 (IL-2) gene[69]. Virus engineered cell based vaccines are centered on more personalized approaches and modify a patient's immune cells *ex vivo* using viral vectors. Notable examples include the recently approved YESCARTA and KYMRIAH both of which target a patients' T cells with a retrovirally inserted anti-CD19 Chimeric

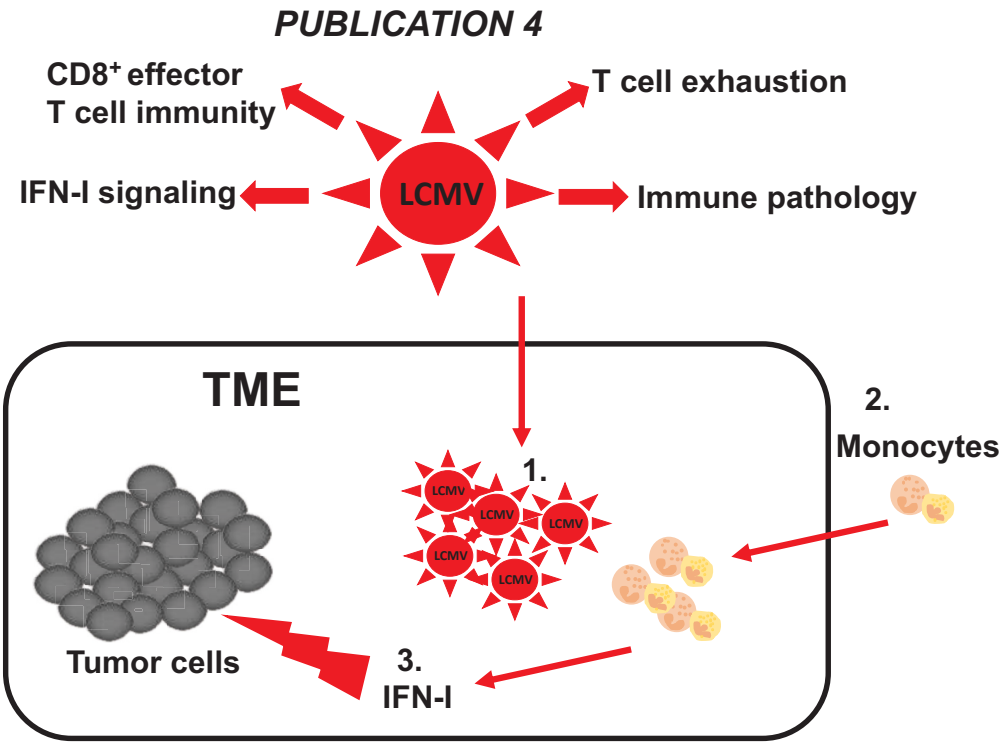

Figure 6: Graphical abstract summary of publication 4. (1) LCMV-selective intra-tumoral replication causes the Infiltration of monocytes (2) whose production of type I Interferons (3) has anti-tumoral effects. The illustration was created by A. Pandyra.

Antigen Receptor (CAR) for the treatment of acute lymphoblastic leukemia[70].

For decades LCMV has been the prototypic experimental arenavirus of choice for immunologists. The Arenaviridae family consists of three genera, *Mammaarenavirus, Reptarenavirus* and *Hartmanivirus*, the first of which infects mammalian hosts. The *Mammaarenavirus* genus consists of 41 distinct viral species capable of infecting mammalian hosts and is geographically, genetically and epidemiologically sub-divided into Old and New World groups. LCMV belongs to the

former group. The genome of arenaviruses is bi-segmented and composed of two single-stranded negative sense RNA biomolecules. The large (L) segment encodes the matrix protein (Z) and the RNA-dependent RNA polymerase L protein (LP). The viral nucleoprotein (NP) and the glycoprotein precursor (GPC) are encoded by the small (S) segment. The GPC is further post-translationally processed to the peripheral virion attachment protein GP1 and the transmembrane protein GP210. The LCMV lifecycle is limited to the hosts' cytoplasm and clathrin-independent or clathrin-dependent endocytotic viral entry is upon others mediated by the surface receptor α-dystroglycan[71]. Not only does infection with LCMV result in robust $CD8^+$ effector T cell responses but also in long-term immunity. LCMV poses a relatively low health hazard making it an ideal model to study $CD8^+$ effector T cell mediated immunity. Indeed, its wide experimental use has led to monumental discoveries such as the discovery of MHC restriction as well as PD-1 and its role during T cell exhaustion[16]. By expressing LCMV-specific epitopes on tumor cells it has been possible to study various aspects of CD8 mediated anti-tumor immunity[72]. **Publication 4 (Kalkavan H, Sharma P, Kasper S, Helfrich I, Pandyra AA, Gassa A, Virchow I, Flatz L, Brandenburg T, Namineni S, Heikenwalder M, Höchst B, Knolle PA, Wollmann G, von Laer D, Drexler I, Rathbun J, Cannon PM, Scheu S, Bauer J, Chauhan J, Häussinger D, Willimsky G, Löhning M, Schadendorf D, Brandau S, Schuler M, Lang PA, Lang KS. Spatiotemporally restricted arenavirus replication induces immune surveillance and type I interferon-dependent tumor regression. Nat Commun; 2017, 8:14447)** demonstrated that direct intravenous or peritumoral injection of the hepatotropic LCMV-WE in several syngeneic or spontaneous murine and human xenograft models of cancer, including subcutaneous, endogenous hepatocellular carcinoma and spontaneous MT/ret melanoma led to regression or complete elimination of early-stage pre-established tumors (Figure 6).

LCMV preferentially replicated in tumor cells and metastatic sites leading to robust immune infiltration with some, albeit minimal accompanying replication in the liver. LCMV replication within the tumor persisted for at least thirty days post-tumor inoculation and tumor regression was dependent on IFN-I production by tumor-infiltrating monocytes. Importantly, IFN-I did not blunt LCMV replication within the tumor allowing for sustained innate immune activation and clearance of LCMV from other organs.

Infection with LCMV has been used for years to elucidate aspects of chronic and acute infections[25, 73], T cell exhaustion[16, 25], interferon responses[74] and the molecular factors in specific immune subsets influencing the course of infection[73, 75, 76]. **In publication 5 (Lang PA*, Meryk A*, Pandyra AA*, Brenner D, Brüstle A, Xu HC, Merches K, Lang F, Khairnar V, Sharma P, Funkner P, Recher M, Shaabani N, Duncan GS, Duhan V, Homey B, Ohashi PS, Häussinger D, Knolle PA, Honke N, Mak TW, Lang KS. Toso regulates differentiation and activation of inflammatory dendritic cells during persistence-prone virus infection. Cell Death Differ; 2015, 22:164.),** responses of inflammatory dendritic cells (iDCs) were investigated

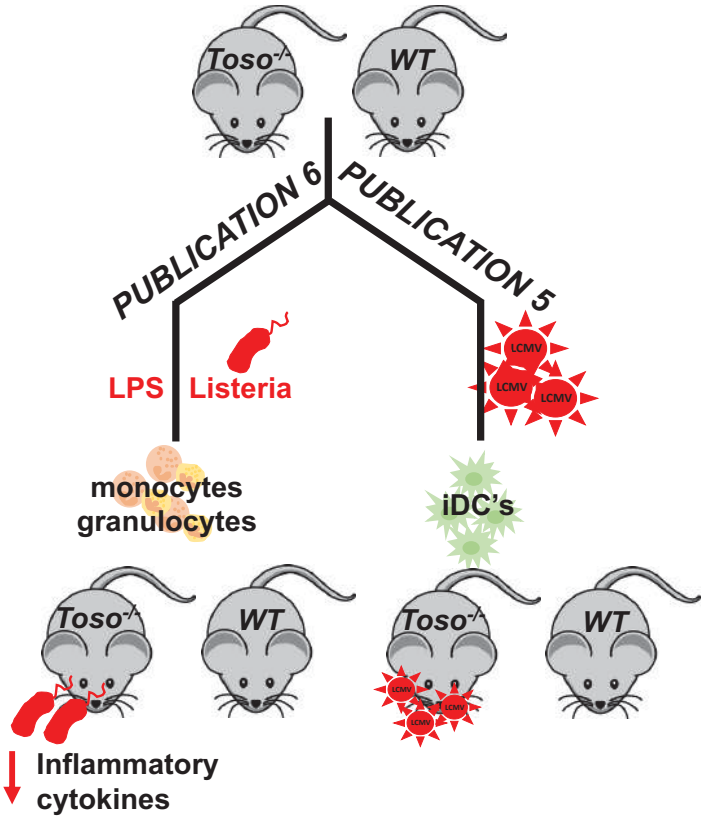

Figure 6: Graphical abstract summary of publications 5 and 6. Infection with LCMV and listeria leads to persistence in *Toso*$^{-/-}$ mice mediated by inflammatory dendritic cells (iDCs) and monocytes/granulocytes respectively. The illustration was created by A. Pandyra.

following chronic infection of wild-type (WT) and Toso-deficient (*Toso*$^{-/-}$) mice (Figure 7). iDCs differentiate from blood monocytes and infiltrate infected tissue and are ontologically different from monocytes. Following acute infection with hepatotropic viruses, iDCs are essential for re-stimulating virus-specific CD8^{+} T cells and therefore contribute to virus control. iDCs have been found in several other inflammation-related pathologies including psoriasis, rheumatoid arthritis and cancer[77]. Importantly, pro-immune roles of iDCs within the TME have been recently identified and shown to correlate with anti-tumoral and Th17 responses as well as T cell activation[78]. Therefore, identifying factors governing iDC function has the potential to shed important light on how to manipulate this subset within the TME to maximize

anti-tumoral efficacy. Toso is a plasma membrane protein that contains an extracellular region with homology to the Ig variable (IgV) domains and a cytoplasmic region with partial homology to Fas-activated serine/threonine kinase (FAST kinase)[79]. Toso was first identified as a molecule expressed on activated T cells capable of protecting T cells from programmed cell death. Toso is additionally expressed on B cells, overexpressed in B-cell lymphomas[80], and is important for macrophage homeostasis[81]. Mechanistically, Toso was originally described to influence Fas signaling[79, 82]. However, the physiological relevance of the diverse functions attributed to Toso remain to be verified which and this is addressed by **publications 5 and 6**.

IV. Inflammation and monocytes

Another important immune infiltrating component affecting anti-tumor immunity are monocytes, the precursors of iDCs. Monocytes, particularly PD-L1 positive monocytes also termed myeloid-derived suppressor cells (MDSC), can exert their immunosuppressive effects through inhibition of anti-tumor functions of T and NK cells, secretion of immunoregulatory cytokines and presentation of surface inhibitory molecules[83]. This monocytic population plays a significant immunosuppressive role at various points in tumor progression[84] including in relapsed tumors[85]. Monocytes are intimately linked with tumor-associated inflammatory processes which paradoxically can contribute to tumor transformation, progression and metastasis[2] through various mechanisms including the production of pro-inflammatory cytokines, [86]. Inflammatory processes and sources of inflammation within the context of cancer are multi-faceted and can occur prior to cancer development through infection, chronic inflammation and autoimmunity. Inflammation also develops within the TME and is supported by dysregulated oncogenic signaling[87], infiltration of immunosuppressive cells such as MDSCs, pre-existing pathogens[88] and metabolic changes facilitated by alterations in the microbiome[89]. **Publication 7 (Maney* SK, McIlwain DR*, Polz R*, Pandyra AA*, Sundaram B, Wolff D, Ohishi K, Maretzky T, Brooke MA, Evers A, Vasudevan AA, Aghaeepour N, Scheller J, Münk C, Häussinger D, Mak TW, Nolan GP, Kelsell DP, Blobel CP, Lang KS, Lang PA Deletions in the cytoplasmic domain of iRhom1 and iRhom2 promote shedding of the TNF receptor by the protease ADAM17. Sci Signal; 2015, 8:ra109.)** highlights the contribution of the cytoplasmic domain of iRhom1 and iRhom2 in promoting shedding of the tumor necrosis factor receptor (TNFR) by the protease A

disintegrin and metalloproteinase 17 (ADAM17 also known as TNF-α converting enzyme TACE, Figure 8)[90]. ADAM17 is a membrane-bound metalloproteinase that processes a wide array of cell surface/membrane proteins. It is a central regulator of epidermal growth factor receptor (EGFR), TNFR signaling pathways, which control cell proliferation, survival, inflammation, oncogenesis, and immunity. ADAM17 plays a critical role in tumor progression and inflammation due to the role in shedding pro-inflammatory molecules, pro-tumorigenic substrates and adhesion molecules[91]. Further inflammatory process were investigated in **Publication 6 (Lang PA*, Meryk A*, Pandyra AA*, Brenner D, Brüstle A, Xu HC, Merches K, Lang F, Khairnar V, Sharma P, Funkner P, Recher M, Shaabani N, Duncan GS, Duhan V, Homey B, Ohashi PS, Häussinger D, Knolle PA, Honke N, Mak TW, Lang KS. Toso regulates differentiation and activation of inflammatory dendritic cells during persistence-prone virus infection. Cell Death Differ; 2015, 22:164.)** where inflammatory immune responses were investigated following infection and administration of innate immune stimulators in wild-type (WT) and Toso-deficient (*Toso*$^{-/-}$) mice (Figure 7). Monocytes were determined to play a critical role in protecting mice against cytokine-induced septic shock following lipopolysaccharide (LPS) administration in *Toso*$^{-/-}$ mice.

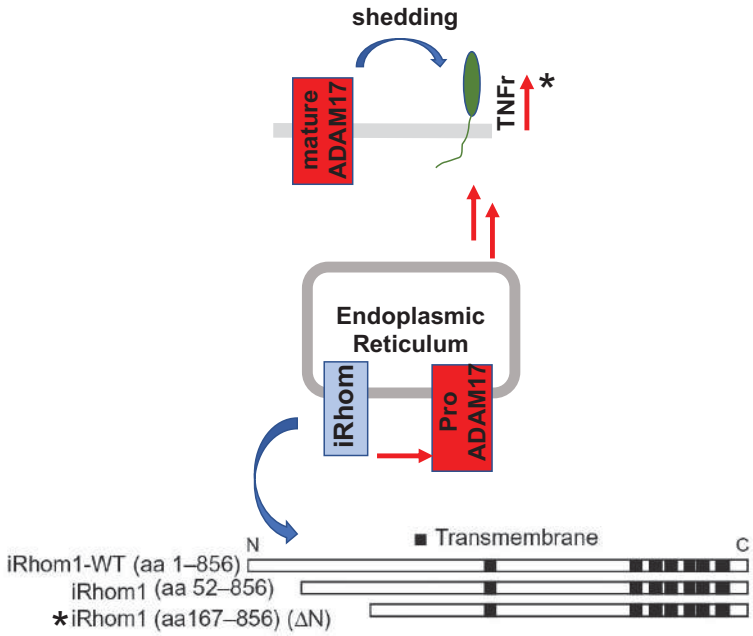

Figure 8: Graphical abstract summary of publication 7. Mutational deletion in the cytoplasmic domain (C) of iRhom1 (*) increased shedding of the TNFr, ADAM17 activity and resistance to TNF-induced cell death. The illustration was created by A. Pandyra, with parts of the figure re-used with permission from AAAS (under License to publish for dissertation purposes)[90].

3. Discussion

The cumulative work presented in this habilitation thesis elucidates several aspects of tumor biology and onco-immunology. Firstly, this work identified novel anti-cancer therapies translatable to several tumor types. Importantly, the use of drugs previously used in the clinic albeit for non-cancer purposes has enabled a more directly translational approach to identify new therapies. The pharmacological and safety profiles of such drugs are readily available making their potential translation into the clinic more rapid. As is the case for many treatment regimens, it is optimal to administer a drug in multimodal and combinatorial treatment strategies to increase tumor-specific anticancer effects. In Publication 1, we provide a complimentary approach of combining statins and already FDA-approved PDE inhibitor agents in the treatment of hematologic malignancies. In Publication 1, we found that dipyridamole and cilostazol potentiated statin-induced cell death in a PKA-independent manner (Figure 5). In addition to PKA, cAMP also regulates specific ion channels and exchange protein directly activated by cAMP EPAC proteins, which are cAMP-dependent guanine nucleotide exchange factors for the RAP GTPases[92]. Future work is required to delineate the mechanism by which elevated cAMP levels sensitize cancer cells to statin-induced apoptosis. We further demonstrated that the PDE inhibitors dipyridamole and cilostazol inhibit the SREBP2-regulated feedback mechanism of the MVA pathway via an additional, cAMP-independent mechanism. Interestingly, cilostazol has previously been reported to inhibit insulin-induced expression of SREBP1[93], but the potential involvement of cAMP signaling was not explored.

The data presented in publication 1 has important clinical implications, as many cAMP-hydrolyzing PDE inhibitors are approved for several non-oncology indications[94]. For example, cilostazol (marketed as Pletal) is currently approved and widely used to treat intermittent claudication. As the combination of cilostazol and statins has already been evaluated clinically in healthy subjects[95, 96] and in patients with cardiovascular indications[97] without added adverse effects, there is the possibility of fast-tracking these agents to phase II trials.

The overexpression of several PDEs has been observed in solid and hematological tumors, and the possibility of cAMP-hydrolyzing PDE inhibition as an anticancer strategy has been preclinically explored alone or in combination with

chemo- and targeted molecular therapies[98, 99]. In hematological malignancies, primary chronic lymphocytic leukemia patient samples were found to have PDE7B overexpression and noted to be sensitive to PDE7 inhibition in a cAMP-dependent manner[98]. Another study found a strong synergistic combinatorial effect between adenosine A2A receptor agonists and cAMP-hydrolyzing PDE inhibitors in MM and diffuse large B-cell lymphoma cell lines and primary patient samples[99]. Given that a number of PDE inhibitors are poised for repurposing and that statins have demonstrated anticancer activity in early-phase clinical trials, further studies are needed to evaluate the therapeutic benefit of a statin-PDE inhibitor combination for the treatment of cancer.

Importantly, it was recently demonstrated that PDE inhibitors exert potent anti-MDSCs activity[100] and have immunostimulatory properties in metastatic melanoma patients. Specifically, a PDE inhibitor, Tadalafil, increased infiltration of $CD8^+$ T cells in melanoma tumors and is suggested as a future agent capable of augmenting immunotherapies[101]. The possibility of testing the statin/PDE combination in order to augment immunotherapies in poorly infiltrating 'cold' tumors is an attractive area of further exploration as is combining Tegaserod, the novel anti-melanoma agent discovered in publication 2 with anti-CTL-4 monoclonal antibodies such as ipilimumab. Tegaserod had potent anti-melanoma activity and was tested *in vivo* in syngeneic murine models which enabled the study of the infiltrates in the TME. The infiltration of Treg's as well as FOXP3 and ROR-γt expression in $CD4^+$ T cells in the TME milieu was decreased in the tumors of Tegaserod treated mice. In tumor cells, Tegaserod suppressed the PI3K/Akt/mTOR pathway in both BRAF WT and mutant tumor cells. Recently, a report has shown phosphorylation of S6 to be marker of sensitivity to BRAF mutated melanoma and that suppression of S6 after MAPK treatment was a predictor of progression-free survival[102]. In our investigation, Tegaserod's suppression of p-S6 and its strong synergy with vemurafenib in BRAF mutated human melanoma cell lines is in accordance with the above report. Importantly, Tegaserod also suppressed S6 phosphorylation in non-BRAF mutated melanoma cell lines indicating a broader therapeutic potential of Tegaserod in patients without the BRAF mutation but where the PI3K/Akt/mTOR pathway is activated such as in patients harboring NRAS mutations[103]. The suppression of S6 phosphorylation is likely mediated by decreased mTORC1 activity as phosphorylation of the direct upstream regulator of S6, p70 S6 kinase was also

blunted. mTORC1 integrates several upstream pathways related to cellular growth and metabolism including MAPK through RSK[104], PI3K/Akt[105] as well as the liver kinase B1 (LKB1)-adenosine monophosphate-activated protein kinase (AMPK)[106].

As Tegaserod did not perturb the MAPK pathway but decreased Akt phosphorylation at a residue known to be phosphorylated by mTORC2, it's likely that S6 is affected through the PI3K/Akt pathway although the potential contribution of AMPK would also have to be explored. Finally, in the remaining part of the directly therapeutically relevant anti-tumoral applications, Publication 4 proposes to use LCMV as a direct anti-cancer immunotherapeutic agent. The ability of viruses to kill cancer cells has been recognized for several decades and is supported by recent Food and Drug Administration and European Union (EU) approval of T-Vec. The specific mechanisms of virotherapy have long been considered to be directly oncolytic. Recently, it was recognized that induction of an inflammatory response contributes to virus mediated tumor regression[107, 108]. In cancer therapies with oncolytic viruses, this is considered to be of limited therapeutic value and merely a collateral effect. By contrast, in our study, we provide evidence that a powerful immune response itself induced by arenavirus replication may lead to complete tumor regression. Treatment with a non-oncolytic arenavirus is advantageous in inducing sustained immune surveillance. First, an arenavirus such as LCMV will not kill the host cell by direct cytopathic effects. Therefore, virus replication is maintained until an immune response is induced within the tumor tissue. Secondly, arenavirus replication will not be limited by strong IFN-I responses[109]. In addition, LCMV usually fails to induce rapid neutralizing antibodies[110]. Thus, arenavirus replication in tumors can only be controlled by infiltration of virus-specific $CD8^+$ T cells. As long as $CD8^+$ T cells do not infiltrate the tumor, arenaviruses can replicate for several days or weeks even if tumor cells respond to IFN-I. In this direct comparison and using IFN-I-responsive tumor models LCMV was therapeutically more potent than the oncolytic viruses VSV-GP and rVACV which require defects in the IFN pathway for efficient replication in tumor cells[111, 112]. However, the relationship between infiltrating $CD8^+$ T cells and arenavirus therapy is LCMV strain dependent. For example, Schadler et al.[113] used the low replicative 'neurotropic strain' LCMV Armstrong (LCMV Armstrong) in addition to lipopolysaccharide (LPS) and anti-CD3, to increase thrombospondin-1 (Tsp1) in T cells and tested the anti-tumoral potency of Tsp1. In their study, growth of B16F10 melanomas was observed for approximately 2 weeks

after LCMV Armstrong infection and anti-tumoral effects after LCMV Armstrong administration were dependent on Tsp1 and T cells. By contrast, our studies with the 'viscerotropic strain' LCMV-WE used in our studies revealed that its potent anti-tumor activity was mediated via IFN-I and was T-cell independent. The differences in mechanism and potency underlying the anti-tumor effects of LCMV in the two studies likely reflect strain-dependent differences between the different arenaviruses used, the impact of the specific cancer types examined and the different timepoints used. In the long-term observation of approximately 80 days, our study showed that the absence of T cells was beneficial for LCMV-WE therapy. Moreover, we based our studies largely on the mechanism of anti-tumoral action of LCMV in a murine head and neck cancer model, whereas Schadler et al. used malignant melanoma, where effective immunotherapies mainly depend on tumor-specific T cells. This may also explain the lower efficiency and efficacy of IFN-dependent LCMV therapy on B16F10 melanoma compared with head and neck or colon cancer.

The use of LCMV-WE could fill a gap in virotherapy in the treatment of IFN-I-responsive cancers. Careful characterization of IFN-I responsiveness and additional LCMV host factors may guide the selection of patients suitable for LCMV cancer therapy. As robust $CD8^+$ T cell tumoral infiltration would blunt LCMV replication, it is unlikely that this therapy would be combined with checkpoint inhibitors. Rather it could be an attractive option for the treatment of patients who have failed to respond to checkpoint inhibitors or typically 'cold' poorly infiltrating tumors where treatment with checkpoint inhibitors is not an option.

Interestingly, in this context of using LCMV-WE as an anti-cancer therapeutic, LCMV-induced anti-tumor immunity depended mainly on the recruitment of IFN-producing $Ly6C^+$ monocytes. Early recruitment of this monocytic population was beneficial in regressing the pre-established tumors. The potential emergence of these immunosuppressive MDSC populations within the TME following LCMV treatment should be further evaluated especially in the longer-term tumor growth models.

Publication 5 and 6 address the question of how monocytes and/or inflammatory cells originating from monocytes behave in the context of chronic viral infection, bacterial acute infection and other inflammatory stimuli including innate immune activators. Both of these studies made use of Toso-deficient (*Toso*$^{-/-}$) mice to address whether Toso functionally contributes to immune responses following

infectious and inflammatory stimuli. Toso has been identified as being functionally important in several subsets of immune cells. Given that Toso can act as a cell surface receptor for secreted IgM, it is not surprising that Toso is critical for maintaining the function of B cells. Recently, using a cell-type specific knockout system where Toso was knocked out in $CD19^+$ B cells (*Toso*$^{-/-}$ *x CD19-Cre*$^+$*),* Nguyen et al. demonstrated that Toso was expressed in the trans-Golgi networking of developing B cells and was critical in curbing the IgM-BCR transport and expression[114]. Accordingly, B cells in *Toso*$^{-/-}$ *x CD19-Cre*$^+$ mice were characterized increased tonic BCR signaling, dysregulated B-2 cell homeostasis and increased B-1 cell differentiation[114]. A critical role for Toso in the function of human T cells was also recently highlighted [115]. Meryk et al. investigated the role of Toso in human T cells in the elderly and discovered that Toso expression was decreased in these individuals and linked to changes in methylation patterns in the gene locus. Furthermore, Toso was found to function as a costimulatory molecule following IgM binding capable of enhancing TCR signaling and cytokine production[115]. Taken together it's clear that Toso affects a wide variety of signaling events following a diverse set of infectious and inflammatory stimuli in granulocytes[116], monocytes[116], dendritic cells[117, 118] and B cells[114].

Although *Toso*$^{-/-}$ mice were more susceptible to Listeria infection, *Toso*$^{-/-}$ granulocytes were still able to uptake Listeria, albeit at decreased levels. However, it is unclear whether additional mechanisms besides Listeria uptake were also defective in the absence of Toso. As activation of innate immune cells can partially depend on the phagocytosis of pathogenic pattern molecules, it's possible that Toso is not only directly affecting innate immune cell effector functions, but perhaps more importantly is regulating immune activation, which strongly impacts pathogen control. Following innate immune LPS treatment, *Toso*$^{-/-}$ mice were characterized by decreased cytokine production which protected the mice from septic shock.

In the context of chronic viral infection (**publication 5**), Toso was essential in clearing the pathogen through enabling the differentiation and maturation of iDCs, a process that is required for the control of persistence-prone virus infection. Impaired function of Toso during infection with non-cytopathic viruses such as LCMV and hepatitis viruses may be beneficial for the host by preventing potentially damaging immunopathology[119]. Interestingly, the presence of virally induced pathology following infection with persistent low cytopathic viruses such as HIV, Hepatitis B and

Hepatitis C virus[119] can differ between individuals, and the underlying cause for such differential outcomes remains unclear. We speculate that differences in expression or function of Toso may contribute to the inter-individual variability of disease outcome following viral infections. On the other hand, Toso deficiency may be disadvantageous for the host following infection with high cytopathic viruses that need to be cleared to ensure host survival. Indeed, Yu et al. found *Toso*$^{-/-}$ mice to be more susceptible to infection with influenza virus strain A/PR8 (H1N1)[120]. Using tissue specific ablation of Toso, the phenotype was recapitulated in *Toso*$^{-/-}$ *x CD19-Cre*$^{+}$ mice, again highlighting the importance of Toso in the B cell compartment and in this context differentiation/maintenance of regulatory B cells[120]. An obvious limitation of our whole body knockout models is the inherent complexity Toso exerts on many immune cells therefore making it difficult to ascertain whether Toso is mechanistically relevant to the immune population in question or whether it is a by-product of impaired interactions with other immune cells where Toso might be more functionally relevant. Due to its over-expression in CLL, Toso has been highlighted as a selective target for CAR-T cell therapies[121] and others have proposed it to be a target of curbing pathogenic T cell responses at local inflammatory sites[120].

Ectodomain shedding facilitated by the proteolytic release of transmembrane proteins such as TNF that are crucial in maintaining tissue homeostasis. However, when this process is deregulated this can result in detrimental effects and contribute to pathology several diseases including rheumatoid arthritis, osteoarthritis, atherosclerosis, IBS, Alzheimer's and cancer[91]. An increased understanding in the factors controlling TNF shedding can give insight in how to better therapeutically target these pathogenic processes. In publication 7, we have identified a high degree of functional overlap for iRhom1 and iRhom2 in controlling the activity of ADAM17. Deletion of part of the cytoplasmic N terminus of either iRhom1 or iRhom2 results in a gain of function by promoting constitutive ADAM17-dependent shedding of TNFRs, thereby blocking downstream signaling and protecting cells from TNF-induced cytotoxicity.

Little is known about how the iRhoms are functionally controlled. Our results suggest that the extended cytoplasmic N-terminal domain is of conserved importance for the actions of both iRhom1 and iRhom2. Dominant inherited human N-terminal mutations in iRhom2 result in overgrowth of epithelial tissues and predisposition to esophageal cancer[122]. Our results involving dominant N-terminal mutated mouse

iRhoms and enhanced TNFR shedding from TOC patient–derived keratinocytes suggest that these human mutations could similarly result in greater or constitutive ADAM17 activity. This could result in direct consequences for neoplasia, such as overproduction of EGFR ligands, strongly implicated in cancer[123] or shedding of TNFRs as an evasion mechanism for tumor cells to escape cell death induced by TNF. Increased abundance of ADAM17 is also known to be associated with breast, ovarian, kidney, colon, and prostate cancers[91].

Interestingly, ADAM17 activity was recently associated with tumor cell immune evasion through PD-L1 cleavage modulation[124]. PD-L1, like PD-1, blunts anti-tumor immunity, inhibits the clonal expansion of antigen-specific anti-tumoral $CD8^+$ T cells and is a major immunotherapeutic target (clinical examples include Durvalumab, atezolizumab and avelumab). As ADAM17, in addition to proteolytically cleaving pro-inflammatory molecules, also processes PD-L1, it is therefore not entirely unexpected that high levels of PD-L1 and ADAM17 are associated with poor cancer prognosis[91]. Although it's difficult to selectively target ADAM17 due its broad expression, involvement in many physiological processes and homology to other ADAM metalloproteases such as ADAM10, efforts are nevertheless underway to develop selective small-molecule inhibitors and monoclonal antibodies. Another potentially attractive therapeutic option is the targeting of iRhoms as they are able to differentiate between substrates ADAM17 and ADAM10[125]. Although both iRhom1 and 2 are expressed in all tissues, only iRhom2 is expressed in immune cells[126] presenting an opportunity to target ADAM17 exclusively in immune cells. Indeed, iRhom2-deficient mice are protected against sepsis and rheumatoid arthritis due to iRhom2/ADAM17/TNF pathway blockage[127]. An interesting subject of future explorations would be investigating the effects of iRhom2 in tumor initiation and progression combined with innate and infectious using iRhom2-deficient mice.

4. Summary – English

The original papers summarized in this habilitation thesis elucidate aspects of tumor treatment through novel combinations and immunomodulating agents. Notably, we identified that a phosphodiesterase (PDE) inhibitor, cilostazol, and other compounds that increase intracellular cyclic adenosine monophosphate (cAMP) levels potentiate statin-induced apoptosis in acute myeloid leukemia and multiple myeloma cells. Using screening approaches, we have identified a drug with anti-melanoma activity in vitro and in vivo that has the potential to be combined with the standard of care agent Vemurafenib and Cobimetinib in both BRAFV600E and BRAF WT melanoma as well as immunotherapies as Tegaserod decreased the infiltration of immunosuppressive FOXP3 and ROR-γt positive CD4+ T cells into the TME. We further identified a novel immunotherapeutic virus by demonstrating that the arenaviruses lymphocytic choriomeningitis virus (LCMV) preferentially replicated in tumor cells in a variety of murine and human cancer models. LCMV replication led to prolonged local immune activation, rapid regression of localized and metastatic cancers, and long-term disease control. Additional original papers in this habilitation thesis presented aspects of immunological responses following chronic viral infections, bacterial infections and innate immune stimulation pertaining to key immune populations that are known to influence anti-tumor immunity. Specifically, we observed that intrinsic expression of Toso (Faim3, FcIR) influenced the differentiation and activation of iDCs in vivo and DCs in vitro. Lack of iDCs in Toso-deficient ($Toso^{-/-}$) mice reduced $CD8^{+}$T-cell function in the liver and resulted in virus persistence. We found Toso to have an essential role in the differentiation and maturation of iDCs, a process that is required for the control of persistence-prone virus infection. Toso also played a critical regulatory function in innate immune activation. Toso-deficient neutrophils exhibited more reactive oxygen species production and reduced phagocytosis of pathogens compared with controls. Cytokine production was also decreased in $Toso^{-/-}$ mice compared with WT animals, rendering them resistant to septic shock induced by lipopolysaccharide but susceptible to bacterial infection. Lastly, we elucidated key molecular aspects of inflammatory processes by demonstrating how loss of the amino terminus in iRhom1 and iRhom2 impairs TNF signaling, despite enhancing ADAM17 activity. This can contribute to our understanding of how mutations in the amino-terminal region

contribute to the cancer predisposition syndrome tylosis with esophageal cancer (TOC).

5. Summary – Deutsch

Die in dieser Habilitationsschrift zusammengefassten Originalarbeiten beleuchten Aspekte der Tumorbehandlung durch neuartige Kombinationen und immunmodulierende Wirkstoffe. Insbesondere haben wir festgestellt, dass Phosphodiesterase (PDE)-Inhibitoren, Cilostazol, und andere Verbindungen, die den intrazellulären Gehalt an zyklischem Adenosinmonophosphat (cAMP) erhöhen, die durch Statine ausgelöste Apoptose bei akuter myeloischer Leukämie und multiplen Myelomzellen verstärken. Mit Hilfe von Screening-Ansätzen haben wir einen Wirkstoff mit Anti-Melanom-Aktivität in vitro und in vivo identifiziert, der das Potenzial hat, mit den Standardtherapeutika Vemurafenib und Cobimetinib sowohl beim BRAFV600E als auch beim BRAF-WT-Melanom sowie mit Immuntherapien kombiniert zu werden, da Tegaserod die Infiltration von immunsuppressiven FOXP3- und ROR-γt-positiven CD4+ T-Zellen in die TME verringert. Darüber hinaus zeigen wir dass das lymphozytäre Choriomeningitis-Virus (LCMV) in einer Reihe von Krebsmodellen bevorzugt in Tumorzellen repliziert. Die LCMV-Replikation führte zu einer verlängerten lokalen Immunaktivierung, zu einer raschen Rückbildung von lokalisierten und metastasierten Krebserkrankungen und zu einer langfristigen Krankheitskontrolle. Weitere Originalarbeiten in dieser Habilitationsschrift befassen sich mit immunologischen Reaktionen nach chronischen Virusinfektionen, bakteriellen Infektionen und der Stimulation des angeborenen Immunsystems in Bezug auf wichtige Immunpopulationen, die eine Anti-Tumor-Immunität beeinflussen. Insbesondere haben wir beobachtet, dass die intrinsische Expression von Toso (Faim3, FcIR) die Differenzierung und Aktivierung von iDCs in vivo und DCs in vitro beeinflusst. Das Fehlen von iDCs in Toso-defizienten (Toso-/-) Mäusen reduzierte die Funktion der CD8+T-Zellen in der Leber und führte zu einer Viruspersistenz. Wir fanden heraus, dass Toso eine wesentliche Rolle bei der Differenzierung und Reifung von iDCs spielt, ein Prozess, der für die Kontrolle der persistenzanfälligen Virusinfektion erforderlich ist. Toso spielt auch eine entscheidende regulatorische Funktion bei der Aktivierung des angeborenen Immunsystems. Toso-defiziente neutrophile Granulozyten produzierten mehr reaktive Sauerstoffspezies und zeigten eine geringere Phagozytose von Krankheitserregern als die Kontrollgruppe. Auch die Zytokinproduktion war bei Toso-/- Mäusen im Vergleich zu WT-Tieren vermindert, was sie resistent gegen einen

durch Lipopolysaccharid ausgelösten septischen Schock, aber auch anfälliger für bakterielle Infektionen machte. Schließlich konnten wir wichtige molekulare Aspekte von Entzündungsprozessen aufklären, indem wir zeigten, wie der Verlust des zytoplasmatischen Teils von iRhom1 und iRhom2 die TNF-Signalübertragung beeinträchtigt, obwohl die ADAM17-Aktivität erhöht wird. Dies könnte bei Mutationen in dem zytoplasmatischen Teil des iRhom2 bei dem Tylosis Syndrom Tylose mit Ösophaguskrebs (TOC) eine wichtige Rolle spielen.

6. References

1. Hanahan, D. & Weinberg, R.A. The hallmarks of cancer. *Cell* **100**, 57-70 (2000).

2. Hanahan, D. & Weinberg, R.A. Hallmarks of cancer: the next generation. *Cell* **144**, 646-674 (2011).

3. Fouad, Y.A. & Aanei, C. Revisiting the hallmarks of cancer. *Am J Cancer Res* **7**, 1016-1036 (2017).

4. Waldman, A.D., Fritz, J.M. & Lenardo, M.J. A guide to cancer immunotherapy: from T cell basic science to clinical practice. *Nat Rev Immunol* (2020).

5. Martinez-Lostao, L., Anel, A. & Pardo, J. How Do Cytotoxic Lymphocytes Kill Cancer Cells? *Clin Cancer Res* **21**, 5047-5056 (2015).

6. Galon, J. & Bruni, D. Approaches to treat immune hot, altered and cold tumours with combination immunotherapies. *Nat Rev Drug Discov* **18**, 197-218 (2019).

7. Rapp, M. *et al.* CCL22 controls immunity by promoting regulatory T cell communication with dendritic cells in lymph nodes. *J Exp Med* **216**, 1170-1181 (2019).

8. Kim, J.H., Kim, B.S. & Lee, S.K. Regulatory T Cells in Tumor Microenvironment and Approach for Anticancer Immunotherapy. *Immune Netw* **20**, e4 (2020).

9. Li, C., Jiang, P., Wei, S., Xu, X. & Wang, J. Regulatory T cells in tumor microenvironment: new mechanisms, potential therapeutic strategies and future prospects. *Mol Cancer* **19**, 116 (2020).

10. Veglia, F., Perego, M. & Gabrilovich, D. Myeloid-derived suppressor cells coming of age. *Nat Immunol* **19**, 108-119 (2018).

11. Jeong, J., Suh, Y. & Jung, K. Context Drives Diversification of Monocytes and Neutrophils in Orchestrating the Tumor Microenvironment. *Front Immunol* **10**, 1817 (2019).

12. Boutilier, A.J. & Elsawa, S.F. Macrophage Polarization States in the Tumor Microenvironment. *Int J Mol Sci* **22** (2021).

13. Ma, Y. *et al.* Anticancer chemotherapy-induced intratumoral recruitment and differentiation of antigen-presenting cells. *Immunity* **38**, 729-741 (2013).

14. Tesone, A.J. *et al.* Satb1 Overexpression Drives Tumor-Promoting Activities in Cancer-Associated Dendritic Cells. *Cell Rep* **14**, 1774-1786 (2016).

15. Larkin, J. *et al.* Combined Nivolumab and Ipilimumab or Monotherapy in Untreated Melanoma. *N Engl J Med* **373**, 23-34 (2015).

16. Barber, D.L. *et al.* Restoring function in exhausted CD8 T cells during chronic viral infection. *Nature* **439**, 682-687 (2006).

17. Wu, Z., Li, S. & Zhu, X. The Mechanism of Stimulating and Mobilizing the Immune System Enhancing the Anti-Tumor Immunity. *Front Immunol* **12**, 682435 (2021).

18. Vitale, C. & Strati, P. CAR T-Cell Therapy for B-Cell non-Hodgkin Lymphoma and Chronic Lymphocytic Leukemia: Clinical Trials and Real-World Experiences. *Front Oncol* **10**, 849 (2020).

19. Hugo, W. *et al.* Genomic and Transcriptomic Features of Response to Anti-PD-1 Therapy in Metastatic Melanoma. *Cell* **165**, 35-44 (2016).

20. McGranahan, N. *et al.* Clonal neoantigens elicit T cell immunoreactivity and sensitivity to immune checkpoint blockade. *Science* **351**, 1463-1469 (2016).

21. Ayers, M. *et al.* IFN-gamma-related mRNA profile predicts clinical response to PD-1 blockade. *J Clin Invest* **127**, 2930-2940 (2017).

22. Prat, A. *et al.* Immune-Related Gene Expression Profiling After PD-1 Blockade in Non-Small Cell Lung Carcinoma, Head and Neck Squamous Cell Carcinoma, and Melanoma. *Cancer Res* **77**, 3540-3550 (2017).

23. Huang, A.C. *et al.* T-cell invigoration to tumour burden ratio associated with anti-PD-1 response. *Nature* **545**, 60-65 (2017).

24. Zou, W. Immunosuppressive networks in the tumour environment and their therapeutic relevance. *Nat Rev Cancer* **5**, 263-274 (2005).

25. Wherry, E.J. *et al.* Molecular signature of CD8+ T cell exhaustion during chronic viral infection. *Immunity* **27**, 670-684 (2007).

26. Li, K.K. & Adams, D.H. Antitumor CD8+ T cells in hepatocellular carcinoma: present but exhausted. *Hepatology* **59**, 1232-1234 (2014).

27. Liu, X., Hoft, D.F. & Peng, G. Senescent T cells within suppressive tumor microenvironments: emerging target for tumor immunotherapy. *The Journal of Clinical Investigation* **130**, 1073-1083 (2020).

28. Wherry, E.J. & Kurachi, M. Molecular and cellular insights into T cell exhaustion. *Nat Rev Immunol* **15**, 486-499 (2015).

29. Zhao, Y., Shao, Q. & Peng, G. Exhaustion and senescence: two crucial dysfunctional states of T cells in the tumor microenvironment. *Cell Mol Immunol* **17**, 27-35 (2020).

30. Dolfi, D.V. *et al.* Increased T-bet is associated with senescence of influenza virus-specific CD8 T cells in aged humans. *J Leukoc Biol* **93**, 825-836 (2013).

31. Crespo, J., Sun, H., Welling, T.H., Tian, Z. & Zou, W. T cell anergy, exhaustion, senescence, and stemness in the tumor microenvironment. *Curr Opin Immunol* **25**, 214-221 (2013).

32. Bour-Jordan, H. *et al.* Intrinsic and extrinsic control of peripheral T-cell tolerance by costimulatory molecules of the CD28/ B7 family. *Immunol Rev* **241**, 180-205 (2011).

33. Liu, W. *et al.* Senescent Tumor CD8(+) T Cells: Mechanisms of Induction and Challenges to Immunotherapy. *Cancers (Basel)* **12** (2020).

34. Buck, M.D., O'Sullivan, D. & Pearce, E.L. T cell metabolism drives immunity. *J Exp Med* **212**, 1345-1360 (2015).

35. O'Neill, L.A. & Pearce, E.J. Immunometabolism governs dendritic cell and macrophage function. *J Exp Med* **213**, 15-23 (2016).

36. Jiang, B. Aerobic glycolysis and high level of lactate in cancer metabolism and microenvironment. *Genes Dis* **4**, 25-27 (2017).

37. Sukumar, M. *et al.* Inhibiting glycolytic metabolism enhances CD8+ T cell memory and antitumor function. *J Clin Invest* **123**, 4479-4488 (2013).

38. Wang, R. *et al.* The transcription factor Myc controls metabolic reprogramming upon T lymphocyte activation. *Immunity* **35**, 871-882 (2011).

39. Angelin, A. *et al.* Foxp3 Reprograms T Cell Metabolism to Function in Low-Glucose, High-Lactate Environments. *Cell Metab* **25**, 1282-1293 e1287 (2017).

40. Hu, C., Pang, B., Lin, G., Zhen, Y. & Yi, H. Energy metabolism manipulates the fate and function of tumour myeloid-derived suppressor cells. *Br J Cancer* **122**, 23-29 (2020).

41. Srivastava, M.K., Sinha, P., Clements, V.K., Rodriguez, P. & Ostrand-Rosenberg, S. Myeloid-derived suppressor cells inhibit T-cell activation by depleting cystine and cysteine. *Cancer Res* **70**, 68-77 (2010).

42. Wu, K. *et al.* Redefining Tumor-Associated Macrophage Subpopulations and Functions in the Tumor Microenvironment. *Front Immunol* **11**, 1731 (2020).

43. Ye, J. *et al.* TLR8 signaling enhances tumor immunity by preventing tumor-induced T-cell senescence. *EMBO Mol Med* **6**, 1294-1311 (2014).

44. Dietsch, G.N. *et al.* Late-Stage Cancer Patients Remain Highly Responsive to Immune Activation by the Selective TLR8 Agonist Motolimod (VTX-2337). *Clin Cancer Res* **21**, 5445-5452 (2015).

45. Chow, L.Q.M. *et al.* Phase Ib Trial of the Toll-like Receptor 8 Agonist, Motolimod (VTX-2337), Combined with Cetuximab in Patients with Recurrent or Metastatic SCCHN. *Clin Cancer Res* **23**, 2442-2450 (2017).

46. Ribas, A. *et al.* Oncolytic Virotherapy Promotes Intratumoral T Cell Infiltration and Improves Anti-PD-1 Immunotherapy. *Cell* **170**, 1109-1119 e1110 (2017).

47. Chesney, J. *et al.* Randomized, Open-Label Phase II Study Evaluating the Efficacy and Safety of Talimogene Laherparepvec in Combination With Ipilimumab Versus Ipilimumab Alone in Patients With Advanced, Unresectable Melanoma. *J Clin Oncol* **36**, 1658-1667 (2018).

48. Das, S. & Johnson, D.B. Immune-related adverse events and anti-tumor efficacy of immune checkpoint inhibitors. *J Immunother Cancer* **7**, 306 (2019).

49. Ovadya, Y. & Krizhanovsky, V. Strategies targeting cellular senescence. *J Clin Invest* **128**, 1247-1254 (2018).

50. Patnaik, A. *et al.* A First-in-Human Phase I Study of the Oral p38 MAPK Inhibitor, Ralimetinib (LY2228820 Dimesylate), in Patients with Advanced Cancer. *Clin Cancer Res* **22**, 1095-1102 (2016).

51. Ebert, P.J.R. *et al.* MAP Kinase Inhibition Promotes T Cell and Anti-tumor Activity in Combination with PD-L1 Checkpoint Blockade. *Immunity* **44**, 609-621 (2016).

52. Keller, H.R., Zhang, X., Li, L., Schaider, H. & Wells, J.W. Overcoming resistance to targeted therapy with immunotherapy and combination therapy for metastatic melanoma. *Oncotarget* **8**, 75675-75686 (2017).

53. Vermaelen, K., Waeytens, A., Kholmanskikh, O., Van den Bulcke, M. & Van Valckenborgh, E. Perspectives on the integration of Immuno-Oncology Biomarkers and drugs in a Health Care setting. *Semin Cancer Biol* **52**, 166-177 (2018).

54. Ashburn, T.T. & Thor, K.B. Drug repositioning: identifying and developing new uses for existing drugs. *Nat Rev Drug Discov* **3**, 673-683 (2004).

55. Goldstein, J.L. & Brown, M.S. Regulation of the mevalonate pathway. *Nature* **343**, 425-430 (1990).

56. Longo, J. *et al.* Cyclic AMP-hydrolyzing phosphodiesterase inhibitors potentiate statin-induced cancer cell death. *Mol Oncol* **14**, 2533-2545 (2020).

57. Mullen, P.J., Yu, R., Longo, J., Archer, M.C. & Penn, L.Z. The interplay between cell signalling and the mevalonate pathway in cancer. *Nat Rev Cancer* **16**, 718-731 (2016).

58. Pandyra, A. *et al.* Immediate utility of two approved agents to target both the metabolic mevalonate pathway and its restorative feedback loop. *Cancer Res* **74**, 4772-4782 (2014).

59. Nielsen, S.F., Nordestgaard, B.G. & Bojesen, S.E. Statin use and reduced cancer-related mortality. *N Engl J Med* **367**, 1792-1802 (2012).

60. Sassano, A. *et al.* Suppressive effects of statins on acute promyelocytic leukemia cells. *Cancer Res* **67**, 4524-4532 (2007).

61. Clendening, J.W. *et al.* Exploiting the mevalonate pathway to distinguish statin-sensitive multiple myeloma. *Blood* **115**, 4787-4797 (2010).

62. Wu, J., Wong, W.W., Khosravi, F., Minden, M.D. & Penn, L.Z. Blocking the Raf/MEK/ERK pathway sensitizes acute myelogenous leukemia cells to lovastatin-induced apoptosis. *Cancer Res* **64**, 6461-6468 (2004).

63. Li, H.Y., Appelbaum, F.R., Willman, C.L., Zager, R.A. & Banker, D.E. Cholesterol-modulating agents kill acute myeloid leukemia cells and sensitize them to therapeutics by blocking adaptive cholesterol responses. *Blood* **101**, 3628-3634 (2003).

64. Freed-Pastor, W.A. *et al.* Mutant p53 disrupts mammary tissue architecture via the mevalonate pathway. *Cell* **148**, 244-258 (2012).

65. Mira, E. *et al.* A lovastatin-elicited genetic program inhibits M2 macrophage polarization and enhances T cell infiltration into spontaneous mouse mammary tumors. *Oncotarget* **4**, 2288-2301 (2013).

66. Thurnher, M., Nussbaumer, O. & Gruenbacher, G. Novel aspects of mevalonate pathway inhibitors as antitumor agents. *Clin Cancer Res* **18**, 3524-3531 (2012).

67. Malfitano, A.M., Di Somma, S., Iannuzzi, C.A., Pentimalli, F. & Portella, G. Virotherapy: From single agents to combinatorial treatments. *Biochem Pharmacol* **177**, 113986 (2020).

68. Chulpanova, D.S. *et al.* Recombinant Viruses for Cancer Therapy. *Biomedicines* **6** (2018).

69. Arriola, E. & Ottensmeier, C. TG4010: a vaccine with a therapeutic role in cancer. *Immunotherapy* **8**, 511-519 (2016).

70. Maude, S.L. *et al.* Tisagenlecleucel in Children and Young Adults with B-Cell Lymphoblastic Leukemia. *N Engl J Med* **378**, 439-448 (2018).

71. Cao, W. *et al.* Identification of alpha-dystroglycan as a receptor for lymphocytic choriomeningitis virus and Lassa fever virus. *Science* **282**, 2079-2081 (1998).

72. Prevost-Blondel, A. *et al.* Tumor-infiltrating lymphocytes exhibiting high ex vivo cytolytic activity fail to prevent murine melanoma tumor growth in vivo. *J Immunol* **161**, 2187-2194 (1998).

73. Grusdat, M. *et al.* IRF4 and BATF are critical for CD8(+) T-cell function following infection with LCMV. *Cell Death Differ* **21**, 1050-1060 (2014).

74. Suprunenko, T. & Hofer, M.J. Complexities of Type I Interferon Biology: Lessons from LCMV. *Viruses* **11** (2019).

75. Huang, A. *et al.* Progranulin prevents regulatory NK cell cytotoxicity against antiviral T cells. *JCI Insight* **4** (2019).

76. Xu, H.C. *et al.* Lymphocytes Negatively Regulate NK Cell Activity via Qa-1b following Viral Infection. *Cell Rep* **21**, 2528-2540 (2017).

77. Segura, E. & Amigorena, S. Inflammatory dendritic cells in mice and humans. *Trends Immunol* **34**, 440-445 (2013).

78. Veglia, F. & Gabrilovich, D.I. Dendritic cells in cancer: the role revisited. *Curr Opin Immunol* **45**, 43-51 (2017).

79. Hitoshi, Y. *et al.* Toso, a cell surface, specific regulator of Fas-induced apoptosis in T cells. *Immunity* **8**, 461-471 (1998).

80. Pallasch, C.P. *et al.* Overexpression of TOSO in CLL is triggered by B-cell receptor signaling and associated with progressive disease. *Blood* **112**, 4213-4219 (2008).

81. Sigruener, A. *et al.* E-LDL upregulates TOSO expression and enhances the survival of human macrophages. *Biochem Biophys Res Commun* **359**, 723-728 (2007).

82. Song, Y. & Jacob, C.O. The mouse cell surface protein TOSO regulates Fas/Fas ligand-induced apoptosis through its binding to Fas-associated death domain. *J Biol Chem* **280**, 9618-9626 (2005).

83. Groth, C. *et al.* Immunosuppression mediated by myeloid-derived suppressor cells (MDSCs) during tumour progression. *Br J Cancer* **120**, 16-25 (2019).

84. Davidov, V., Jensen, G., Mai, S., Chen, S.H. & Pan, P.Y. Analyzing One Cell at a TIME: Analysis of Myeloid Cell Contributions in the Tumor Immune Microenvironment. *Front Immunol* **11**, 1842 (2020).

85. Witkowski, M.T. *et al.* Extensive Remodeling of the Immune Microenvironment in B Cell Acute Lymphoblastic Leukemia. *Cancer Cell* **37**, 867-882 e812 (2020).

86. Greten, F.R. & Grivennikov, S.I. Inflammation and Cancer: Triggers, Mechanisms, and Consequences. *Immunity* **51**, 27-41 (2019).

87. Komarova, E.A. *et al.* p53 is a suppressor of inflammatory response in mice. *FASEB J* **19**, 1030-1032 (2005).

88. Woo, S.R., Corrales, L. & Gajewski, T.F. Innate immune recognition of cancer. *Annu Rev Immunol* **33**, 445-474 (2015).

89. Grivennikov, S.I. *et al.* Adenoma-linked barrier defects and microbial products drive IL-23/IL-17-mediated tumour growth. *Nature* **491**, 254-258 (2012).

90. Maney, S.K. *et al.* Deletions in the cytoplasmic domain of iRhom1 and iRhom2 promote shedding of the TNF receptor by the protease ADAM17. *Sci Signal* **8**, ra109 (2015).

91. Calligaris, M. *et al.* Strategies to Target ADAM17 in Disease: From its Discovery to the iRhom Revolution. *Molecules* **26** (2021).

92. Bos, J.L. Epac proteins: multi-purpose cAMP targets. *Trends Biochem Sci* **31**, 680-686 (2006).

93. Jung, Y.A. *et al.* Cilostazol inhibits insulin-stimulated expression of sterol regulatory binding protein-1c via inhibition of LXR and Sp1. *Exp Mol Med* **46**, e73 (2014).

94. Maurice, D.H. *et al.* Advances in targeting cyclic nucleotide phosphodiesterases. *Nat Rev Drug Discov* **13**, 290-314 (2014).

95. Kim, J.R. *et al.* Effect of Cilostazol on the Pharmacokinetics of Simvastatin in Healthy Subjects. *Biomed Res Int* **2019**, 1365180 (2019).

96. Bramer, S.L., Brisson, J., Corey, A.E. & Mallikaarjun, S. Effect of multiple cilostazol doses on single dose lovastatin pharmacokinetics in healthy volunteers. *Clin Pharmacokinet* **37 Suppl 2**, 69-77 (1999).

97. Hiatt, W.R., Money, S.R. & Brass, E.P. Long-term safety of cilostazol in patients with peripheral artery disease: the CASTLE study (Cilostazol: A Study in Long-term Effects). *J Vasc Surg* **47**, 330-336 (2008).

98. Zhang, L. *et al.* Cyclic nucleotide phosphodiesterase profiling reveals increased expression of phosphodiesterase 7B in chronic lymphocytic leukemia. *Proc Natl Acad Sci U S A* **105**, 19532-19537 (2008).

99. Rickles, R.J. *et al.* Adenosine A2A receptor agonists and PDE inhibitors: a synergistic multitarget mechanism discovered through systematic combination screening in B-cell malignancies. *Blood* **116**, 593-602 (2010).

100. Leukes, V., Walzl, G. & du Plessis, N. Myeloid-Derived Suppressor Cells as Target of Phosphodiesterase-5 Inhibitors in Host-Directed Therapeutics for Tuberculosis. *Front Immunol* **11**, 451 (2020).

101. Hassel, J.C. *et al.* Tadalafil has biologic activity in human melanoma. Results of a pilot trial with Tadalafil in patients with metastatic Melanoma (TaMe). *Oncoimmunology* **6**, e1326440 (2017).

102. Corcoran, R.B. *et al.* TORC1 suppression predicts responsiveness to RAF and MEK inhibition in BRAF-mutant melanoma. *Sci Transl Med* **5**, 196ra198 (2013).

103. Posch, C. *et al.* Combined targeting of MEK and PI3K/mTOR effector pathways is necessary to effectively inhibit NRAS mutant melanoma in vitro and in vivo. *Proc Natl Acad Sci U S A* **110**, 4015-4020 (2013).

104. Roux, P.P. *et al.* RAS/ERK signaling promotes site-specific ribosomal protein S6 phosphorylation via RSK and stimulates cap-dependent translation. *J Biol Chem* **282**, 14056-14064 (2007).

105. Manning, B.D., Tee, A.R., Logsdon, M.N., Blenis, J. & Cantley, L.C. Identification of the tuberous sclerosis complex-2 tumor suppressor gene product tuberin as a target of the phosphoinositide 3-kinase/akt pathway. *Mol Cell* **10**, 151-162 (2002).

106. Inoki, K. *et al.* TSC2 integrates Wnt and energy signals via a coordinated phosphorylation by AMPK and GSK3 to regulate cell growth. *Cell* **126**, 955-968 (2006).

107. Huang, H., Xiao, T., He, L., Ji, H. & Liu, X.Y. Interferon-beta-armed oncolytic adenovirus induces both apoptosis and necroptosis in cancer cells. *Acta Biochim Biophys Sin (Shanghai)* **44**, 737-745 (2012).

108. Hasegawa, Y. *et al.* Urokinase-targeted fusion by oncolytic Sendai virus eradicates orthotopic glioblastomas by pronounced synergy with interferon-beta gene. *Mol Ther* **18**, 1778-1786 (2010).

109. Moskophidis, D. *et al.* Resistance of lymphocytic choriomeningitis virus to alpha/beta interferon and to gamma interferon. *J Virol* **68**, 1951-1955 (1994).

110. Recher, M. *et al.* Extralymphatic virus sanctuaries as a consequence of potent T-cell activation. *Nat Med* **13**, 1316-1323 (2007).

111. Stojdl, D.F. *et al.* Exploiting tumor-specific defects in the interferon pathway with a previously unknown oncolytic virus. *Nat Med* **6**, 821-825 (2000).

112. Moerdyk-Schauwecker, M. *et al.* Resistance of pancreatic cancer cells to oncolytic vesicular stomatitis virus: role of type I interferon signaling. *Virology* **436**, 221-234 (2013).

113. Schadler, K.L. *et al.* Immunosurveillance by antiangiogenesis: tumor growth arrest by T cell-derived thrombospondin-1. *Cancer Res* **74**, 2171-2181 (2014).

114. Nguyen, T.T. *et al.* The IgM receptor FcmuR limits tonic BCR signaling by regulating expression of the IgM BCR. *Nat Immunol* **18**, 321-333 (2017).

115. Meryk, A. *et al.* Fcmu receptor as a Costimulatory Molecule for T Cells. *Cell Rep* **26**, 2681-2691 e2685 (2019).

116. Lang, K.S. *et al.* Involvement of Toso in activation of monocytes, macrophages, and granulocytes. *Proc Natl Acad Sci U S A* **110**, 2593-2598 (2013).

117. Brenner, D. *et al.* Toso controls encephalitogenic immune responses by dendritic cells and regulatory T cells. *Proc Natl Acad Sci U S A* **111**, 1060-1065 (2014).

118. Lang, P.A. *et al.* Toso regulates differentiation and activation of inflammatory dendritic cells during persistence-prone virus infection. *Cell Death Differ* **22**, 164-173 (2015).

119. Rehermann, B. & Nascimbeni, M. Immunology of hepatitis B virus and hepatitis C virus infection. *Nat Rev Immunol* **5**, 215-229 (2005).

120. Yu, J. *et al.* Surface receptor Toso controls B cell-mediated regulation of T cell immunity. *J Clin Invest* **128**, 1820-1836 (2018).

121. Faitschuk, E., Hombach, A.A., Frenzel, L.P., Wendtner, C.M. & Abken, H. Chimeric antigen receptor T cells targeting Fc mu receptor selectively eliminate CLL cells while sparing healthy B cells. *Blood* **128**, 1711-1722 (2016).

122. Nitoiu, D., Etheridge, S.L. & Kelsell, D.P. Insights into desmosome biology from inherited human skin disease and cardiocutaneous syndromes. *Cell Commun Adhes* **21**, 129-140 (2014).

123. Hirsch, F.R., Varella-Garcia, M. & Cappuzzo, F. Predictive value of EGFR and HER2 overexpression in advanced non-small-cell lung cancer. *Oncogene* **28 Suppl 1**, S32-37 (2009).

124. Romero, Y., Wise, R. & Zolkiewska, A. Proteolytic processing of PD-L1 by ADAM proteases in breast cancer cells. *Cancer Immunol Immunother* **69**, 43-55 (2020).

125. Dulloo, I., Muliyil, S. & Freeman, M. The molecular, cellular and pathophysiological roles of iRhom pseudoproteases. *Open Biol* **9**, 190003 (2019).

126. Christova, Y., Adrain, C., Bambrough, P., Ibrahim, A. & Freeman, M. Mammalian iRhoms have distinct physiological functions including an essential role in TACE regulation. *EMBO Rep* **14**, 884-890 (2013).

127. Qing, X. *et al.* iRhom2 promotes lupus nephritis through TNF-alpha and EGFR signaling. *J Clin Invest* **128**, 1397-1412 (2018).

7. Acknowledgements

I would like to thank my other mentors Prof. Dr. Linda Penn, Prof. Dr. Karl Lang and Prof. Dr. Dieter Häussinger. Linda, not only are you a great scientist, but have taught me so many other crucial skills: how to teach others, how to effectively communicate scientific knowledge and put stories together. Karl, you turned me into an immunologist and have taught me to always think outside the box, come up with creative solutions and never be daunted by obstacles. Moreover I would like to thank Prof. Dr. Dieter Häussinger for his mentorship and support.

I would like to thank my team, Wei Liu, Pawel Stachura, Agnès Wlodarczyk and Olivia Stencel. Without you guys, your hard work and dedication much of this work would not be possible. Thanks for sticking with me and putting your trust in me.

I would like to thank Prof. Dr. Arndt Borkhardt for his encouragement and continued support. From the very beginning of joining his department, I have found myself in a scientifically stimulating and challenging environment and I am extremely grateful for the opportunity to work with him and am lucky to be mentored by him.

I would like to thank my work colleagues and friends, Sanil Bhatia, Ute Fischer, Filio Brozou, Rabea Wagener and Daniel Picard. A special thanks goes to Chris Xu, one of the best scientists I know.

Finally I would like to thank my family for their continuous support and love. We have traveled many worlds together.

8. Thesis Publications

In this habilitation thesis the following original works are summarized:

1. Longo, J*, **Pandyra, AA***, Stachura P, Minden MD, Schimmer AD, Penn LZ. Cyclic AMP-hydrolyzing phosphodiesterase inhibitors potentiate statin-induced cancer cell death. *Mol Onco*l; 2020, 14:2545. **Published under a Creative Commons Attribution (CC BY) License. Copyright on any research article published is retained by the author(s).**
   IF: 6.574

2. Liu W, Stachura P, Xu HC, Umesh Ganesh N, Cox F, Wang R, Lang KS, Gopalakrishnan J, Haussinger D, Homey B, Lang PA, **Pandyra AA**. Repurposing the serotonin agonist Tegaserod as an anticancer agent in melanoma: molecular mechanisms and clinical implications. *J Exp Clin Cancer Res*, 2020, 39:38. **Published under a Creative Commons Attribution (CC BY) License. Copyright on any research article published is retained by the author(s)**
   IF: 7.068

3. Liu, W, Stachura P, Xu HC, Bhatia S, Borkhardt A, Lang PA, **Pandyra AA**. Senescent Tumor CD8(+) T Cells: Mechanisms of Induction and Challenges to Immunotherapy. *Cancers (Basel)*; 2020, 12:2828. *Review* **Published under a Creative Commons Attribution (CC BY) License. Copyright on any research article published is retained by the author(s).**
   IF: 6.126

4. Kalkavan H, Sharma P, Kasper S, Helfrich I, **Pandyra AA**, Gassa A, Virchow I, Flatz L, Brandenburg T, Namineni S, Heikenwalder M, Höchst B, Knolle PA, Wollmann G, von Laer D, Drexler I, Rathbun J, Cannon PM, Scheu S, Bauer J, Chauhan J, Häussinger D, Willimsky G, Löhning M, Schadendorf D, Brandau S, Schuler M, Lang PA, Lang KS. Spatiotemporally restricted arenavirus replication induces immune surveillance and type I interferon-dependent tumor regression. *Nat Commun;* 2017, 8:14447. **Permission to re-use by authors in thesis is granted by Springer Nature.** IF: 10.759

5. Lang PA*, Meryk A*, **Pandyra AA***, Brenner D, Brüstle A, Xu HC, Merches K, Lang F, Khairnar V, Sharma P, Funkner P, Recher M, Shaabani N, Duncan GS, Duhan V, Homey B, Ohashi PS, Häussinger D, Knolle PA, Honke N, Mak TW, Lang KS. Toso regulates differentiation and activation of inflammatory dendritic cells during persistence-prone virus infection. *Cell Death Differ;* 2015, 22:164. **Permission to re-use by authors in thesis is granted by Springer Nature.**
   IF: 10.759

6. Lang KS*, Lang PA*, Meryk A*, Pandyra AA*, Boucher LM, Pozdeev VI, Tusche MW, Göthert JR, Haight J, Wakeham A, You-Ten AJ, McIlwain DR, Merches K, Khairnar V, Recher M, Nolan GP, Hitoshi Y, Funkner P, Navarini AA, Verschoor A, Shaabani N, Honke N, Penn LZ, Ohashi PS, Häussinger D, Lee KH, Mak TW. Involvement of Toso in activation of monocytes, macrophages, and granulocytes. *Proc Natl Acad Sci U S A;* 2013, 110:2593. **Permission to re-use by authors in thesis is granted by *PNAS*.**

IF: 9.412

7. Maney* SK, McIlwain DR*, Polz R*, **Pandyra AA*,** Sundaram B, Wolff D, Ohishi K, Maretzky T, Brooke MA, Evers A, Vasudevan AA, Aghaeepour N, Scheller J, Münk C, Häussinger D, Mak TW, Nolan GP, Kelsell DP, Blobel CP, Lang KS, Lang PA Deletions in the cytoplasmic domain of iRhom1 and iRhom2 promote shedding of the TNF receptor by the protease ADAM17. *Sci Signal;* 2015, 8:ra109. **Permission to re-use by authors in thesis is granted by AAAS.**

IF: 6.460

9. **Declarations**

I hereby declare that with regards to the work presented in my habilitation thesis, ethical principles to ensure good scientific practice were adhered to by me.

Düsseldorf, 26.08.2021 _____
Dr. phil. Aleksandra Pandyra

I hereby declare that no other habilitation procedures have been initiated or and that there have been no other unsuccessful habilitation attempts.

Düsseldorf, 26.08.2021 _____
Dr. phil. Aleksandra Pandyra

I hereby declare in lieu of an oath that I have independently made that the contributions to the publications on which on which my habilitation thesis is based have been made independently.

Düsseldorf, 26.08.2021 _____
Dr. phil. Aleksandra Pandyra

10. Appended Publications

Molecular Oncology

FEBS PRESS science publishing by scientists

Cyclic AMP-hydrolyzing phosphodiesterase inhibitors potentiate statin-induced cancer cell death

Joseph Longo[1,2], Aleksandra A. Pandyra[1,2,3,4], Paweł Stachura[3], Mark D. Minden[1,2], Aaron D. Schimmer[1,2] and Linda Z. Penn[1,2]

1 Princess Margaret Cancer Centre, University Health Network, Toronto, Canada
2 Department of Medical Biophysics, University of Toronto, Toronto, Canada
3 Department of Molecular Medicine II, Medical Faculty, Heinrich Heine University, Düsseldorf, Germany
4 Department of Gastroenterology, Hepatology, and Infectious Diseases, Heinrich Heine University, Düsseldorf, Germany

Keywords
cilostazol; dipyridamole; mevalonate pathway; phosphodiesterase inhibitor; SREBP2; statins

Correspondence
L. Z. Penn, Princess Margaret Cancer Centre, University Health Network, Princess Margaret Cancer Research Tower, 101 College Street, 13-706, Toronto, ON M5G 1L7, Canada
Tel: +1 416 634 8770
E-mail: lpenn@uhnresearch.ca

Joseph Longo and Aleksandra A. Pandyra contributed equally to this work

(Received 17 February 2020, revised 13 July 2020, accepted 30 July 2020, available online 25 August 2020)

doi:10.1002/1878-0261.12775

Dipyridamole, an antiplatelet drug, has been shown to synergize with statins to induce cancer cell-specific apoptosis. However, given the polypharmacology of dipyridamole, the mechanism by which it potentiates statin-induced apoptosis remains unclear. Here, we applied a pharmacological approach to identify the activity of dipyridamole specific to its synergistic anticancer interaction with statins. We evaluated compounds that phenocopy the individual activities of dipyridamole and assessed whether they could potentiate statin-induced cell death. Notably, we identified that a phosphodiesterase (PDE) inhibitor, cilostazol, and other compounds that increase intracellular cyclic adenosine monophosphate (cAMP) levels potentiate statin-induced apoptosis in acute myeloid leukemia and multiple myeloma cells. Additionally, we demonstrated that both dipyridamole and cilostazol further inhibit statin-induced activation of sterol regulatory element-binding protein 2, a known modulator of statin sensitivity, in a cAMP-independent manner. Taken together, our data support that PDE inhibitors such as dipyridamole and cilostazol can potentiate statin-induced apoptosis via a dual mechanism. Given that several PDE inhibitors are clinically approved for various indications, they are immediately available for testing in combination with statins for the treatment of hematological malignancies.

1. Introduction

The synthesis of cholesterol and other isoprenoids via the mevalonate (MVA) pathway is tightly regulated to maintain homeostasis. In many cancer cells, an increased dependency on isoprenoid biosynthesis for growth and survival confers sensitivity to the statin family of drugs, which inhibits the rate-limiting enzyme of the MVA pathway, HMG-CoA reductase (HMGCR) [1]. However, in normal cells and many cancer cells, treatment with statins activates the transcription factor sterol regulatory element-binding protein 2 (SREBP2), which functions to upregulate genes involved in MVA metabolism to restore homeostasis. Activation of this feedback response has been associated with statin resistance in cancer cells [2–4]. In contrast, subsets of cancer cells that do not induce this feedback loop following statin treatment readily undergo apoptosis [2,4].

Abbreviations
AML, acute myeloid leukemia; ANOVA, analysis of variance; cAMP, cyclic adenosine monophosphate; cGMP, cyclic guanosine monophosphate; GGPP, geranylgeranyl pyrophosphate; HMG-CoA, 3-hydroxy-3-methylglutaryl coenzyme A; HMGCR, HMG-CoA reductase; MM, multiple myeloma; MVA, mevalonate; PDE, phosphodiesterase; PKA, protein kinase A; qRT–PCR, quantitative reverse transcription–PCR; SD, standard deviation; sgRNAs, small guide RNAs; SREBP, sterol regulatory element-binding protein.

We previously demonstrated that inhibition of this feedback response via RNAi-mediated knockdown of SREBP2 potentiates statin-induced cell death in lung and breast cancer cell lines [5]. Moreover, through a drug screening approach, our laboratory identified that the drug dipyridamole, an antiplatelet agent approved for secondary stroke prevention, can synergize with statins to induce apoptosis in acute myeloid leukemia (AML) and multiple myeloma (MM) cells [6]. We further demonstrated that dipyridamole inhibits statin-induced SREBP2 cleavage and activation, thus abrogating the restorative feedback loop of the MVA pathway (Fig. 1) [6]. Since these initial observations in AML and MM, dipyridamole has been shown to inhibit statin-induced SREBP2 activation and potentiate statin-induced cell death in breast [3] and prostate [4] cancer; however, the mechanism by which dipyridamole inhibits SREBP2 and potentiates statin-induced cancer cell death remains poorly characterized.

In this manuscript, we present data to suggest that the synergistic anticancer interaction between statins and dipyridamole is twofold. In part, the ability of dipyridamole to function as a phosphodiesterase (PDE) inhibitor and increase cyclic adenosine monophosphate (cAMP) levels sensitizes cancer cells to statin-induced apoptosis. Additionally, dipyridamole and another cAMP-hydrolyzing PDE inhibitor, cilostazol, are able to inhibit statin-induced SREBP2 activity, and thus potentiate the proapoptotic activity of statins through a second, cAMP-independent mechanism. Collectively, these data warrant further investigation into the combination of a statin and cAMP-hydrolyzing PDE inhibitor for the treatment of hematological malignancies.

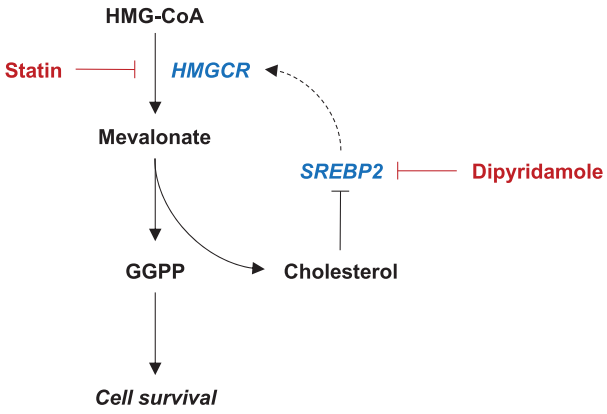

Fig. 1. Dipyridamole inhibits the sterol-regulated feedback loop of the MVA pathway. Schematic representation of the MVA pathway. Statins inhibit the rate-limiting enzyme of the pathway, HMGCR, which catalyzes the conversion of HMG-CoA to MVA. MVA is subsequently used to synthesize various metabolites that are important for cell growth and survival, including GGPP and cholesterol. Statin-mediated cholesterol depletion induces the cleavage and activation of SREBP2, which in turn induces the transcription of genes involved in MVA metabolism to restore homeostasis. We previously identified that the drug dipyridamole can inhibit statin-induced SREBP2 activation; however, the mechanism by which dipyridamole inhibits SREBP2 cleavage remains poorly understood.

2. Materials and methods

2.1. Cell culture and compounds

KMS11, LP1, OCI-AML-2, and OCI-AML-3 cell lines were cultured as described previously [6]. S49 wild-type (CCLZR352) and kin- (CCLZR347) cells were purchased from the University of California, San Francisco (UCSF) Cell Culture Facility and were cultured in Dulbecco's modified Eagle medium supplemented with 10% heat-inactivated horse serum, 100 units·mL^{-1} penicillin, and 100 μg·mL^{-1} streptomycin. Cell lines were routinely confirmed to be mycoplasma-free using the MycoAlert Mycoplasma Detection Kit (Lonza, Mississauga, Canada). Atorvastatin calcium (21CEC Pharmaceuticals Ltd., Markham, Canada) and fluvastatin sodium (US Biological, Burlington, Canada) were dissolved in ethanol. Dipyridamole (Sigma, Oakville, Canada), cilostazol (Tocris Bioscience, Burlington, Canada), *S*-(4-nitrobenzyl)-6-thioinosine (NBMPR) (Tocris Bioscience), 4-{[3′,4′-(methylenedioxy)benzyl] amino}-6-methoxyquinazoline (MBMQ) (Calbiochem, Oakville, Canada), fasentin (Sigma), and forskolin (Sigma) were dissolved in DMSO. Mevalonate and dibutyryl-cAMP (db-cAMP) were purchased from Sigma and dissolved in water. Geranylgeranyl pyrophosphate (GGPP) (methanol : ammonia solution) was purchased from Sigma.

2.2. Cell viability assays

3-(4,5-Dimethylthiazol-2-yl)-2,5-diphenyltetrazolium bromide (MTT) assays were performed as previously described [7]. Briefly, cells were seeded at 15 000–20 000 cells/well in 96-well plates and treated as indicated for 48 h. Percent cell viability was calculated relative to cells treated with solvent control(s). Fluvastatin dose–response curves were plotted, and area under the dose–response curve (AUC) values were computed using GRAPHPAD PRISM v6 software (San Diego, CA, USA).

2.3. Cell death assays

Cells were seeded at 750 000 cells/well in 6-well plates and treated as indicated for 48 h. For propidium

iodide (PI) staining, cells were fixed in 70% ethanol for at least 24 h, stained with PI, and analyzed by flow cytometry for the % pre-G1 DNA population as a measure of cell death, as previously described [2]. For Annexin V staining, cells were processed and stained using the Annexin V-FITC Apoptosis Kit (BioVision Inc., Burlington, Canada) as per the manufacturer's protocol, or washed and stained as indicated in Annexin V Binding Buffer (BD Biosciences, Mississauga, Canada). Apoptosis assays using primary AML cells were performed as described previously [6]. Patient samples were obtained with informed consent under a protocol approved by the University Health Network Research Ethics Board in accordance with the Declaration of Helsinki.

2.4. CCLE data mining

RNA sequencing data for the selected AML and MM human cell lines from the Cancer Cell Line Encyclopedia (CCLE) [8] were analyzed using the UCSC Xena Functional Genomics Explorer (https://xenabrowser.net/) [9].

2.5. CRISPR/Cas9-mediated gene knockout

Independent small guide RNAs (sgRNAs) that target *PRKACA* were cloned into lentiCRISPR v2 (Addgene plasmid #52961, Watertown, MA, USA). A sgRNA targeting a random locus on chromosome 10 was used as a negative control. HEK-293Tv cells were co-transfected with the sgRNA constructs, pMD2.G and psPAX2 using calcium-phosphate. LP1 cells were transduced with the lentiviral supernatants in the presence of 8 $\mu g \cdot mL^{-1}$ polybrene, after which they were selected with 1 $\mu g \cdot mL^{-1}$ puromycin. The sequences for the sgRNAs were obtained from Ref. [10] and are as follows:

gC10 Random: AAACATGTATAACCCTGCGC
gPRKACA #1: ACGAATCAAGACCCTCGGCA
gPRKACA #2: AGATGTTCTCACACCTACGG

2.6. Immunoblotting

For proteins other than HMGCR, immunoblotting was performed as previously described [4], using the following primary antibodies: SREBP2 (1 : 250; BD Biosciences, 557037), Actin (1 : 3000; Sigma, A2066), PKA C-α (1 : 1000; Cell Signaling Technology, #4782), α-Tubulin (1 : 3000; Calbiochem, CP06), and Ku80 (1 : 3000; Cell Signaling Technology, #2180). For HMGCR immunoblots, cells were seeded at 750 000 cells/well in 6-well plates and treated as indicated for 24 h. Whole cell lysates were prepared by washing cells twice with cold PBS and lysing cells in ~ 80 μL of buffer (20 mM Tris pH 7.5, 150 mM NaCl, 1 mM EDTA, 1 mM EGTA, 0.5% Triton X-100, protease inhibitors) on ice for 30 min. Lysates were cleared by centrifugation and protein concentrations determined using the Pierce 660 nm Protein Assay Kit (Thermo Fisher Scientific). Dithiothreitol (DTT) was added to a final concentration of 1 M. 4x Laemmli sample buffer was then added to the DTT-containing lysates at room temperature. Samples were not boiled to limit aggregation of membrane proteins. Blots were probed with primary antibodies against HMGCR (A9) (1 : 1000; prepared in-house) and actin.

2.7. Quantitative RT–PCR

Total RNA was isolated using TRIzol Reagent (Invitrogen, Mississauga, Canada). cDNA was synthesized from 500 ng RNA using SuperScript III (Invitrogen), or RNA was directly used for RT–PCR analysis using the iTaq Universal Probe One-Step Kit (Bio-Rad, Mississauga, Canada), according to the manufacturer's instructions. Quantitative reverse transcription–PCR (qRT–PCR) was performed using TaqMan probes (Applied Biosystems, Mississauga, Canada) for the following genes: *HMGCR* (Hs00168352), *HMGCS1* (Hs00266810), *INSIG1* (Hs01650979), and *GAPDH* (Hs99999905).

2.8. Intracellular cAMP quantification

Intracellular levels of cAMP were measured using the Cyclic AMP Chemiluminescent Immunoassay Kit (Cell Technology, Hayward, CA, USA) as per the manufacturer's protocol. Briefly, 1.5×10^6 cells/well (6-well plate) were incubated with the compounds as indicated, washed with PBS, and lysed in 150 μL of the provided lysis buffer.

3. Results

3.1. The cAMP-hydrolyzing PDE3 inhibitor cilostazol phenocopies dipyridamole to potentiate statin-induced cancer cell death

Dipyridamole has been reported to have multiple targets and can function as an inhibitor of nucleoside transport [11], glucose uptake [12], and PDEs [13] (Fig. 2A). To test which, if any, of these reported functions of dipyridamole are important for

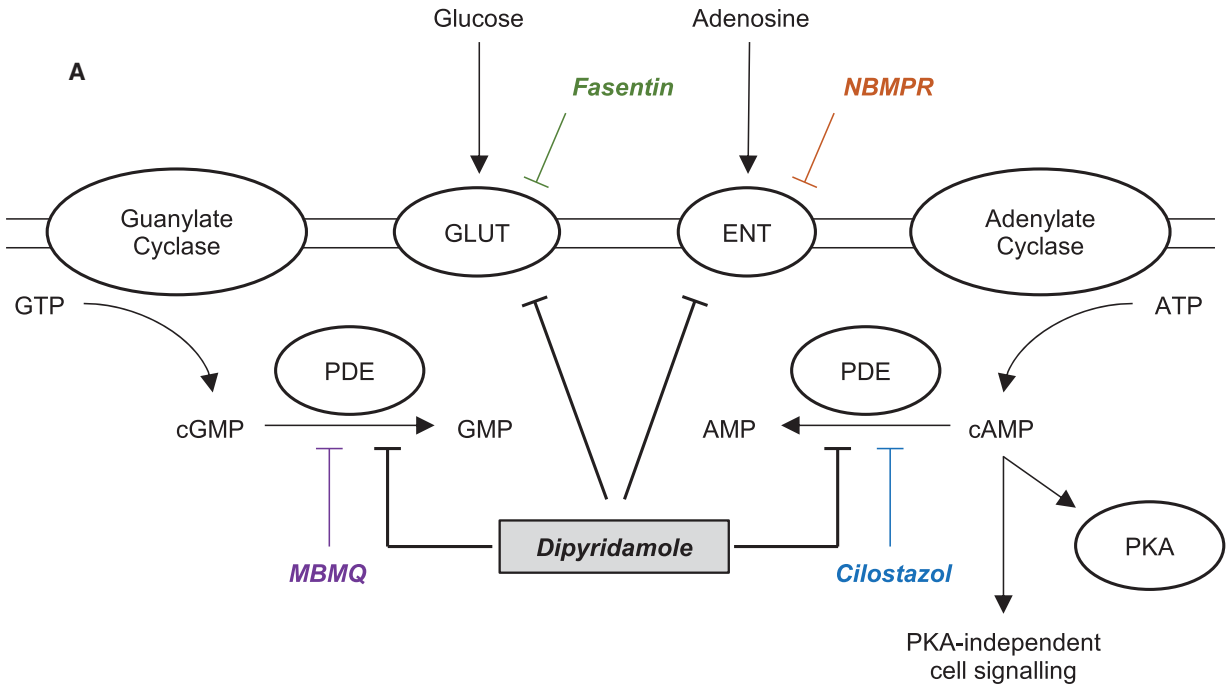
A
Glucose
Adenosine
Fasentin
NBMPR
Guanylate Cyclase
GLUT
ENT
Adenylate Cyclase
GTP
ATP
PDE
PDE
cGMP
GMP
AMP
cAMP
MBMQ
Dipyridamole
Cilostazol
PKA
PKA-independent cell signalling

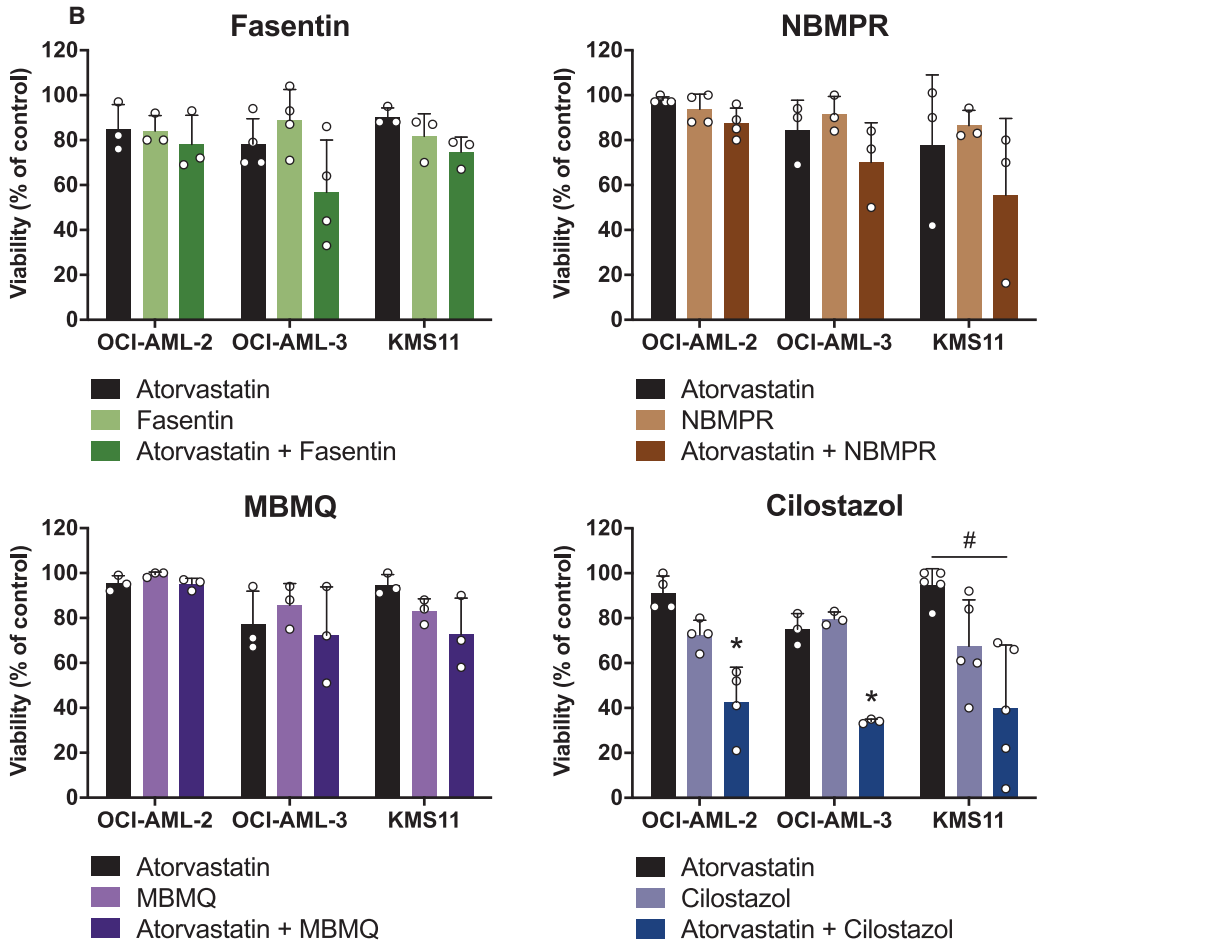
B
Fasentin
Viability (% of control)
OCI-AML-2
OCI-AML-3
KMS11
Atorvastatin
Fasentin
Atorvastatin + Fasentin
NBMPR
Atorvastatin
NBMPR
Atorvastatin + NBMPR
MBMQ
Atorvastatin
MBMQ
Atorvastatin + MBMQ
Cilostazol
#
*
Atorvastatin
Cilostazol
Atorvastatin + Cilostazol

Fig. 2. The cAMP-hydrolyzing PDE3 inhibitor cilostazol phenocopies dipyridamole to potentiate statin-induced cancer cell death. (A) Schematic representation of the reported targets of dipyridamole and additional compounds that target these proteins. ENT, equilibrative nucleoside transporter; GLUT, glucose transporter; PDE, phosphodiesterase; PKA, protein kinase A. (B) OCI-AML-2, OCI-AML-3, and KMS11 cells were treated with atorvastatin (4, 2 and 4 μM for OCI-AML-2, OCI-AML-3, and KMS11 cells, respectively) ± a glucose uptake inhibitor (fasentin; 12.5, 6.3, and 12.5 μM for OCI-AML-2, OCI-AML-3, and KMS11 cells, respectively), ENT inhibitor (NBMPR; 20 μM), cGMP-hydrolyzing PDE5 inhibitor (MBMQ; 10 μM), or cAMP-hydrolyzing PDE3 inhibitor (cilostazol; 25, 12.5, and 25 μM for OCI-AML-2, OCI-AML-3, and KMS11 cells, respectively). After 48 h, cell viability was evaluated by MTT assays. Data are represented as the mean + SD. $^{*}P < 0.05$ (one-way ANOVA with Tukey's multiple comparisons test, where the indicated groups were compared to the other groups of that cell line). $^{\#}P < 0.05$ (one-way ANOVA with Tukey's multiple comparisons test, comparing the two indicated groups).

potentiating statin-induced cancer cell death, we assayed additional compounds with similar activities for their ability to phenocopy dipyridamole. For these experiments, we evaluated the following compounds: NBMPR [equilibrative nucleoside transporter 1 (ENT1) inhibitor], fasentin [glucose transporter 1 (GLUT1) inhibitor], MBMQ (PDE5 inhibitor), and cilostazol (PDE3 inhibitor). AML (OCI-AML-2, OCI-AML-3) and MM (KMS11) cells were treated with each compound alone or in combination with atorvastatin. The concentrations of each compound were chosen such that they had minimal single-agent effects on cell viability (< 20%), but were still within the range known to inhibit the target under investigation [14–20]. Of the four compounds evaluated, only the combination of atorvastatin and cilostazol was observed to decrease AML and MM cell viability in all three cell lines (Fig. 2B). We further demonstrated that these effects were on-target and not specific to atorvastatin, as a similar decrease in cell viability was observed when cilostazol was combined with fluvastatin, another statin drug (Fig. S1). Moreover, the addition of exogenous MVA or GGPP was able to fully rescue the decrease in cell viability caused by the statin–cilostazol combination (Fig. S1), further supporting that these effects were due to MVA pathway inhibition.

3.2. Compounds that increase cAMP levels phenocopy dipyridamole to potentiate statin-induced apoptosis

PDEs catalyze the hydrolysis of cAMP and cyclic guanosine monophosphate (cGMP) (Fig. 2A), thereby regulating the intracellular concentrations of these secondary messengers. There are 11 PDE proteins that can be expressed in mammalian cells, which differ in their cellular functions, structures, expression patterns, and affinities for cAMP and cGMP [21,22]. Dipyridamole is known to inhibit multiple cAMP- and cGMP-hydrolyzing PDEs with varying affinities [13,22]. In contrast, cilostazol is reported to be a specific inhibitor of PDE3, which is a cAMP-hydrolyzing PDE [13,21]. Given our observation that the statin–cilostazol combination was uniquely able to decrease the viability of AML and MM cells, we hypothesized that inhibition of cAMP hydrolysis by dipyridamole may be responsible, at least in part, for its ability to synergize with statins to induce cancer cell death. Indeed, dipyridamole treatment, at the concentration used throughout this study (5 μM), resulted in a 2.5-fold increase in intracellular cAMP levels (Fig. S2).

To evaluate whether the PDEs targeted by dipyridamole and cilostazol are expressed in AML and MM cells, we mined the Cancer Cell Line Encyclopedia (CCLE) database [8]. Indeed, multiple PDEs, including isoforms of PDE3, PDE5, PDE6, PDE7, and PDE8, are highly and consistently expressed in a panel of AML and MM cell lines, including previously characterized statin-sensitive (e.g., KMS11, OCI-AML-3) and insensitive (e.g., LP1) cell lines (Fig. 3A) [6,23,24]. We subsequently evaluated the ability of an adenylate cyclase activator (forskolin) and cell-permeable analog of cAMP (db-cAMP) to potentiate statin-induced apoptosis in AML cells. The combination of fluvastatin and dipyridamole, cilostazol, forskolin, or db-cAMP significantly induced apoptosis in OCI-AML-2 and OCI-AML-3 cells, whereas no significant apoptosis was observed in response to treatment with each cAMP-modulating compound on its own (Fig. 3B). To determine whether primary cells were similarly sensitive to the combination of a statin and PDE inhibitor, we treated primary AML cells with fluvastatin and/or cilostazol for 48 h, after which apoptosis was quantified by Annexin V staining using flow cytometry. Indeed, the fluvastatin–cilostazol combination significantly induced apoptosis in these cells (Fig. 3C). This is consistent with our previous report that the statin–dipyridamole combination can induce apoptosis in primary AML cells [6]. Notably, we evaluated the statin–cilostazol combination in primary cells from three of the same patients as in our previous report with dipyridamole, and observed concordant results [6]. Collectively, these data suggest that elevating intracellular levels of cAMP may be an effective way to

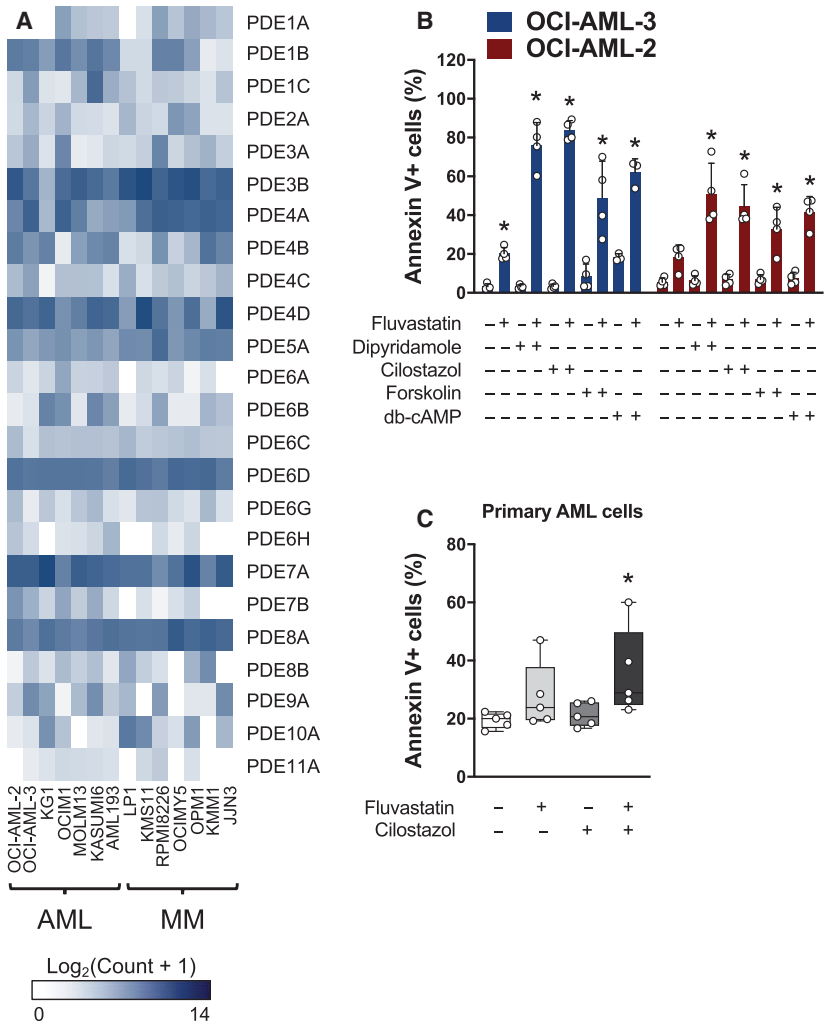

Fig. 3. Compounds that increase cAMP levels phenocopy dipyridamole to potentiate statin-induced apoptosis. (A) RNA expression of the different PDEs in a panel of human AML and MM cell lines. Data were mined from the CCLE database. (B) OCI-AML-2 and OCI-AML-3 cells were treated with fluvastatin (4 μM for OCI-AML-2 and 2 μM for OCI-AML-3) ± a PDE3 inhibitor (cilostazol; 20 μM), an adenylate cyclase activator (forskolin; 10 μM) or db-cAMP (0.1 mM). After 48 h, cells were labeled with FITC-conjugated Annexin V and apoptotic cells were quantified by flow cytometry. $*P < 0.05$ (one-way ANOVA with Dunnett's multiple comparisons test, where the indicated groups were compared to the solvent controls group of that cell line). Data are represented as the mean + SD. (C) Primary AML cells were cultured in the presence of solvent controls, 5 μM fluvastatin, 20 μM cilostazol, or the combination. After 48 h, cells were labeled with FITC-conjugated Annexin V and analyzed by flow cytometry. Data from four independent AML patient samples are represented as box plots with whiskers depicting the maximum and minimum values. $*P < 0.05$ (one-way ANOVA with Dunnett's multiple comparisons test, where the indicated group was compared to the solvent controls group).

sensitize hematological cancer cells to statin-induced apoptosis.

3.3. Compounds that increase cAMP levels differentially modulate sterol metabolism

We previously demonstrated that dipyridamole inhibits statin-induced SREBP2 cleavage and activation, which sensitizes cancer cells to statin-induced apoptosis [4,6]. To test whether compounds that increase cAMP levels similarly inhibit the induction of sterol metabolism gene expression in response to statin treatment, we treated LP1 cells with fluvastatin as a single agent or in combination with a PDE inhibitor (dipyridamole or cilostazol), forskolin or db-cAMP, and then evaluated the expression of three SREBP2 target genes by qRT–PCR: *HMGCR*, HMG-CoA synthase 1 (*HMGCS1*), and insulin-induced gene 1 (*INSIG1*). We chose LP1

cells for these experiments because we previously demonstrated that this cell line robustly activates SREBP2 in response to statin exposure, and cotreatment with dipyridamole sensitizes them to statin-induced apoptosis [6]. As expected, treatment of LP1 cells with fluvastatin resulted in the induction of all three sterol-regulated genes, a response which was completely blocked by dipyridamole cotreatment (Fig. 4A). Cilostazol similarly inhibited fluvastatin-induced expression of these SREBP2 target genes (Fig. 4A). In contrast, forskolin and db-cAMP had weaker, if any, effects on the expression of these sterol-regulated genes in this cell line, and yet both compounds potentiated statin-induced apoptosis (Figs 3B and 4A, Fig. S3). Concordantly, only dipyridamole and cilostazol decreased statin-induced HMGCR protein expression (Fig. 4B), which was associated with the inhibition of SREBP2 cleavage following statin treatment (Fig. 4C).

cAMP can regulate several effectors, the most well studied of which is cAMP-dependent protein kinase A (PKA). PKA phosphorylates a multitude of proteins with diverse roles in signal transduction, metabolism, ion transport, and transcription regulation [25]. In particular, PKA has been shown to phosphorylate and negatively regulate SREBP1 (the master transcriptional regulator of fatty acid biosynthesis) *in vitro* at a residue that is conserved between SREBP1 and SREBP2 [26]. However, given our observation that db-cAMP did not inhibit statin-induced SREBP2 target gene expression (Fig. 4A), we reasoned that the effects of dipyridamole and cilostazol on SREBP2 were likely independent of cAMP/PKA signaling. To validate this model, we knocked out the alpha catalytic subunit of PKA (PKA Cα, encoded by *PRKACA*) in LP1 cells and evaluated the subsequent effects on dipyridamole and cilostazol activity. Consistent with a cAMP/PKA-independent mechanism, both dipyridamole and cilostazol retained their ability to inhibit SREBP2 and potentiate statin-induced cell death in PKA-depleted LP1 cells (Figs S4 and S5).

To further confirm the above observation, we evaluated dipyridamole and cilostazol activity in isogenic wild-type and PKA-null (kin-) S49 cells [27]. S49 kin- cells have no detectable PKA activity due to improper *cis*-autophosphorylation at serine 338 during translation, which renders the catalytic subunit of PKA insoluble [28]. Indeed, dipyridamole and cilostazol potentiated statin-induced cell death in both S49 wild-type and kin- cells (Fig. S4).

Taken together, these data suggest that compounds that increase cAMP levels, including PDE inhibitors and forskolin, can sensitize hematological cancer cells to statin-induced apoptosis. Furthermore, PDE inhibitors such as dipyridamole and cilostazol further possess cAMP/PKA-independent activity against statin-induced SREBP2 activation (Fig. 5).

4. Discussion

Our laboratory previously reported a novel role for the drug dipyridamole as an inhibitor of the SREBP family of transcription factors [4,6]. As a result, dipyridamole can sensitize certain cancer cells to statin-induced apoptosis (Fig. 1) [4,6]. However, given the polypharmacology of dipyridamole, the mechanism by which it inhibits the SREBP proteins and synergizes with statins remains to be fully understood. As a step toward elucidating this mechanism, we evaluated individual compounds that phenocopied the different known functions of dipyridamole for their ability to sensitize AML and MM cell lines to statin-induced cell death. Through this approach, we were able to dissect the polypharmacology of dipyridamole and implicate its role as a cAMP-hydrolyzing PDE inhibitor in potentiating statin-induced apoptosis.

Our study revealed that cAMP-hydrolyzing PDE inhibitors, including dipyridamole and cilostazol, sensitize hematological cancer cells to statin-induced apoptosis via a dual mechanism (Fig. 5). By inhibiting PDE activity, dipyridamole and cilostazol increase intracellular cAMP levels (Fig. S2) [18]. We demonstrated

Fig. 4. Compounds that increase cAMP levels differentially modulate sterol metabolism. (A) LP1 cells were treated with 4 μM fluvastatin ± 5 μM dipyridamole, 20 μM cilostazol, 10 μM forskolin, or 0.1 mM db-cAMP for 16 h, and RNA was isolated to assay for *HMGCR*, *HMGCS1* and *INSIG1* expression by qRT–PCR. mRNA expression data are normalized to *GAPDH* expression. Data are represented as the mean + SD. $^{*}P < 0.05$ (one-way ANOVA with Tukey's multiple comparisons test, where the indicated groups were compared to the solvent controls group), $^{\#}P < 0.05$ (one-way ANOVA with Tukey's multiple comparisons test, comparing the two indicated groups). (B) LP1 cells were treated with 4 μM fluvastatin ± 5 μM dipyridamole, 20 μM cilostazol, 10 μM forskolin, or 0.1 mM db-cAMP for 24 h, and protein was isolated to assay for HMGCR expression by immunoblotting. 1 = HMGCR oligomer, 2 = HMGCR monomer. Immunoblots are representative of three independent experiments. (C) LP1 cells were treated with 4 μM fluvastatin ± 5 μM dipyridamole or 20 μM cilostazol for 8 h, and protein was isolated to assay for SREBP2 cleavage (activation) by immunoblotting. F, full-length SREBP2; C, cleaved SREBP2. Immunoblots are representative of three independent experiments.

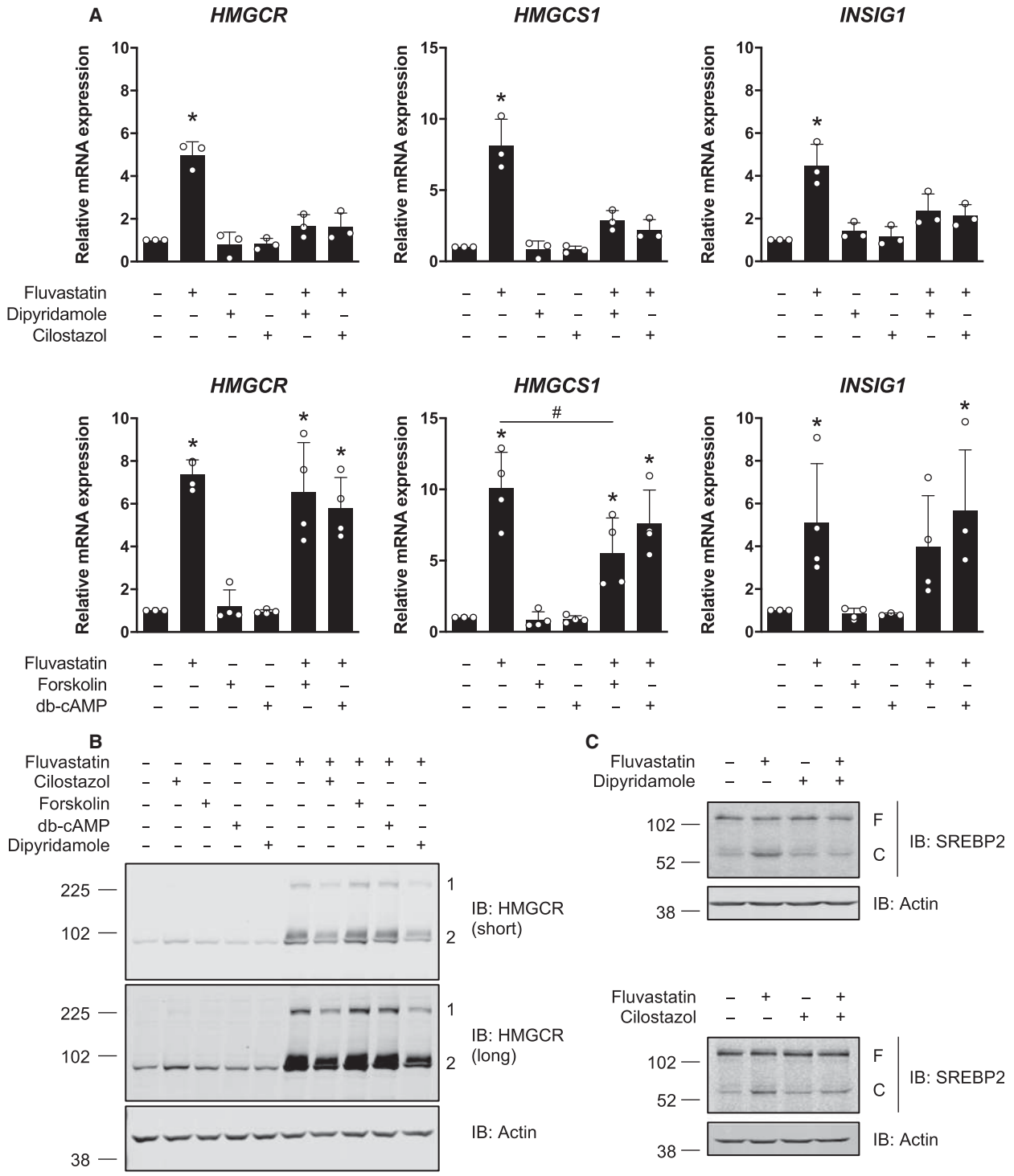

that other compounds that increase cAMP levels, including forskolin, similarly sensitize cancer cells to statin-induced cell death. Importantly, cotreatment with a statin and cAMP-modulating agent was effective at potentiating cell death in both statin-sensitive (e.g., KMS11, OCI-AML-3) and statin-insensitive (e.g., LP1) cell lines (Fig. 3B, Figs S1, S3,and S4D). Our data are consistent with a previous report, where the combination of lovastatin and db-cAMP was shown to enhance differentiation and cytotoxicity in

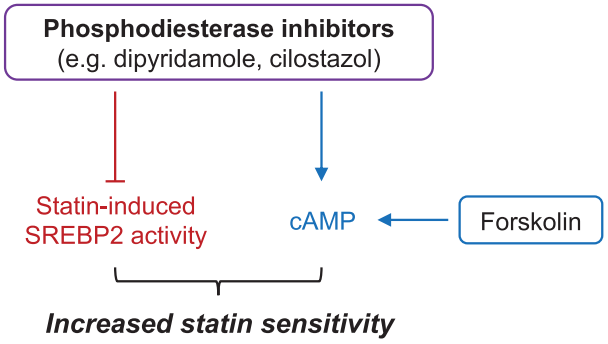

Fig. 5. Proposed model for how cAMP-hydrolyzing PDE inhibitors potentiate statin-induced cancer cell death. Compounds that increase intracellular cAMP levels, including PDE inhibitors (e.g., dipyridamole, cilostazol) and forskolin, can sensitize cancer cells to statin-induced apoptosis. Dipyridamole and cilostazol also inhibit statin-induced activation of SREBP2 through a cAMP-independent mechanism, which abrogates the restorative feedback loop of the MVA pathway and further sensitizes cancer cells to statin-induced apoptosis.

embryonal carcinoma and neuroblastoma cell lines [29]. However, the critical cAMP-regulated effector that modulates statin sensitivity in cancer cells remains to be identified. In the present study, we found that dipyridamole and cilostazol potentiate statin-induced cell death in a PKA-independent manner (Fig. S4). In addition to PKA, cAMP also regulates specific ion channels and the EPAC (exchange protein directly activated by cAMP) proteins, which are cAMP-dependent guanine nucleotide exchange factors for the RAP GTPases [30]. Future work is required to delineate the mechanism by which elevated cAMP levels sensitize cancer cells to statin-induced apoptosis.

We further demonstrated that the PDE inhibitors dipyridamole and cilostazol inhibit the SREBP2-regulated feedback mechanism of the MVA pathway via an additional, cAMP-independent mechanism (Fig. 4). Interestingly, cilostazol has previously been reported to inhibit insulin-induced expression of SREBP1 [31], but the potential involvement of cAMP signaling was not explored. Data in the literature are conflicting as to the effects of PDE inhibitors on lipid metabolism. A recent study demonstrated that combined inhibition of PDE4 and PDE8 in Leydig cells promotes SREBP2 signaling, cholesterol metabolism, and steroidogenesis [32]. In contrast, data from a randomized controlled trial in patients with type 2 diabetes revealed that cilostazol treatment significantly lowered serum triglyceride and low-density lipoprotein (LDL) cholesterol levels [33]. The data we present here clearly show that dipyridamole (a pan-PDE inhibitor) and cilostazol (a PDE3 inhibitor) can abrogate SREBP2 cleavage and activation in AML and MM cells exposed to a statin. It is therefore possible that different PDEs play unique roles in regulating SREBP2 signaling and sterol metabolism and that PDE-mediated regulation of SREBP2 is tissue type- and context-dependent. In the context of cancer, dipyridamole has been shown to inhibit statin-induced SREBP2 cleavage and activation in AML, MM, breast cancer, and prostate cancer cells [3,4,6], suggesting similar regulation in many different cell types. A rigorous analysis of the effects of different PDE inhibitors on lipid metabolism and investigation into the mechanism(s) by which these clinically approved drugs act to modulate cancer cell metabolism should be a focus of future studies. Interestingly, unlike many other PDE inhibitors, dipyridamole and cilostazol also inhibit adenosine uptake [11,34]. While we did not observe enhanced cell death when the adenosine reuptake inhibitor NBMPR was combined with a statin (Fig. 2B), it remains possible that dipyridamole and cilostazol inhibit sterol metabolism via a PDE-independent mechanism or through simultaneous modulation of multiple targets.

The data presented here may have important clinical implications, as many cAMP-hydrolyzing PDE inhibitors are approved for several nononcology indications [21]. For example, cilostazol (marketed as Pletal) is currently approved and widely used to treat intermittent claudication. The overexpression of several PDEs has been observed in solid and hematological tumors, and the possibility of cAMP-hydrolyzing PDE inhibition as an anticancer strategy has been preclinically explored alone or in combination with chemo- and targeted molecular therapies [35–40]. In hematological malignancies, primary chronic lymphocytic leukemia patient samples were found to have PDE7B overexpression and noted to be sensitive to PDE7 inhibition in a cAMP-dependent manner [38]. Another study found a strong synergistic combinatorial effect between adenosine A2A receptor agonists and cAMP-hydrolyzing PDE inhibitors in MM and diffuse large B-cell lymphoma cell lines and primary patient samples [41]. Given that a number of PDE inhibitors are poised for repurposing and that statins have demonstrated anticancer activity in early-phase clinical trials [42–49], further studies are needed to evaluate the therapeutic benefit of a statin-PDE inhibitor combination for the treatment of cancer. As the combination of cilostazol and statins has already been evaluated clinically in healthy subjects [50,51] and in patients with cardiovascular indications [52,53] without added adverse effects, there is the possibility of fast-tracking these agents to phase II trials in AML and MM.

5. Conclusion

In summary, we propose a working model whereby cAMP-hydrolyzing PDE inhibitors, such as dipyridamole and cilostazol, increase cAMP levels and inhibit SREBP2 activation via independent mechanisms, both of which converge to potentiate statin-induced apoptosis in hematological cancer cells (Fig. 5). Given that statins and a number of PDE inhibitors are already approved for various nononcology indications, future studies are needed to thoroughly evaluate the potential therapeutic benefit of these agents for the treatment of hematological malignancies. Moreover, our experimental approach to dissect the polypharmacology of dipyridamole is one that may be useful when interrogating novel functions of other repurposed drugs.

Acknowledgements

We thank all members of the Penn laboratory for helpful discussions. LZP holds a Tier 1 Canada Research Chair in Molecular Oncology. This work was supported by funding from the Canadian Institutes of Health Research (CIHR) (FRN: 142263; LZP), Canadian Cancer Society (Grant #706394; LZP), and Office of the Assistant Secretary of Defense for Health Affairs, through the Breast Cancer Research Program (Award No. W81XWH-16-1-0068; LZP). Opinions, interpretations, conclusions, and recommendations are those of the author and are not necessarily endorsed by the Department of Defense. JL and AAP were supported by CIHR Doctoral Research Awards. AAP was further supported by a Canadian Breast Cancer Foundation Doctoral Award.

Conflict of interest

The authors declare no conflict of interest.

Author contributions

JL, AAP, and LZP conceived and designed the study. JL, AAP, and PS performed experiments, as well as analyzed and interpreted the experimental data. MDM and ADS provided the primary AML cells and clinical expertise. JL, AAP, and LZP wrote the manuscript. All authors read and approved the manuscript. LZP supervised the study.

Data accessibility

The RNA expression data in Fig. 3A were obtained through the CCLE database [8]. All other raw data are available from the corresponding author upon reasonable request.

References

1 Mullen PJ, Yu R, Longo J, Archer MC & Penn LZ (2016) The interplay between cell signalling and the mevalonate pathway in cancer. *Nat Rev Cancer* **16**, 718–731.

2 Clendening JW, Pandyra A, Li Z, Boutros PC, Martirosyan A, Lehner R, Jurisica I, Trudel S & Penn LZ (2010) Exploiting the mevalonate pathway to distinguish statin-sensitive multiple myeloma. *Blood* **115**, 4787–4797.

3 Göbel A, Breining D, Rauner M, Hofbauer LC & Rachner TD (2019) Induction of 3-hydroxy-3-methylglutaryl-CoA reductase mediates statin resistance in breast cancer cells. *Cell Death Dis* **10**, 91.

4 Longo J, Mullen PJ, Yu R, van Leeuwen JE, Masoomian M, Woon DTS, Wang Y, Chen EX, Hamilton RJ, Sweet JM *et al.* (2019) An actionable sterol-regulated feedback loop modulates statin sensitivity in prostate cancer. *Mol Metab* **25**, 119–130.

5 Pandyra AA, Mullen PJ, Goard CA, Ericson E, Sharma P, Kalkat M, Yu R, Pong JT, Brown KR, Hart T *et al.* (2015) Genome-wide RNAi analysis reveals that simultaneous inhibition of specific mevalonate pathway genes potentiates tumor cell death. *Oncotarget* **6**, 26909–26921.

6 Pandyra A, Mullen PJ, Kalkat M, Yu R, Pong JT, Li Z, Trudel S, Lang KS, Minden MD, Schimmer AD *et al.* (2014) Immediate utility of two approved agents to target both the metabolic mevalonate pathway and its restorative feedback loop. *Cancer Res* **74**, 4772–4782.

7 Dimitroulakos J, Ye LY, Benzaquen M, Moore MJ, Kamel-Reid S, Freedman MH, Yeger H & Penn LZ (2001) Differential sensitivity of various pediatric cancers and squamous cell carcinomas to lovastatin-induced apoptosis: therapeutic implications. *Clin Cancer Res* **7**, 158–167.

8 Barretina J, Caponigro G, Stransky N, Venkatesan K, Margolin AA, Kim S, Wilson CJ, Lehár J, Kryukov GV, Sonkin D *et al.* (2012) The Cancer Cell Line Encyclopedia enables predictive modelling of anticancer drug sensitivity. *Nature* **483**, 603–607.

9 Goldman M, Craft B, Hastie M, Repečka K, Kamath A, McDade F, Rogers D, Brooks AN, Zhu J & Haussler D (2019) The UCSC Xena platform for cancer genomics data visualization and interpretation. *bioRxiv*. https://doi.org/10.1101/326470

10 Hart T, Chandrashekhar M, Aregger M, Steinhart Z, Brown KR, MacLeod G, Mis M, Zimmermann M, Fradet-Turcotte A, Sun S *et al.* (2015) High-resolution CRISPR screens reveal fitness genes and genotype-specific cancer liabilities. *Cell* **163**, 1515–1526.

11 King AE, Ackley MA, Cass CE, Young JD & Baldwin SA (2006) Nucleoside transporters: from scavengers to novel therapeutic targets. *Trends Pharmacol Sci* **27**, 416–425.
12 Steinfelder HJ & Joost HG (1988) Inhibition of insulin-stimulated glucose transport in rat adipocytes by nucleoside transport inhibitors. *FEBS Lett* **227**, 215–219.
13 Bender AT & Beavo JA (2006) Cyclic nucleotide phosphodiesterases: molecular regulation to clinical use. *Pharmacol Rev* **58**, 488–520.
14 Wood TE, Dalili S, Simpson CD, Hurren R, Mao X, Saiz FS, Gronda M, Eberhard Y, Minden MD, Bilan PJ *et al.* (2008) A novel inhibitor of glucose uptake sensitizes cells to FAS-induced cell death. *Mol Cancer Ther* **7**, 3546–3555.
15 Boleti H, Coe IR, Baldwin SA, Young JD & Cass CE (1997) Molecular identification of the equilibrative NBMPR-sensitive (es) nucleoside transporter and demonstration of an equilibrative NBMPR-insensitive (ei) transport activity in human erythroleukemia (K562) cells. *Neuropharmacology* **36**, 1167–1179.
16 Hourani SMO, Boon K, Fooks HM & Prentice DJ (2001) Role of cyclic nucleotides in vasodilations of the rat thoracic aorta induced by adenosine analogues. *Br J Pharmacol* **133**, 833–840.
17 Kim M-J, Park K-G, Lee K-M, Kim H-S, Kim S-Y, Kim C-S, Lee S-L, Chang Y-C, Park J-Y, Lee K-U *et al.* (2005) Cilostazol inhibits vascular smooth muscle cell growth by downregulation of the transcription factor E2F. *Hypertension* **45**, 552–556.
18 Shakur Y, Fong M, Hensley J, Cone J, Movsesian MA, Kambayashi J-I, Yoshitake M & Liu Y (2002) Comparison of the effects of cilostazol and milrinone on cAMP-PDE activity, intracellular cAMP and calcium in the heart. *Cardiovasc Drugs Ther* **16**, 417–427.
19 Bouley R, Pastor-Soler N, Cohen O, McLaughlin M, Breton S & Brown D (2005) Stimulation of AQP2 membrane insertion in renal epithelial cells in vitro and in vivo by the cGMP phosphodiesterase inhibitor sildenafil citrate (Viagra). *Am J Physiol Ren Physiol* **288**, F1103–F1112.
20 Lu J, Montgomery BK, Chatain GP, Bugarini A, Zhang Q, Wang X, Edwards NA, Ray-Chaudhury A, Merrill MJ, Lonser RR *et al.* (2018) Corticotropin releasing hormone can selectively stimulate glucose uptake in corticotropinoma via glucose transporter 1. *Mol Cell Endocrinol* **470**, 105–114.
21 Maurice DH, Ke H, Ahmad F, Wang Y, Chung J & Manganiello VC (2014) Advances in targeting cyclic nucleotide phosphodiesterases. *Nat Rev Drug Discov* **13**, 290–314.
22 Baillie GS, Tejeda GS & Kelly MP (2019) Therapeutic targeting of 3′,5′-cyclic nucleotide phosphodiesterases: inhibition and beyond. *Nat Rev Drug Discov* **18**, 770–796.
23 Wong WW-L, Clendening JW, Martirosyan A, Boutros PC, Bros C, Khosravi F, Jurisica I, Stewart AK, Bergsagel PL & Penn LZ (2007) Determinants of sensitivity to lovastatin-induced apoptosis in multiple myeloma. *Mol Cancer Ther* **6**, 1886–1897.
24 Dimitroulakos J, Nohynek D, Backway KL, Hedley DW, Yeger H, Freedman MH, Minden MD & Penn LZ (1999) Increased sensitivity of acute myeloid leukemias to lovastatin-induced apoptosis: a potential therapeutic approach. *Blood* **93**, 1308–1318.
25 Sassone-Corsi P (2012) The cyclic AMP pathway. *Cold Spring Harb Perspect Biol* **4**, a011148.
26 Lu M & Shyy JYJ (2006) Sterol regulatory element-binding protein 1 is negatively modulated by PKA phosphorylation. *Am J Physiol Cell Physiol* **290**, 1477–1486.
27 Orellana SA & McKnight GS (1990) The S49 Kin- cell line transcribes and translates a functional mRNA coding for the catalytic subunit of cAMP-dependent protein kinase. *J Biol Chem* **265**, 3048–3053.
28 Keshwani MM, Klammt C, von Daake S, Ma Y, Kornev AP, Choe S, Insel PA & Taylor SS (2012) Cotranslational cis-phosphorylation of the COOH-terminal tail is a key priming step in the maturation of cAMP-dependent protein kinase. *Proc Natl Acad Sci USA* **109**, E1221–E1229.
29 Arnold DE, Gagne C, Niknejad N, McBurney MW & Dimitroulakos J (2010) Lovastatin induces neuronal differentiation and apoptosis of embryonal carcinoma and neuroblastoma cells: enhanced differentiation and apoptosis in combination with dbcAMP. *Mol Cell Biochem* **345**, 1–11.
30 Bos JL (2006) Epac proteins: multi-purpose cAMP targets. *Trends Biochem Sci* **31**, 680–686.
31 Jung YA, Kim HK, Bae KH, Seo HY, Kim HS, Jang BK, Jung GS, Lee IK, Kim MK & Park KG (2014) Cilostazol inhibits insulin-stimulated expression of sterol regulatory binding protein-1c via inhibition of LXR and Sp1. *Exp Mol Med* **46**, e73.
32 Shimizu-Albergine M, Van Yserloo B, Golkowski MG, Ong SE, Beavo JA & Bornfeldt KE (2016) SCAP/SREBP pathway is required for the full steroidogenic response to cyclic AMP. *Proc Natl Acad Sci USA* **113**, E5685–E5693.
33 Katakami N, Kim YS, Kawamori R & Yamasaki Y (2010) The phosphodiesterase inhibitor cilostazol induces regression of carotid atherosclerosis in subjects with type 2 diabetes mellitus: principal results of the Diabetic Atherosclerosis Prevention by Cilostazol (DAPC) study: a randomized trial. *Circulation* **121**, 2584–2591.
34 Sun B, Le SN, Lin S, Fong M, Guertin M, Liu Y, Tandon NN, Yoshitake M & Kambayashi J (2002) New mechanism of action for cilostazol: interplay

between adenosine and cilostazol in inhibiting platelet activation. *J Cardiovasc Pharmacol* **40**, 577–585.
35 Moon EY & Lerner A (2003) PDE4 inhibitors activate a mitochondrial apoptotic pathway in chronic lymphocytic leukemia cells that is regulated by protein phosphatase 2A. *Blood* **101**, 4122–4130.
36 Noonan KA, Ghosh N, Rudraraju L, Bui M & Borrello I (2014) Targeting immune suppression with PDE5 inhibition in end-stage multiple myeloma. *Cancer Immunol Res* **2**, 725–731.
37 Lerner A & Epstein PM (2006) Cyclic nucleotide phosphodiesterases as targets for treatment of haematological malignancies. *Biochem J* **393**, 21–41.
38 Zhang L, Murray F, Zahno A, Kanter JR, Chou D, Suda R, Fenlon M, Rassenti L, Cottam H, Kipps TJ *et al.* (2008) Cyclic nucleotide phosphodiesterase profiling reveals increased expression of phosphodiesterase 7B in chronic lymphocytic leukemia. *Proc Natl Acad Sci USA* **105**, 19532–19537.
39 Lin DC, Xu L, Ding LW, Sharma A, Liu LZ, Yang H, Tan P, Vadgama J, Karlan BY, Lester J *et al.* (2013) Genomic and functional characterizations of phosphodiesterase subtype 4D in human cancers. *Proc Natl Acad Sci USA* **110**, 6109–6114.
40 Zhou S, Xu H, Tang Q, Xia H & Bi F (2020) Dipyridamole enhances the cytotoxicities of trametinib against colon cancer cells through combined targeting of HMGCS1 and MEK pathway. *Mol Cancer Ther* **19**, 135–146.
41 Rickles RJ, Pierce LT, Giordano TP, Tam WF, McMillin DW, Delmore J, Laubach JP, Borisy AA, Richardson PG & Lee MS (2010) Adenosine A2A receptor agonists and PDE inhibitors: a synergistic multitarget mechanism discovered through systematic combination screening in B-cell malignancies. *Blood* **116**, 593–602.
42 Kornblau SM, Banker DE, Stirewalt D, Shen D, Lemker E, Verstovsek S, Estrov Z, Faderl S, Cortes J, Beran M *et al.* (2007) Blockade of adaptive defensive changes in cholesterol uptake and synthesis in AML by the addition of pravastatin to idarubicin + high-dose Ara-C: a phase 1 study. *Blood* **109**, 2999–3006.
43 Knox JJ, Siu LL, Chen E, Dimitroulakos J, Kamel-Reid S, Moore MJ, Chin S, Irish J, LaFramboise S & Oza AM (2005) A phase I trial of prolonged administration of lovastatin in patients with recurrent or metastatic squamous cell carcinoma of the head and neck or of the cervix. *Eur J Cancer* **41**, 523–530.
44 Hus M, Grzasko N, Szostek M, Pluta A, Helbig G, Woszczyk D, Adamczyk-Cioch M, Jawniak D, Legiec W, Morawska M *et al.* (2011) Thalidomide, dexamethasone and lovastatin with autologous stem cell transplantation as a salvage immunomodulatory therapy in patients with relapsed and refractory multiple myeloma. *Ann Hematol* **90**, 1161–1166.
45 Goss GD, Jonker DJ, Laurie SA, Weberpals JI, Oza AM, Spaans JN, la Porte C & Dimitroulakos J (2016) A phase I study of high-dose rosuvastatin with standard dose erlotinib in patients with advanced solid malignancies. *J Transl Med* **14**, 83.
46 Bjarnadottir O, Romero Q, Bendahl PO, Jirström K, Rydén L, Loman N, Uhlén M, Johannesson H, Rose C, Grabau D *et al.* (2013) Targeting HMG-CoA reductase with statins in a window-of-opportunity breast cancer trial. *Breast Cancer Res Treat* **138**, 499–508.
47 Murtola TJ, Syvälä H, Tolonen T, Helminen M, Riikonen J, Koskimäki J, Pakarainen T, Kaipia A, Isotalo T, Kujala P *et al.* (2018) Atorvastatin versus placebo for prostate cancer before radical prostatectomy – a randomized, double-blind, placebo-controlled clinical trial. *Eur Urol* **74**, 697–701.
48 Garwood ER, Kumar AS, Baehner FL, Moore DH, Au A, Hylton N, Flowers CI, Garber J, Lesnikoski BA, Hwang ES *et al.* (2010) Fluvastatin reduces proliferation and increases apoptosis in women with high grade breast cancer. *Breast Cancer Res Treat* **119**, 137–144.
49 Longo J, Hamilton RJ, Masoomian M, Khurram N, Branchard E, Mullen PJ, Elbaz M, Hersey K, Chadwick D, Ghai S *et al.* (2020) A pilot window-of-opportunity study of preoperative fluvastatin in localized prostate cancer. *Prostate Cancer Prostatic Dis.* https://doi.org/10.1038/s41391-020-0221-7.
50 Bramer SL, Brisson J, Corey AE & Mallikaarjun S (1999) Effect of multiple cilostazol doses on single dose lovastatin pharmacokinetics in healthy volunteers. *Clin Pharmacokinet* **37**, 69–77.
51 Kim J-R, Jung JA, Kim S, Huh W, Ghim J-L, Shin J-G & Ko J-W (2019) Effect of cilostazol on the pharmacokinetics of simvastatin in healthy subjects. *Biomed Res Int* **2019**, 1365180.
52 Hiatt WR, Money SR & Brass EP (2008) Long-term safety of cilostazol in patients with peripheral artery disease: the CASTLE study (Cilostazol: a study in long-term effects). *J Vasc Surg* **47**, 330–336.
53 Ari H, Emlek N, Ari S, Coşar S, Doğanay K, Aydin C, Tenekecioğlu E, Tütüncü A, Yontar OC, Gürdoğan M *et al.* (2015) The effect of high dose cilostazol and rosuvastatin on periprocedural myocardial injury in patients with elective percutaneous coronary intervention. *Acta Cardiol Sin* **31**, 292–300.

Supporting information

Additional supporting information may be found online in the Supporting Information section at the end of the article.

Fig. S1. Statin-cilostazol-induced cancer cell death can be rescued by exogenous MVA or GGPP. KMS11 and

OCI-AML-3 cells were treated as indicated with fluvastatin (2 μM for KMS11 and 0.5 μM for OCI-AML-3 cells), cilostazol (12.5 μM), mevalonate (0.2 mM) and/or GGPP (2 μM). After 48 hr, cell viability was evaluated by MTT assays. Data are represented as the mean + SD. *p < 0.05 (one-way ANOVA with Tukey's multiple comparisons test, where the indicated groups were compared to the other groups of that cell line).

Fig. S2. Dipyridamole treatment increases intracellular cAMP. OCI-AML-3 cells were treated with 2 μM fluvastatin ± 5 μM dipyridamole for 15 min and intracellular cAMP levels were quantified. Data are represented as the mean + SD. *p < 0.05 (one-way ANOVA with Dunnett's multiple comparisons test, where the indicated groups were compared to the solvent controls group).

Fig. S3. Forskolin and db-cAMP sensitize LP1 cells to fluvastatin-induced apoptosis. LP1 cells were treated with 4 μM fluvastatin ± 10 μM forskolin or 0.1 mM db-cAMP for 48 hr, after which apoptotic cells (double Annexin V-positive and 7AAD-positive cells) were quantified by flow cytometry. Data are represented as the mean + SD. *p < 0.05 (one-way ANOVA with Dunnett's multiple comparisons test, where the indicated groups were compared to the solvent controls group).

Fig. S4. Potentiation of statin-induced cancer cell death by dipyridamole and cilostazol is independent of PKA. (A) Immunoblot for PKA C-α expression in LP1 cells expressing Cas9 and a sgRNA to a random locus on chromosome 10 (gC10 Random) or one of two different locations within *PRKACA* (representative of three independent experiments). (B) LP1 gC10 Random and gPRKACA sublines were treated with a range of fluvastatin concentrations (0-24 μM) ± 5 μM dipyridamole or 10 μM cilostazol. After 48 hr, cell viability was evaluated by MTT assays. The area under each fluvastatin dose-response curve is plotted. Data are represented as the mean + SD. *p < 0.05 (one-way ANOVA with Dunnett's multiple comparisons test, where the indicated groups were compared to the fluvastatin alone group of that subline). (C) Immunoblot for PKA C-α expression in S49 wildtype (WT) or kin- (PKA-null) cells (representative of three independent experiments). (D) S49 WT and kin- cells were treated with 5 μM fluvastatin ± 2.5 μM dipyridamole or 5 μM cilostazol for 48 hr, fixed in ethanol and assayed for DNA fragmentation (% pre-G1 population) as a marker of cell death by propidium iodide staining. Data are represented as the mean + SD. *p < 0.05 (one-way ANOVA with Dunnett's multiple comparisons test, where the indicated groups were compared to the solvent controls group of that cell line).

Fig. S5. Dipyridamole and cilostazol inhibit the sterol-regulated feedback loop of the MVA pathway independent of PKA. (A) LP1 gPRKACA sublines were treated with 4 μM fluvastatin ± 5 μM dipyridamole or 20 μM cilostazol for 16 hr, and RNA was isolated to assay for *HMGCS1* expression by qRT-PCR. mRNA expression data are normalized to *GAPDH* expression. Data are represented as the mean + SD. *p < 0.05 (one-way ANOVA with Sidak's multiple comparisons test, where the indicated groups were compared to the solvent controls group of that subline). (B) LP1 gC10 Random or gPRKACA #1 cells were treated with 4 μM fluvastatin ± 5 μM dipyridamole or 20 μM cilostazol for 8 hr, and protein was isolated to assay for SREBP2 cleavage (activation) by immunoblotting. F = full-length SREBP2, C = cleaved SREBP2. Immunoblots are representative of three independent experiments.

Liu et al. Journal of Experimental & Clinical Cancer Research (2020) 39:38
https://doi.org/10.1186/s13046-020-1539-7

Journal of Experimental & Clinical Cancer Research

RESEARCH Open Access

Repurposing the serotonin agonist Tegaserod as an anticancer agent in melanoma: molecular mechanisms and clinical implications

Wei Liu[1†], Paweł Stachura[1†], Haifeng C. Xu[1,2], Nikkitha Umesh Ganesh[1], Fiona Cox[1], Ruifeng Wang[1], Karl S. Lang[2], Jay Gopalakrishnan[3], Dieter Häussinger[4], Bernhard Homey[5], Philipp A. Lang[1] and Aleksandra A. Pandyra[1,4*]

Abstract

Background: New therapies are urgently needed in melanoma particularly in late-stage patients not responsive to immunotherapies and kinase inhibitors.

Methods: Drug screening, IC50 determinations as well as synergy assays were detected by the MTT assay. Apoptosis using Annexin V and 7AAD staining was assessed using flow cytometry. TUNEL staining was performed using immunocytochemistry. Changes in phosphorylation of key molecules in PI3K/Akt/mTOR and other relevant pathways were detected by western blot as well as immunocytochemistry. To assess in vivo anti-tumor activity of Tegaserod, syngeneic intravenous and subcutaneous melanoma xenografts were used. Immunocytochemical staining was performed to detect expression of active Caspase-3, cleaved Caspase 8 and p-S6 in tumors. Evaluation of immune infiltrates was carried out by flow cytometry.

Results: Using a screen of 770 pharmacologically active and/or FDA approved drugs, we identified Tegaserod (Zelnorm, Zelmac) as a compound with novel anti-cancer activity which induced apoptosis in murine and human malignant melanoma cell lines. Tegaserod (TM) is a serotonin receptor 4 agonist (HTR4) used in the treatment of irritable bowel syndrome (IBS). TM's anti-melanoma apoptosis-inducing effects were uncoupled from serotonin signaling and attributed to PI3K/Akt/mTOR signaling inhibition. Specifically, TM blunted S6 phosphorylation in both $BRAF^{V600E}$ and BRAF wildtype (WT) melanoma cell lines. TM decreased tumor growth and metastases as well as increased survival in an in vivo syngeneic immune-competent model. In vivo, TM also caused tumor cell apoptosis, blunted PI3K/Akt/mTOR signaling and decreased S6 phosphorylation. Furthermore TM decreased the infiltration of immune suppressive regulatory $CD4^+CD25^+$ T cells and FOXP3 and ROR-γt positive $CD4^+$ T cells. Importantly, TM synergized with Vemurafenib, the standard of care drug used in patients with late stage disease harboring the $BRAF^{V600E}$ mutation and could be additively or synergistically combined with Cobimetinib in both $BRAF^{V600E}$ and BRAF WT melanoma cell lines in inducing anti-cancer effects.

(Continued on next page)

* Correspondence: aleksandra.pandyra@uni-duesseldorf.de
†Wei Liu and Paweł Stachura contributed equally to this work.
[1]Department of Molecular Medicine II, Medical Faculty, Heinrich-Heine-University, Universitätsstraße 1, 40225 Düsseldorf, Germany
[4]Department of Gastroenterology, Hepatology and Infectious Diseases, Heinrich-Heine-University, Moorenstrasse 5, 40225 Düsseldorf, Germany
Full list of author information is available at the end of the article

(Continued from previous page)
Conclusion: Taken together, we have identified a drug with anti-melanoma activity in vitro and in vivo that has the potential to be combined with the standard of care agent Vemurafenib and Cobimetinib in both $BRAF^{V600E}$ and BRAF WT melanoma.

Keywords: Tegaserod, Melanoma, PI3K/Akt/mTOR pathway, Apoptosis

Background

Melanoma accounts for a large proportion of skin-related deaths and its incidence and mortality is on the rise [1, 2]. Despite advances in treatment options, the 5-year survival for patients suffering from late stage disease is only 20% [2]. The current therapeutic landscape encompasses surgery to remove early stage melanomas, traditional chemotherapy and radiation therapy for the more advanced stages, targeted therapies as well as immunotherapy. An increased understanding of the molecular landscape driving melanoma particularly activating mutations such as $BRAF^{V600E}$ harbored by 50% of melanoma patients, has led to the development of small molecule inhibitors designed to specifically target multiple nodes of the MAPK pathway [3]. The approval of the Anti-CTLA checkpoint inhibitor Ipilimumab [4] in 2011 ushered immunotherapies focused on targeting the PD1/PD-L1 axis. This has had a tremendous impact on the therapy landscape in treating patients with advanced melanoma improving not only overall survival but leading to long-term survival in some patients. However, resistance to targeted therapies as well immunotherapy where bio-markers of response are not yet well-established [5, 6], present challenges in the treatment of melanoma. Although combinatorial approaches of the various targeted therapies together with immunotherapies are underway [7], the high-costs [5] associated with immunotherapy highlights an urgent need for novel anti-melanoma therapeutic options. The application of drugs used for alternate diseases as novel anti-cancer therapeutics, known as drug repositioning, has been successfully implemented in the clinical setting [8] and these compounds can be a rich potential source of novel, readily available anti-cancer therapeutics.

We conducted a pharmacologic screen composed of the NIH Clinical Collection (NCC) of 770 small molecules, FDA-approved or which have been previously used in human clinical trials to identify novel anti-melanoma agents. Each molecule was screened in the murine B16F10 cell line and its half maximal inhibitory concentrations (IC50) was determined. Amongst the compounds whose IC50 values were in the low micromolar range, Tegaserod (TM), a serotonin receptor 4 (HTR4) agonist, validated successfully in secondary screening approaches with BRAF WT and $BRAF^{V600E}$ human melanoma cell lines and was pursued in further in vitro and in vivo studies. In melanoma, serotonin has been found to increase melanogenesis via HTR2A, an effect that was reversed by HTR antagonists [9]. And while HTR2B-C antagonists have been shown to inhibit migration in uveal [10] and metastatic melanoma [11], little is known about serotonin agonists, particularly HTR4 agonists in the context of this tumor type.

TM induced apoptosis in the B16F10 murine melanoma cell line as well as several human melanoma cell lines. In vivo, TM was well tolerated and efficacy was demonstrated in a syngeneic melanoma model testing primary tumor growth and metastasis. Importantly, TM strongly synergized with the standard of care $BRAF^{V600E}$ targeting Vemurafenib in human melanoma cell lines harboring this mutation. Mechanistically, TM suppressed PI3K/Akt/mTOR signaling converging on the ribosomal protein S6 (S6) in vitro and in vivo. PI3K/Akt/mTOR inhibition was likely responsible for TM's pro-apoptotic effects and anti-metastatic effects in melanoma cell lines as pharmacological inhibition of the pathway using specific inhibitors recapitulated the apoptotic phenotype confirming the sensitivity of melanoma cells to PI3K/Akt/mTOR pathway perturbation.

Results

A screen of pharmacologically active drugs identifies Tegaserod (TM) as having anti-melanoma activity

To identify drugs with novel anti-melanoma activities using an unbiased approach, we tested the NIH Clinical Collection (NCC) composed of 770 small molecules against the murine B16F10 (B16F10) melanoma cell line. A murine cell line was chosen with the intent of testing sensitivity in an in vivo immune-competent syngeneic model where immune cell-host interactions could also be evaluated. B16F10 cells were exposed to a concentration range (10 μM-78 nM) for 72 h and the IC50 values for each compound were determined by assessing cell viability at each dose using the MTT assay (Additional file 1: Figure S1A). From the compounds with determinable IC50 values, many had IC50 values in the low micromolar range (< 2 μM) that could be subdivided into broad pharmacological and/or functional classes (Fig. 1a). Positive hits included members of the statin, antifungal and antihelmintics categories, most of which are already being pre-clinically evaluated as therapeutics in melanoma or other cancers [12–14]. Others,

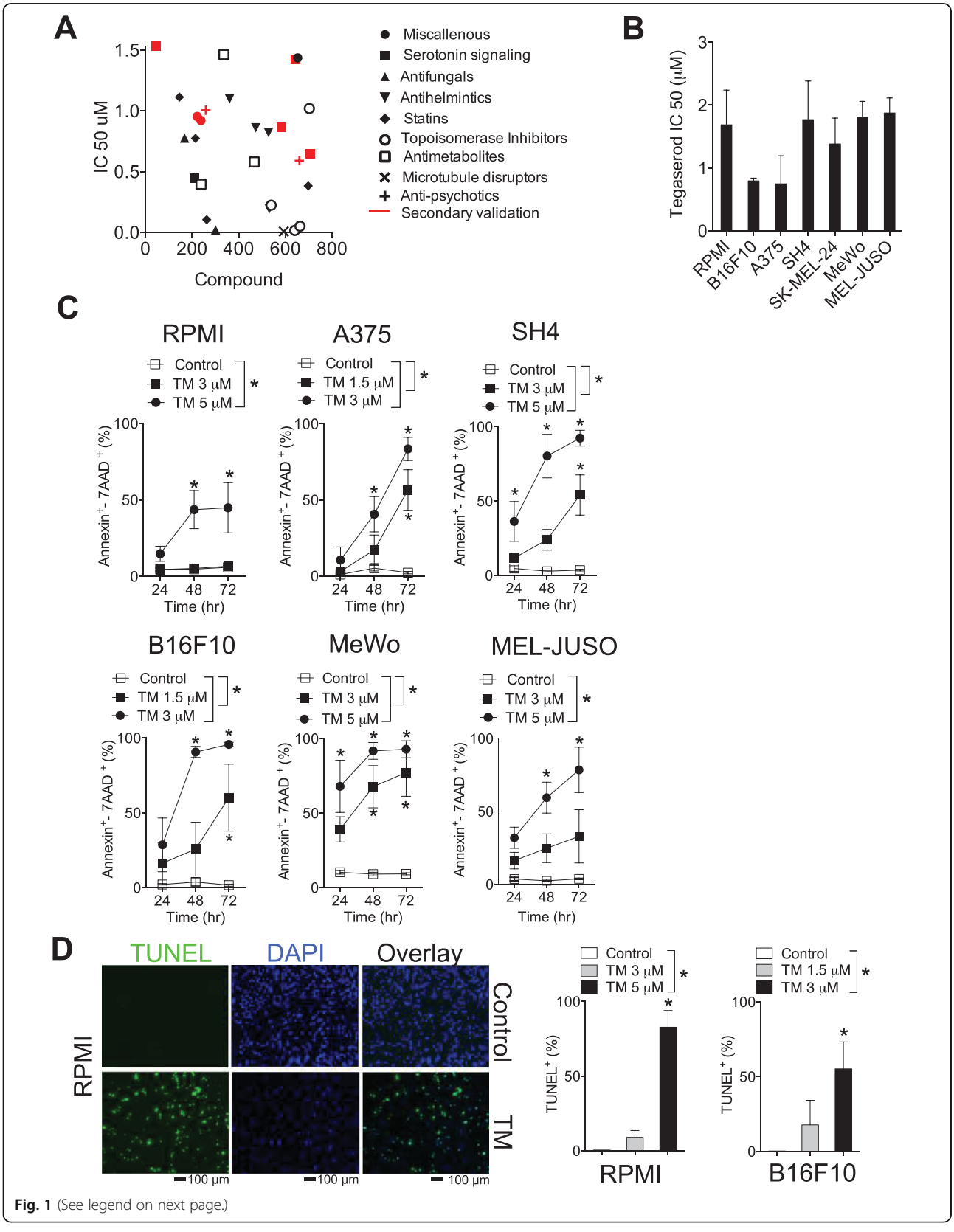

Fig. 1 (See legend on next page.)

(See figure on previous page.)
Fig. 1 A pharmacological screen identifies Tegaserod (TM) as having anti-melanoma activity. **a** B16F10 murine melanoma cells were treated with 770 pharmacologically active compounds at a concentration range of 10 μM-78 nM. Several classes of compounds had anti-cancer activity with IC50 values in the low micromolar range as assessed by MTT assay following 72 h of exposure. **b** Tageserod (TM) a serotonin agonist was further validated and found to have anti-cancer effects in the B16F10 cell line and a panel of human malignant melanoma cell lines, A375, RPMI-7951 (RPMI), SH4, SK-MEL-24, MeWo and MEL-JUSO (n = 3–6). **c** Treatment with low micromolar doses of TM induced apoptosis in a time and dose-dependent manner as assessed by Annexin V/7AAD staining (n = 4–6). Percent apoptosis was ascertained by summing up the Annexin $V^+/7AAD^-$ and Annexin $V^+/7AAD^+$ populations. *$P < 0.05$ as determined by a 2-way ANOVA with a Dunnett's post-hoc test. **d**, left panel Immunofluorescent TUNEL staining of RPMI cells 48 h post TM (5 μM) treatment is shown (A representative image of n = 3–5 is shown). *P < 0.05 as determined by a 1-way ANOVA with a Dunnett's post-hoc test. Scale bar indicates 100 μm. **d**, right panel Quantification of the TUNEL apoptosis staining is shown (n = 3–5). Error bars in the all experiments indicate SEM

belonging to the microtubule disruptors, antimetabolite and topoisomerase inhibitors are already in use as anti-cancer agents [15]. Secondary screening validation focused on compounds in the serotonin signaling categories. Tegaserod (TM), a serotonin agonist had IC50 values in the low micromolar ranges in B16F10 cells as well as several human malignant melanoma cell lines (Fig. 1b). The chosen melanoma cell lines have both wildtype (WT) and mutated BRAF. Specifically, the A375, SH4, RPMI-7951 (RPMI) and SK-MEL-24 harbor the $BRAF^{V600E}$ mutation while the B16F10 murine cells and the human MeWo and MEL-JUSO cell lines are BRAF WT. As the MTT assay is only an indirect indicator of cell viability, we next assessed whether TM is capable of inducing apoptosis. There was a significant time and dose-dependent increase in apoptosis in all cell lines tested as determined by measuring Annexin V and 7AAD staining following treatment with TM (Fig. 1c).

To further verify and characterize cell death observed following treatment of melanoma cells with TM, we assessed apoptosis using TUNEL staining in representative $BRAF^{V600E}$ and BRAF WT melanoma cell lines, RPMI and B16F10 cell lines respectively. Treatment with TM induced an increase in TUNEL staining relative to untreated controls (Fig. 1d). Taken together, we have identified a compound with previously unknown anti-melanoma activity that induces apoptosis in melanoma cell lines.

Tegaserod (TM) exerts its anti-cancer effects independently of serotonin signaling

We wondered whether melanoma cancer cell lines express serotonin receptors 5-HTRs. We mined expression data from the Cancer Cell Line Encyclopedia (CCLE) [16] and found that some receptors particularly HTR7 have a high expression relative to the others in the human melanoma cell lines used in our system (Fig. 2a). TM was synthesized with the primary intent of functioning as a 5-HTR4 agonist [17]. HTR4 mRNA was weakly detected (not detectable in the MeWo cell line) but HTR4 protein expression was undetectable in all melanoma cell lines tested (Fig. 2b).

The main transduction mechanisms of the G-coupled 5-HTR1 and 5-HTR4–7's occur through modulation of cAMP levels [18]. We therefore wondered whether TM alters cAMP levels in melanoma cell lines. Treatment of melanoma cell lines with TM did not alter cAMP levels (Additional file 1: Figure S2A). The expression of genes that have been previously shown to be upregulated upon serotonin (5-HT) treatment through PKA signaling, *PDE2A*, *MET*, *TREM1*, *THBS1*, *SERPINB2* and *S1PR1* [19] was not changed following TM treatment (Additional file 1: Figure S2B). As expected, with the lack of change in cAMP levels, there was no significant increase in the phosphorylation of the cAMP response element binding protein (CREB) in RPMI, B16F10, A375, SK-MEL-24, MeWo cells although p-CREB was increased in SH4 and MEL-JUSO cells (Fig. 2c). To further address the question of whether serotonin agonist signaling is responsible for the apoptotic phenotype, we treated melanoma cancer cells with a wide range (100 μM–0.4 μM) of 5-HT. Treatment with 5-HT had little effect on the melanoma cells (Fig. 2d) and co-treatment of 5-HT with TM had no effect on apoptosis induced by TM (Fig. 2e). Taken together, the anti-melanoma effects caused by TM are likely not being mediated through 5-HTR4 signaling.

Tegaserod (TM) blunts of ribosomal protein S6 (S6) phosphorylation through the PI3K/Akt/mTOR pathway

We wondered what signaling pathways perturbed by treatment with TM are responsible for the apoptotic phenotype in melanoma cells.

Common driver oncogenic pathways critical to melanoma pathogenesis are the MAPK and PI3K/Akt and mTOR pathways [20]. ERK phosphorylation was not significantly affected following treatment of melanoma cells with TM at early time-points, 8 and 18 h, prior to apoptosis induction (Additional file 1: Figure S3). Phosphorylation of ribosomal protein S6 (S6) on the $Ser^{235/236}$ phosphorylation sites was inhibited in all human melanoma cell lines tested (Fig. 3a and Additional file 1: Figure S4A). Phosphorylation of S6 on the $Ser^{240/244}$ phosphorylation sites was also inhibited in the RPMI and SH4 cells lines (Additional file 1: Figure S4B). As there was no difference in S6 phosphorylation between control and TM treated B16F10 cells at 8 and 18 h we also assessed

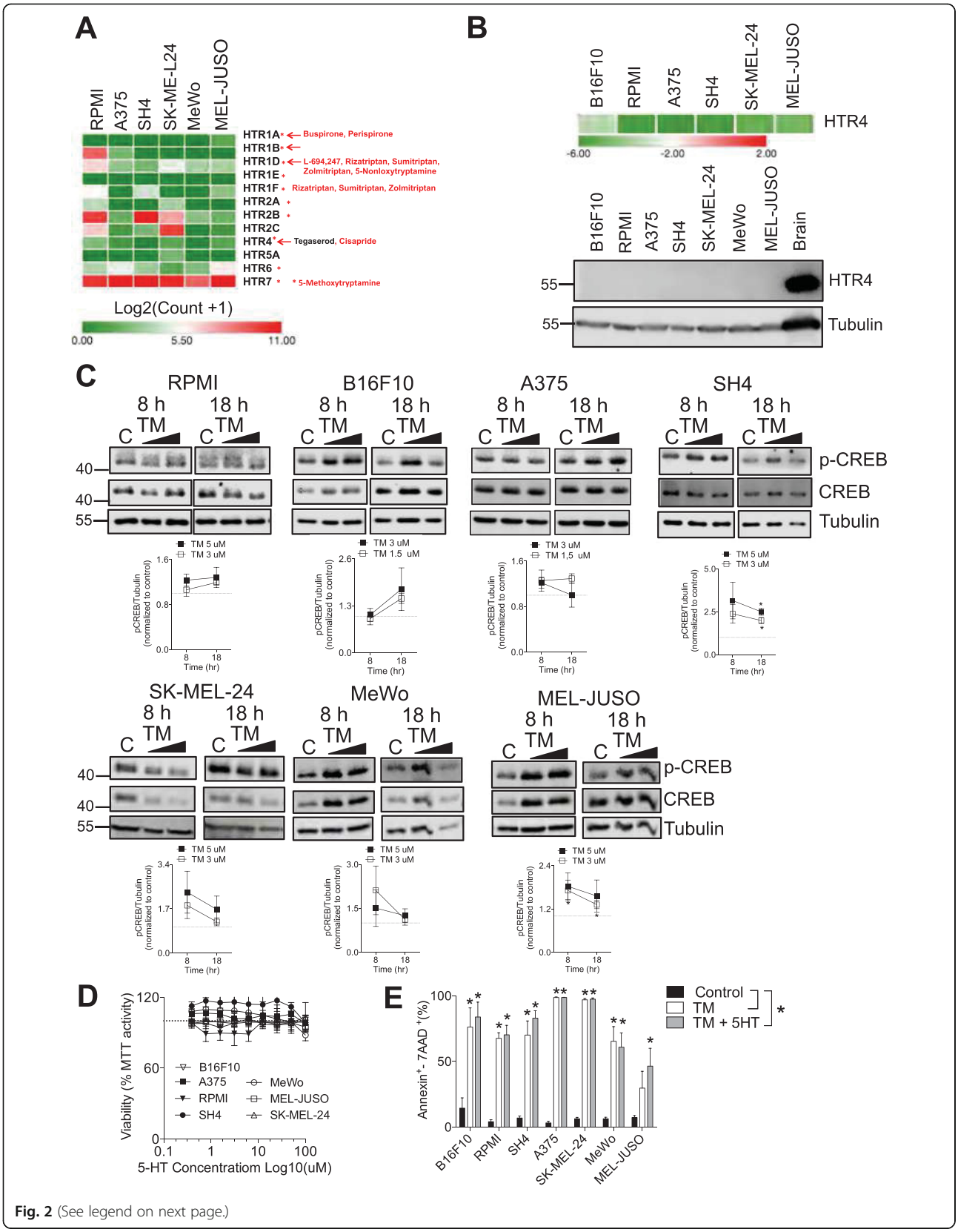

Fig. 2 (See legend on next page.)

(See figure on previous page.)
Fig. 2 TM induces apoptosis independently of serotonin signaling (**a**) Expression of the different serotonin receptors (5-HTRs) in our panel of human melanoma cell lines. Data was mined from the Cancer Cell Line Encyclopedia. **b**, upper panel mRNA expression of 5-HTR4 which is targeted by TM is shown. Expression values are represented as Log10 (CT*HTR4*- CT*GAPDH*) and visualized through Morpheus software (Broad Institute) (n = 3–5). **b**, lower panel Protein expression of HTR4 in melanoma cell lines is shown using mouse brain as a positive control (A representative immunoblot of n = 3 is shown). **c**, upper panel Changes in phosphorylation of the transcription factor CREB 8 and 18 h post TM treatment are shown (A representative immunoblot of n = 3–5 is shown). Quantification of immunoblots is shown in C (lower panel). **d** Treatment with serotonin (5-HT) for 72 h did not have anti-proliferative effects in melanoma cells (n = 3–4). **e** Co-treatment of TM (3 μM for B16F10 and A375 and 5 μM for RPMI, SH4, MeWo and MelJuso melanoma cells) with serotonin (5-HT, 100 μM) did not impact the anti-melanoma effects of TM and did not alter TM induced apoptosis as assessed 72 h post treatment using the Annexin V/7AAD assay ($n = 3–6$). Error bars in the all experiments indicate SEM; *$P < 0.05$ as determined by a Student's t-test (unpaired, 2 tailed), or a one-way ANOVA with a Dunnett's post-hoc test

earlier time-points. At 2 and 4 h post TM treatment, p-S6 was also blunted as assessed by immunofluorescence staining (Fig. 3b).

S6 is phosphorylated by the p70 S6 kinase directly downstream of the mammalian target of rapamycin (mTOR) complex 1 (TORC1) [21]. TORC1 converges on multiple upstream signaling pathways including the MAPK [22] and PI3K/Akt /mTOR pathways [23–25]. The MAPK pathway activity, as assessed by ERK phosphorylation was unperturbed in response to TM treatment (Additional file 1: Figure S3). Through the PI3K/Akt pathways, activated Akt can activate TORC1 through tuberous sclerosis complex 2 (TSC2) or PRAS40 phosphorylation [25, 26]. AKT phosphorylation on Ser473 was suppressed at 8 or 18 h post treatment with TM in RPMI, SH4 and B16F10 cells (Fig. 3a). Not surprisingly, phosphorylation of the kinase directly upstream of S6, p70 S6 at Thr^{421}/Ser^{424}, was also decreased in RPMI, B16F10 and SH4 cells post TM treatment (Fig. 3a). Maximal Akt activation occurs through phosphorylation of two key residues, Ser 473 by mTORC2 [27] or DNA-dependent protein kinase (DNA-PK) [28] and by phosphoinositide-dependent kinase 1 (PDK1) at Thr^{308} [29]. However, as PDK1 phosphorylation at Ser^{241} was not blunted following treatment with TM (Additional file 1: Figure S4B) and phospho-Akt at residue Thr 308 was not detectable in our system under normal cell growth conditions (data not shown) Akt activity by TM might be rather suppressed through mTORC2 or DNA-PK. However, there is the possibility that suppression of phosphorylation at alternative Akt sites occurs through other regulators such CK2 [30] or GSK-3α [31] and this would have to be further explored.

To confirm that melanoma cells used in our system are sensitive to PI3K/Akt/mTOR inhibition, we treated melanoma cells with specific inhibitors of AKT (MK-2206, a highly selective Akt1/2/3 inhibitor), PI3K (ZSTK474, a class I PI3K isoforms inhibitor) and mTOR (KU-0063794, a specific dual-mTOR inhibitor of mTORC1 and mTORC2). All our tested melanoma cell lines both $BRAF^{V600E}$ and BRAF WT were sensitive to AKT, PI3K and pan-mTOR inhibition with IC50 values in a similar range as that of TM (Additional file 1: Figure S5 and Table 1). ZSTK474 and/or MK-2206 and/or KU-0063794 also induced apoptosis in both $BRAF^{V600E}$ and BRAF WT melanoma cell lines (Fig. 3c). Taken together, TM suppresses p-S6 through blunting PI3K/Akt/mTOR signaling in melanoma cells, an effect that is likely responsible for the pro-apoptotic effects observed as treatment with various inhibitors of the pathway was able to recapitulate the phenotype.

Tegaserod (TM) delays tumor growth, reduces metastases, increases survival and suppresses p-S6 in vivo

To evaluate the efficacy of TM against melanoma tumor growth we used a syngeneic immune-competent model. Mice were subcutaneously inoculated with B16F10 cells, and 7 days later, randomized and treated with daily injections of TM or vehicle for 5 days. Treatment significantly decreased tumor growth (Fig. 4a) and resulted in only slight decreases in weight following treatment (Additional file 1: Figure S6A). There were no changes in liver damage markers AST, LDH and ALT (Additional file 1: Figure S6B). The in vitro TM-mediated PI3K/Akt/mTOR signaling inhibition was re-capitulated in vivo. When immunohistochemical staining of tumor tissue harvested 13 days post inoculation was performed for phosphorylation of S6 (Ser235/236), one third of control tumor slides were classified as having a high positive score. This is sharp contrast to tumors from TM treated mice where only one slide scored as having a high positive score (Fig. 4b). Images were scored for positive staining using the IHC profiler which employs an automated, unbiased approach to evaluate antibody staining in tissue sections [32]. Furthermore, tumor lysates from TM treated mice had significantly lower Akt and S6 phosphorylation levels (Fig. 4c).

To assess tumor apoptosis, immunohistochemical staining of tumor tissue harvested 13 days post inoculation was performed for active Caspase-3 and cleaved Caspase-8 (Fig. 4d and Additional file 1: Figure S6D). 50% of tumor slides from TM-treated mice stained for active Caspase-3 had a positive score and the other 50% were scored as low positive. In contrast, tumor slides

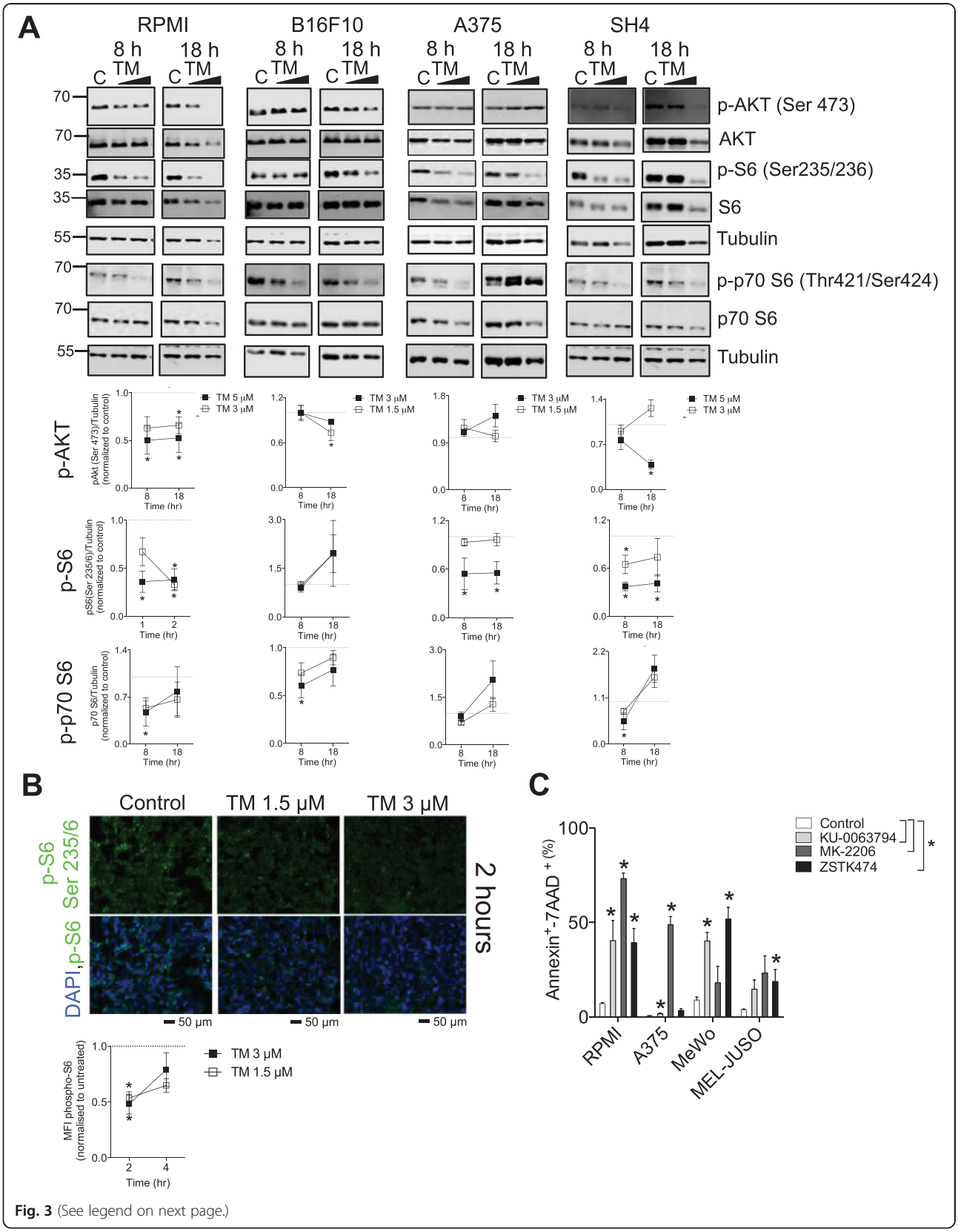

Fig. 3 (See legend on next page.)

(See figure on previous page.)
Fig. 3 TM blunts ribosomal protein S6 (S6) phosphorylation through the PI3K/Akt/mTOR pathway. **a** Treatment with increasing doses of TM at the indicated time-points prior to apoptosis induction decreased phosphorylation of Akt (p-Akt) at Ser 473, phospho-S6 (p-S6) at Ser235/6 and phospho-p70 S6 (p-p70 S6) in RPMI, B16F10, A375 and RPMI cells (representative immunoblots of n = 3–7 are shown) and quantified below. **b** Immunofluorescent p-S6 staining of B16F10 cells treated with TM for 2 h is shown (A representative image of n = 3 is shown) and quantified in B, lower panel). Scale bar indicates 50 μm. **c** Treatment for 48 h with the PI3K inhibitor ZSTK474 (2 μM for MeWo, 6 μM for MEL-JUSO and A375 and 1 μM for RPMI), pan-Akt inhibitor MK-2206 (2 μM for MeWo, 6 μM for MEL-JUSO, 10 μM for A375 and 4 μM for RPMI) and mTORC1/mTORC2 inhibitor KU-0063794 (2 μM for MeWo and 4 μM for all other cell lines) induced apoptosis in melanoma cells as assessed by Annexin V/7AAD staining (n = 3–6). Percent apoptosis was ascertained by summing up the Annexin $V^+/7AAD^-$ and Annexin $V^+/7AAD^+$. Error bars in the all experiments indicate SEM. *$P < 0.05$ as determined by a Student's t-test (unpaired, 2 tailed) or a one-way ANOVA with a Dunnett's post-hoc test

from vehicle-treated mice were 5% negative for cleaved Caspase-3, and only 27% scored positive and 68% scored low positive (Fig. 4d). There was a significantly higher contribution from the high positive stained areas for active Caspase-3 in the tumors of TM-treated mice (Additional file 1: Figure S6C) indicating that TM treatment caused tumor cell apoptosis in vivo. When tumor lysates were probed for cleaved Caspase-8, tumors from TM treated mice demonstrated a trend towards increased cleaved Caspase-8 but differences were not significant (Additional file 1: Figure 6E).

To evaluate the ability of TM to decrease metastasis in vivo, we intravenously injected B16F10 melanoma cells into C57BL/6 J mice and monitored lung metastases in control and TM treated mice. Mice treated with TM had significantly less lung metastases (Fig. 4e). As a result, the mice treated with TM survived significantly longer than control mice (Fig. 4f). Taken together, we have shown that in vivo TM is well tolerated, can retard tumor growth, induces tumor apoptosis and blunts p-S6.

Tegaserod (TM) decreases the infiltration of regulatory T cells and synergizes with BRAF and MEK inhibitors

Next, we wondered whether TM treatment impacted immune infiltrates. We harvested tumors from mice at day 13 post inoculation when there were no significant differences in tumor size and found that the numbers of $NK1.1^+CD3^-$ natural killer (NK) cells, $Ly6C^{high}Ly6G^-$ monocytes, $Ly6C^{low}Ly6G^{high}$ granulocytes and $CD8^+$ T cells were not different between tumors harvested from control and TM treated mice (Fig. 5a). However, tumors harvested from TM treated mice were characterized by lower amounts of infiltrating $CD4^+$ T cells (Fig. 5a). As regulatory $CD4^+CD25^+$ T cells play a crucial role in suppressing anti-tumoral immunity [33] and have been shown to be susceptible to PI3K/PTEN/mTOR axis inhibition [34], we next checked whether there were any differences in the percentage of infiltrating regulatory $CD4^+CD25^+$ T cells between TM treated and control tumors. Not only was the percentage of $CD4^+CD25^+$ T cells lower in tumors harvested from TM-treated mice (Fig. 5b), but the infiltration of FOXP3 expressing $CD4^+$ cells was decreased (Fig. 5c). By contrast, surface markers of exhaustion (PD-1), activation (KLRG1, Granzyme B, perforin, Interferon gamma (IFNγ)) and death (CD95) were no different on tumor infiltrating $CD8^+$ T cells between TM and vehicle treated mice (Fig. 5c).

Any potential novel therapy will not be used as in a mono-therapeutic setting but will be combined with the current standard of care. We therefore ascertained whether TM could be combined with Vemurafenib, a B-Raf inhibitor approved for the treatment of late-stage melanoma [35]. We tested the combination in human cell lines harboring the $BRAF^{V600E}$ mutation targeted by Vemurafenib, namely RPMI, A375 and the SK-MEL-24 cells. TM synergized with Vemurafenib in all cell lines tested (Fig. 5d). Other kinase inhibitors currently in use for the treatment of late stage melanoma include the MEK inhibitor Cobimetinib. TM also synergized with Cobimetinib in A375 cells at higher effective doses (ED75 and ED90) and was additive in RPMI, B16F10, MeWo and MEL-JUSO melanoma cell lines (Fig. 5d). Taken together, we have shown that TM inhibited tumor growth in vivo and can be successfully combined with the current standard of care.

Discussion

Our screen identified several potential hits with anti-melanoma activity including serotonin agonists and other compounds, such as statins, antihelmintics and antifungals which are already being re-purposed as anti-cancer agents pre-clinically or in the clinical setting. The

Table 1 Melanoma cell line sensitivity to PI3K/Akt and mTOR pathway inhibition

Compound	Target	IC50±SEM					
		B16.F10	A375	RPMI	SH4	MeWo	MEL-JUSO
MK-2206	Pan-AKT	0.29±0.05	4.76±0.58	1.92±0.36	3.11±0.91	1.26±0.01	3.03±0.35
ZSTK474	PI3K	0.95±0.33	2.69±1.14	0.51±0.05	2.80±0.81	1.06±0.07	3.47±0.28
KU-0063794	Pan-mTOR	0.68±0.26	1.90±1.45	1.63±0.28	1.71±0.86	0.97±0.05	1.84±0.12

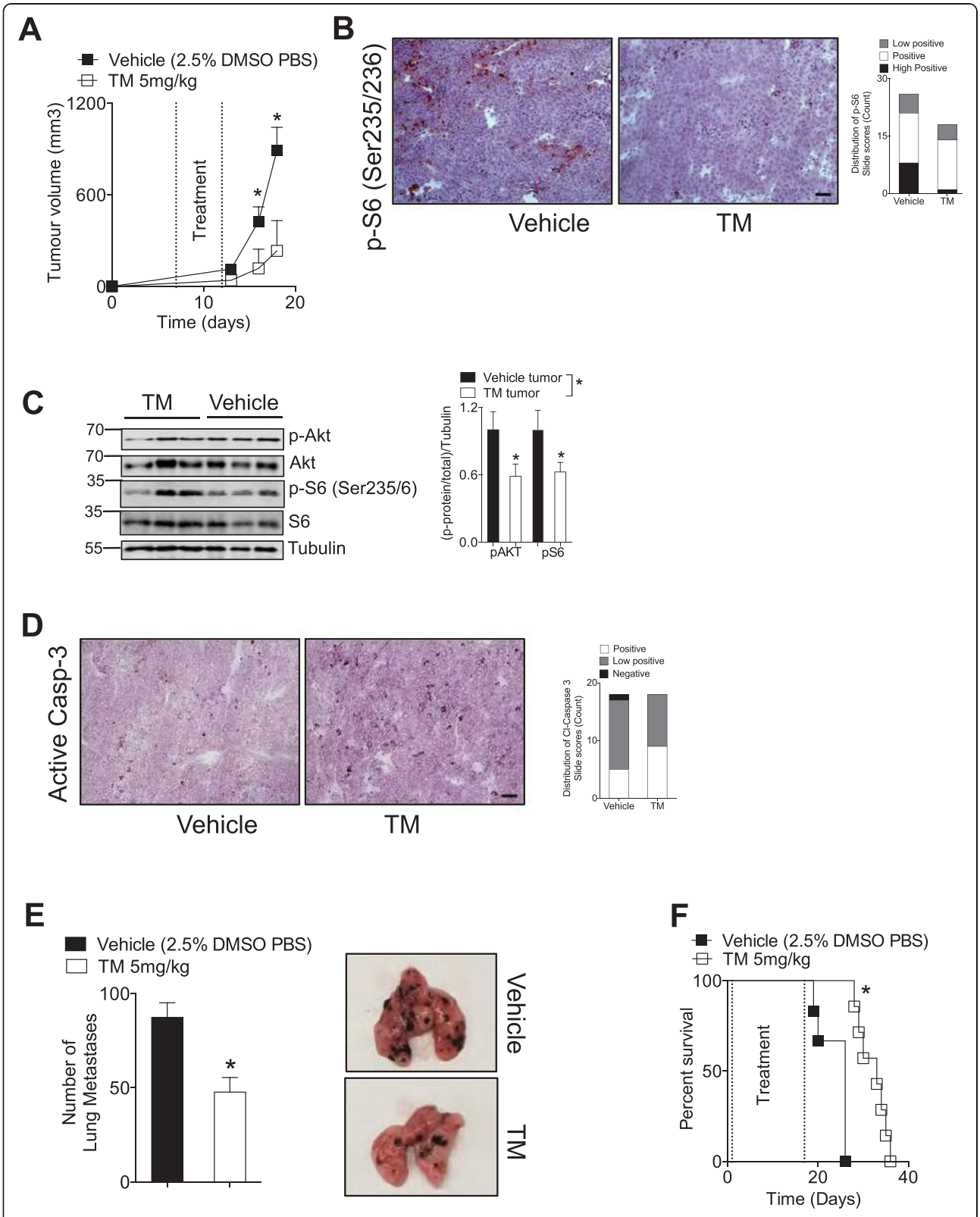

Fig. 4 (See legend on next page.)

(See figure on previous page.)
Fig. 4 Tegaserod (TM) delays tumor growth, induces tumor cell apoptosis and inhibits Akt and p-S6 phosphorylation in vivo. **a** C57BL/6 J mice were subcutaneously injected with 5×10^5 B16F10 cells. Seven days post-tumor injection, mice were randomized and into two groups and treated daily with 5 mg/kg of Tegaserod or vehicle for five consecutive days. **a** Tumor volume was measured for 18 days after which mice were sacrificed (n = 6–8). **b** Mice were sacrificed on Day 13 post tumor-inoculation and immunohistochemical staining of tumor tissue for p-S6 is shown (a representative image of n = 6 mice is shown). A third of pictures from tumors of mice treated with vehicle were classified as 'high positive' for p-S6 compared to only 1 slide from TM treated mice (3–5 pictures from different fields of view were obtained of tumors from each independent mouse, for a total of 26 and 18 tumor pictures for vehicle and TM treated mice respectively). **c**, left panel Immunoblots of tumor lysates from TM or control treated mice confirmed decreased Akt (Ser473) and S6 (Ser235/6) phosphorylation (n = 6–9 mice, with 3 mice being shown on one immunoblot) quantified in **c**, right panel. **d** Mice were sacrificed on Day 13 post tumor-inoculation and **d**, left panel immunohistochemical staining of tumor tissue revealed that tumors of mice treated with TM had increased active Caspase-3 expression (a representative image of n = 6 is shown). **d**, right panel. The relative score distribution of tumor slides is shown (3 pictures from different fields of view were obtained of tumors from each independent mouse (n = 6), for a total of 18 tumor pictures for each stain and treatment group. **e** C57BL/6 J mice were intravenously injected with 2×10^5 B16F10 cells. Starting at day 1 post inoculation, mice were treated with 5 mg/kg of Tegaserod or vehicle three times a week. Mice were sacrificed at Day 14 post tumor inoculation and lung metastases counted with representative lung images shown in the right panel (n = 10). **f** C57BL/6 J mice were intravenously injected with 10^5 B16F10 cells. Starting at day 1 post inoculation, mice were treated with 5 mg/kg of Tegaserod or vehicle three times a week till day 17 post-inoculation. Mice were monitored for survival (n = 6-7). All Scale bars indicate 50 μm. Error bars in the all experiments indicate SEM. *P < 0.05 as determined by a determined by a Student's t-test (unpaired, 2 tailed) or and log-rank test for analysis of Kaplan Meier survival curves

serotonin signaling class of compounds that were positive hits in the original screen included serotonin agonists as well as the anti-depressants indatraline and maprotiline. The latter two are multi-functional and not only prevent the re-uptake of serotonin but also dopamine and norepinephrine and did not have appreciable anti-melanoma activity when compared to the other compounds in the serotonin signaling class including TM. Serotonin signaling occurs when serotonin, a neurotransmitter present in the gut, blood platelets and the central nervous system (CNS), binds to serotonin receptors (5-HTRs) resulting in complex physiological and behavioral changes affecting mood, cognition, digestion, pain perception [18, 36]. The pharmacological opportunities to modulate these physiological processes and impact human disease are vast and have resulted in a plethora of 5-HTR agonist and antagonist ligands. There are seven families of human serotonin receptors mostly part of the G-protein coupled receptor family differentially expressed throughout the CNS, liver, kidney, heart, gut [18]. We were intrigued by the possibility of investigating TM because the role of serotonin signaling in cancer remains controversial. Serotonin and 5-HTR2A agonists were found to induce melanogenesis in melanoma cell lines [9]. Jiang et al. reported increased levels of serotonin and 5-HTR2B in human pancreatic ductal adenocarcinomas which promoted pancreatic tumor growth in mice [37]. Many other studies have similarly reported growth stimulatory effects of serotonin signaling through various 5-HTRs and inhibitory effects of 5-HTR antagonists in many tumor types [38, 39]. However, there have also been reports, albeit much fewer, suggesting that treatment with serotonin agonists might also have anti-cancer effects in glioma [40] and breast cancer cells [41]. Involvement within the autocrine loops and activation of the MAPK, JNK, PI3K/Akt/mTOR [37, 38] pathways has been implicated in serotonin's mitogenic role.

We did not observe any pro or anti-mitogenic effects following treatment with serotonin (5-HT) in melanoma cells. Co-treatment of TM with 5-HT did not effect the compound's ability to induce apoptosis in the melanoma cells. This suggests that the affinity of the synthetic ligand TM is stronger for the 5-HTR's than for the natural ligand 5-HT, and/or that the pro-apoptotic effects of TM can be uncoupled from serotonin signaling. Treatment with 5-HTR ligands, agonists or antagonist presents a complex scenario. As previously reported [38] treatment with one ligand can yield opposing concentration dependent results. Serotonin signaling following TM treatment might occurring through other 5-HTRs. TM has been reported to be an agonist for the 5-HTR1A-D and an antagonist for 5-HTR2A-B [42]. In our case, we used doses in the low micromolar range, high enough to elicit tumor apoptosis inducing pleiotropic effects [42, 43]. Although we did not observe significant changes in cAMP levels and 5-HT responsive genes following TM treatment in most of the cell lines, increased p-CREB levels were observed in the SH4 and MEL-JUSO cells suggesting a possible involvement of other serotonin receptors including ones previously unidentified as being targets for TM. However, other antagonists and agonists present in the screen including the 5-HTR4 agonists (Cisparide) that did not have any anti-cancer effects further suggesting that TM is uniquely acting to distinctly target other molecules, likely upstream receptors or kinases of the PI3K/Akt/mTOR pathways.

The current repertoire of clinically approved treatment options in melanoma encompasses agents that inhibit proliferation and induce cell death [44]. This includes targeted inhibitors of the BRAF pathway and checkpoint inhibitors. The former class of agents such as Vemurafenib cause cell arrest and trigger apoptosis [35, 45] while

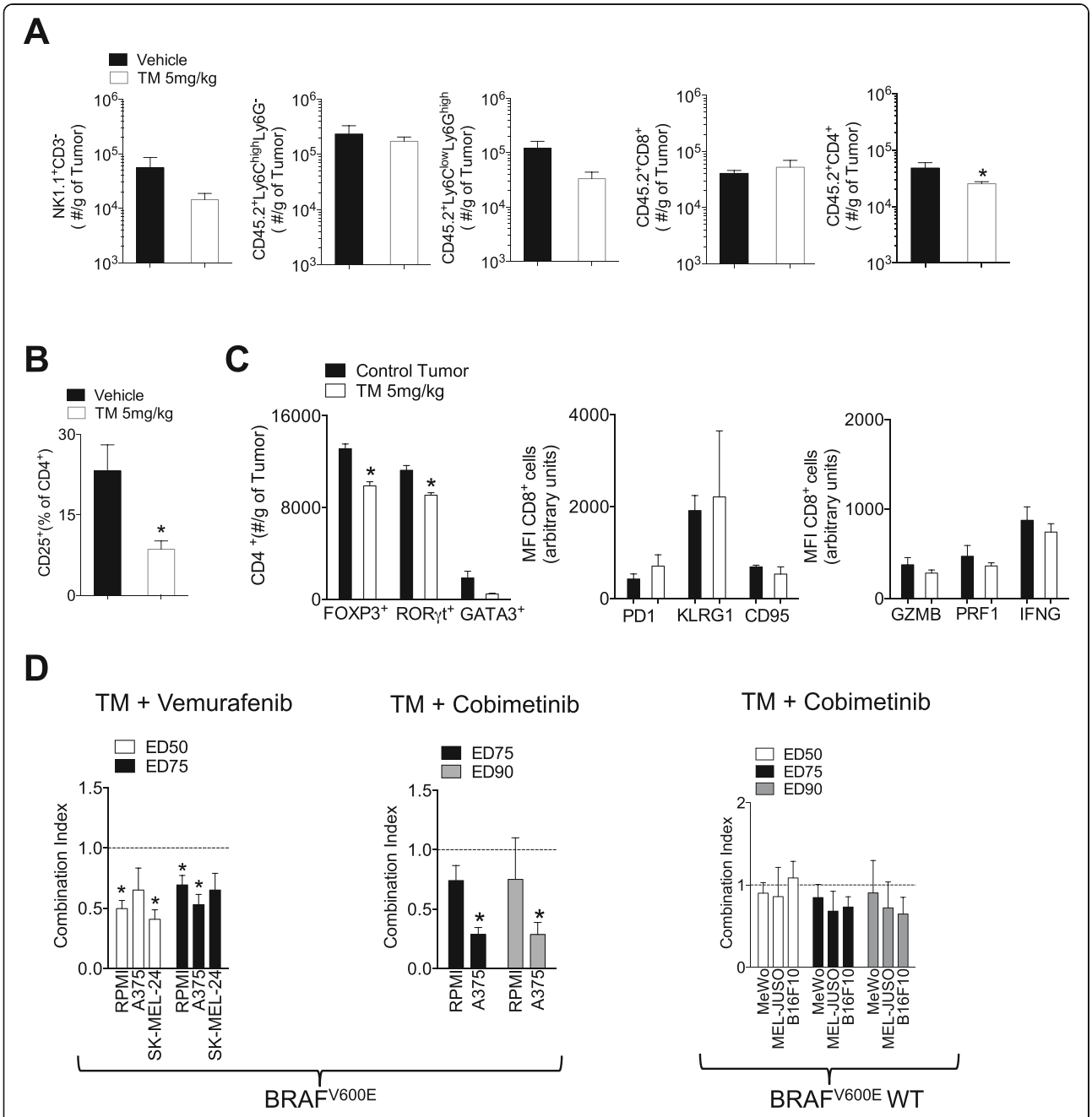

Fig. 5 Tegaserod (TM) decreases tumor infiltration of $CD25^+CD4^+$ T cells and synergizes with Vemurafenib and Cobimetinib. **a-c** C57BL/6 J mice were subcutaneously injected with 5×10^5 B16F10 cells. Seven days post-tumor injection, mice were randomized and into two groups and treated daily with 5 mg/kg of Tegaserod or vehicle for five consecutive days. Mice were sacrificed on Day 13 post tumor-inoculation and tumor infiltrating lymphocytes using were assessed using FACS analysis (n = 3–6). **d** Melanoma cell lines harboring the $BRAF^{V600E}$ mutation, A375, RPMI-7951 (RPMI) and SK-MEL-24 were exposed to a dose range of TM and Vemurafenib in a fixed 1:1 ratio. $BRAF^{V600E}$ and BRAF WT melanoma cell lines were exposed to a dose range of TM and Cobimetinib in a fixed ratio (RPMI, 1:2, A375 64:1, MeWo 4:1, MEL-JUSO 4:1, B16F10 1:1). Synergy was evaluated using the combination index (CI) from the dose-response curves. CI < 1 indicates synergy, CI = 1 indicates additivity, and CI > 1 indicates antagonism. The EC50 (50% effective concentration) and EC75 (75% effective concentration) or EC90 (90% effective concentration) are shown (n = 3–6). *P < 0.05 as determined by a one-sample Student's t-test

the checkpoint inhibitors cause immunogenic cell death through lytic and apoptotic cell death mediated by activated $CD8^+$ T and NK cells respectively [6, 44]. Resistance to the targeted inhibitors and variable checkpoint inhibitor response rates has shifted the focus in recent years interest to finding novel combination

treatments to overcome resistance and increase response rates [7]. Strategies include targeting other forms of cell death such as necroptosis [46], inhibiting MAPK reactivation that occurs following targeted therapy treatment, and concomitantly inhibiting other pathways including the PI3K/Akt/mTOR [47, 48].

Recently, a report has shown phosphorylation of S6 to be marker of sensitivity to BRAF mutated melanoma and that suppression of S6 after MAPK treatment was a predictor of progression-free survival [23]. In our investigation, TM's suppression of p-S6 and its strong synergy with vemurafenib in BRAF mutated human melanoma cell lines is in accordance with the above report. Importantly, TM also suppressed S6 phosphorylation in non-BRAF mutated melanoma cell lines indicating a broader therapeutic potential of TM in patients without the BRAF mutation but where the PI3K/Akt/mTOR pathway is activated such as in patients harboring NRAS mutations [48]. The suppression of S6 phosphorylation is likely mediated by decreased mTORC1 activity as phosphorylation of the direct upstream regulator of S6, p70 S6 kinase was also blunted. mTORC1 integrates several upstream pathways related to cellular growth and metabolism including MAPK through RSK [22], PI3K/Akt [25] as well as the liver kinase B1 (LKB1)-adenosine monophosphate-activated protein kinase (AMPK) [49]. As TM did not perturb the MAPK pathway but decreased Akt phosphorylation at a residue known to be phosphorylated by mTORC2 [27], it's likely that S6 is affected through the PI3K/Akt pathway although the potential contribution of AMPK would also have to be explored. Interestingly, Yoon et al. found that dual mTORC1/2 inhibition following treatment with Torin1 in A375 melanoma cells induced focal adhesion reorganization, increased the size of focal adhesions and increased migration and invasion *in vitro* [29]. TM did not phenocopy Torin 1 using B16F10 cells, as treatment with TM decreased the number metastases in vivo in an immuno-competent murine model where the presence of tumor infiltrating lymphocytes was considered. The immunosuppressive and pro-tumorigenic contribution of regulatory $CD4^+$ T cells in the tumor microenvironment is well established [50]. As the infiltration of FOXP3 expressing $CD4^+$ T cells and regulatory $CD4^+$ T cells in TM treated tumors was decreased, this likely contributes to TM's anti-cancer effects in vivo.

Tegaserod (Zelnorm, Zelmac) which is used for the treatment of irritable bowel syndrome (IBS) [51, 52] was also shown to be effective against chronic constipation [53]. Although Tegaserod was well-tolerated and effective, it was removed off the market in the Unites States in 2007 at the FDA's request [54] chiefly due cardiovascular (CV) safety concerns raised through retrospective clinical trial analysis. However, all adverse cardiovascular events occurred in patients with CV disease and/or CV risk factors. Furthermore, the link between Tegaserod and adverse CV outcomes was not recapitulated in subsequent epidemiological studies [55, 56] which found no association between Tegaserod use and adverse CV's. The tolerability and availability of the drug would likely outweigh the relatively low cardiovascular risk (0.1%) associated with Tegaserod usage especially in melanoma patients with few treatment options. In vivo, TM retarded decreased metastatic and primary tumor growth, induced apoptosis and suppressed p-Akt and p-S6 in tumor cells. TM is available in generic form and has the potential to be re-purposed as an anti-melanoma agent. The dose we used in mice, 5 mg/kg, once daily, is roughly equivalent to a Human Equivalent Dose (HED) [57] of 0.405 mg/kg. Given that TM is available as a 6 mg pill administered twice daily, the doses we used in our in vivo studies are within the physiological range. Furthermore, as the compound synergized with Vemurafenib and other kinase inhibitors currently used in melanoma patients with late-stage disease, this is likely a favorable point of clinical entry especially since most patients eventually develop resistance to Vemurafenib and other kinase inhibitors [7, 47]. Furthermore, as the BRAF WT cohort of patients are a diverse group, treatment options are much less clear cut [44, 58] although immunotherapies, as with $BRAF^{V600E}$ melanoma are a promising albeit costly treatment approach [59]. Currently there are a lot of different combinations in clinical trials using MEK in combination with inhibitors of the PI3K/AKT/mTOR axis [58] (NCT01941927, NCT01363232, NCT01337765).

Conclusions

Taken together, we have identified a compound that is effective in inducing apoptosis in both $BRAF^{V600E}$ and BRAF WT melanoma and has the potential to be readily translated to the clinic especially in the case of BRAF WT melanoma where fewer approved treatment options exist. Tegaserod blunted phosphorylation of S6 through inhibition of the PI3K/Akt/mTOR pathway in vitro and in vivo. Tegaserod synergized with Vemurafenib in $BRAF^{V600E}$ human cell lines and could also be combined with Cobimetinib in BRAF WT cell lines.

Materials and methods

Cell culture and compounds

B16F10, A375, SH4, RPMI-7951 and SK-MEL-24 melanoma cell lines were purchased from ATCC. MeWo and MEL-JUSO cell lines were kindly provided by Dr. A. Roesh (Universitätsklinikum Essen, Essen, Germany). The MEL-JUSO and MeWo cell lines were both originally purchased from ATCC. B16F10 murine cells, A375 and SH4 human malignant melanoma cell lines were maintained

Dulbecco Modified Eagle's Medium (DMEM). Human RPMI-7951 malignant melanoma cells were maintained in Eagle's MEM. SK-MEL-24 were maintained in Eagle in Earle's BSS with non-essential amino acids. MeWo and MEL-JUSO cell lines were maintained in Roswell Park Memorial Institute (RPMI) medium. All media were supplemented with 10% FCS (15% for SK-MEL-24) and penicillin streptomycin. Cells were incubated at 37 °C in 5% CO^2, and all cell lines were routinely confirmed to be mycoplasma-free (MycoAlert Mycoplasma Detection Kit, Lonza). The NIH Clinical Collection (NCC) composed of 770 small molecules mainly dissolved in DMSO at a concentration of 10 μM was obtained from the NIH, Tegaserod (Sigma) was dissolved in DMSO, serotonin (Sigma) was dissolved in water. MK-2206, ZSTK474, KU-0063794, Vemurafenib, Cobimetinib (Selleckchem) were dissolved in DMSO.

MTT assays

For the MTT colorimetric assay, cells were seeded in 96 well plates and viability was assessed following addition of the MTT (Sigma) reagent. Half-maximal inhibitory concentrations (IC50) values were computed from dose–response curves using Prism (v5.0, GraphPad Software).

Flow Cytometry

For Annexin V/7AAD apoptosis assays, trypsinized cells were washed and stained in Annexin V binding buffer (BD Biosciences). Melanoma cells were treated at doses of 2 x – 4x IC50 values for TM and 2 x IC50 for PI3K/Akt/mTOR inhibitors. Stainings of $CD4^+$ cells for FOXP3, RORγ and GATA3 and of $CD8^+$ cells for Granzyme B, perforin and IFNγ were performed using the Foxp3 mouse Treg cell staining buffer kit (eBioscience). Cells were analyzed using FACS (FACS Fortessa, BD Biosciences).

Immunofluorescence

For TUNEL staining, cells were seeded on cover slips, treated and 48 h later fixed by 4% formaldehyde in PBS for 30 min, permeabilized with 0.1% Triton X-100, 0.1% sodium citrate in PBS for 2 min and stained using the TUNEL staining kit as per manufacturer's protocol (Roche). For p-S6 staining, cells seeded on cover slips were stained with primary anti-p-S6 antibody (Ser 235/6, Cell Signaling) overnight, followed by incubation with secondary anti-Rabbit IgG Cy3 conjugate antibody. Cover slips were incubated with DAPI in PBS for 30 min. Images were taken with an Axiocam 503 color microscope (ZEISS).

Immunoblotting

Cells were lysed using boiling hot SDS lysis buffer (1.1% SDS, 11% glycerol, 0.1 mol/L Tris, pH 6.8) with 10% β-mercaptoethanol. Tumor tissue was crushed using a tissue lyser (TissueLyser II, QIAGEN) and cells were gently lysed using Triton X-100. Blots were probed with anti-α-tubulin (Merck), anti-HTR4 (ThermoFischer), anti-cleaved Caspase 8, anti-Akt, anti-p-Akt (Ser 473), anti-S6, anti-p-S6 (Ser235/6, Ser240/4), anti-p70 S6, anti-p-p70 S6 (Thr421/Ser424), anti-p-ERK1/2, anti-ERK1/2, anti-p-CREB (Ser133) and anti-CREB (all from Cell Signaling) and detected using the Odyssey infrared imaging system (Odyssey Fc, LI-COR Biosciences). Immunoblots were quantified using ImageJ.

Combination index (CI) determination

Synergy between TM and Vemurafenib, and Cobimetinib was evaluated by calculating the CI [60]. Dose–response curves were generated for TM, Vemurafenib and Cobimetinib alone and each drug in combination with TM at a constant ratio following compound exposure for 72 h. Viability was assessed by the MTT assay. CompuSyn software was used to evaluate synergy using the median-effect model.

Histology

Histological analysis was performed on snap frozen tissue. Briefly, snap-frozen tissue sections fixed in acetone, blocked with 10% FCS and stained with anti-active Caspase 3 (BD Biosciences), cleaved Caspase 8 (Cell Signaling). For p-S6 (Cell Signaling) staining, snap-frozen tissue sections were fixed in 10% neutral buffered formalin and blocked with 5% FCS/ 0.3% Triton X-100 in PBS. Images were taken with an Axiocam 503 color microscope (ZEISS) and quantified using Image J. For conventional immunohistochemistry tumor slides, IHC profiler Image J plugin was used as previously described in detail [32].

Serum biochemistry

Aspartate aminotransferase (AST), alanine aminotransferase (ALT) and L-Lactatdehydrogenase (LDH) were measured using the automated biochemical analyser Spotchem EZ SP-4430 (Arkray, Amstelveen, Netherlands) and the Spotchem EZ Reagent Strips Liver-1.

Quantitative RT-PCR

RNA was isolated using Trizol (Invitrogen) and RT-PCR analyses were performed using the iTaq™ Universal SYBR® GreenOne-Step RT-qPCR Kit (Biorad) according to the manufacturer's instructions. For analysis, expression levels were normalized to *GADPH*.

Intracellular CAMP assay

Intracellular CAMP levels were determined as per manfacturer's instructions (Enzo Life Biosciences).

Mice and in vivo treatments

C57BL/6 J mice were maintained under specific pathogen-free conditions. Seven to nine week old C57BL/6 J mice were subcutaneously injected with 5×10^5 B16F10 cells. Seven days post injection, when tumor volume reached approximately 50 mm^3, mice were randomized and treated daily for 5 consecutive days with 5 mg/kg Tegaserod or vehicle control (2.5% DMSO in PBS). Tegaserod and vehicle were administered intraperitoneally (i.p.). Tumors were measured using calipers and tumor volume was calculated using the following formula: (tumor length x width^2)/2. For metastases quantification experiments, C57BL/6 J mice were intravenously injected with 2×10^5 B16F10 cells and treatment with Tegaserod and vehicle (administered i.p.) occurred 1 day post inoculation and continued three times weekly till day 14 post inoculation at which time mice were sacrificed. Metastases from lungs, stored in PBS for short term storage, were manually counted. For survival experiments, C57BL/6 J mice were intravenously injected with 10^5 B16F10 cells. Treatment with Tegaserod and vehicle (administered i.p.) occurred 1 day post inoculation and continued three times weekly till day 17 post inoculation. Experiments were performed under the authorization of LANUV in accordance with German law for animal protection.

Data mining using the CCLE

RNA-Seq expression data (Read Count) from the Cancer Cell Line Encyclopedia (CCLE) [16] (Broad Institute and Genomics Institute of the Novartis Research Foundation) for the selected human melanoma cell lines was analyzed using Xena Functional Genomics Explorer [61] and visualized using the MORPHEUS matrix visualization software (https://software.broadinstitute.org/morpheus).

Statistical analyses

Data are expressed as mean ± S.E.M. Statistically significant differences between two groups were determined using the student's t-test and between three or more groups, the one-way ANOVA was used with a post-hoc Dunnett test. To assess significance between Kaplan Meier survival curves, the log-rank test was used. Values of $P < 0.05$ were considered statistically significant.

Supplementary information

Supplementary information accompanies this paper at https://doi.org/10.1186/s13046-020-1539-7.

Additional file 1: Figure S1. B16F10 cells were treated (10 μM-78 nM) for 72 h and IC50 compound values determined. Compounds for which IC50 values were not determinable or were above 10 μM were placed on the 10 μM line. **Figure S2.** (A) Treatment at the indicated time points with TM (3 μM for B16F10 and A375, 5 μM for RPMI and SH4) did not induce changes in CAMP levels (n = 3-4). (B) Treatment with TM for 18 h did not induce changes in serotonin responsive genes. Expression was normalized to GAPDH (n = 3–4). **Figure S3.** TM did not affect the MAPK pathway. Melanoma cells were treated as indicated with increasing concentrations of TM (representative immunoblots of n = 3-5 are shown). Blots are quantified in (B). **Figure S4.** (A) Changes in phospho-S6 (p-S6) at Ser235/6 in MeWo and MEL-JUSO melanoma cells (n = 5–6) following TM treatment are shown. (B) Changes in p-S6 (Ser240/244) (n = 2–3) and p-PDK1 (Ser241) (n = 3–4) following treatment with TM are shown. **Figure S5.** Dose response curves following treatment with the PI3K inhibitor ZSTK474, pan-Akt inhibitor MK-2206 and mTORC1/mTORC2 inhibitor KU-0063794 are shown (n = 3–4). **Figure S6.** (A) TM-treated mice as described in Fig. 4a. experienced a small decrease in body weight (n = 6–8). (B) Treatment with TM did not alter liver damage parameters (n = 3). (C) Quantification of the active Caspase-3 staining for Fig. 4d is shown (n = 6 mice). (D) Immunohistochemical staining of tumor tissue for cleaved Caspase-8 is shown and quantified (n = 6 mice). (E) Tumor lysates probed for cleaved Caspase-8 are shown (n = 6–9 mice, with 3 mice shown). Error bars in all experiments indicate SEM. *$P < 0.05$ as determined by a Student's t-test (unpaired, 2 tailed) or a one-way ANOVA with a Dunnett's post-hoc test.

Abbreviations

ALT: Alanine aminotransferase; AST: Aspartate aminotransferase; CCLE: Cancer Cell Line Encyclopedia; CREB: CAMP response element binding protein; IC50: Half maximal inhibitory concentrations; JNK: c-Jun N-terminal kinases; LDH: Lactate dehydrogenase; MAPK: Mitogen-activated protein kinase; NCC: NIH Clinical Collection; PKA: Protein kinase A; TM: Tegaserod; TUNEL: Terminal deoxynucleotidyl transferase dUTP nick end labeling

Acknowledgements

We thank Professor A. Rösch, University of Duisburg-Essen, Essen, Germany for providing the MeWo and MEL-JUSO melanoma cell lines.

Availability of data and materials

All data are available within the article and supplementary files, or available from the authors upon request.

Authors' contributions

WL, PS, HCX, NUG, FC, RW and AAP performed the experiments. AAP directed the study and wrote the manuscript. KSL, PAL, DH, BH, and JG discussed the project and provided suggestions. PAL funded and supervised the study. All authors read and approved the final manuscript.

Funding

This work was supported by the funds from the Deutsche Forschungsgemeinschaft (DFG) SFB974, RTG1949 and the Düsseldorf School of Oncology (DSO).

Ethics approval and consent to participate

Experiments were performed under the authorization of LANUV in accordance with German law for animal protection.

Consent for publication

All authors have agreed to the publication of this manuscript.

Competing interests

The authors have declared that no competing interests exist.

Author details

[1]Department of Molecular Medicine II, Medical Faculty, Heinrich-Heine-University, Universitätsstraße 1, 40225 Düsseldorf, Germany. [2]Institute of Immunology, Medical Faculty, University of Duisburg-Essen, Hufelandstrasse 55, 45147 Essen, Germany. [3]Institute of Human Genetics, Heinrich-Heine-University, Universitätsstrasse 1, 40225 Düsseldorf, Germany. [4]Department of Gastroenterology, Hepatology and Infectious Diseases, Heinrich-Heine-University, Moorenstrasse 5, 40225 Düsseldorf, Germany. [5]Department of Dermatology, Medical Faculty, Heinrich-Heine-University, Universitätsstraße 1, 40225 Düsseldorf, Germany.

Received: 23 September 2019 Accepted: 5 February 2020
Published online: 21 February 2020

References

1. Shellenberger R, Nabhan M, Kakaraparthi S. Melanoma screening: a plan for improving early detection. Ann Med. 2016;48(3):142–8.
2. NA HN, Krapcho M, Miller D, Bishop K, Kosary CL, Yu M, Ruhl J, Tatalovich Z, Mariotto A, Lewis DR, Chen HS, Feuer EJ, Cronin KA, editors. SEER Cancer Statistics Review, 1975-2014. Bethesda, https://seer.cancer.gov/csr/1975_2014/, based on November 2016 SEER data submission, posted to the SEER web site, April 2017: National Cancer Institute; 2017.
3. Rozeman EA, Dekker TJA, Haanen J, Blank CU. Advanced Melanoma: Current Treatment Options, Biomarkers, and Future Perspectives. Am J Clin Dermatol. 2018;19(3):303-17.
4. Eggermont AM, Chiarion-Sileni V, Grob JJ, Dummer R, Wolchok JD, Schmidt H, et al. Adjuvant ipilimumab versus placebo after complete resection of high-risk stage III melanoma (EORTC 18071): a randomised, double-blind, phase 3 trial. Lancet Oncol. 2015;16(5):522–30.
5. Vermaelen K, Waeytens A, Kholmanskikh O, Van den Bulcke M, Van Valckenborgh E. Perspectives on the integration of Immuno-Oncology Biomarkers and drugs in a Health Care setting. Semin Cancer Biol. 2018; 52(Pt 2):166-77.
6. Schachter J, Ribas A, Long GV, Arance A, Grob JJ, Mortier L, et al. Pembrolizumab versus ipilimumab for advanced melanoma: final overall survival results of a multicentre, randomised, open-label phase 3 study (KEYNOTE-006). Lancet. 2017;390(10105):1853–62.
7. Keller HR, Zhang X, Li L, Schaider H, Wells JW. Overcoming resistance to targeted therapy with immunotherapy and combination therapy for metastatic melanoma. Oncotarget. 2017;8(43):75675–86.
8. Ashburn TT, Thor KB. Drug repositioning: identifying and developing new uses for existing drugs. Nat Rev Drug Discov. 2004;3(8):673–83.
9. Lee HJ, Park MK, Kim SY, Park Choo HY, Lee AY, Lee CH. Serotonin induces melanogenesis via serotonin receptor 2A. Br J Dermatol. 2011;165(6):1344–8.
10. Weidmann C, Berube J, Piquet L, de la Fouchardiere A, Landreville S. Expression of the serotonin receptor 2B in uveal melanoma and effects of an antagonist on cell lines. Clin Exp Metastasis. 2018;35(3):123–34.
11. Uzawa K, Kasamatsu A, Shimizu T, Saito Y, Baba T, Sakuma K, et al. Suppression of metastasis by mirtazapine via restoration of the Lin-7C/beta-catenin pathway in human cancer cells. Sci Rep. 2014;4:5433.
12. Minden MD, Dimitroulakos J, Nohynek D, Penn LZ. Lovastatin induced control of blast cell growth in an elderly patient with acute myeloblastic leukemia. Leuk Lymphoma. 2001;40(5–6):659–62.
13. Spagnuolo PA, Hu J, Hurren R, Wang X, Gronda M, Sukhai MA, et al. The antihelmintic flubendazole inhibits microtubule function through a mechanism distinct from Vinca alkaloids and displays preclinical activity in leukemia and myeloma. Blood. 2010;115(23):4824–33.
14. Liang G, Liu M, Wang Q, Shen Y, Mei H, Li D, et al. Itraconazole exerts its anti-melanoma effect by suppressing hedgehog, Wnt, and PI3K/mTOR signaling pathways. Oncotarget. 2017;8(17):28510–25.
15. Cameron D, Morden JP, Canney P, Velikova G, Coleman R, Bartlett J, et al. Accelerated versus standard epirubicin followed by cyclophosphamide, methotrexate, and fluorouracil or capecitabine as adjuvant therapy for breast cancer in the randomised UK TACT2 trial (CRUK/05/19): a multicentre, phase 3, open-label, randomised, controlled trial. Lancet Oncol. 2017;18(7): 929–45.
16. Barretina J, Caponigro G, Stransky N, Venkatesan K, Margolin AA, Kim S, et al. The Cancer cell line encyclopedia enables predictive modelling of anticancer drug sensitivity. Nature. 2012;483(7391):603–7.
17. Mikami T, Sugimoto H, Naganeo R, Ohmi T, Saito T, Eda H. Contribution of active and inactive states of the human 5-HT4d receptor to the functional activities of 5-HT4-receptor agonists. J Pharmacol Sci. 2008;107(3):251–9.
18. Nichols DE, Nichols CD. Serotonin receptors. Chem Rev. 2008;108(5):1614–41.
19. Dominguez-Soto A, Usategui A, Casas-Engel ML, Simon-Fuentes M, Nieto C, Cuevas VD, et al. Serotonin drives the acquisition of a profibrotic and anti-inflammatory gene profile through the 5-HT7R-PKA signaling axis. Sci Rep. 2017;7(1):14761.
20. Paluncic J, Kovacevic Z, Jansson PJ, Kalinowski D, Merlot AM, Huang ML, et al. Roads to melanoma: key pathways and emerging players in melanoma progression and oncogenic signaling. Biochim Biophys Acta. 2016;1863(4):770–84.
21. Burnett PE, Barrow RK, Cohen NA, Snyder SH, Sabatini DM. RAFT1 phosphorylation of the translational regulators p70 S6 kinase and 4E-BP1. Proc Natl Acad Sci U S A. 1998;95(4):1432–7.
22. Roux PP, Shahbazian D, Vu H, Holz MK, Cohen MS, Taunton J, et al. RAS/ERK signaling promotes site-specific ribosomal protein S6 phosphorylation via RSK and stimulates cap-dependent translation. J Biol Chem. 2007;282(19):14056–64.
23. Corcoran RB, Rothenberg SM, Hata AN, Faber AC, Piris A, Nazarian RM, et al. TORC1 suppression predicts responsiveness to RAF and MEK inhibition in BRAF-mutant melanoma. Sci Transl Med. 2013;**5**(196):196ra198.
24. Kleffel S, Posch C, Barthel SR, Mueller H, Schlapbach C, Guenova E, et al. Melanoma cell-intrinsic PD-1 receptor functions promote tumor growth. Cell. 2015;162(6):1242–56.
25. Manning BD, Tee AR, Logsdon MN, Blenis J, Cantley LC. Identification of the tuberous sclerosis complex-2 tumor suppressor gene product tuberin as a target of the phosphoinositide 3-kinase/akt pathway. Mol Cell. 2002;10(1):151–62.
26. Meyuhas O. Ribosomal protein S6 phosphorylation: four decades of research. Int Rev Cell Mol Biol. 2015;320:41–73.
27. Sarbassov DD, Guertin DA, Ali SM, Sabatini DM. Phosphorylation and regulation of Akt/PKB by the rictor-mTOR complex. Science (New York, N Y). 2005;307(5712):1098–101.
28. Feng J, Park J, Cron P, Hess D, Hemmings BA. Identification of a PKB/Akt hydrophobic motif Ser-473 kinase as DNA-dependent protein kinase. J Biol Chem. 2004;279(39):41189–96.
29. Yoon S-O, Shin S, Karreth FA, Buel GR, Jedrychowski MP, Plas DR, et al. Focal Adhesion- and IGF1R-Dependent Survival and Migratory Pathways Mediate Tumor Resistance to mTORC1/2 Inhibition. Mol Cell. 2017;67(3):512–27 e514.
30. Di Maira G, Salvi M, Arrigoni G, Marin O, Sarno S, Brustolon F, et al. Protein kinase CK2 phosphorylates and upregulates Akt/PKB. Cell Death Differ. 2005; 12(6):668–77.
31. Gulen MF, Bulek K, Xiao H, Yu M, Gao J, Sun L, et al. Inactivation of the enzyme GSK3alpha by the kinase IKKi promotes AKT-mTOR signaling pathway that mediates interleukin-1-induced Th17 cell maintenance. Immunity. 2012;37(5):800–12.
32. Varghese F, Bukhari AB, Malhotra R, De A. IHC profiler: an open source plugin for the quantitative evaluation and automated scoring of immunohistochemistry images of human tissue samples. PLoS One. 2014;9(5):e96801.
33. Ohue Y, Nishikawa H. Regulatory T (Treg) cells in cancer: can Treg cells be a new therapeutic target? Cancer Sci. 2019;110(7):2080–9.
34. Ali K, Soond DR, Pineiro R, Hagemann T, Pearce W, Lim EL, et al. Inactivation of PI(3)K p110delta breaks regulatory T-cell-mediated immune tolerance to cancer. Nature. 2014;510(7505):407–11.
35. Larkin J, Del Vecchio M, Ascierto PA, Krajsova I, Schachter J, Neyns B, et al. Vemurafenib in patients with BRAF(V600) mutated metastatic melanoma: an open-label, multicentre, safety study. Lancet Oncol. 2014;15(4):436–44.
36. Berger M, Gray JA, Roth BL. The expanded biology of serotonin. Annu Rev Med. 2009;60:355–66.
37. Jiang SH, Li J, Dong FY, Yang JY, Liu DJ, Yang XM, et al. Increased serotonin signaling contributes to the Warburg effect in pancreatic tumor cells under metabolic stress and promotes growth of pancreatic tumors in mice. Gastroenterology. 2017;153(1):277–91 e219.
38. Sarrouilhe D, Clarhaut J, Defamie N, Mesnil M. Serotonin and cancer: what is the link? Curr Mol Med. 2015;15(1):62–77.
39. Etxabe A, Lara-Castillo MC, Cornet-Masana JM, Banus-Mulet A, Nomdedeu M, Torrente MA, et al. Inhibition of serotonin receptor type 1 in acute myeloid leukemia impairs leukemia stem cell functionality: a promising novel therapeutic target. Leukemia. 2017;31(11):2288–302.
40. Pollard SM, Yoshikawa K, Clarke ID, Danovi D, Stricker S, Russell R, et al. Glioma stem cell lines expanded in adherent culture have tumor-specific phenotypes and are suitable for chemical and genetic screens. Cell Stem Cell. 2009;4(6):568–80.
41. Jose J, Tavares CDJ, Ebelt ND, Lodi A, Edupuganti R, Xie X, et al. Serotonin Analogues as Inhibitors of Breast Cancer Cell Growth. Med Chem Lett. 2017; 8:1072–6.
42. De Maeyer JH, Lefebvre RA, Schuurkes JA. 5-HT4 receptor agonists: similar but not the same. Neurogastroenterol Motil. 2008;20(2):99–112.
43. Beattie DT, Smith JA, Marquess D, Vickery RG, Armstrong SR, Pulido-Rios T, et al. The 5-HT4 receptor agonist, tegaserod, is a potent 5-HT2B receptor antagonist in vitro and in vivo. Br J Pharmacol. 2004;143(5):549–60.
44. Mattia G, Puglisi R, Ascione B, Malorni W, Care A, Matarrese P. Cell death-based treatments of melanoma:conventional treatments and new therapeutic strategies. Cell Death Dis. 2018;9(2):112.

45. Joseph EW, Pratilas CA, Poulikakos PI, Tadi M, Wang W, Taylor BS, et al. The RAF inhibitor PLX4032 inhibits ERK signaling and tumor cell proliferation in a V600E BRAF-selective manner. Proc Natl Acad Sci U S A. 2010;107(33):14903–8.
46. Broussard L, Howland A, Ryu S, Song K, Norris D, Armstrong CA, et al. Melanoma cell death mechanisms. Chonnam Med J. 2018;54(3):135–42.
47. Torres-Collado AX, Knott J, Jazirehi AR. Reversal of Resistance in Targeted Therapy of Metastatic Melanoma: Lessons Learned from Vemurafenib (BRAFV600E-Specific Inhibitor). Cancers (Basel). 2018;10(6):157-76.
48. Posch C, Moslehi H, Feeney L, Green GA, Ebaee A, Feichtenschlager V, et al. Combined targeting of MEK and PI3K/mTOR effector pathways is necessary to effectively inhibit NRAS mutant melanoma in vitro and in vivo. Proc Natl Acad Sci U S A. 2013;110(10):4015–20.
49. Inoki K, Ouyang H, Zhu T, Lindvall C, Wang Y, Zhang X, et al. TSC2 integrates Wnt and energy signals via a coordinated phosphorylation by AMPK and GSK3 to regulate cell growth. Cell. 2006;126(5):955–68.
50. Togashi Y, Shitara K, Nishikawa H. Regulatory T cells in cancer immunosuppression - implications for anticancer therapy. Nat Rev Clin Oncol. 2019;16(6):356–71.
51. Muller-Lissner SA, Fumagalli I, Bardhan KD, Pace F, Pecher E, Nault B, et al. Tegaserod, a 5-HT(4) receptor partial agonist, relieves symptoms in irritable bowel syndrome patients with abdominal pain, bloating and constipation. Aliment Pharmacol Ther. 2001;15(10):1655–66.
52. Nyhlin H, Bang C, Elsborg L, Silvennoinen J, Holme I, Ruegg P, et al. A double-blind, placebo-controlled, randomized study to evaluate the efficacy, safety and tolerability of tegaserod in patients with irritable bowel syndrome. Scand J Gastroenterol. 2004;39(2):119–26.
53. Johanson JF, Wald A, Tougas G, Chey WD, Novick JS, Lembo AJ, et al. Effect of tegaserod in chronic constipation: a randomized, double-blind, controlled trial. Clin Gastroenterol Hepatol. 2004;2(9):796–805.
54. Thompson CA. Novartis suspends tegaserod sales at FDA's request. Am J Health Syst Pharm. 2007;64(10):1020.
55. Anderson JL, May HT, Bair TL, Muhlestein JB, Horne BD, Carlquist JF. Lack of association of tegaserod with adverse cardiovascular outcomes in a matched case-control study. J Cardiovasc Pharmacol Ther. 2009;14(3):170–5.
56. Loughlin J, Quinn S, Rivero E, Wong J, Huang J, Kralstein J, et al. Tegaserod and the risk of cardiovascular ischemic events: an observational cohort study. J Cardiovasc Pharmacol Ther. 2010;15(2):151–7.
57. Nair AB, Jacob S. A simple practice guide for dose conversion between animals and human. J Basic Clin Pharm. 2016;7(2):27–31.
58. Johnpulle RAN, Johnson DB, Sosman JA. Molecular targeted therapy approaches for BRAF wild-type melanoma. Curr Oncol Rep. 2016;18(1):6.
59. Larkin J, Lao CD, Urba WJ, McDermott DF, Horak C, Jiang J, et al. Efficacy and safety of Nivolumab in patients with BRAF V600 mutant and BRAF wild-type advanced melanoma: a pooled analysis of 4 clinical trials. JAMA Oncol. 2015;1(4):433–40.
60. Chou TC, Talalay P. Quantitative analysis of dose-effect relationships: the combined effects of multiple drugs or enzyme inhibitors. Adv Enzym Regul. 1984;22:27–55.
61. Goldman M, Craft B, Swatloski T, Cline M, Morozova O, Diekhans M, et al. The UCSC Cancer genomics browser: update 2015. Nucleic Acids Res. 2015; 43(Database issue):D812–7.

Publisher's Note

cancers

MDPI

Review

Senescent Tumor CD8$^+$ T Cells: Mechanisms of Induction and Challenges to Immunotherapy

Wei Liu [1,†], Paweł Stachura [1,†], Haifeng C. Xu [1], Sanil Bhatia [2], Arndt Borkhardt [2], Philipp A. Lang [1] and Aleksandra A. Pandyra [1,2,3,*]

1 Department of Molecular Medicine II, Medical Faculty, Heinrich-Heine-University, 40225 Düsseldorf, Germany; weliu100@uni-duesseldorf.de (W.L.); stachura@uni-duesseldorf.de (P.S.); xuh@uni-duesseldorf.de (H.C.X.); langp@uni-duesseldorf.de (P.A.L.)

2 Department of Pediatric Oncology, Hematology and Clinical Immunology, Medical Faculty, Center of Child and Adolescent Health, Heinrich-Heine-University, 40225 Düsseldorf, Germany; Sanil.Bhatia@uni-duesseldorf.de (S.B.); arndt.borkhardt@hhu.de (A.B.)

3 Department of Gastroenterology, Hepatology, and Infectious Diseases, Heinrich-Heine-University, 40225 Düsseldorf, Germany

* Correspondence: aleksandra.pandyra@uni-duesseldorf.de; Tel.: +49-211-81-17258

† These authors contributed equally to this work.

Received: 7 September 2020; Accepted: 29 September 2020; Published: 30 September 2020

Simple Summary: Immunotherapies harness the hosts' immune system to combat cancer and are currently used to treat many tumor types. Immunotherapies mainly target T cells, the major immune population responsible for tumor-cell killing. One of the reasons that T cells may not respond to immunotherapeutic treatment is that they are in a dysfunctional state termed senescence. This review seeks to describe the molecular mechanisms that characterize and induce T cell senescence within the context of the tumor microenvironment and how this might affect treatment responses.

Abstract: The inability of tumor-infiltrating T lymphocytes to eradicate tumor cells within the tumor microenvironment (TME) is a major obstacle to successful immunotherapeutic treatments. Understanding the immunosuppressive mechanisms within the TME is paramount to overcoming these obstacles. T cell senescence is a critical dysfunctional state present in the TME that differs from T cell exhaustion currently targeted by many immunotherapies. This review focuses on the physiological, molecular, metabolic and cellular processes that drive CD8$^+$ T cell senescence. Evidence showing that senescent T cells hinder immunotherapies is discussed, as are therapeutic options to reverse T cell senescence.

Keywords: CD8$^+$ T cells; senescence; immunotherapy; metabolism

1. Introduction

Harnessing the immune system to treat solid and hematological malignancies has ushered a novel therapeutic era. The tumor micro-environment (TME) is complex, with many targeting opportunities due to the signaling networks and cross-talk between immune, tumor and stromal cells. However, the modulation of cytotoxic antigen-activated CD8$^+$ T (T_c) cells has been at the forefront of the immunotherapy revolution [1]. The antigen-specific process requires the engagement of the T cell antigen receptor (TCR)-CD3 complex on T_c cells with a major histocompatibility complex (MHC) class I-bound tumor antigen-derived peptide as well as co-stimulatory signals. Responsible for the direct tumor cell killing through granule exocytosis [2], T_c cells are integral in eradicating tumors and are currently targeted by many approved immunotherapies. The monoclonal antibody checkpoint

inhibitors such as nivolumab [3] are currently used to treat solid tumors, and they target the inhibitory programmed cell death 1 (PD-1) [4] receptor expressed on T cells. In the adoptive T cell therapy field, a patient's T cells are expanded ex vivo, transduced with synthetic chimeric antigen receptors (CAR) targeting a tumor specific target antigen such as CD19, and transferred back to lymphodepleted patients. Currently approved CAR-T cell therapies include the second generation anti-CD19 CAR T-cell products axicabtagene ciloleucel and tisagenlecleucel for the treatment of B-cell malignancies [5,6]. Many more T cell based therapies are currently in the experimental phase of pre-clinical or clinical testing [7]. While immunotherapies have made remarkable progress in increasing the survival of some patients, low response rates, toxicities, as well as lack of available bio-markers in predicting response, make the successful implementation of these therapies challenging. A major obstacle is the inability to effectively target T_c cells. This can occur through T_c intrinsic or acquired resistance helped by dysfunctional states present within the immunosuppressive networks [8] of the TME: exhaustion and senescence. While T cell exhaustion has been extensively studied and targeted, T cell senescence, especially within the context of anti-tumor immunity, is an emerging concept in the field of T cell dysfunction. This review focuses on senescence in the $CD8^+$ T cell compartment. It aims to explore the different mechanisms that induce senescence in the context of TME, ways in which T cell senescence affects responses to immunotherapies and how T cell senescence can be therapeutically reversed.

2. Exhaustion and Senescence

Both exhausted and senescent T cells have been found to accumulate during chronic viral infections [9,10] and cancers [11,12]. Exhaustion and senescence are both considered dysfunctional states. They are characterized by dampened granzyme B (GzmB)—mediated effector function and impaired proliferation [13]. However, they are defined by distinct surface marker, cytokine, transcriptional and metabolic profiles (Table 1).

Table 1. Characteristics of senescent and exhausted T cells.

	Senescent T Cells	**Exhausted T Cells**
Stimulus	Repetitive Ag Stimulation, Stress	Continuous Ag Stimulation
Cytokine Secretion	↑ IFN–γ, IL-6, IL-8, IL-10, TNF, TGF-β	↓ IFN-γ, IL-2, TNF
Surface Markers	↑ CD57, Tim-3, TGIT, CD45RA, KLRG1, ↓ CD28, CD27	↑ PD-1, LAG-3, CD 160, 2B4, CTLA-4, Tim-3, TGIT
Metabolism	↑ Glycolysis, ↓ Mitochondrial Biogenesis	↓ Glycolysis, ↓ Mitochondrial Biogenesis
Transcriptional	T-bet	Eomes, NFAT, TOX, T-bet, Nr4a
Effector Functions	↓ Granzyme B, ↓Perforin	↓ Granzyme B
Phenotypic Characteristic	↓ Proliferative Capacity, ↑ DNA Damage Molecules, ↑ SA-β-gal activity	↓ Proliferative Capacity, Cell Cycle Arrest

↓ Decrease, ↑ Increase.

When T_c cells are exhausted through excessive and continuous stimulation, they upregulate inhibitory cell surface receptors such as PD-1 and LAG-3 and possess a decreased capacity to secrete interleukin 2 (IL-2) and interferon gamma (IFN-γ) [14] (Figure 1). The exhausted transcriptional T_c profile is very context dependent and is driven, during varying stages of exhaustion, by nuclear factor of activated T cell (NFAT), nuclear receptor Nr4a, thymocyte selection-associated HMG box (TOX), eomesodermin (Eomes) and T-Bet [15]. While exhausted and senescent T_c cells share characteristics such as the upregulation of surface markers Tim-3 and tyrosine-based inhibitory motif (ITIM) domain (TIGIT), senescent T_c cells also upregulate CD57 and CD45RA (Figure 1). The cytokine secretory profile of senescent T_c cells sharply contrasts that of exhausted T cells (Figure 1). Senescent T_c cells secrete high levels of inflammatory cytokines such as IL-2, IL-6, IL-8, TNF, IFN-γ and the immunosuppressive IL-10 and TGF-β (Figure 1), a program known as senescence-associated secretory phenotype (SASP). This in turn has critical consequences not only for T cell themselves, but for other immune cells within the TME milieu, including antigen presenting cells (APCs) such as dendritic cells (DCs), tumor-associated

macrophages (TAMs) and myeloid-derived suppressor cells (MDSC). Transcriptional programs in senescent T_cs have been shown to be mediated by T-bet [16] but otherwise are poorly characterized. Senescence-inducing stimuli include exposure to DNA damaging agents, stress signals and repetitive stimulation linked but not limited to the ageing process. It should be pointed out that dysfunctional T cell states other than exhaustion and senescence such as anergy have also been described. Anergic T cells are hypo-responsive, produce low levels of IL-2 and generally have little effector function. T cell anergy is caused by insufficient CD28 dependent co-stimulation of the TCR, but the surface markers of anergic T cells are poorly characterized [17]. Insufficient CD28 stimulation within the TME combined with tumor cell expressing factors, such as PD-L1 and CD95, is also closely linked to deletion of effector T cells through a process known as tolerance. Tolerance is exacerbated by TGF-β and IL-10 [18]. Taken together, senescent, anergic and exhausted T_c cells often co-exist in the TME or circulation and simultaneously exert immunosuppressive effects [11,19]. The current limitations of check-point inhibitors suggest that targeting multiple dysfunctional T_c cell states would be therapeutically beneficial. A deeper understanding of the mechanisms and functional consequences of T cell senescence are urgently needed.

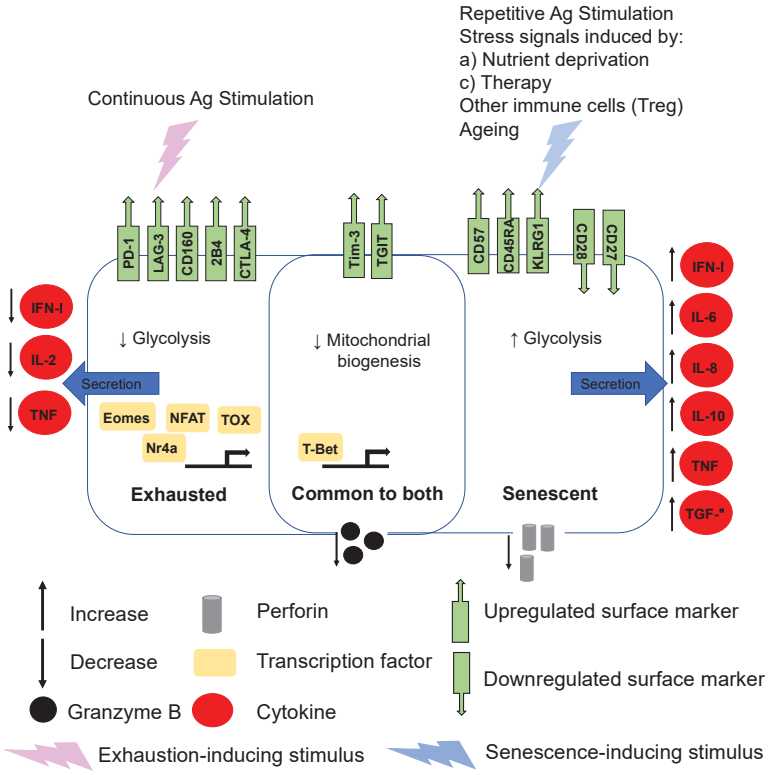

Figure 1. Surface phenotypic, metabolic and transcriptional differences between $CD8^+$ dysfunctional senescent and exhaustive states. Characteristics common to both dysfunctional states are shown the in the middle, purple overlapping section. While both T cell state exhibit decreased effector function, senescent T cells have a very distinct senescence-associated secretory phenotype (SASP) with increased cytokine production of IFN-γ, IL-6, IL-8, IL-10, TNF and TGF-β. In contrast. exhausted T cells are characterized by decreased IL-2, TNF and IFN-γ production. While some surface markers such as Tim-3 and TGIT are common to both dysfunctional T cell states, there is otherwise quite a distinct pattern of expression. Ag = antigen.

3. Mechanisms of T Cell Senescence Induction

Senescent T cells have been found in primary and metastatic solid tumor sites [19–23] as well as hematological malignancies [11,24]. T_c senescence can be classified into two major cellular mechanisms which are however not entirely separated from one another: premature and replicative senescence.

Premature senescence is caused by external factors such as stress within the TME incurred by (i) effects of immune and tumor cells, (ii) TME metabolic changes, (iii) and drug and radiation therapy, all of which are closely interlinked and not necessarily independently occurring events (Figure 2). Replicative senescence is linked to age-related changes and to telomeric shortening. T cell anergy on the other hand, is closely linked to peripheral tolerance.

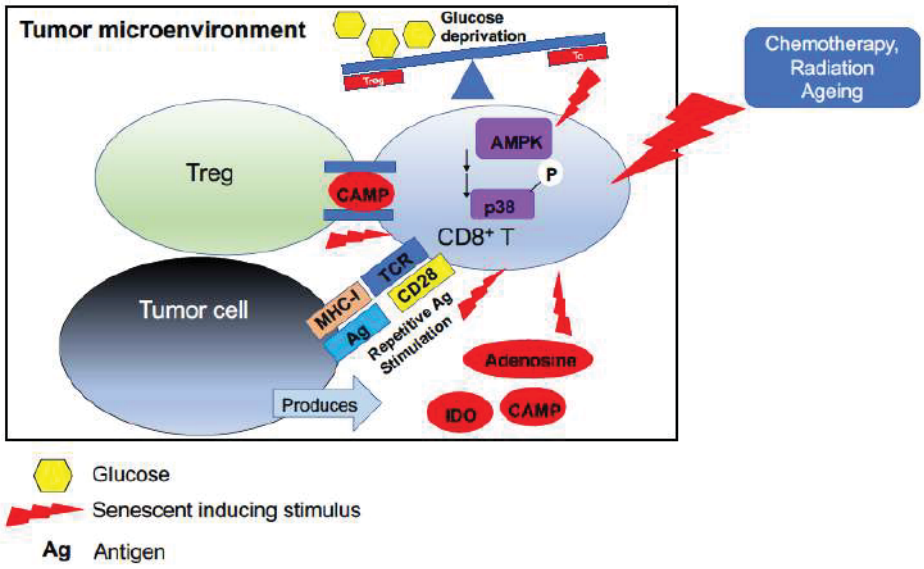

Figure 2. T cell senescence can occur via multiple mechanisms within the tumor microenvironment. Tregs, through glucose metabolic competition and transfer of cAMP produced by tumors, can induce $CD8^+$ T cell senescence, as can other metabolites produced by tumor cells, such as adenosine. Repeated antigen stimulation and external factors such as chemotherapeutic and radiation therapy also induce premature senescence. A key molecular pathway involved in $CD8^+$ T cell senescence induction is non-canonical signaling through p38-MAPK.

3.1. Signaling Pathways Involved in T_c Senescence

The intrinsic molecular pathways governing premature and replicative senescence are not completely defined but involve the MAPK pathway. The diverse and complex MAPK pathway with its three subgroups, Erk, Jnk and p38, is involved in many aspects of innate and acquired immune regulation. Classical engagement of the MAPK pathway downstream of the TCR does not occur in senescent T_c cells as they lack the costimulatory molecule CD28. p38-MAPK activation however, can also be mediated by environmental stressors such as low glucose, DNA damage and by proinflammatory cytokines which trigger AMPK to auto-phosphorylate p38. Henson et al. showed that p38 MAPK expression was elevated in human senescent $CD8^+$ T cells and that blocking p38 following inhibitor treatment resulted in increased mitochondrial mass, improved mitochondrial function and enhanced proliferation [25]. Human senescent $CD27^-CD28^-CD4^+$ T cells prompt AMPK-stimulated recruitment of p38, resulting in p38 autophosphorylation, facilitated by the protein scaffold TAB1, which inhibits telomerase activity and parts of the TCR signalosome [26]. In addition to p38, involvement of the other MAPK members Erk and Jnk have been found to impact T cell senescence in the context of a new immune inhibitory complex termed the sestrin—MAPK activation complex (sMAC). sMAC formation is increased with age [27]. In human and murine $CD4^+$ T cells, sestrins induced senescence through binding and simultaneous activation of Erk, Jnk and p38 to form sMAC. Silencing sestrin enhanced T cell activity. Although $CD4^+$ T cells were experimentally used in this study, the authors did show that sestrin deficiency increased vaccine responses in aged mice and increased the frequency of splenic $CD8^+$ T cells. A follow-up study specifically examining the effects of sestrin in $CD27^-CD28^-CD8^+$ T cells, showed that a divergent mechanism was responsible for sestrin-dependent senescence in

$CD27^{-}CD28^{-}CD8^{+}$ T cells linked to a natural killer group 2 member D (NKG2D)–DNAX Activating Protein of 12KDa (DAP12)–sestrin 2 complex. Disturbance of the NKG2D–DAP12–sestrin 2 complex through sestrin 2 genetic inhibition, restored TCR signaling [28]. T cell mitochondrial dysfunction also accelerates senescence. It was recently demonstrated that $Tfam^{fl/fl}$ $Cd4^{Cre}$ mice (where mitochondrial transcription factor A (TFAM) is depleted in $CD4^{+}$ and $CD8^{+}$ lymphocytes) prematurely died due to multiple age-related changes [29]. Taken together, the full extent of the molecular pathways involved T_c senescence are not completely elucidated. The current knowledge, however, presents targetable opportunities to potentially reverse senescence and understand how senescent T_c cells might impact immunotherapies in the treatment of cancer.

3.2. The TME Drives Tc Premature Senescence

3.2.1. Immune and Tumor Cells

A tumor's ability to evade the immune system is dynamic, complex and partially dependent on the immunosuppressive activities of infiltrating immune cells. T_c effector function is similarly complicated and shaped by the spatiotemporal distribution of APCs in the tumor milieu and tumor-draining lymph nodes, cytokines and the presence of other immune cells such as regulatory $CD4^{+}CD25^{hi}FoxP3^{+}$ T (Treg) cells. Initial priming of naïve T cells occurs in the lymph node through direct interaction with antigen present on APCs such as DCs. DCs also co-express receptors such as CD80 necessary for binding to CD28 and inducing co-stimulatory signals. Upon migration of primed T_c cells into the TME, the tumor cells expressing the antigenic peptide become targets. The numbers of infiltrating $CD8^{+}$ T cells varies widely across tumor types. Some tumors, such as melanoma and non-small cell lung cancer (NSCLC), generally have a high degree T_c infiltration. Other tumors, such as pancreatic and neuroblastoma, typically have a low degree of T_c infiltrates, although of course within a specific tumor type, there is a lot of intra-tumoral heterogeneity [30]. Many factors during this process can impact the ability of T_c cells to target tumor cells.

Regulatory $CD4^{+}CD25^{hi}FoxP3^{+}$ T (Treg) cells are subsets of T cells which play a role in maintaining immune homeostasis and present a critical barrier for immunotherapies through their suppressive effects on T_c cells. Tregs have been found in lymph nodes where they impact DC function through CCL22. CCL22, a chemokine produced by dendritic cells, enables cell-to-cell contact between DCs and Treg through Treg-expressed CCR4 [31]. Tregs accumulate within the TME, and their ability to infiltrate into tumors has been linked to the expression of multiple chemokine receptors such as CCR4, CCR5, CCR8 and CCR10. Within the TME, Tregs usually express immunosuppressive molecules such as CTL-4, which binds to CD80 and CD86 on APCs thereby affecting T_c effector function [32]. Treg suppressive mediated-effects on APCs and T_c effector cells can also occur through inhibitory cytokine secretion of IL-10, TGF-β, and IL-35. These inhibitory cytokines suppress antigen presentation in APCs. IL-35 and IL-10 promote T cell exhaustion. Metabolic competition for the consumption of IL-2 through the expression of CD25 on Tregs also suppresses T_c effector functions [33]. Tregs are also found in peripheral circulation, but their precise role in facilitating immune evasion are not as well characterized as with the TME-associated Tregs [32].

Relating specifically to Treg-mediated T_c senescence induction, an important study demonstrated that co-transfer of Tregs and naïve $CD8^{+}$ T cells into $Rag1^{-/-}$ mice transformed naïve T cells into senescent T cells (as assessed by SA-β-Gal positivity). Furthermore, the senescent T cells acquired immunosuppressive functions both in vitro and in vivo. Involvement of the mitogen-activated protein kinase (MAPK) pathway was implicated, as pre-treatment with ERK and p38 inhibitors abrogated these immunosuppressive effects [34]. Another critical study by Liu at al. using ex vivo cultured primary human T cells demonstrated that human Tregs induced nuclear kinase ataxia–telangiectasia-mutated protein (ATM)-associated DNA damage responses in T_cs [35]. The majority of subsequent mechanistic experiments demonstrated that senescence was mediated by competition for glucose, which triggered phosphorylation of the energy sensor AMP-activated protein kinase (AMPK) in cooperation with

Stat1 and Stat3. These mechanistic studies were performed using naïve $CD4^+$ T cells. However, the authors did show that Treg-induced naïve $CD8^+$ T cell senescence was blocked by pre-treatment with ATM or STAT inhibitors in NOD SCID gamma (NSG) mice, indicating that similar mechanisms of senescence induction also occur in $CD8^+$ T cells. These studies did not directly explore the specific co-localized induction of Treg-induced T_c senescence within the TME. However, as Tregs and T_cs are often co-expressed within tumors [36,37] and tumor-draining lymph nodes [38], the clinical relevance of these in vivo and ex vivo studies is plausible. These interactions, however, would likely be mediated by APCs, which these studies did not address. APCs might guide the cellular interaction between Tregs and T_cs through costimulatory (CD28/CD80 and CD86, OXO/OXOL, CD95/CD95L) on $CD8^+$ T cells or co-inhibitory (PD-1/PD-L1 and CTLA-4/CD80) signals on $CD8^+$ and $CD4^+$ T cells, respectively. Other immune cells within the TME might also indirectly impact T_c senescence. Treg and MDSC populations often support each other's expansion through positive feedback loops involving TGF-β and other cytokines [33]. In turn, MDSCs can be expanded by many of the SASP cytokines secreted by T_c senescent cells such as TGF-β, IL-6 and IFN-γ [39].

Tumor cells are the targets of T_cs following priming in the lymph nodes. T_c-mediated tumor cell killing occurs through TCR-mediated T_c cell binding to MHC-I-restricted tumor antigens on tumor cells. This interaction releases cytolytic perforin and granzymes causing tumor cell killing. Tumor cell killing can also occur through the death receptor pathway mediated by the expression of CD95 on tumor cells and CD95L on T_c cells. Receptors present on tumor cells such as PD-L1 can diminish T_c cells responses through the PD-1–PD–L1 axis [2]. Tumor cells can also downregulate MHC-I and CD95 expression to dampen responses and evade apoptosis. Immunosuppressive cytokines produced by tumor cells such as TGF-β and IL-10 also influence T_c effector function. Metabolites produced by tumor cells, elaborated on in the section below, can also affect T_cs.

Tumor cells have been shown to induce T_c senescence in in vitro and in vivo models. Montes et al. showed that ex vivo incubation of human T cells isolated from healthy donors with a variety of human tumor cell lines triggered downregulation of CD28 expression. Activation of ATM, shortening of telomere length and an ability to suppress antigen nonspecific and allogeneic-induced proliferation of responder T cells were also observed [40]. Tumor-induced senescence was dependent on direct tumor-T cell contact [40]. Another pivotal investigation demonstrated that adoptive transfer of tumor-specific $CD8^+$ tumor-infiltrating lymphocytes (TIL) 586 cells into tumor-bearing (586 mel cells) NSG mice induced senescence, as assessed by SA-β-Gal^+ staining in TILs [41]. Activation of TLR8 signaling in tumor cells was able to reverse the tumor-induced senescence [42]. Taken together, tumor-infiltrating immune cells such as Tregs as well as tumor cells have been shown to be capable of inducing T cell senescence. As this evidence largely stems from ex vivo studies, the role of critical cells mediating T_c priming such as DCs in facilitating this process remains to be explored.

3.2.2. Metabolic Changes

Metabolic re-programming within the TME is critical to many pro-tumorigenic processes, including driving senescence [43,44]. Cancer cells have a high rate of glucose consumption through aerobic glycolysis, resulting in low glucose and high lactate concentrations in the TME [45]. Antigen-activated effector T cells, once they become primed and activated in the lymph nodes, begin their clonal expansion and rapid proliferation [43]. Therefore, they have metabolic requirements different to those of circulating naïve cells which rely on oxidative phosphorylation for their energy requirements. Rapidly proliferating T cells have higher glycolytic activity [46] and increased amino acid metabolism [47]. TCR-mediated T cell activation is followed by metabolic re-programming and biomass accumulation. Changes in metabolism include a switch to aerobic glycolysis despite there being enough oxygen present to generate glucose through the tricarboxylic acid (TCA) cycle [43]. Aerobic glycolysis provides important intermediates for cell growth, such as glucose-6-phosphate, 3-phosphoglycerate (3PG) and citrate. Molecularly, this metabolic transition is supported by mTOR, PI3K activity, the transcription factor Myc and hypoxia-inducible factor-1α (HIF-1α) [43,47]. As already described above in the study

by Liu et al., increased glucose consumption by Tregs reduced the glucose pool available for naïve T cells, initiating AMPK signaling cascades and DNA damage responses [35]. Effector T cell activity is sensitive towards intracellular NAD depletion, often occurring in the TME. Tregs, however, have developed re-programming strategies mediated by the transcription factor FOXP3 to maintain their proliferative capabilities and suppressive functions, despite low glucose and high lactate levels [48]. It remains to be elucidated whether within the TME Treg numbers would be high enough to deplete glucose pools. However, in addition to Treg competing for glucose consumption, other immune cells within the TME also have distinct metabolic requirements which can affect glucose pools. MDSCs have high glucose uptake rates and can contribute to the dysfunction of other immune cells by limiting pools of available glucose [39]. MDSCs can also affect the T cell activation through depletion of amino acids such as cystine and cysteine [49], but whether that eventually also contributes to T_c senescence induction is not known. Conditions of hypoxia within the TME compounded by increased tumor acidity can cause an accumulation of immunosuppressive M2 polarized TAMs, which are critical in maintaining a tolerogenic phenotype, expanding Tregs and suppressing T_c function [50].

Tumor cells also produce metabolites that are inducers of T_c cell senescence. For instance adenosine, whose production is catalyzed by the surface ectonucleotidases CD39 and CD73, accumulates in the TME through CD38 and CD73 expression on cancer exosomes [51]. Adenosine exposure triggered replicative senescence in human $CD8^+$ T cells, decreased proliferative capacity and reduced IL-2 production [52]. Furthermore, adenosine can impact APCs that are critical for T_c function. Tumor-produced adenosine has been shown to decrease DC maturation and immune function [53]. Another example is cyclic adenosine monophosphate (cAMP), produced by tumor cells and a suppressor of T cell function [54]. In ex vivo co-culturing experiments, cAMP was shown to be transferred from Tregs to T_cs through direct gap junction formation, thereby suppressing proliferation of T_cs and decreasing IL-2 production [55]. However, the in vivo relevance of these findings in the context of the TME has yet to be validated. Other TME-associated metabolites such as indoleamine 2,3-dioxygenase (IDO) [56], although not yet shown to directly induce T_c senescence, plausibly contribute to the induction of T_c dysfunction through activation of Tregs.

3.2.3. Chemotherapeutics and Radiation Therapy

DNA damage caused by commonly used chemotherapeutics can lead to senescence induction in both tumor and normal cells [57]. Most chemotherapeutic agents are genotoxic and cause DNA damage by triggering chromosomal breaks or double stranded DNA breaks. This is followed by induction of the DNA damage response (DDR) mediated by ATM and ATR kinases, whose downstream targets are cell cycle regulatory proteins checkpoint homologs 1 and 2 (Chk1 and Chk2). Chk1 and Chk2 trigger the activation of various cyclin-dependent kinase inhibitors causing cell cycle arrest [58]. It is not surprising that treatment with such agents can also lead to immuno-senescence, especially in rapidly proliferating populations such as T_c cells following antigen exposure. A six months longitudinal study tracked shifts in $CD8^+$ T cell populations in DNA-damaging chemotherapy-treated breast cancer patients. The study found that senescent-enriched $CD28^-CD57^+$ cells were more pre-dominant in cancer patients compared to the untreated healthy age-matched group. The study also found that immuno-senescence and immune risk parameters were more pronounced in the chemotherapy-treated group [22]. When peripheral $CD8^+$ T lymphocytes were assessed in metastatic breast cancer patients during the post-salvage taxane chemotherapy follow-up, it was found that $CD8^+CD28^-$ populations were increased in breast cancer patients compared to the control cohort [23]. In another longitudinal study, radiotherapy and chemotherapy in early-stage breast cancer patients increased senescent cytotoxic T lymphocytes [59]. Shortened telomere length was observed in peripheral blood mononuclear cells in non-Hodgkin's lymphoma patients undergoing chemotherapy [60]. These results are correlative, and the functional consequences of T_c cell senescence induction in these clinical settings should be mechanistically explored. Tumor senescence might be beneficial to the organism under some contexts, as it stops tumor-cell proliferation. However, the unintended potentially

detrimental consequences of T_c cell senescence should be considered during the course of therapy, especially if immunotherapy treatment such as CAR-T cell therapy is to be further applied.

3.3. Age-Related Replicative Senescence

Replicative senescence in normal somatic cells is telomere dependent and occurs as a result of telomere shortening or a classical DNA damage response triggered by a dysfunctional telomerase [61]. Telomerase dysfunction can be triggered by oxidative stress [62]. This is paralleled in T_c cells. The natural aging process is accompanied by blunted immune responses to anti-viral, bacterial and other stimuli as well as decreased responsiveness to vaccines [63,64]. Repeated antigen stimulation throughout an individual's life time is one potential cause of aging-induced T_c senescence. Others include physiological changes such as thymic shrinking which limits the naïve T cell pool, changes in the bone marrow, and obesity [62,65,66]. While ex vivo stimulated human $CD8^+$ T cells have been shown to have high initial telomerase activity, their telomere lengths shorten following several rounds of antigen stimulation, and their telomerase activity dramatically decreases [67]. A decrease in the number of naïve $CD8^+$ T cells and suppressed functionality in terms proliferation and decreased cytokine production accompany age-related dysfunction [63,68]. In aged mice, proliferative defects have also been demonstrated in anti-viral memory $CD8^+$ T cells [69]. Senescence has also been observed in $CD8^+$ T cells which have not undergone repetitive antigen stimulation. A recent study explored a specialized subset of semi-differentiated antigen naïve but semi-primed T cells expressing the activation marker CD44 termed "virtual memory" $CD8^+$ T cells ($CD44^{hi}CD49d^{lo}$; T_{VM}). The investigation found T_{VM} cells accumulated in aged mice and humans and acquired a dysfunctional senescent but not exhausted phenotype [70]. The presence of T_{VM} cells in aged individuals would be expected to diminish primary $CD8^+$ T cell responses while still maintaining a base effector function and the ability to secrete cytokines.

4. Tc Cell Senescence and Effects on Immunotherapy Response

4.1. Checkpoint Inhibitors

Given the increased accumulation of senescent T_c cells in older individuals, it would be reasonable to expect that age would dimmish response to immunotherapies. Curiously, however, some reports indicate that advanced age positively correlates with anti-PD-1 therapy response [71]. In this study, when a total of 538 metastatic melanoma patients treated with pembrolizumab were stratified according to age and response, a smaller percentage of patients aged over 62 years had progressive disease. The study, which controlled for prior MAPK inhibitor therapy, did not control for mutational burden but did corroborate the patient data with murine models. Genetically identical tumors experienced better, albeit minor, anti-PD-1 responses in aged mice. The study found that in younger patients, Tregs were increased and $CD8^+$ T cells decreased in the TME. The authors speculated that memory $CD8^+$ T cells, which accumulate with age and expand in response to immunotherapy, may be responsible for improved anti-PD-1 responses. However, accumulation of memory $CD8^+$ T cells in aged individuals is not absolute and is relative to a decrease in naïve T cells due to thymic shrinking. Other studies in various tumor types have found no correlation [72,73], or a negative correlation between age and checkpoint inhibitor response [74]. The study citing the negative correlation was carried out in patients with advanced renal cell carcinoma with a small sub-group of older patients. Furthermore, the study did not assess infiltrates in the TME. Age-induced senescence might affect other critical immune cells which could impact responses to checkpoint inhibitors, including the abovementioned T_{vM} cells [70]. The phagocytic function of macrophages/monocytes is decreased during aging and might impair release of antigens into the micro-environment. Aging also decreases numbers and antigen presenting functions of APCs, which would impact T cell effector function [75].

It is difficult to conclusively ascertain whether older patients fare better/worse following immunotherapy treatment given the usually low numbers of elderly patients included in clinical trials.

Immunotherapy response, particularly to checkpoint inhibitors, is complex, and no successful biomarker of response has been established. Several biomarkers have been suggested, including neo-antigen burden, PD-L1 expression, genomic and transcriptomic signatures and immune infiltration [76,77]. While age-induced T_c cell senescence might impact response to immunotherapy treatment, other more significant factors could over-ride these effects. For example, a recent study reported that tumors in younger female individuals accumulated more poorly presented driver mutations than those in older and male patients. Accordingly, these female patients had poorer immune checkpoint therapy responses [78]. Taken together, it remains to be proven whether age is a predictor of immunotherapy response

Irrespective of age, patients with accumulated senescent T_c cells within the TME might respond poorly to checkpoint inhibition, which seeks to de-repress the exhaustive T_c phenotype but does not target the senescent one. A small pilot study of melanoma patients was able to identify patients with primary resistance to checkpoint inhibitors by using lymphocyte phenotyping for senescence markers CD27, CD28, Tim-3 and CD57 [79]. The study tracked senescence markers in the peripheral blood for 12 weeks post diagnosis of metastatic melanoma. Another study found that in multiple myeloma, T-cell clones exhibited hypo-responsiveness and a telomere-independent senescent ($KLRG\text{-}1^+/CD57^+/CD160^+/CD28^-$) phenotype. These senescent T cells also expressed low levels of PD-1 and CTL-4 [24]. Although limited in the numbers of assessed patients, these studies suggest that senescent T_c impede responses to checkpoint inhibitors.

4.2. CAR-T Cell Therapy

CAR-T cell therapy has the potential to be curative in patients with hematological malignancies such as leukemia and lymphoma. However, CAR-T cell therapy application to solid tumors whose targetable antigen repertoire can be difficult to predict will be more challenging. CAR-T cell therapy depends on the isolation and expansion of a patient's T cells harvested from the periphery. It is plausible to speculate that functionally impaired senescent T cells in this context would provide an impediment to successful T cell expansion and/or CAR activity once in the TME. In vivo, murine studies have shown that PD-1 upregulation within the tumor microenvironment impeded the function of CD28-CAR-T cells, which was restored by concomitant treatment with anti-PD-1 antibodies [80]. Furthermore, introduction of a patient's expanded T cells into the TME might lead to terminal differentiation of the T cells caused by TME-induced T_c senescence or exhaustion [81]. Taken together, although this requires further exploration, there is reasonable correlative evidence to suggest that senescent T_c cells impact immunotherapy responses.

4.3. Targeting T Cell Senescence

As 40–85 percent of patients treated with checkpoint inhibitors fail to exhibit a sustained clinical response [82], combinatorial approaches that also reverse T_c cell senescence could be of therapeutic benefit. As induction of tumor cell senescence can be advantageous in the context of tumor clearance, strategies to reverse T cell senescence should be carefully considered. While induction of tumor cell senescence can initially stop uncontrolled proliferation, the SASP profile of senescent tumor cells can promote tumor relapse, inflammation and recruit immunosuppressive immune cells to the TME. Agents that induce apoptosis in senescent cells termed "senolytics" (e.g., dasatanib and quercetin), are currently being tested in pulmonary fibrosis and after radiotherapy to improve clinical symptoms [83,84]. Whether these agents can be used in neoplastic malignancies to clear senescent tumor cells and/or senescent T_c cells is an area warranting further exploration.

Agents such as ralimetinib that target p38 MAPK, which are safe and have already being used in clinical trials [85], are an attractive option as they could dually target T_c senescence signaling and tumor proliferation. In addition to their direct anti-tumoral effects, other inhibitors of the MAPK pathway already approved for the treatment of metastatic melanoma are also promising. These include the B-Raf-targeting inhibitor vemurafenib or MEK1/2 targeting inhibitor trametinib. These drugs have

already been shown to increase the number of $CD8^+$ TILs and enhance checkpoint inhibition in murine models [86,87]. During senescence, upregulation of BCL-2 family members (BCL-XL, BCL-W) have been reported in several studies, across various cell types [84]. Of note, inhibitors targeting the BCL-2 protein family, including novitoclax, are selectively senolytic in some cell types [88]. Moreover, several other pro-survival pathways have been implicated in eliminating senescence, including the p53/p21 axis, receptor tyrosine kinase, HIF-1α and serpine anti-apoptotic pathways [84,89]. HSP90, a member of the chaperone protein family, was identified as a new class of senolytics [90,91]. HSP90 is upregulated in several tumor types and promotes the stabilization of PI3K/Akt, ERK and other pro-survival signaling pathways upregulated during cellular senescence [92]. Therefore, downregulation of pro-survival signaling pathways upon HSP90 inhibition may be responsible for its senolytic activity [90]. Whether these inhibitors also reverse T_c senescence and enhance checkpoint inhibition in the clinical setting remains to be elucidated. However, combinatorial therapy is paramount in achieving clinical success. Therefore, these strategies might present good therapeutic opportunities. They also have the advantage of using already approved therapies.

Combining checkpoint inhibitors with other activators of the immune system such as TLR8 agonists could maximize the benefits of immunotherapy. TLR8 agonists have already been shown to reverse the T cell tumor-induced senescence in mouse models of cancer [41]. They have the added benefit of increasing immune infiltration and activating other anti-tumoral immune cells such as dendritic and NK cells. The TLR8 agonist motolimod (VTX-2337) has been evaluated in clinical trials, is well tolerated and shows promise activating the immune system in cancer patients [93,94]. Other approaches exist, such as the reprogramming of senescent T_c cells from pluripotent stem cells (T-IPSCs). However, this approach is complicated by the unpredictable re-arrangement of the TCR [81].

Taken together, as our molecular understanding of the pathways governing T_c cell senescence increases, so will the ability to effectively target this dysfunctional subset of T cells, reverse their immunosuppression and augment currently used immunotherapies. Furthermore, assessing senescent T cell accumulation following treatment with currently used therapies in cancer patients might help to optimize treatment strategies and uncover novel bio-markers of immunotherapy response.

5. Conclusions

Senescent T_c cells are phenotypically distinct from exhausted T_c cells. Their immunosuppressive function brings new obstacles to successful immunotherapy. Regardless of whether the tumor-specific T cell senescence is of replicative or premature origin, a deeper molecular understating of the molecular pathways driving this process is needed. This will open new therapeutic options to eradicate challenges imposed by a suppressive TME. Currently, MAPK pathway inhibitors and TLR8a agonists are amongst the most clinically promising candidates to reverse T cell senescence. They can potentially be used in combinatorial approaches with checkpoint inhibitors to target many levels of immune dysfunction and maximize anti-tumor immunity. Much progress has been made in defining T cell senescence as a distinct dysfunctional state. However, clinical evidence showing the functional importance of T cell senescence in solid tumors and hematological malignancies is largely correlative and needs to be further explored.

Author Contributions: W.L., P.S., S.B. and A.A.P. performed data research. A.A.P. wrote the manuscript. All authors edited the manuscript. H.C.X., S.B., A.B., P.A.L. and A.A.P. conceptualized the design of the study. All authors have read and agreed to the published version of the manuscript.

Funding: S.B. acknowledges the support by Forschungskommission (2018-04) and DSO-Netzwerkverbundes, HHU Düsseldorf. This work was supported by the funds from the Deutsche Forschungsgemeinschaft (DFG) SFB974, RTG1949 and the Düsseldorf School of Oncology (DSO).

Conflicts of Interest: The authors declare no conflict of interest.

References

1. Waldman, A.D.; Fritz, J.M.; Lenardo, M.J. A guide to cancer immunotherapy: From T cell basic science to clinical practice. *Nat. Rev. Immunol.* **2020**, 1–18. [CrossRef]
2. Martinez-Lostao, L.; Anel, A.; Pardo, J. How Do Cytotoxic Lymphocytes Kill Cancer Cells? *Clin. Cancer Res.* **2015**, *21*, 5047–5056. [CrossRef]
3. Larkin, J.; Chiarion-Sileni, V.; Gonzalez, R.; Grob, J.-J.; Cowey, C.L.; Lao, C.D.; Schadendorf, D.; Dummer, R.; Smylie, M.; Rutkowski, P.; et al. Combined Nivolumab and Ipilimumab or Monotherapy in Untreated Melanoma. *New Engl. J. Med.* **2015**, *373*, 23–34. [CrossRef]
4. Barber, D.L.; Wherry, E.J.; Masopust, D.; Zhu, B.; Allison, J.; Sharpe, A.H.; Freeman, G.J.; Ahmed, R. Restoring function in exhausted CD8 T cells during chronic viral infection. *Nature* **2006**, *439*, 682–687. [CrossRef]
5. Locke, F.L.; Neelapu, S.S.; Bartlett, N.L.; Siddiqi, T.; Chavez, J.C.; Hosing, C.M.; Ghobadi, A.; Budde, L.E.; Bot, A.; Rossi, J.M.; et al. Phase 1 Results of ZUMA-1: A Multicenter Study of KTE-C19 Anti-CD19 CAR T Cell Therapy in Refractory Aggressive Lymphoma. *Mol. Ther.* **2017**, *25*, 285–295. [CrossRef] [PubMed]
6. Neelapu, S.S.; Locke, F.L.; Bartlett, N.L.; Lekakis, L.J.; Miklos, D.B.; Jacobson, C.A.; Braunschweig, I.; Oluwole, O.O.; Siddiqi, T.; Lin, Y.; et al. Axicabtagene Ciloleucel CAR T-Cell Therapy in Refractory Large B-Cell Lymphoma. *N. Engl. J. Med.* **2017**, *377*, 2531–2544. [CrossRef] [PubMed]
7. Vitale, C.; Strati, P. CAR T-Cell Therapy for B-Cell non-Hodgkin Lymphoma and Chronic Lymphocytic Leukemia: Clinical Trials and Real-World Experiences. *Front. Oncol.* **2020**, *10*, 849. [CrossRef] [PubMed]
8. Zou, W. Immunosuppressive networks in the tumour environment and their therapeutic relevance. *Nat. Rev. Cancer* **2005**, *5*, 263–274. [CrossRef]
9. Appay, V.; Nixon, D.F.; Donahoe, S.M.; Gillespie, G.M.; Dong, T.; King, A.; Ogg, G.S.; Spiegel, H.M.; Conlon, C.; Spina, C.A.; et al. HIV-Specific Cd8+ T Cells Produce Antiviral Cytokines but Are Impaired in Cytolytic Function. *J. Exp. Med.* **2000**, *192*, 63–76. [CrossRef]
10. Wherry, E.J.; Ha, S.-J.; Kaech, S.M.; Haining, W.N.; Sarkar, S.; Kalia, V.; Subramaniam, S.; Blattman, J.N.; Barber, D.L.; Ahmed, R. Molecular Signature of CD8+ T Cell Exhaustion during Chronic Viral Infection. *Immunity* **2007**, *27*, 670–684. [CrossRef]
11. Zelle-Rieser, C.; Thangavadivel, S.; Biedermann, R.; Brunner, A.; Stoitzner, P.; Willenbacher, E.; Greil, R.; Jöhrer, K. T cells in multiple myeloma display features of exhaustion and senescence at the tumor site. *J. Hematol. Oncol.* **2016**, *9*, 116. [CrossRef]
12. Li, K.-K.; Adams, D.H. Antitumor CD8+ T cells in hepatocellular carcinoma: Present but exhausted. *Hepatology* **2014**, *59*, 1232–1234. [CrossRef] [PubMed]
13. Liu, X.; Hoft, D.F.; Peng, G. Senescent T cells within suppressive tumor microenvironments: Emerging target for tumor immunotherapy. *J. Clin. Investig.* **2020**, *130*, 1073–1083. [CrossRef] [PubMed]
14. Wherry, E.J.; Kurachi, M. Molecular and cellular insights into T cell exhaustion. *Nat. Rev. Immunol.* **2015**, *15*, 486–499. [CrossRef] [PubMed]
15. Zhao, Y.; Shao, Q.; Peng, G. Exhaustion and senescence: Two crucial dysfunctional states of T cells in the tumor microenvironment. *Cell. Mol. Immunol.* **2019**, *17*, 27–35. [CrossRef]
16. Dolfi, D.V.; Mansfield, K.D.; Polley, A.M.; Doyle, S.A.; Freeman, G.J.; Pircher, H.; Schmader, K.E.; Wherry, E.J. Increased T-bet is associated with senescence of influenza virus-specific CD8 T cells in aged humans. *J. Leukoc. Biol.* **2013**, *93*, 825–836. [CrossRef]
17. Crespo, J.; Sun, H.; Welling, T.H.; Tian, Z.; Zou, W. T cell anergy, exhaustion, senescence, and stemness in the tumor microenvironment. *Curr. Opin. Immunol.* **2013**, *25*, 214–221. [CrossRef]
18. Bour-Jordan, H.; Esensten, J.H.; Martínez-Llordella, M.; Penaranda, C.; Stumpf, M.; Bluestone, J.A. Intrinsic and extrinsic control of peripheral T-cell tolerance by costimulatory molecules of the CD28/B7 family. *Immunol. Rev.* **2011**, *241*, 180–205. [CrossRef]
19. Papalampros, A.; Vailas, M.; Ntostoglou, K.; Chiloeches, M.L.; Sakellariou, S.; Chouliari, N.V.; Samaras, M.G.; Veltsista, P.D.; Theodorou, S.D.P.; Margetis, A.T.; et al. Unique Spatial Immune Profiling in Pancreatic Ductal Adenocarcinoma with Enrichment of Exhausted and Senescent T Cells and Diffused CD47-SIRPα Expression. *Cancers* **2020**, *12*, 1825. [CrossRef]
20. Li, H.; Wu, K.; Tao, K.; Chen, L.; Zheng, Q.; Lu, X.; Liu, J.; Shi, L.; Liu, C.; Wang, G.; et al. Tim-3/galectin-9 signaling pathway mediates T-cell dysfunction and predicts poor prognosis in patients with hepatitis B virus-associated hepatocellular carcinoma. *Hepatology* **2012**, *56*, 1342–1351. [CrossRef]

21. Gruber, I.; El Yousfi, S.; Dürr-Störzer, S.; Wallwiener, D.; Solomayer, E.F.; Fehm, T. Down-regulation of CD28, TCR-zeta (zeta) and up-regulation of FAS in peripheral cytotoxic T-cells of primary breast cancer patients. *Anticancer Res.* **2008**, *28*, 779–784. [PubMed]
22. Onyema, O.O.; DeCoster, L.; Njemini, R.; Forti, L.N.; Bautmans, I.; De Waele, M.; Mets, T. Chemotherapy-induced changes and immunosenescence of CD8+ T-cells in patients with breast cancer. *Anticancer Res.* **2015**, *35*, 1481–1489. [PubMed]
23. Song, G.; Wang, X.; Jia, J.; Yuan, Y.; Wan, F.; Zhou, X.; Yang, H.; Ren, J.; Gu, J.; Lyerly, H.K. Elevated level of peripheral CD8+CD28− T lymphocytes are an independent predictor of progression-free survival in patients with metastatic breast cancer during the course of chemotherapy. *Cancer Immunol. Immunother.* **2013**, *62*, 1123–1130. [CrossRef] [PubMed]
24. Suen, H.; Brown, R.; Yang, S.; Weatherburn, C.; Ho, P.J.; Woodland, N.; Nassif, N.; Barbaro, P.; Bryant, C.; Hart, D.; et al. Multiple myeloma causes clonal T-cell immunosenescence: Identification of potential novel targets for promoting tumour immunity and implications for checkpoint blockade. *Leukemia* **2016**, *30*, 1716–1724. [CrossRef] [PubMed]
25. Henson, S.M.; Lanna, A.; Riddell, N.; Franzese, O.; Macaulay, R.; Griffiths, S.J.; Puleston, D.J.; Watson, A.S.; Simon, A.K.; Tooze, S.A.; et al. p38 signaling inhibits mTORC1-independent autophagy in senescent human CD8+ T cells. *J. Clin. Investig.* **2014**, *124*, 4004–4016. [CrossRef]
26. Lanna, A.; Henson, S.M.; Escors, D.; Akbar, A.N. The kinase p38 activated by the metabolic regulator AMPK and scaffold TAB1 drives the senescence of human T cells. *Nat. Immunol.* **2014**, *15*, 965–972. [CrossRef]
27. Lanna, A.; Gomes, D.C.; Müller-Durovic, B.; McDonnell, T.; Escors, D.; Gilroy, D.W.; Lee, J.H.; Karin, M.; Akbar, A.N. A sestrin-dependent Erk–Jnk–p38 MAPK activation complex inhibits immunity during aging. *Nat. Immunol.* **2017**, *18*, 354–363. [CrossRef]
28. Pereira, B.I.; De Maeyer, R.P.H.; Covre, L.P.; Nehar-Belaid, D.; Lanna, A.; Ward, S.; Marches, R.; Chambers, E.S.; Gomes, D.C.O.; Riddell, N.E.; et al. Sestrins induce natural killer function in senescent-like CD8+ T cells. *Nat. Immunol.* **2020**, *21*, 684–694. [CrossRef]
29. Desdín-Micó, G.; Soto-Heredero, G.; Aranda, J.F.; Oller, J.; Carrasco, E.; Gabandé-Rodríguez, E.; Blanco, E.M.; Alfranca, A.; Cussó, L.; Desco, M.; et al. T cells with dysfunctional mitochondria induce multimorbidity and premature senescence. *Science* **2020**, *368*, 1371–1376. [CrossRef]
30. Galon, J.; Bruni, D. Approaches to treat immune hot, altered and cold tumours with combination immunotherapies. *Nat. Rev. Drug Discov.* **2019**, *18*, 197–218. [CrossRef]
31. Rapp, M.; Wintergerst, M.W.M.; Kunz, W.G.; Vetter, V.K.; Knott, M.M.L.; Lisowski, D.; Haubner, S.; Moder, S.; Thaler, R.; Eiber, S.; et al. CCL22 controls immunity by promoting regulatory T cell communication with dendritic cells in lymph nodes. *J. Exp. Med.* **2019**, *216*, 1170–1181. [CrossRef] [PubMed]
32. Kim, J.-H.; Kim, B.S.; Lee, S.-K. Regulatory T Cells in Tumor Microenvironment and Approach for Anticancer Immunotherapy. *Immune Netw.* **2020**, *20*, e4. [CrossRef] [PubMed]
33. Li, C.; Jiang, P.; Wei, S.; Xu, X.; Wang, J. Regulatory T cells in tumor microenvironment: New mechanisms, potential therapeutic strategies and future prospects. *Mol. Cancer* **2020**, *19*, 1–23. [CrossRef] [PubMed]
34. Ye, J.; Huang, X.; Hsueh, E.C.; Zhang, Q.; Ma, C.; Zhang, Y.; Varvares, M.A.; Hoft, D.F.; Peng, G. Human regulatory T cells induce T-lymphocyte senescence. *Blood* **2012**, *120*, 2021–2031. [CrossRef]
35. Liu, X.; Mo, W.; Ye, J.; Li, L.; Zhang, Y.; Hsueh, E.C.; Hoft, D.F.; Peng, G. Regulatory T cells trigger effector T cell DNA damage and senescence caused by metabolic competition. *Nat. Commun.* **2018**, *9*, 249. [CrossRef]
36. Ji, A.L.; Rubin, A.J.; Thrane, K.; Jiang, S.; Reynolds, D.L.; Meyers, R.M.; Guo, M.G.; George, B.M.; Mollbrink, A.; Bergenstråhle, J.; et al. Multimodal Analysis of Composition and Spatial Architecture in Human Squamous Cell Carcinoma. *Cell* **2020**, *182*, 497–514.e22. [CrossRef]
37. Sakuishi, K.; Ngiow, S.F.; Sullivan, J.M.; Teng, M.W.L.; Kuchroo, V.K.; Smyth, M.J.; Anderson, A.C. TIM3+FOXP3+regulatory T cells are tissue-specific promoters of T-cell dysfunction in cancer. *OncoImmunology* **2013**, *2*, e23849. [CrossRef]
38. Zhou, X.; Zhao, S.; He, Y.; Geng, S.; Shi, Y.; Wang, B. Precise Spatiotemporal Interruption of Regulatory T-cell–Mediated CD8+ T-cell Suppression Leads to Tumor Immunity. *Cancer Res.* **2018**, *79*, 585–597. [CrossRef]
39. Hu, C.; Pang, B.; Lin, G.; Zhen, Y.; Yi, H. Energy metabolism manipulates the fate and function of tumour myeloid-derived suppressor cells. *Br. J. Cancer* **2020**, *122*, 23–29. [CrossRef]

40. Montes, C.L.; Chapoval, A.; Nelson, J.A.; Orhue, V.; Zhang, X.; Schulze, D.H.; Strome, S.E.; Gastman, B.R. Tumor-induced senescent T cells with suppressor function: A potential form of tumor immune evasion. *Cancer Res.* **2008**, *68*, 870–879. [CrossRef]
41. Ye, J.; Ma, C.; Hsueh, E.C.; Dou, J.; Mo, W.; Liu, S.; Han, B.; Huang, Y.; Zhang, Y.; Varvares, M.; et al. TLR 8 signaling enhances tumor immunity by preventing tumor-induced T-cell senescence. *EMBO Mol. Med.* **2014**, *6*, 1294–1311. [CrossRef] [PubMed]
42. Li, L.; Liu, X.; Sanders, K.L.; Edwards, J.L.; Ye, J.; Si, F.; Gao, A.; Huang, L.; Hsueh, E.C.; Ford, D.A.; et al. TLR8-Mediated Metabolic Control of Human Treg Function: A Mechanistic Target for Cancer Immunotherapy. *Cell Metab.* **2019**, *29*, 103–123.e5. [CrossRef] [PubMed]
43. Buck, M.D.; O'Sullivan, D.; Pearce, E.L. T cell metabolism drives immunity. *J. Exp. Med.* **2015**, *212*, 1345–1360. [CrossRef] [PubMed]
44. O'Neill, L.A.; Pearce, E.J. Immunometabolism governs dendritic cell and macrophage function. *J. Exp. Med.* **2015**, *213*, 15–23. [CrossRef] [PubMed]
45. Jiang, B. Aerobic glycolysis and high level of lactate in cancer metabolism and microenvironment. *Gene Funct. Dis.* **2017**, *4*, 25–27. [CrossRef]
46. Sukumar, M.; Liu, J.; Ji, Y.; Subramanian, M.; Crompton, J.G.; Yu, Z.; Roychoudhuri, R.; Palmer, D.C.; Muranski, P.; Karoly, E.D.; et al. Inhibiting glycolytic metabolism enhances CD8+ T cell memory and antitumor function. *J. Clin. Investig.* **2013**, *123*, 4479–4488. [CrossRef]
47. Wang, R.; Dillon, C.P.; Shi, L.Z.; Milasta, S.; Carter, R.; Finkelstein, D.; McCormick, L.L.; Fitzgerald, P.; Chi, H.; Munger, J.; et al. The Transcription Factor Myc Controls Metabolic Reprogramming upon T Lymphocyte Activation. *Immunity* **2011**, *35*, 871–882. [CrossRef]
48. Angelin, A.; Gil-de-Gómez, L.; Dahiya, S.; Jiao, J.; Guo, L.; Levine, M.H.; Wang, Z.; Quinn, W.J., III; Kopinski, P.K.; Wang, L.; et al. Foxp3 Reprograms T Cell Metabolism to Function in Low-Glucose, High-Lactate Environments. *Cell Metab.* **2017**, *25*, 1282–1293.e7. [CrossRef]
49. Srivastava, M.K.; Sinha, P.; Clements, V.K.; Rodriguez, P.; Ostrand-Rosenberg, S. Myeloid-derived suppressor cells inhibit T-cell activation by depleting cystine and cysteine. *Cancer Res.* **2010**, *70*, 68–77. [CrossRef]
50. Wu, K.; Lin, K.; Li, X.; Yuan, X.; Xu, P.; Ni, P.; Xu, D. Redefining Tumor-Associated Macrophage Subpopulations and Functions in the Tumor Microenvironment. *Front. Immunol.* **2020**, *11*, 1731. [CrossRef]
51. Clayton, A.; Al-Taei, S.; Webber, J.P.; Mason, M.D.; Tabi, Z. Cancer Exosomes Express CD39 and CD73, Which Suppress T Cells through Adenosine Production. *J. Immunol.* **2011**, *187*, 676–683. [CrossRef]
52. Parish, S.T.; Kim, S.; Sekhon, R.K.; Wu, J.E.; Kawakatsu, Y.; Effros, R.B. Adenosine Deaminase Modulation of Telomerase Activity and Replicative Senescence in Human CD8 T Lymphocytes. *J. Immunol.* **2010**, *184*, 2847–2854. [CrossRef]
53. Lee, J.-H.; Choi, S.-Y.; Jung, N.-C.; Song, J.-Y.; Seo, H.G.; Lee, H.S.; Lim, D.-S. The Effect of the Tumor Microenvironment and Tumor-Derived Metabolites on Dendritic Cell Function. *J. Cancer* **2020**, *11*, 769–775. [CrossRef]
54. Vang, T.; Torgersen, K.M.; Sundvold, V.; Saxena, M.; Levy, F.O.; Skålhegg, B.S.; Hansson, V.; Mustelin, T.; Taskén, K. Activation of the COOH-terminal Src Kinase (Csk) by cAMP-dependent Protein Kinase Inhibits Signaling through the T Cell Receptor. *J. Exp. Med.* **2001**, *193*, 497–508. [CrossRef]
55. Bopp, T.; Becker, C.; Klein, M.; Klein-Hessling, S.; Palmetshofer, A.; Serfling, E.; Heib, V.; Becker, M.; Kubach, J.; Schmitt, S.; et al. Cyclic adenosine monophosphate is a key component of regulatory T cell–mediated suppression. *J. Exp. Med.* **2007**, *204*, 1303–1310. [CrossRef]
56. Ustun, C.; Miller, J.S.; Munn, D.H.; Weisdorf, D.J.; Blazar, B.R. Regulatory T cells in acute myelogenous leukemia: Is it time for immunomodulation? *Blood* **2011**, *118*, 5084–5095. [CrossRef]
57. Campisi, J.; d'Adda di Fagagna, D. Cellular senescence: When bad things happen to good cells. *Nat. Rev. Mol. Cell Biol.* **2007**, *8*, 729–740. [CrossRef]
58. Faheem, M.M.; Seligson, N.D.; Ahmad, S.M.; Rasool, R.U.; Gandhi, S.G.; Bhagat, M.; Goswami, A. Convergence of therapy-induced senescence (TIS) and EMT in multistep carcinogenesis: Current opinions and emerging perspectives. *Cell Death Discov.* **2020**, *6*, 1–12. [CrossRef]
59. Sehl, M.E.; Carroll, J.E.; Horvath, S.; Bower, J.E. The acute effects of adjuvant radiation and chemotherapy on peripheral blood epigenetic age in early stage breast cancer patients. *NPJ Breast Cancer* **2020**, *6*, 23. [CrossRef]
60. Lee, J.-J.; Nam, C.-E.; Cho, S.-H.; Park, K.-S.; Chung, I.-J.; Kim, H.-J. Telomere length shortening in non-Hodgkin's lymphoma patients undergoing chemotherapy. *Ann. Hematol.* **2003**, *82*, 492–495. [CrossRef]

61. d'Adda di Fagagna, F.; Reaper, P.M.; Clay-Farrace, L.; Fiegler, H.; Carr, P.; Von Zglinicki, T.; Saretzki, G.; Carter, N.P.; Jackson, S.P. A DNA damage checkpoint response in telomere-initiated senescence. *Nature* **2003**, *426*, 194–198. [CrossRef] [PubMed]
62. Chou, J.P.; Effros, R.B. T Cell Replicative Senescence in Human Aging. *Curr. Pharm. Des.* **2013**, *19*, 1680–1698. [CrossRef]
63. Briceno, O.; Lissina, A.; Wanke, K.; Afonso, G.; Von Braun, A.; Ragon, K.; Miquel, T.; Gostick, E.; Papagno, L.; Stiasny, K.; et al. Reduced naïve CD8+ T-cell priming efficacy in elderly adults. *Aging Cell* **2016**, *15*, 14–21. [CrossRef] [PubMed]
64. Jiang, J.; Fisher, E.M.; Murasko, D.M. CD8 T cell responses to influenza virus infection in aged mice. *Ageing Res. Rev.* **2011**, *10*, 422–427. [CrossRef]
65. Brenchley, J.M.; Karandikar, N.J.; Betts, M.R.; Ambrozak, D.R.; Hill, B.J.; Crotty, L.E.; Casazza, J.P.; Kuruppu, J.; Migueles, S.A.; Connors, M.; et al. Expression of CD57 defines replicative senescence and antigen-induced apoptotic death of CD8+ T cells. *Blood* **2003**, *101*, 2711–2720. [CrossRef]
66. Wang, Z.; Aguilar, E.G.; Luna, J.I.; Dunai, C.; Khuat, L.T.; Le, C.T.; Mirsoian, A.; Minnar, C.M.; Stoffel, K.M.; Sturgill, I.R.; et al. Paradoxical effects of obesity on T cell function during tumor progression and PD-1 checkpoint blockade. *Nat. Med.* **2019**, *25*, 141–151. [CrossRef] [PubMed]
67. Valenzuela, H. Divergent Telomerase and CD28 Expression Patterns in Human CD4 and CD8 T Cells Following Repeated Encounters with the Same Antigenic Stimulus. *Clin. Immunol.* **2002**, *105*, 117–125. [CrossRef]
68. Renkema, K.R.; Li, G.; Wu, A.; Smithey, M.J.; Nikolich-Zugich, J. Two Separate Defects Affecting True Naive or Virtual Memory T Cell Precursors Combine To Reduce Naive T Cell Responses with Aging. *J. Immunol.* **2014**, *192*, 151–159. [CrossRef] [PubMed]
69. Decman, V.; Laidlaw, B.J.; DiMenna, L.J.; Abdulla, S.; Mozdzanowska, K.; Erikson, J.; Ertl, H.C.J.; Wherry, E.J. Cell-Intrinsic Defects in the Proliferative Response of Antiviral Memory CD8 T Cells in Aged Mice upon Secondary Infection. *J. Immunol.* **2010**, *184*, 5151–5159. [CrossRef]
70. Quinn, K.M.; Fox, A.; Harland, K.L.; Russ, B.E.; Li, J.; Nguyen, T.H.O.; Loh, L.; Olshanksy, M.; Naeem, H.; Tsyganov, K.; et al. Age-Related Decline in Primary CD8+ T Cell Responses Is Associated with the Development of Senescence in Virtual Memory CD8+ T Cells. *Cell Rep.* **2018**, *23*, 3512–3524. [CrossRef]
71. Kugel, C.H., III; Douglass, S.M.; Webster, M.R.; Kaur, A.; Liu, Q.; Yin, X.; Weiss, S.A.; Darvishian, F.; Al-Rohil, R.N.; Ndoye, A.; et al. Age Correlates with Response to Anti-PD1, Reflecting Age-Related Differences in Intratumoral Effector and Regulatory T-Cell Populations. *Clin. Cancer Res.* **2018**, *24*, 5347–5356. [CrossRef]
72. Hodi, F.S.; O'Day, S.J.; McDermott, D.F.; Weber, R.W.; Sosman, J.A.; Haanen, J.B.; Gonzalez, R.; Robert, C.; Schadendorf, D.; Hassel, J.C.; et al. Improved Survival with Ipilimumab in Patients with Metastatic Melanoma. *N. Engl. J. Med.* **2010**, *363*, 711–723. [CrossRef]
73. Chiarion-Sileni, V.; Pigozzo, J.; Ascierto, P.; Grimaldi, A.M.; Maio, M.; Di Guardo, L.; Marchetti, P.; de Rosa, F.; Nuzzo, C.; Testori, A.; et al. Efficacy and safety of ipilimumab in elderly patients with pretreated advanced melanoma treated at Italian centres through the expanded access programme. *J. Exp. Clin. Cancer Res.* **2014**, *33*, 30. [CrossRef]
74. Motzer, R.J.; Escudier, B.; George, S.; Hammers, H.J.; Srinivas, S.; Tykodi, S.S.; Sosman, J.A.; Plimack, E.R.; Procopio, G.; McDermott, D.F.; et al. Nivolumab versus everolimus in patients with advanced renal cell carcinoma: Updated results with long-term follow-up of the randomized, open-label, phase 3 CheckMate 025 trial. *Cancer* **2020**, *126*, 4156–4167. [CrossRef]
75. Daste, A.; Domblides, C.; Gross-Goupil, M.; Chakiba, C.; Quivy, A.; Cochin, V.; De Mones, E.; Larmonier, N.; Soubeyran, P.; Ravaud, A. Immune checkpoint inhibitors and elderly people: A review. *Eur. J. Cancer* **2017**, *82*, 155–166. [CrossRef]
76. McGranahan, N.; Furness, A.J.S.; Rosenthal, R.; Ramskov, S.; Lyngaa, R.; Saini, S.K.; Jamal-Hanjani, M.; Wilson, G.A.; Birkbak, N.J.; Hiley, C.; et al. Clonal neoantigens elicit T cell immunoreactivity and sensitivity to immune checkpoint blockade. *Science* **2016**, *351*, 1463–1469. [CrossRef]
77. Hugo, W.; Zaretsky, J.M.; Sun, L.; Song, C.; Moreno, B.H.; Hu-Lieskovan, S.; Berent-Maoz, B.; Pang, J.; Chmielowski, B.; Cherry, G.; et al. Genomic and Transcriptomic Features of Response to Anti-PD-1 Therapy in Metastatic Melanoma. *Cell* **2016**, *165*, 35–44. [CrossRef]

78. Castro, A.; Pyke, R.M.; Zhang, X.; Thompson, W.K.; Day, C.-P.; Alexandrov, L.B.; Zanetti, M.; Carter, H. Strength of immune selection in tumors varies with sex and age. *Nat. Commun.* **2020**, *11*, 1–9. [CrossRef]
79. Moreira, A.; Gross, S.; Kirchberger, M.C.; Erdmann, M.; Schuler, G.; Heinzerling, L.; Groß, S. Senescence markers: Predictive for response to checkpoint inhibitors. *Int. J. Cancer* **2019**, *144*, 1147–1150. [CrossRef]
80. Cherkassky, L.; Morello, A.; Villena-Vargas, J.; Feng, Y.; Dimitrov, D.S.; Jones, D.R.; Sadelain, M.; Adusumilli, P.S. Human CAR T cells with cell-intrinsic PD-1 checkpoint blockade resist tumor-mediated inhibition. *J. Clin. Investig.* **2016**, *126*, 3130–3144. [CrossRef]
81. Kasakovski, D.; Xu, L.; Li, Y. T cell senescence and CAR-T cell exhaustion in hematological malignancies. *J. Hematol. Oncol.* **2018**, *11*, 91. [CrossRef]
82. Das, S.; Johnson, D.B. Immune-related adverse events and anti-tumor efficacy of immune checkpoint inhibitors. *J. Immunother. Cancer* **2019**, *7*, 306–311. [CrossRef]
83. Battram, A.M.; Bachiller, M.; Martin-Antonio, B. Senescence in the Development and Response to Cancer with Immunotherapy: A Double-Edged Sword. *Int. J. Mol. Sci.* **2020**, *21*, 4346. [CrossRef]
84. Ovadya, Y.; Krizhanovsky, V. Strategies targeting cellular senescence. *J. Clin. Investig.* **2018**, *128*, 1247–1254. [CrossRef]
85. Patnaik, A.; Haluska, P.; Tolcher, A.W.; Erlichman, C.; Papadopoulos, K.P.; Lensing, J.L.; Beeram, M.; Molina, J.R.; Rasco, D.; Arcos, R.R.; et al. A First-in-Human Phase I Study of the Oral p38 MAPK Inhibitor, Ralimetinib (LY2228820 Dimesylate), in Patients with Advanced Cancer. *Clin. Cancer Res.* **2015**, *22*, 1095–1102. [CrossRef]
86. Ebert, P.J.; Cheung, J.; Yang, Y.; McNamara, E.; Hong, R.; Moskalenko, M.; Gould, S.E.; Maecker, H.; Irving, B.A.; Kim, J.M.; et al. MAP Kinase Inhibition Promotes T Cell and Anti-tumor Activity in Combination with PD-L1 Checkpoint Blockade. *Immunity* **2016**, *44*, 609–621. [CrossRef]
87. Loi, S.; Dushyanthen, S.; Beavis, P.A.; Salgado, R.; Denkert, C.; Savas, P.; Combs, S.; Rimm, D.L.; Giltnane, J.M.; Estrada, M.V.; et al. RAS/MAPK Activation Is Associated with Reduced Tumor-Infiltrating Lymphocytes in Triple-Negative Breast Cancer: Therapeutic Cooperation Between MEK and PD-1/PD-L1 Immune Checkpoint Inhibitors. *Clin. Cancer Res.* **2015**, *22*, 1499–1509. [CrossRef]
88. Chang, J.; Wang, Y.; Shao, L.; Laberge, R.-M.; Demaria, M.; Campisi, J.; Janakiraman, K.; Sharpless, N.E.; Ding, S.; Feng, W.; et al. Clearance of senescent cells by ABT263 rejuvenates aged hematopoietic stem cells in mice. *Nat. Med.* **2016**, *22*, 78–83. [CrossRef]
89. Zhu, Y.; Tchkonia, T.; Pirtskhalava, T.; Gower, A.C.; Ding, H.; Giorgadze, N.; Palmer, A.K.; Ikeno, Y.; Hubbard, G.B.; Lenburg, M.; et al. The Achilles' heel of senescent cells: From transcriptome to senolytic drugs. *Aging Cell* **2015**, *14*, 644–658. [CrossRef]
90. Fuhrmann-Stroissnigg, H.; Ling, Y.Y.; Zhao, J.; McGowan, S.J.; Zhu, Y.; Brooks, R.W.; Grassi, D.; Gregg, S.Q.; Stripay, J.L.; Dorronsoro, A.; et al. Identification of HSP90 inhibitors as a novel class of senolytics. *Nat. Commun.* **2017**, *8*, 422. [CrossRef]
91. Deschênes-Simard, X.; Gaumont-Leclerc, M.-F.; Bourdeau, V.; Lessard, F.; Moiseeva, O.; Forest, V.; Igelmann, S.; Mallette, F.A.; Saba-El-Leil, M.K.; Meloche, S.; et al. Tumor suppressor activity of the ERK/MAPK pathway by promoting selective protein degradation. *Genes Dev.* **2013**, *27*, 900–915. [CrossRef]
92. Astle, M.V.; Hannan, K.M.; Ng, P.Y.; Lee, R.S.; George, A.J.; Hsu, A.K.; Haupt, Y.; Hannan, R.D.; Pearson, R.B. AKT induces senescence in human cells via mTORC1 and p53 in the absence of DNA damage: Implications for targeting mTOR during malignancy. *Oncogene* **2011**, *31*, 1949–1962. [CrossRef]
93. Dietsch, G.N.; Randall, T.D.; Gottardo, R.; Northfelt, D.W.; Ramanathan, R.K.; Cohen, P.A.; Manjarrez, K.L.; Newkirk, M.; Bryan, J.K.; Hershberg, R.M. Late Stage Cancer Patients Remain Highly Responsive to Immune Activation by the Selective TLR8 Agonist Motolimod (VTX-2337). *Clin. Cancer Res.* **2015**, *21*, 5445–5452. [CrossRef]
94. Chow, L.Q.M.; Morishima, C.; Eaton, K.D.; Baik, C.S.; Goulart, B.H.; Anderson, L.N.; Manjarrez, K.L.; Dietsch, G.N.; Bryan, J.K.; Hershberg, R.M.; et al. Phase Ib Trial of the Toll-like Receptor 8 Agonist, Motolimod (VTX-2337), Combined with Cetuximab in Patients with Recurrent or Metastatic SCCHN. *Clin. Cancer Res.* **2017**, *23*, 2442–2450. [CrossRef]

nature COMMUNICATIONS

ARTICLE

Received 7 Nov 2016 | Accepted 30 Dec 2016 | Published 1 Mar 2017

DOI: 10.1038/ncomms14447 OPEN

Spatiotemporally restricted arenavirus replication induces immune surveillance and type I interferon-dependent tumour regression

Halime Kalkavan[1,2], Piyush Sharma[1], Stefan Kasper[2], Iris Helfrich[3], Aleksandra A. Pandyra[1], Asmae Gassa[1,4], Isabel Virchow[2], Lukas Flatz[5], Tim Brandenburg[1], Sukumar Namineni[6], Mathias Heikenwalder[6], Bastian Höchst[7], Percy A. Knolle[7], Guido Wollmann[8], Dorothee von Laer[8], Ingo Drexler[9], Jessica Rathbun[10], Paula M. Cannon[10], Stefanie Scheu[11], Jens Bauer[11], Jagat Chauhan[12], Dieter Häussinger[13], Gerald Willimsky[14,15], Max Löhning[16], Dirk Schadendorf[3,17], Sven Brandau[18,*], Martin Schuler[2,17,*], Philipp A. Lang[19,*] & Karl S. Lang[1,*]

Immune-mediated effector molecules can limit cancer growth, but lack of sustained immune activation in the tumour microenvironment restricts antitumour immunity. New therapeutic approaches that induce a strong and prolonged immune activation would represent a major immunotherapeutic advance. Here we show that the arenaviruses lymphocytic choriomeningitis virus (LCMV) and the clinically used Junin virus vaccine (Candid#1) preferentially replicate in tumour cells in a variety of murine and human cancer models. Viral replication leads to prolonged local immune activation, rapid regression of localized and metastatic cancers, and long-term disease control. Mechanistically, LCMV induces antitumour immunity, which depends on the recruitment of interferon-producing Ly6C$^+$ monocytes and additionally enhances tumour-specific CD8$^+$ T cells. In comparison with other clinically evaluated oncolytic viruses and to PD-1 blockade, LCMV treatment shows promising antitumoural benefits. In conclusion, therapeutically administered arenavirus replicates in cancer cells and induces tumour regression by enhancing local immune responses.

[1] Institute of Immunology, Medical Faculty, University Duisburg-Essen, 45122 Essen, Germany. [2] Department of Medical Oncology, West German Cancer Center, University Hospital Essen, University Duisburg-Essen, 45122 Essen, Germany. [3] Department of Dermatology, West German Cancer Center, University Hospital Essen, University Duisburg-Essen, 45122 Essen, Germany. [4] Department of Cardiothoracic Surgery, Cologne University Heart Center, Kerpener Strasse 62, 50937 Cologne, Germany. [5] Department of Dermatology/Allergology, Cantonal Hospital, Rorschacher Strasse 95, St. Gallen 9007, Switzerland. [6] Department of Virology, Technical University of Munich, Schneckenburgstrasse 8, 81675 Munich, Germany. [7] Institute of Molecular Immunology/Experimental Oncology, München Klinikum rechts der Isar, Technical University Munich, 81675 Munich, Germany. [8] Division for Virology, Medical University Innsbruck, Peter-Mayr-Strasse 4b, 6020 Innsbruck, Austria. [9] Institute of Virology, Düsseldorf University Hospital, Heinrich Heine University, Universitätsstrasse 1, 40225 Düsseldorf, Germany. [10] Department of Molecular Microbiology and Immunology, University of Southern California, Los Angeles, 90033 California, USA. [11] Institute of Medical Microbiology and Hospital Hygiene, University of Düsseldorf, Universitätsstrasse 1, 40225 Düsseldorf, Germany. [12] Ludwig Institute for Cancer Research, University of Oxford, Old Road Campus, Research Building, Old Road Campus, Headington, Oxford OX3 7DQ, UK. [13] Department of Gastroenterology, Hepatology and Infectious Diseases, University of Düsseldorf, Universitätsstrasse 1, 40225 Düsseldorf, Germany. [14] Institute of Immunology (Charité - University Medicine Berlin), 3125 Berlin, Germany. [15] German Cancer Research Center (DKFZ), 13125 Heidelberg, Germany. [16] Department of Rheumatology and Clinical Immunology, Charité—University Medicine Berlin and German Rheumatism Research Center (DRFZ), Charitéplatz 1, D-10117 Berlin, Germany. [17] German Cancer Consortium (DKTK), Partner Site University Hospital Essen, 45122 Essen, Germany. [18] Department of Otorhinolaryngology, West German Cancer Center, University Hospital Essen, University Duisburg-Essen, 45122 Essen, Germany. [19] Department of Molecular Medicine II, Medical Faculty, Heinrich Heine University, Universitätsstrasse 1, D-40225 Düsseldorf, Germany. * These authors contributed equally to this work. Correspondence and requests for materials should be addressed to M.S. (email: martin.schuler@uk-essen.de) or to K.S.L. (email: karlsebastian.lang@uk-essen.de).

Effective treatment of advanced tumours remains a major challenge because of limited availability of tumour-specific agents and development of drug resistance. Next to chemotherapy and targeted therapies, immunotherapy is one promising approach to treat cancer[1].

The immune system can directly attack tumour cells via antigen-specific cytotoxic $CD8^+$ T cells, activated natural killer (NK) cells or antibody-mediated cytotoxicity[2,3]. In addition, cytokines such as tumour necrosis factor-α, interferon (IFN)-γ or type I IFN (IFN-I) can directly exert antiproliferative and pro-apoptotic effects on tumour cells, or indirectly, through modulation of the tumour microenvironment[1,4]. Despite the physiological existence of these potent anticancer effector molecules, neoplastic cells can survive and expand in immune-competent individuals. Escape from immune surveillance is mainly explained by limited immune activation or tumour-induced immunosuppression within the microenvironment[2]. Effective induction of strong and sustained immune activation at the tumour sites would therefore be a promising therapeutic approach against cancer.

Viruses have a very high capacity to activate the innate and adaptive immune system. This is mainly explained by three mechanisms. First, viruses introduce new antigens to the immune system, which are recognized by the host as foreign[5]. Second, viruses carry ligands for pattern recognition receptors, which trigger the innate immune system[5]. Third, viruses are usually drained from peripheral sites to the lymphatic system where they undergo spatiotemporally restricted replication in antigen-presenting cells and thereby specifically activate innate and adaptive immune cells[6,7].

Arenaviruses are enveloped and pleiomorphic, with a diameter of 60–300 nm and two single-stranded RNA genome segments. The non-cytopathic arenaviruses propagate rapidly without directly harming susceptible tissues. Rather, it is the immune response against infected cells that may cause severe tissue damage and disease symptoms[8,9]. Arenaviruses can infect humans and disease outcome depends on the specific strain. Lassa virus and Junin virus are responsible for the Lassa and Argentine haemorrhagic fever, respectively[10]. In contrast, human infection with the arenavirus strains lymphocytic choriomeningitis virus (LCMV, strain WE) and Candid#1, which is a clinically applied vaccine virus to protect against Argentine haemorrhagic fever, is usually asymptomatic or causes non-specific symptoms such as fever and malaise[11,12]. LCMV-WE induces a strong T-cell response, which can be antitumoural in cancer models[13,14]. Therefore, recombinant single-cycle LCMV is considered a vaccine virus with potential to immunize against tumour antigens[15].

Here we investigate whether neoplastic cells can serve as natural reservoir for arenavirus replication and whether such replication can induce spatiotemporally restricted innate immunity, virus-specific and tumour-specific adaptive immune activation. We show that LCMV and Candid#1 preferentially replicate in cancer cells and induce immune surveillance resulting in IFN-I-dependent tumour regression.

Results

Arenavirus preferentially replicates in cancer cells. In recent times, we found that fast replication of arenavirus in dendritic cells led to massive activation of the innate and adaptive immune system[6]. As cancer cells are characterized by altered cell cycle, metabolism and translation[16] relative to their normal counterparts, we wondered whether arenaviruses might preferentially replicate in tumour cells and whether this affects the antitumoural immune response. To explore the replication capacity of arenaviruses in tumour cells, we infected human cancer cells and the healthy parenchymal counterpart they originated from with the non-cytopathic LCMV. Primary hepatocytes, colon epithelial cells, melanocytes and bronchial epithelial cells showed limited LCMV replication as compared with malignant cells originating from these tissues (Fig. 1a,b). Having established that arenaviruses preferentially replicate in tumour cells, we next infected a tumorigenic cell line that is capable of forming tumours in a syngeneic setting using immune-competent mice. Specifically, we infected the murine squamous oropharynx carcinoma cell line (MOPC)[17] with LCMV-WE *in vitro*. Within 72 h, all cancer cells revealed LCMV replication without affected cell survival (Fig. 1c and Supplementary Fig. 1). Next, we established palpable tumours in C57BL/6 mice by subcutaneous injection of MOPC cells and infected the mice with 2×10^4 plaque-forming unit (PFU) LCMV peritumourally. Immunofluorescence revealed viral replication within these tumours, but not in other regions of the skin (Fig. 1d). The presence of subcutaneous MOPC tumours significantly increased local and splenic virus propagation in C57BL/6 mice (Fig. 1e) and virus persisted in tumours for more than 30 days (Fig. 1f). To generalize this phenomenon, we analysed the replication of LCMV in a broad panel of other murine cancer models. Peritumoural injection of LCMV in subcutaneously established B16F10 melanoma[18] and MC38 colon cancer[19], as well as intravenous administration of LCMV in endogenously hepatocellular carcinoma bearing LoxP-TAg[20] resulted in intratumoural propagation of LCMV (Fig. 1g–i).

B-Myb promotes arenavirus replication. Lack of IFN-I receptor and deregulated IFN signalling is proposed to be one mechanism accounting for enhanced viral replication and IFN-unresponsiveness in cancer cells[21,22]. However, analysis of the Cancer Genome Atlas (TCGA) database revealed high expression of *Ifnar1* and *Ifnar2* in a range of cancer entities (Supplementary Fig. 2a) and human cancer cell lines showed expression of *Ifnar1* and *Ifnar2* (Supplementary Fig. 2b). To test whether human cancer cell lines can respond to some of the many murine IFN-I in a xenograft system, we treated Sw480 cells and HeLa cells with different IFN-I subtypes *in vitro*. Sw480 and HeLa cells responded to murine IFN-α2 and human IFN-α4 but not to murine IFN-α4 (Supplementary Fig. 2c). Moreover, all the murine cancer cells tested in our *in vivo* studies expressed *Ifnar1* (Supplementary Fig. 2d). In comparison with MC38, B16F10, LoxP-TAg and MT/ret, MOPC cells showed highest expression levels (Supplementary Fig. 2d).

We hypothesized that the fast cell cycle and metabolism of cancer cells promote replication of arenavirus and thereby explains the fast propagation of LCMV in cancer cells. Recent reports show that the expression of the cell cycle kinase CDK2 is associated with increased HIV replication in myeloid and lymphoid cells[23]. CDK2 phosphorylates B-Myb, which enhances the transcription of a number of genes involved in cell proliferation and metabolism[24,25]. To explore whether B-Myb (*Mybl2*) is one factor in cancer cells contributing to enhanced arenavirus replication, we studied *Mybl2* expression and phosphorylation in cancer tissues and non-malignant controls. Indeed, tumours expressed higher *Mybl2* RNA levels and exhibited increased B-Myb phosphorylation (Supplementary Fig. 2e,f). The presence of B-Myb correlated with higher expression of known viral host factors in MOPC tumours than control tissue (Supplementary Fig. 2g). In line, knockdown of B-Myb limited LCMV replication (Supplementary Fig. 2h). Therefore, we concluded that B-myb overexpression is one viral susceptibility factor in cancer cells.

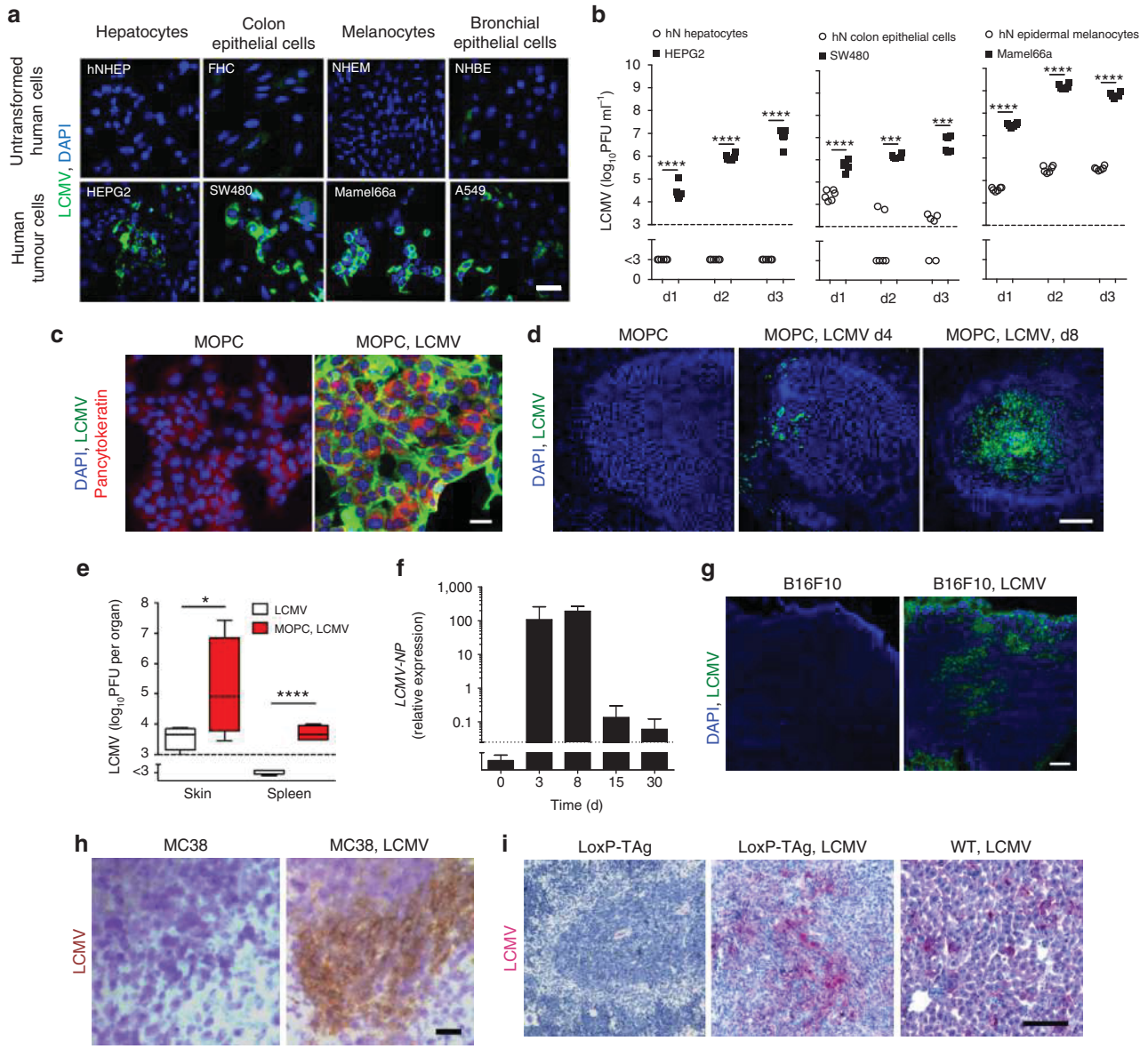

Figure 1 | Arenavirus preferentially replicates and persists in cancer cells. (**a**) Immunofluorescence in tissue-matched human normal untransformed and tumour cells 2 days after LCMV infection (MOI 1) ($n=3$ per group). Scale bar, 20 μm. (**b**) Infectious virus particles in supernatants from human normal (hN) untransformed and tumour cells, which were infected with LCMV (MOI 1) and analysed on indicated days ($n=6$ per group). (**c**) Immunofluorescence of MOPC cells untreated or infected with LCMV (MOI 1) 72 h after infection ($n=3$/group). Scale bar, 20 μm. (**d**) Immunofluorescence of tumours in MOPC-tumour-bearing C57BL/6 mice (day −10) treated with or without 2×10^4 PFU LCMV peritumourally (LCMV, green; 4,6-diamidino-2-phenylindole (DAPI), blue, $n=3$ per group). Scale bar, 200 μm. (**e**) Infectious virus particles in skin and spleen (day 8) of C57BL/6 mice or MOPC-tumour-bearing mice (day −3) treated with 2×10^4 PFU LCMV subcutaneously ($n=4$ per group). (**f**) LCMV-NP RNA in tumours of MOPC-tumour-bearing C57BL/6 mice (day −10) treated with 2×10^4 PFU LCMV intratumourally ($n=8$ per group). (**g**) Immunofluorescence of tumours (day 7, $n=3$) from B16F10-tumour-bearing C57BL/6 mice (day −3) treated with or without 2×10^4 PFU LCMV peritumourally. Scale bar, 200 μm. (**h**) Immunohistochemistry of tumours (day 7, $n=3$) from MC38-bearing C57BL/6 mice (day −3) treated with ($n=6$) or without ($n=7$) 2×10^4 PFU LCMV peritumourally. Scale bar, 200 μm. (**i**) Immunohistochemistry (day 6, $n=3$) of livers from LoxP-Tag-tumour-bearing or WT mice, which were treated with or without 2×10^6 PFU LCMV systemically. Scale bar, 200 μm. Data are shown as mean ± s.e.m. and analysed by unpaired Student's *t*-test. $^*P<0.05$, $^{***}P<0.001$ and $^{****}P<0.0001$.

Arenavirus replication leads to tumour regression. Next we wondered whether LCMV replication in tumour cells influences tumour progression. We infected C57BL/6 mice bearing small tumours with LCMV peritumourally. Untreated control tumours grew robustly and mice succumbed to the tumour within 30 days (Fig. 2a). Peritumoural LCMV injection completely abolished tumour growth and mice survived relapse-free for an observational time of 80 days (Fig. 2a), without virus- or tumour-related symptoms. In mice bearing very advanced MOPC tumours, LCMV infection induced considerable tumour regression and significantly prolonged survival (Fig. 2b). To explore the activity of LCMV virotherapy in metastatic cancers, we compared local and systemic virus administration in mice bearing simultaneous MOPC tumours in the left shoulder and the right flank. Peritumoural injection of LCMV in the right flank resulted in virus replication only in the flank (Supplementary Fig. 3a). Systemically administered LCMV reached both tumour sites (Supplementary Fig. 3a). In agreement, intravenous LCMV application, but not

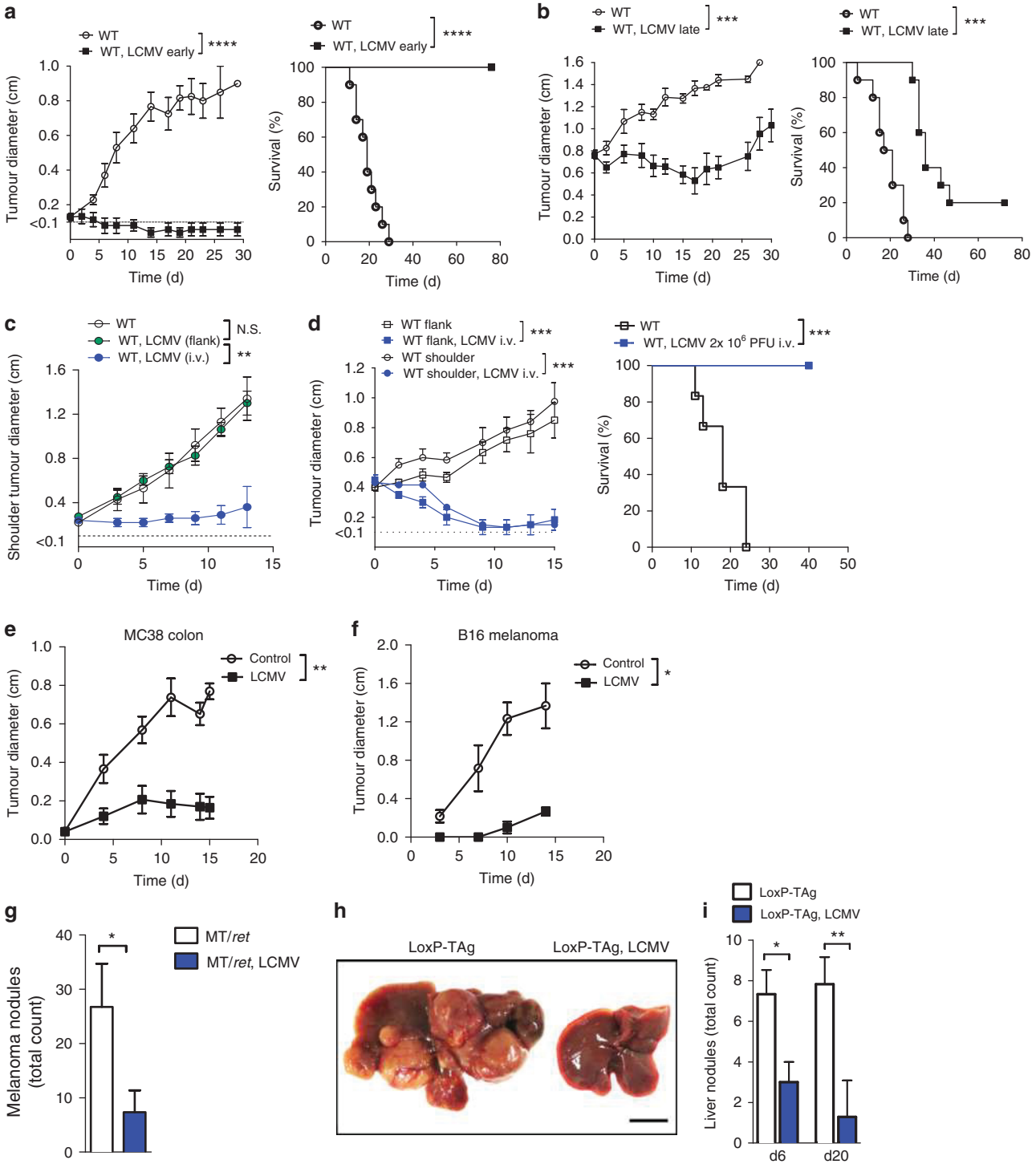

Figure 2 | Persistence of arenavirus leads to tumour regression. (**a**) Tumour diameter and survival of MOPC-tumour-bearing mice (day −3) treated with or without 2×10^4 PFU LCMV peritumourally ($n=10$ per group, three experiments pooled). (**b**) Tumour diameter and survival of MOPC-tumour-bearing mice (day −10) treated with or without 2×10^4 PFU LCMV intratumourally ($n=10$ per group, three experiments pooled). (**c**) Tumour diameter of the shoulder tumour from C57BL/6 mice receiving simultaneously subcutaneously 5×10^5 MOPC cells in the flank and shoulder (day −3), treated without ($n=5$) or with 2×10^4 PFU LCMV given into the flank ($n=4$) or intravenously ($n=5$). (**d**) Tumour diameters (shoulder and flank) and survival of WT mice bearing MOPC tumours simultaneously in the shoulder and flank, treated with or without 2×10^6 PFU LCMV intravenously on day 0 ($n=6$ per group). (**e**) Tumour diameter from MC38-bearing C57BL/6 mice (day −3) treated with ($n=6$) or without ($n=7$) 2×10^4 PFU LCMV peritumourally. (**f**) Tumour diameters from B16F10-tumour-bearing C57BL/6 mice (day −3) treated with or without 2×10^4 PFU LCMV peritumourally ($n=6$ per group). (**g**) Number of melanomas (day 15) in MT/*ret* mice treated with ($n=3$) or without ($n=4$) 2×10^4 PFU LCMV systemically. (**h**,**i**) Representative picture (**h**, day 6, $n=3$) and quantification of tumour nodules (**i**, day 6 $n=3$, day 20 $n=6$) of/in the livers from LoxP-Tag-tumour-bearing or WT mice, which were treated with or without 2×10^6 PFU LCMV systemically. Scale bar, 0.5 cm. Data are shown as mean ± s.e.m. and analysed by unpaired Student's *t*-test. $^*P<0.05$, $^{**}P<0.01$, $^{***}P<0.001$ and $^{****}P<0.0001$.

local LCMV injection into the flank tumour, induced regression of distant shoulder tumours (Fig. 2c). Conclusively, control of multiple tumour sites and prolonged survival of mice with advanced stage metastatic tumours can be achieved by systemic LCMV therapy (Fig. 2d). Next, we analysed the antitumoural activity of LCMV against a broad panel of murine cancer models including MC38 colon cancer[19], B16F10 melanoma[18], the endogenous hepatocellular carcinoma model LoxP-TAg[20] and spontaneous MT/*ret* melanoma model[26]. Peritumoural injection of LCMV limited the growth of subcutaneous MC38 (Fig. 2e) and B16F10 melanoma tumours (Fig. 2f). To test the activity of LCMV virotherapy on spontaneously developing malignant melanomas in the MT/*ret* mouse model[26], LCMV was injected intravenously once cutaneous tumours became palpable. Strikingly, LCMV-infected MT/*ret* mice developed significantly less macroscopically visible tumour nodules than untreated mice (Fig. 2g). Next, we studied LCMV virotherapy in endogenously developing liver cancers. Nine-month-old LoxP-TAg mice harbouring palpable liver tumours either received an intravenous injection of LCMV (2×10^6 PFU) or were left untreated. Intriguingly, 20 days after LCMV injection tumour nodules had largely disappeared (Fig. 2h,i). Consistent with these findings, serum liver enzyme levels, which reflect tumour burden in the liver, were significantly lower in LCMV-treated LoxP-TAg mice than in uninfected LoxP-TAg controls (Supplementary Fig. 3b).

IFN-I was essential for tumour regression. To dissect whether LCMV replication or LCMV-induced immune infiltration impacts tumour growth, we studied tumour growth in *Map3-k14*$^{aly/aly}$ mice, which have defective nuclear factor-κB signalling and therefore lack lymph nodes and immune functions[27]. LCMV-induced tumour regression was dependent on *Map3k14* (Supplementary Fig. 4), suggesting that immune infiltration is crucial. Indeed, LCMV replication induced a dense infiltrate composed of T cells (CD90.2, CD4 and CD8) and inflammatory Ly6C$^+$ monocytes (Fig. 3a). Strong infiltrates of Ly6C$^+$ monocytes were detected in draining lymph nodes (dLNs) of LCMV-treated subcutaneous MOPC tumours (Fig. 3b). Monocytes have the plasticity to execute diverse effector functions and are therefore equipped to inhibit tumour growth[28]. As inflammatory monocytes also produce IFN-I after innate sensing[29], we postulated that LCMV-induced IFN-I secretion in Ly6C$^+$ monocytes impacts tumour growth. To analyse IFN-I production in Ly6C$^+$ monocytes, we established MOPC tumours in IFN-β reporter mice (IFNβ$^{mob/mob}$) and infected them with LCMV[30]. IFN-β-producing Ly6C$^+$ monocytes were detected in the dLN of tumour-bearing mice after infection with LCMV (Fig. 3c). Ly6C$^+$ monocytes were further characterized as mPDCA-1^{hi}, CD11c^{med} and B220^{med} (Fig. 3c), suggesting that they were differentiated into IFN-I-producing cells[31]. Consistently, quantitative real-time PCR (qRT–PCR) analysis revealed high expression of IFN-I-associated genes in dLN after LCMV infection, and IFN-α serum levels were enhanced in LCMV-infected tumour-bearing mice (Fig. 3d,e). To dissect the role of monocytes and IFN-I on tumour regression, we studied tumour growth in mice depleted of myeloid cells *in vivo* using different antibodies. First, we treated mice with an antibody against the myeloid differentiation antigen Gr-1 (clone RB6-8C5), which depletes Ly6G$^+$ and Ly6C$^+$ cells[32–34] (Supplementary Fig.5a). Another experimental group was treated with an antiLy6G antibody (clone 1A8), which only binds to Ly6G$^+$ cells (Supplementary Fig. 5b). Depletion of Ly6C$^+$ and Ly6G$^+$ cells (monocytes and granulocytes) with clone RB6-8C5 abrogated LCMV-mediated tumour suppression (Fig. 3f), whereas depletion of Ly6G$^+$ cells (granulocytes) with clone 1A8 alone had no impact on the antitumoural effect of LCMV (Supplementary Fig. 5c). This suggests that monocytes are centrally involved in LCMV-induced tumour regression. The role of monocytes was confirmed using *Ccr2*$^{-/-}$ mice, which have reduced monocyte numbers[28] and in which LCMV-mediated tumour suppression was significantly blunted (Fig. 3g). To corroborate the involvement of IFN-I in LCMV-mediated tumour regression, we used *Irf3*$^{-/-}$*xIrf7*$^{-/-}$ mice, which lack IFN-I induction after LCMV infection[35]. LCMV infection failed to suppress tumour growth in *Irf3*$^{-/-}$*xIrf7*$^{-/-}$ mice (Fig. 3h), supporting the functional importance of IFN-I for the antitumour effect of arenavirus infection. Analysis of T cells (Supplementary Fig. 6a), B cells (Supplementary Fig. 6b) and NK cells (Supplementary Fig. 6c,d) failed to reveal an impact of these immune cell subsets on LCMV-induced control of early stage tumours, suggesting that IFN-I acts independent of these cell subsets on tumour regression.

Monocyte recruitment and IFN-I induction in human cancer. To gain further insights into the possible translation of arenaviruses to human cancer therapy we studied primary tumour biopsies from 34 patients with oropharyngeal cancers. Multigene expression analysis by qRT–PCR revealed a strong correlation between the expression of human monocytic markers *CD14* or *CD16* and diverse IFN-I-related genes such as *IFNB1*, *USP18* and *IRF7* (Supplementary Fig. 7a,b), indicating that human monocytic infiltrates can produce IFN-I within human tumour tissues. To investigate whether our observation is expandable to different human cancer types, we accomplished a gene-set enrichment analysis (GSEA) by using the human cancer TCGA database. Indeed, *CD14*$^+$ cell populations were enriched for IFN-I-related genes (Supplementary Fig. 7c)[36].

Ambiguous role of CD8$^+$ T cells in cancer virotherapy. So far, we found that monocytes and IFN-I were essential factors needed for tumour regression, and that T cells were dispensable for LCMV cancer therapy of early stage tumours. However, we wondered how the presence of CD8$^+$ T cells might also contribute to tumour regression. We hypothesized that CD8$^+$ T cells have a dual role in arenavirus-based therapy. On the one hand, they are essential in controlling virus, therefore limiting viral persistence. On the other hand, tumour-specific CD8$^+$ T cells might be activated by arenavirus and might therefore contribute to tumour regression. Indeed, we found that virus-specific CD8$^+$ T cells were induced during arenavirus therapy (Fig. 4a). The presence of virus-specific CD8$^+$ T cells limited replication and effectiveness of LCMV therapy during systemic treatment (Supplementary Fig. 8a). Conversely, lack of virus-specific CD8$^+$ T cells prolonged the antitumoural effects of IFN-I and enhanced survival even in an advanced tumour stage (Supplementary Fig. 8b,c).

To analyse the role of LCMV on tumour-specific CD8$^+$ T cells, we infected mice bearing Ovalbumin-expressing B16F10 tumours in the presence of tumour-specific CD8$^+$ T cells. LCMV enhanced expression of IL-2Rβ (CD122) and IL-7Rα (CD127) on tumour-specific CD8$^+$ T cells, both of which promote cell survival (Fig. 4b)[8]. Moreover, LCMV infection enhanced tumour-specific CD8$^+$ T cells in tumour infiltrates after vaccination with tumour antigen (Fig. 4c). Accordingly, the combination of LCMV and tumour-specific CD8$^+$ T cells was most effective in suppressing tumour growth in the B16F10 melanoma model and in the EL4 subcutaneous lymphoma model (Fig. 4d,e). This suggests that LCMV enhances the infiltration and function of tumour-specific CD8$^+$ T cells, which contributes to LCMV-mediated tumour regression.

Reduced vasculature correlates with LCMV treatment. Next, we investigated the mechanism of IFN-I-induced tumour suppression in our models. As MOPC cells express the IFN-α/β receptor subunit 1 (IFNAR1) (Supplementary Fig. 2d), we analysed LCMV-induced tumour regression in *Ifnar*$^{-/-}$ mice, which are deficient in the IFN-I receptor. LCMV infection equally suppressed tumour growth in wild type (WT) and *Ifnar*$^{-/-}$ mice (Supplementary Fig. 9), suggesting that IFN-I secreted by infiltrating Ly6C^{+} monocytes directly acts on tumour cells. As IFN-Is are potent inhibitors of tumour associated angiogenesis[37], we studied the expression of angiogenic factors by tumour cells in relation to LCMV treatment. Interestingly, almost all angiogenic

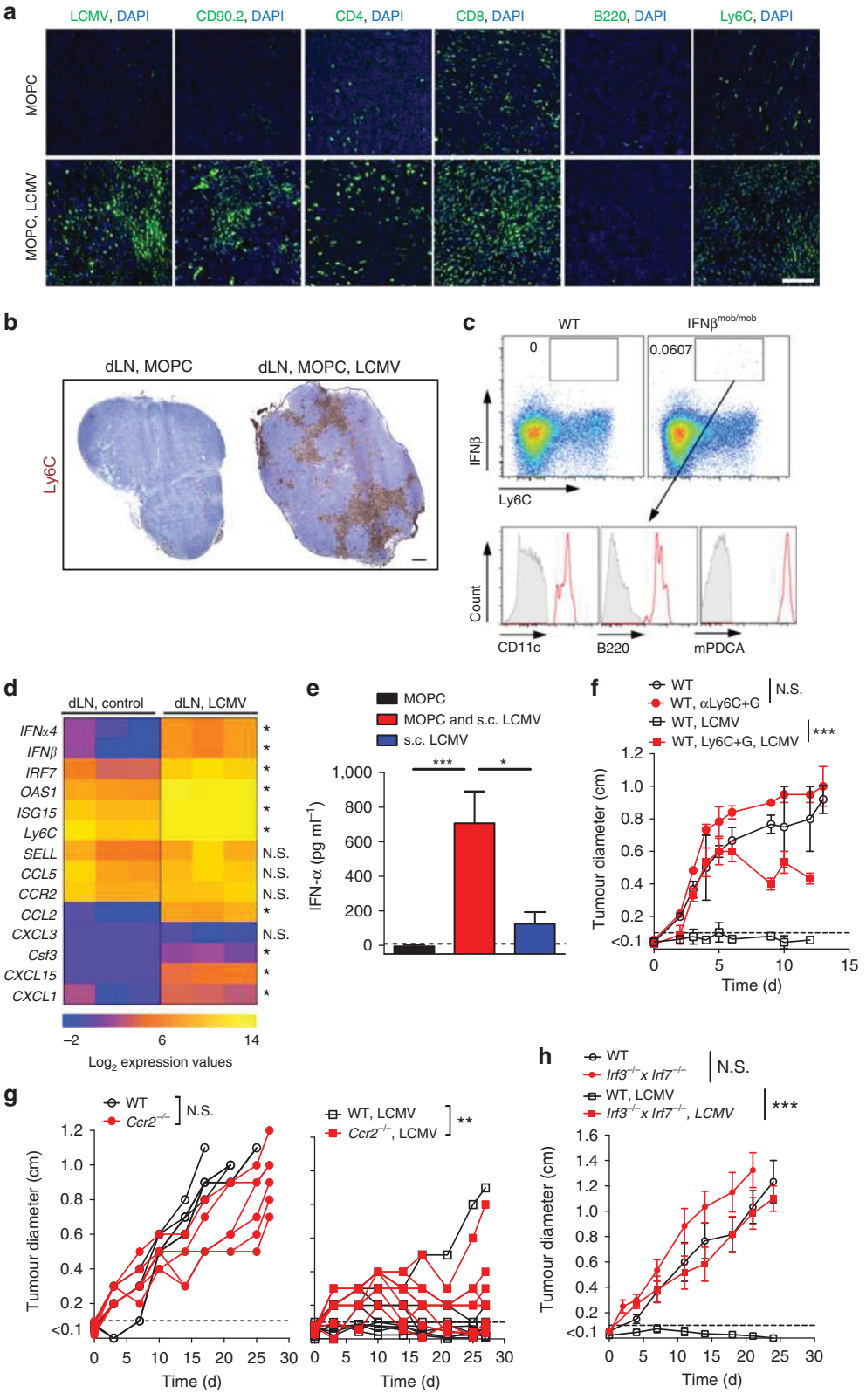

regulators studied were suppressed by LCMV infection (Supplementary Fig. 10a). Moreover, CD31$^+$ vessel formation was severely blunted in LCMV-infected tumours (Supplementary Fig. 10b), leading to reduced microvessel density (MVD) and increased vessel-to-vessel distances (Supplementary Fig. 10c). Consistent with reduced angiogenesis, we observed hypoxic areas in LCMV-treated tumours (Supplementary Fig. 10d) that were characterized by limited tumour cell proliferation and increased apoptosis (Supplementary Fig. 10e).

Arenaviruses induce regression of human tumours. To explore whether arenavirus therapy could be translated to the human system, we used human xenograft models in NOD/SCID mice. Peritumoural LCMV injection led to regression of subcutaneously established HeLa and FaDu tumours in NOD/SCID mice (Fig. 5a,b). Next, we studied the clinically used Junin virus vaccine, Candid#1 (refs 11,12). Candid#1 replicated in Sw480- and HepG2-tumours *in vivo* (Fig. 5c,d). Infection with LCMV and with Candid#1 limited growth of Sw480 tumours (Fig. 5e). Similarly, Candid#1 limited growth of HepG2 and Sw872 tumours (Fig. 5f,g). These data suggest that the vaccine virus Candid#1 has antitumoural properties much similar to the laboratory strain LCMV-WE.

LCMV is superior to oncolytic viruses and PD1 blockade. Next, we compared LCMV with two oncolytic viruses presently in clinical or preclinical development: a chimeric variant of vesicular stomatitis virus (VSV-GP)[38] and a recombinant TK-depleted vaccinia virus (TK$^-$ VACV-GFP/LacZ, rVACV)[39]. Although VSV-GP is currently being developed (www.viratherapeutics.com), another very similar VSV variant (VSV-IFN) is being investigated in a Phase I study for hepatocellular carcinoma (ClinicalTrials.gov NCT01628640). rVACV is so far tested as a double deletion mutant (TK$^-$ and VGF$^-$) in a phase I study, with patients with advanced solid tumours[40]. In the MOPC tumour model, intravenous and intratumoural application of VSV-GP and rVACV showed limited antitumoural effects when compared with LCMV (Fig. 6a,b). Even a 100-fold higher dose of VSV-GP or rVACV did not reach the efficacy of LCMV-induced tumour regression in the MOPC tumour model (Fig. 6b). In line, human Sw480 xenografts were more susceptible to intratumoural LCMV therapy than to VSV-GP or rVACV (Fig. 6c). Next, we analysed the effects of PD-1 blockade together with LCMV treatment. We observed strong expression of PD-L1 in MOPC tumours (Fig. 6d). Blockade of PD-1 (in *Pdcd1*$^{-/-}$ mice) had no impact on tumour regression in the MOPC model (Fig. 6e). In contrast, combination of PD-1 blockade with LCMV had the strongest impact on tumour regression in advanced tumour stage (Fig. 6e).

Discussion

The ability of viruses to kill cancer cells has been recognized for several decades and is supported by recent Food and Drug Administration and European Union (EU) approval of an oncolytic herpesvirus (Talimogene laherparepvec, Amgen, Inc.)[41]. The specific mechanisms of virotherapy have long been considered to be directly oncolytic. Recently, it was recognized that induction of an inflammatory response contributes to virus-mediated tumour regression[42–49]. In cancer therapies with oncolytic viruses, this is considered to be a limited collateral effect. By contrast, in our study, we provide evidence that a powerful immune response itself induced by arenavirus replication may lead to complete tumour regression.

Treatment with a non-oncolytic arenavirus is advantageous in inducing sustained immune surveillance. First, an arenavirus such as LCMV will not kill the host cell by direct cytopathic effects. Therefore, virus replication is maintained until an immune response is induced within the tumour tissue. Second, arenavirus replication cannot solely be limited by a strong IFN-I response[9,50,51]. In addition, LCMV usually fails to induce rapid neutralizing antibodies[52]. Thus, arenavirus replication in tumours can only be controlled by infiltration of virus-specific CD8$^+$ T cells. Consequently, as long as CD8$^+$ T cells do not infiltrate the tumour, arenaviruses can replicate for several days or weeks even if tumour cells respond to IFN-I. In a direct comparison of the IFN-I-responsive tumour models MOPC and Sw480, we found that LCMV was therapeutically more potent than the oncolytic viruses VSV-GP and rVACV. These results could have been expected, because, in contrast to LCMV, VSV-GP and rVACV require defects in the IFN pathway for efficient replication in tumour cells[53–55]. Consequently, arenavirus therapy could fill a gap in virotherapy in the treatment of IFN-I-responsive cancers. Careful characterization of IFN-I responsiveness and additional LCMV host factors may guide the selection of patients suitable for LCMV cancer therapy.

Treatment with arenaviruses might also have certain disadvantages. The broad tropism of arenaviruses[56] might induce adverse events. Live arenaviruses could also replicate in healthy, non-malignant tissue. This replication could induce an immune response in normal tissue, leading to immunopathological side effects[9,52]. Although >5% of humans show evidence of previous LCMV exposure without severe symptoms[10], especially in highly immunocompromised patients overwhelming replication of attenuated vaccine virus could lead to life-threatening disease[52,57] or to gain of selection mutants of the virus[58]. Both risks can be limited by intervention with neutralizing antibodies against the arenavirus strain or antiviral therapy[57]. In our murine models we observed initially enhanced LCMV replication in the presence of tumours, but viral replication lead to an immune response that was capable to control intratumoural virus load.

Figure 3 | IFN-I was essential for arenavirus-induced tumour regression. (**a**) Immunofluorescence (day 10) of tumours from MOPC-tumour-bearing C57BL/6 mice (day −10) treated with or without 2×10^4 PFU LCMV peritumourally ($n=3$/group). Scale bar, 200 μm. (**b**) Immunohistochemistry of dLNs from MOPC-tumour-bearing mice treated with 2×10^4 PFU LCMV subcutaneously ($n=3$/group). Scale bar, 200 μm. (**c**) Representative FACS blots (day 2) from dLNs of MOPC-tumour-bearing C57BL/6 mice (day −3) and IFN-β-reporter mice (IFNβ$^{mob/mob}$) treated with 2×10^4 PFU LCMV peritumourally (day 0, $n=4$ per group). Grey area indicates isotype control. (**d**) qRT-PCR analysis of dLNs (day 3) from MOPC-tumour-bearing C57BL/6 mice (day −3) treated with or without 2×10^4 PFU LCMV peritumourally ($n=3$ per group). (**e**) IFN-α serum ELISA (day 3) from MOPC-tumour-bearing C57BL/6 mice (day −3) treated with or without 2×10^4 PFU LCMV ($n=4$ per group). (**f**) Tumour diameters of MOPC-tumour-bearing C57BL/6 mice (day −3) injected with or without anti-Ly6C + G antibody (200 μg, days −2, 2 and 7) and treated with ($n=6$ per group) or without ($n=6$ control; $n=7$ anti-Ly6C + G-dep.) 2×10^4 PFU LCMV peritumourally (two experiments pooled). (**g**) Tumour diameters of MOPC-tumour-transplanted WT and *Ccr2*$^{-/-}$ mice (day −3) treated with ($n=9$ per group) or without ($n=6$ per group) 2×10^4 PFU LCMV peritumourally (two experiments pooled). (**h**) Tumour diameter from MOPC-tumour-bearing WT and *Irf3*$^{-/-}$ *x Irf7*$^{-/-}$ mice (day ×3) treated with or without 2×10^4 PFU LCMV peritumourally ($n=6$ per group, two experiments pooled). Data are shown as mean ± s.e.m. and analysed by unpaired Student's *t*-test. Survival is shown in Kaplan–Meier method and analysed by log-rank test. NS, nonsignificant; $^*P<0.05$, $^{**}P<0.01$ and $^{***}P<0.001$.

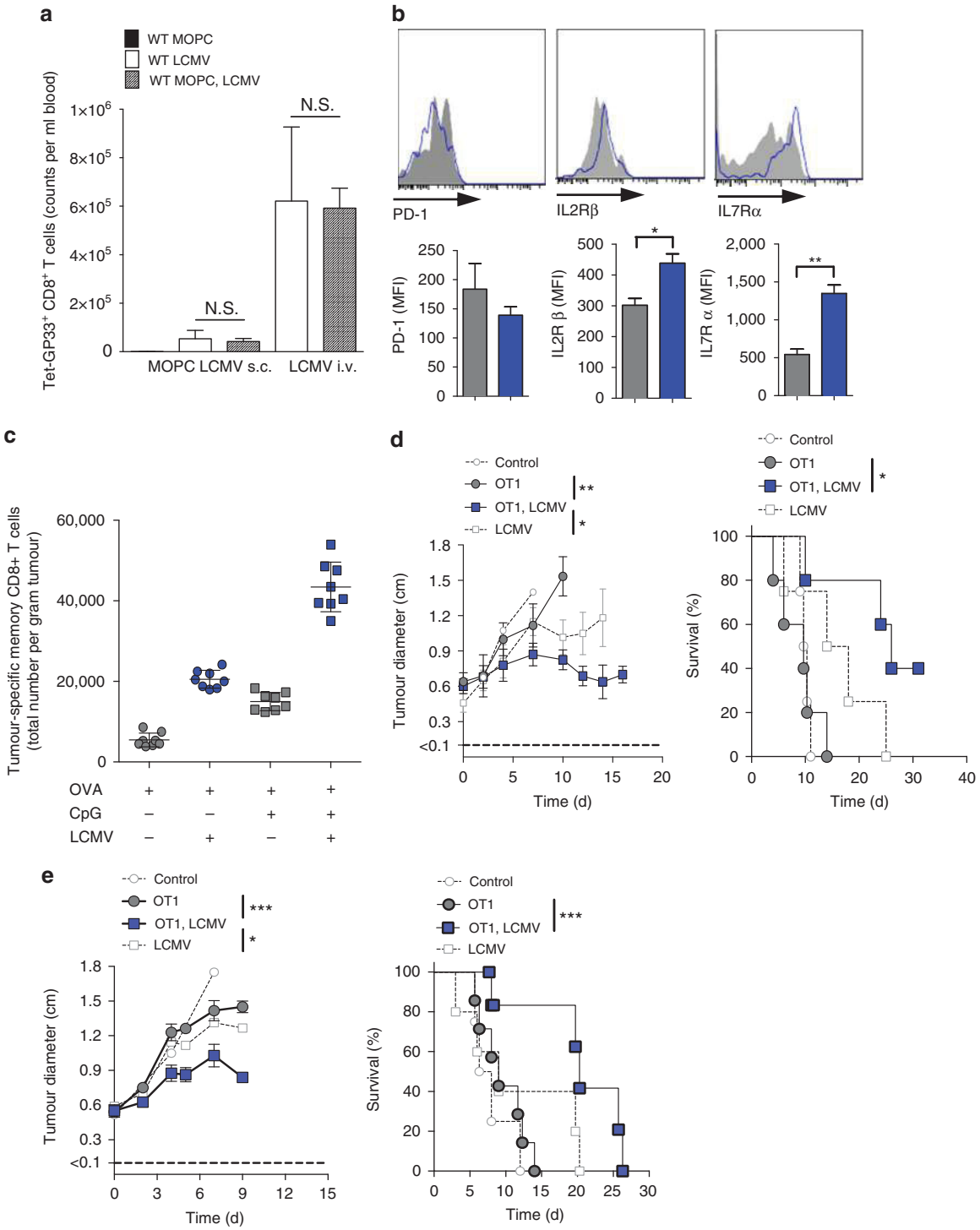

Figure 4 | CD8$^+$ T-cell activation contributes to arenavirus-mediated tumour regression. (**a**) LCMV-specific CD8$^+$ T cells in the blood (day 8) of MOPC-tumour-bearing or control mice, which where infected with LCMV ($n=3$). (**b**) Expression of PD-1, IL-2Rβ and IL-7Rα on tumour-specific CD8$^+$ T cells (OT1, day 8) of B16-OVA-tumour-bearing C57BL/6 mice (day -10) transferred with 5×10^6 OT1 splenocytes (day -1) and additionally treated with ($n=5$) or without ($n=3$) LCMV (i.t. 2×10^4 PFU). (**c**) Total numbers of tumour-specific (OVA), antigen-exposed (CD44$^+$) CD8$^+$ T cells (day 2) in tumours of B16-OVA-tumour-bearing C57BL/6 mice (day -13), which were vaccinated with ovalbumin (200 μg, day -3, i.v.) with or without CpG (20 μg, day -3, i.v.) and additionally treated with or without LCMV (5×10^5 PFU, i.t., $n=8$). (**d**) Tumour diameter and survival of B16-OVA-tumour-bearing C57BL/6 mice (day -10) treated with ($n=5$ per group) or without ($n=4$ per group) 5×10^6 OT1 splenocytes (day -1) and additionally treated with or without LCMV (i.t. 2×10^4 PFU). (**e**) Tumour diameter and survival of EL4-OVA-lymphoma-bearing C57BL/6 mice (day -6) treated with ($n=7$ per group) or without ($n=4$–5 per group) 5×10^6 OT1 splenocytes (day -1) and additionally treated with or without LCMV (i.t. 2×10^6 PFU, day 0). Data are shown as mean ± s.e.m. and analysed by unpaired Student's *t*-test. NS, nonsignificant; $^*P<0.05$, $^{**}P<0.01$ and $^{***}P<0.001$.

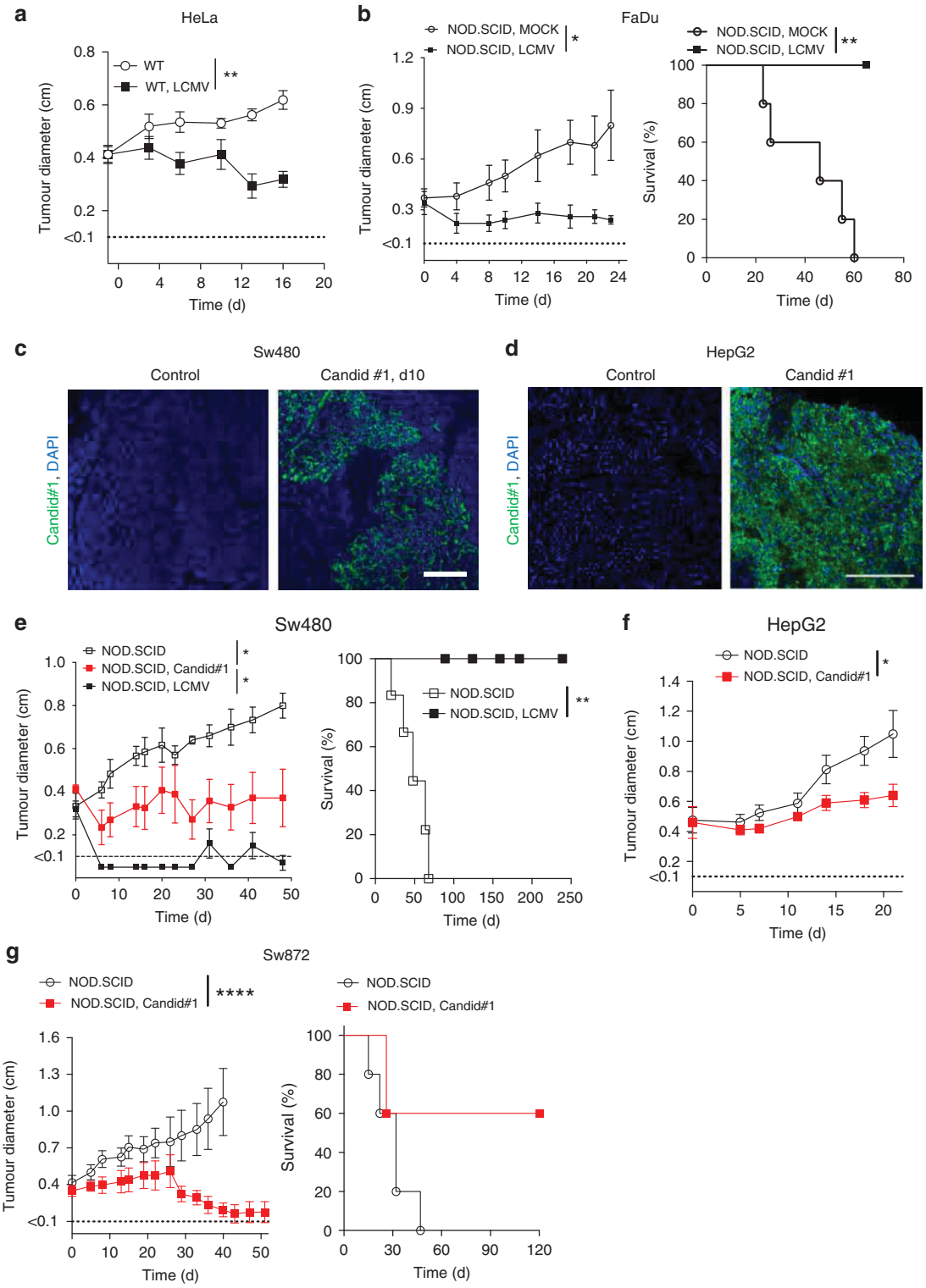

Figure 5 | LCMV and arenavirus vaccine Candid#1 induce regression of human tumours. (**a**) Tumour diameter from HeLa-tumour-bearing NOD/SCID mice (day −8) treated with or without 2×10^4 PFU LCMV intratumourally ($n=8$ per /group). (**b**) Tumour diameter and survival from FaDu-tumour-bearing NOD/SCID mice (day −10) treated with or without 2×10^6 PFU LCMV i.t. ($n=5$ per group) (**c**) Immunofluorescence (day 10) of tumours from Sw480-tumour-bearing NOD/SCID mice (day −10) treated with or without 2×10^4 PFU Candid#1 intratumoural ($n=3$ per group). Scale bar, 200 µm. (**d**) Immunofluorescence (day 10, $n=3$ per group) from HepG2-tumour-bearing NOD/SCID mice treated with or without 5×10^5 PFU Candid#1 intratumourally. Scale bar, 200 µm. (**e**) Tumour diameter and survival from Sw480-tumour-bearing NOD/SCID mice (day −11) treated with ($n=5$) or without ($n=6$) 5×10^5 PFU LCMV or 2×10^4 PFU Candid#1 ($n=7$) intratumourally. (**f**) Tumour diameter from HepG2-tumour-bearing NOD/SCID mice treated with ($n=5$) or without ($n=4$) 5×10^5 PFU Candid#1 intratumourally. (**g**) Tumour diameter (untreated $n=6$; treated $n=8$) and survival ($n=5$ per group) from Sw872 liposarcoma-bearing NOD/SCID mice treated with or without 5×10^5 PFU Candid#1. Data are shown as mean ± s.e.m. and analysed by unpaired Student's *t*-test. Survival is shown in Kaplan–Meier method and analysed by log-rank test. *$P<0.05$, **$P<0.01$ and ****$P<0.0001$

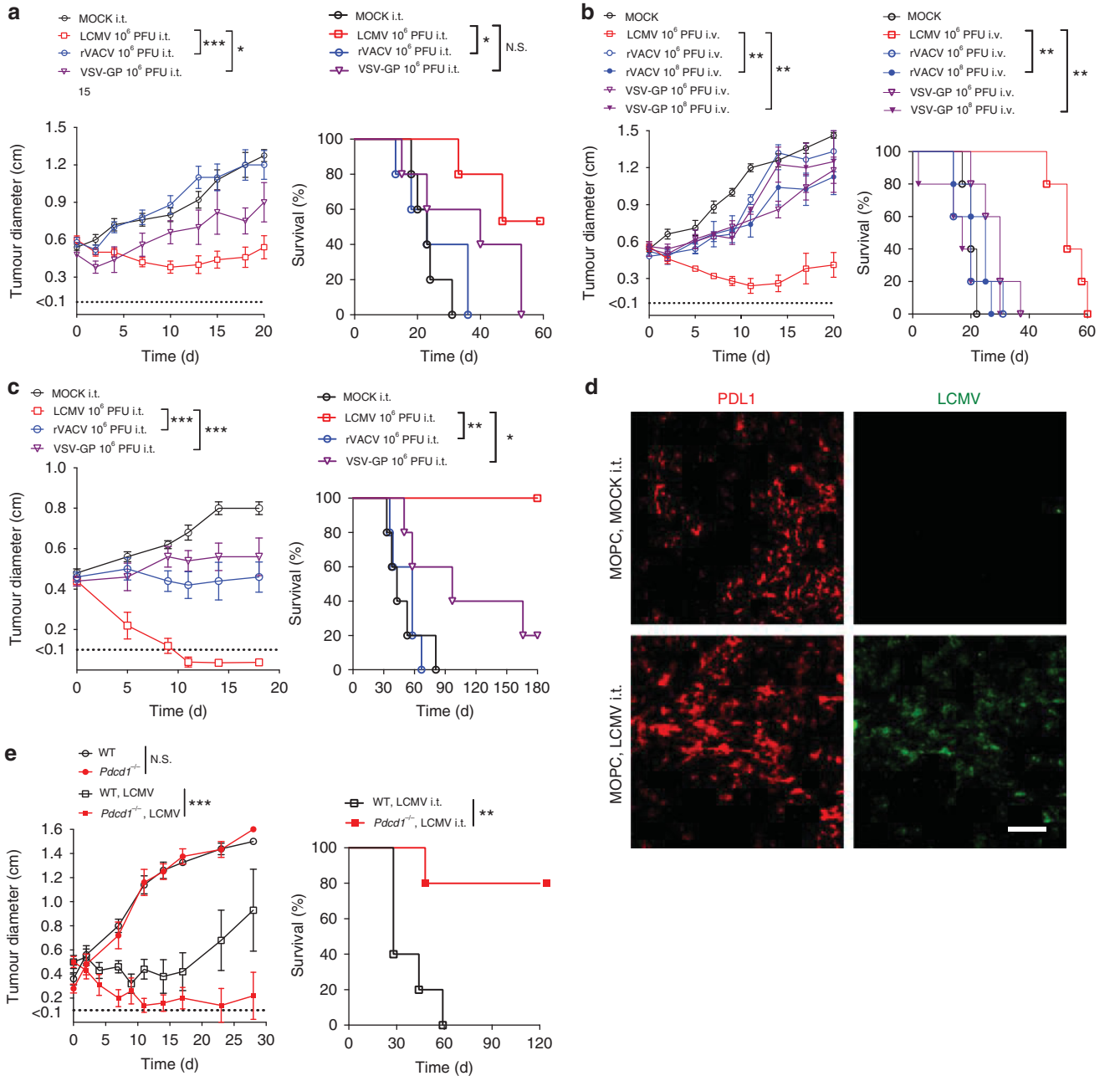

Figure 6 | LCMV induces the strongest tumour regression compared with oncolytic viruses and PD1 blockade. (**a**,**b**) Tumour diameter and survival of MOPC-tumour-bearing C57BL/6 mice (day −10) treated intratumourally (**a**) or intravenously (**b**) with LCMV, VSV-GP, rVACV or vehicle ($n=5$ per group). (**c**) Tumour diameter and survival of Sw480-tumour-bearing NOD/SCID mice treated i.t. with 2×10^6 PFU of LCMV, rVACV, VSV-GP or MOCK control ($n=5$ per group). (**d**) Immunofluorescence of tumours from MOPC-tumour-bearing mice (day −10) treated with or without 2×10^4 PFU LCMV peritumourally on day 0 (LCMV, green; red PD-L1; $n=3$ per group). (**e**) Tumour diameter and survival of MOPC-tumour-bearing C57BL/6 and *Pdcd1*$^{-/-}$ mice (day −10) treated with or without 2×10^4 PFU LCMV peritumourally on day 0 ($n=5$ per group). Data are shown as mean ± s.e.m. and analysed by unpaired Student's *t*-test. Survival is shown in Kaplan–Meier method and analysed by log-rank test. NS, nonsignificant; $^*P<0.05$, $^{**}P<0.01$ and $^{***}P<0.001$; scale bar, 200 μm.

Using the hepatotropic LCMV strain WE, we observed some viral replication in livers of B16F10 mice, but liver enzymes were under the upper limit of normal when tested 20 days after virus injection. LCMV-treated WT, transgenic and NOD/SCID mice did not show any virus or immunopathology related signs of sickness. Nevertheless, the clinical applicability of arenavirus-based treatment has to be carefully evaluated.

We found that arenavirus-based tumour therapy required IFN-I. IFN-I has substantial antiproliferative activity in different cancer types[59]. Three major mechanisms could be responsible for these effects: first, IFN-I can directly induce cell cycle arrest in cancer cells[60,61]; second, IFN-I can trigger an antigen-specific antitumour immune response[4]; and third, IFN-I can inhibit angiogenesis[37]. We found in the MOPC model that arenavirus infection enhanced IFN-I induction, enhanced antitumour immune response and limited angiogenesis.

LCMV treatment did not influence PD-L1 expression in the tumour nor PD-1 expression on $CD8^+$ T cells. In contrast, it

enhanced tumour-infiltrating tumour-specific CD8$^+$ T cells, as well as survival signals in these cells. In line with these findings, a combination of CD8$^+$ T cells and LCMV, or a combination of PD-1 blockade and LCMV, were the most effective tumour treatments.

To date, different strains of LCMV are in laboratory use for the investigation of acute and chronic viral infections, as well as an efficient tool to enhance and examine T-cell responses in murine models of infection, autoimmune disease and cancer[13,15,56,62]. For example, Schadler *et al.*[14] used the low replicative 'neurotropic strain' LCMV Armstrong (LCMVarm) in addition to lipopolysaccharide (LPS) and anti-CD3, to increase thrombospondin-1 (Tsp1) in T cells and tested the antitumoural potency of Tsp1. In their study, growth of B16F10 melanomas was observed for approximately 2 weeks after LCMVarm infection and antitumoural effects after LCMVarm administration were dependent on Tsp1 and T cells. By contrast, our studies with the 'viscerotropic strain' LCMV-WE revealed that its potent antitumour activity was mediated via IFN-I and was T-cell independent. The differences in mechanism and potency underlying the antitumour effects of LCMV in the two studies may reflect strain-dependent differences between the different arenaviruses used, the impact of the specific cancer types examined and the different timepoints used. Thus, similar to Schadler *et al.*[14] we observed an impaired antitumoural effect of LCMV in *Rag1*$^{-/-}$ mice compared with WT mice within the first 2 weeks after LCMV treatment of established tumours, indicating the involvement of T cells (Supplementary Fig. 8b, middle panel). However, in the long-term observation of approximately 80 days, we show that the absence of T cells is beneficial for LCMV-WE therapy (Supplementary Fig. 8b). Moreover, we based our studies largely on the mechanism of antitumoural action of LCMV in a murine head and neck cancer model (MOPC), whereas Schadler *et al.*[14] used malignant melanoma, where effective immunotherapies mainly depend on tumour-specific T cells[63]. This may also explain the lower efficiency and efficacy of IFN-dependent LCMV therapy on B16F10 (Fig. 2f) compared with MOPC (Fig. 2a) or MC38 colon cancer (Fig. 2e).

Studies from others, such as Ochsenbein *et al.*[13] and Flatz *et al.*[15], used LCMV as a model to activate tumour-specific CD8$^+$ T cells. In agreement with their work, we use transgenic tumour models to show that OVA-specific T cells show enhanced antitumoural effects, when additional T-cell activation via LCMV infection is performed. However, we demonstrate that T cells exhibit an ambiguous role in LCMV treatment of tumours. In the presence of tumour-specific T cells, LCMV enhances antitumoural immune defenses, but the presence of virus-specific T cells limits the antitumoural activity of LCMV by controlling viral replication (Supplementary Fig. 4). Moreover, studying the mechanism of antitumoural action of LCMV-WE, we found that T cells were largely dispensable in our MOPC tumour model in *Tcrab*$^{-/-}$, *Rag1*$^{-/-}$ and NOD/SCID mice. Rather, LCMV-induced antitumour immunity depends mainly on the recruitment of IFN-producing Ly6C$^+$ monocytes.

We found that monocytes, which infiltrate into human tumours, have the ability to produce IFN-I. It remains an open question whether local or systemic injection of Candid#1 in humans could be similar to mice in enhancing the local IFN-I response and thereby inducing tumour regression. In recent times it was found that IFN-free therapy of chronic hepatitis C virus-related hepatocellular cancer leads to unexpected early tumour recurrence[64]. This finding underlines the potent antitumoural effects of IFN-I on cancer growth during persistence of virus.

In conclusion, we found that locally or systemically administered arenaviruses preferentially replicate in murine and human cancer cells, and strongly induce a local innate immune response, leading to effective regression of disseminated cancers *in vivo*.

Methods

Human material. Formalin-fixed, paraffin-embedded primary tumour tissue was retrieved from the archives of the Department of Otorhinolaryngology, University Hospital Essen, from patients who had signed their informed consent according to the Declaration of Helsinki and with approval from the institutional review board at the University Hospital Essen.

Viruses. The LCMV strain WE and VSV (strain Indiana) were kindly provided by Rolf Zinkernagel (Institute of Experimental Immunology, ETH, Zurich, Switzerland). LCMV was propagated in L929 cells, which were purchased from ATCC (CCL-1). VSV was propagated in BHK cells, which were bought from ATCC (CRL-8544). Virus titres in tissue of infected mice were measured using plaque assays. For detection of virus in the skin, about 10 mg of the infected skin area was used. Candid#1 was grown in Vero E6 cells purchased from ATCC (CRL-1586). Recombinant VSV-GP (provided by Professor von Laer, Division of Virology, Medical University Innsbruck, Austria) was generated as previously described[38]. VSV-GP was grown on Vero cells under serum-free conditions. Recombinant Tk− Vaccinia virus strain Western Reserve containing the green fluorescent protein gene expressed under the P7.5 promoter within the Tk (thymidine kinase) locus of the genome (originally provided by B. Moss, National Institutes of Health, Bethesda, MD) was propagated, purified and titrated following standard methodology[65].

Cell lines and depletion antibodies. MOPC cells (murine oropharynx cancer) were initially named MTEC and were provided by Dr H.J. Lee of the University of Iowa. Cells were cultured in previously described culture medium[17]. MaMel66a cells (human malignant melanoma) were provided by Professor Schadendorf[66].

MC38-OVA (MC38 cells, murine colon carcinoma) and EL4-OVA cells (murine ovalbumin-expressing lymphoma) were a kind gift of Bertrand Huard (University Medical Center, Geneva, Switzerland). B16F10 cells (murine malignant melanoma) were purchased from ATCC (CRL-6475). B16-OVA (OVA-expressing B16 malignant melanoma cells) were provided by Professor P. Knolle, Technical University, Munich, Germany. SW480 (human colon carcinoma, CCL-228) and FaDu cells (human oropharyngeal carcinoma, HTB-43), A549 cells (human bronchial carcinoma, CCL-185), HepG2 cells (human hepatoma, HB-8065) and HeLa cells (human cervix carcinoma, CCL-2) were purchased from ATCC. SW872 cells were kindly provided from Professor Bauer (University Hospital, Essen, Germany).

Human normal untransformed cells were purchased from ATCC (FHC CRL-183), LONZA (NHBE CC-2540; HRE CC2556) and PromoCell (NHEM C-12453), which were cultured and maintained according to the companies' protocols.

Monoclonal fluorescence-labelled antibodies against LCMV-NP (VL4) and LCMV-GP (clone KL25), and unlabelled anti-NK1.1 antibodies were produced in-house (Professor P.A. Lang, Heinrich Heine University, Düsseldorf, Germany).

Anti-Ly-6G (1A8), anti-Gr-1 Ab (RB6-8C5) and anti-IFNAR1 (clone MAR1-5A3) depletion antibodies were purchased from Bio X Cell. All other antibodies used for immunofluorescence are listed in Supplementary Table 1.

Mice. C57BL/6J (Jackson Laboratory; 00664), *Map3k14*$^{aly/aly}$ (Professor Shibata, Kyoto, Japan), *Ifnar1*$^{-/-}$ (Jackson Laboratory; 028288), *Tcrab*$^{-/-}$ (Jackson Laboratory; 002116), *Jh*$^{-/-}$ (Jackson Laboratory; 002438), *Rag1*$^{-/-}$ (provided by Professor P.A. Lang, Heinrich Heine University, Düsseldorf, Germany), *Ccr2*$^{-/-}$ (Jackson Laboratory; 004999), OT-1 (kindly provided by Professor J. Fandrey, University Hospital, Essen) and *Irf3 x Irf7*$^{-/-}$ (Provided by Professor Löhning, Charite Hospital Berlin) were maintained on the C57BL/6 background. IFNβ$^{mob/mob}$ mice (provided by Professor Scheu, University of Düsseldorf, Germany) express the yellow fluorescent protein under the IFNβ promoter and therefore IFN-I-producing cells can be detected in fluorescein isothiocyanate channel[30]. The spontaneous tumour models LoxP-TAg9 (liver cancer) and MT/*ret* (melanoma) were used on C57BL/6 background. LoxP-TAg9 mice were provided by Professor Willimsky (Charite, University of Berlin, Germany). MT/*ret* mice were provided by Dr Helfrich (University Hospital Essen, Germany). For human xenografts, NOD/SCID mice were used (Charles River; 001303). Six- to 8-week-old, age- and sex-matched mice were used for all the studies. All mice were maintained in single ventilated cages, with the authorization of the Veterinäramt Nordrhein Westfalen (Düsseldorf, Germany) in accordance with the German law for animal protection or institutional guidelines of the Ontario Cancer Institute.

For *in vivo* depletion of NK cells, 50 μg anti-NK1.1 (in 400 μl, in house) was injected intraperitoneally (i.p.) on days −3 and −1. For depletion of Ly-6C and Ly-6G cells (monocytes and granulocytes), 200 μg anti-Ly6C + G antibody (Gr-1, clone RB6-8C5, Bio X Cell BE0075) was given i.p. on days −2, 2 and 7.

For depletion of Ly6-G cells (granulocytes), 500 µg anti-Ly6G (clone 1A8, Bio X Cell BE0075-1) was given starting on day −2 and repeated on day 2 and day 7. For depletion of IFNAR1, 1 mg anti-IFNAR1 antibody (clone MAR1-5A3, Bio X Cell BE0241) was given i.p. on day −1 and repeated by i.p. injections of 250 µg IFNAR1 on days 2 and 8. Same amounts of the IgG1 Isotype control (clone MOPC21, Bio X cell) were injected to the control group. PolyI:C was provided by Sigma (P9582).

Therapeutic application of arenavirus. The time of infection with virus was set to day = 0. In subcutaneous tumour models, tumour cells where injected 13–3 days before as stated (that is, day −10). The optimal dose to guarantee persistence of virus in the tumour was 2×10^4 PFU LCMV peritumourally or 2×10^6 PFU intravenously. Viral doses are indicated in the figure legends. Cell supernatant was used for vehicle control.

Histological analysis and immunocytochemistry. Histological analysis were performed on snap-frozen tissue as previously described[67]. In brief, sections were fixed with acetone for 10 min and nonspecific antigens were blocked in PBS containing 2% FCS for 15 min, followed by various stainings for 45 min.

Immunocytochemistry was performed on cells grown on coverslips[50]. In brief, cells were fixed in 4% Formalin/PBS for 10 min, washed in PBS and then permeabilized in 1% Triton X–PBS for 10 min. After blocking with 10% FCS/PBS for 30–60 min, various stainings for 45 min were followed. Coverslips were mounted on microscope slides using mounting medium (S3023, Dako).

Images were acquired with a fluorescence microscope (KEYENCE BZ II analyser). Quantifications were performed using the Image J software (NIH).

Morphometric analysis of tumour vessels and hypoxia. Morphogenic analyses were performed using consecutive cryosections stained for the endothelial cell marker CD31. MVD was quantified by using the average of three tumour sections per tumour (top, middle and base). For MVD and vessel–vessel distances $n = 1{,}168$ peritumoural vessel–vessel distances (50–100 vessels/tumour), 5 regions of interests per sample were quantified from $n = 3$ histological samples. MVD was calculated as number of vessels per tumour area. Vessel-to-vessel distance was calculated using the middle section of the three generated using corresponding Cell P Software (Olympus, Germany). For analysis of hypoxic tumour areas, Pimonidazole was injected 30 min before killing the mice. Hypoxic tumour areas were detected by the formation of pimonidazole adducts. Tumour sections were immunostained using the Hypoxyprobe-1 Plus kit according to the manufacturer's protocol (Natural Pharmacia International, Inc.) and the hypoxic area index quantified as the percentage of positive tumour area per total tumour area in tumours of corresponding volumes.

Flow cytometric analysis. Single-cell suspensions of cells were incubated with anti-CD16/32 (anti-FcgIII/II receptor, clone 2.4G2) in a 1:100 dilution for 10 min, then stained with conjugated antibodies. All fluorescently labelled monoclonal antibodies (Supplementary Table 1) were diluted 1:100 to their original concentration in FACS buffer. Tetramer was used from NIH tetramer core facility. All stained cells were analysed on LSRII/FACS Fortessa (BD Biosciences) flow cytometer and data were analysed with Flowjo software.

IFN-α ELISA assay. Serum IFN-α levels were determined according to the manufacturers' specifications (Research Diagnostics RDI, Flanders, NJ).

Reverse transcription and qRT–PCR. Total RNA was isolated by using TRIzol (Ambion), reverse transcribed into complementary DNA using Quantitect Reverse Transcription Kit (Qiagen) and analysed by qRT–PCR using the SYBR Green Master Mix (Applied Biosystems, Darmstadt, Germany) or using Taqman gene expression assay (Life Technologies). Either commercially available Primer sets (Supplementary Table 2–4) or self-designed primers ordered from Eurofins Genomics (Ebersberg, Germany) (Supplementary Table 5) were used. For analysis, the expression levels of all target genes were normalized to either 18S or glyceraldehyde 3-phosphate dehydrogenase messenger RNA expression. Relative gene expression levels were calculated with the ΔCt method.

VSV assay. Cells per well (1×10^5) were plated in a 24-well plate on day −1. On day 0, cells were treated with different concentrations of human IFNα4 (11100-1, PBL Assay Science), murine IFNα4 (12115-1, PBL Assay Science) or murine IFNα2 (14-8312-62, eBiosciences) and then infected with 500 PFU/ per well VSV. After 2 h Methylcellulose overlay was added. On day 1, cell layer was stained with crystal violet.

Small interfering RNA transient transfections. MCF7 cells were seeded at 4×10^4 cells per well in a 24-well plate and, 24 h later, transfected with control or B-Myb small interfering RNA duplexes (Origene SR419327) using Hiperfect (Qiagen 301705) as a transfection reagent. Transfected cells were infected for 24 h with LCMV-WE, 24 h post-small interfering RNA transfection.

Statistical analysis. Mean values were compared using an unpaired Student's two-tailed *t*-test. Data are expressed as means ± s.e.m. Student's *t*-test was used to detect significant differences between groups. Chi-Quadrat test was additionally used. Survival was compared with log-rank (Mantel–Cox) tests. The level of statistical significance was set at $P < 0.05$.

Gene set enrichment analysis. RNA-sequencing gene expression data from the TCGA for different types of cancer were downloaded using the cgdsr package of the cBioportal gateway for Cancer Genomics (http://www.cbioportal.org) and mRNA expression z-scores (RNA Seq V2 RSEM) used. TCGA tumours were ranked based on CD14 expression and selected top and bottom samples used as the input for GSEA. GSEA was performed with 1000 permutations using the Browne IFN-response gene set.

Data availability. The authors declare that all data supporting the findings of this study are available within the article and its Supplementary Information files, or are available from the authors upon request.

References

1. Schreiber, R. D., Old, L. J. & Smyth, M. J. Cancer immunoediting: integrating immunity's roles in cancer suppression and promotion. *Science* **331,** 1565–1570 (2011).
2. Kitamura, T., Qian, B. Z. & Pollard, J. W. Immune cell promotion of metastasis. *Nat. Rev. Immunol.* **15,** 73–86 (2015).
3. Gajewski, T. F., Schreiber, H. & Fu, Y.-X. Innate and adaptive immune cells in the tumor microenvironment. *Nat. Immunol.* **14,** 1014–1022 (2013).
4. Dunn, G. P., Koebel, C. M. & Schreiber, R. D. Interferons, immunity and cancer immunoediting. *Nat. Rev. Immunol.* **6,** 836–848 (2006).
5. Getts, D. R., Chastain, E. M., Terry, R. L. & Miller, S. D. Virus infection, antiviral immunity, and autoimmunity. *Immunol. Rev.* **255,** 197–209 (2013).
6. Honke, N. *et al.* Usp18 driven enforced viral replication in dendritic cells contributes to break of immunological tolerance in autoimmune diabetes. *PLoS Pathog.* **9,** e1003650 (2013).
7. Honke, N. *et al.* Enforced viral replication activates adaptive immunity and is essential for the control of a cytopathic virus. *Nat. Immunol.* **13,** 51–57 (2012).
8. Lang, P. A., Recher, M., Haussinger, D. & Lang, K. S. Genes determining the course of virus persistence in the liver: lessons from murine infection with lymphocytic choriomeningitis virus. *Cell. Physiol. Biochem.* **26,** 263–272 (2010).
9. Lang, P. A. *et al.* Aggravation of viral hepatitis by platelet-derived serotonin. *Nat. Med.* **14,** 756–761 (2008).
10. McLay, L., Liang, Y. & Ly, H. Comparative analysis of disease pathogenesis and molecular mechanisms of New World and Old World arenavirus infections. *J. Gen. Virol.* **95,** 1–15 (2014).
11. Enria, D. A. & Oro, J. G. B. Junin virus vaccines. *Curr. Top. Microbiol. Immunol.* **263,** 239–261 (2002).
12. Enria, D. A., Briggiler, A. M. & Sanchez, Z. Treatment of Argentine hemorrhagic fever. *Antiviral Res.* **78,** 132–139 (2008).
13. Ochsenbein, A. F. *et al.* Roles of tumour localization, second signals and cross priming in cytotoxic T-cell induction. *Nature* **411,** 1058–1064 (2001).
14. Schadler, K. L. *et al.* Immunosurveillance by antiangiogenesis: tumor growth arrest by T cell-derived thrombospondin-1. *Cancer Res.* **74,** 2171–2181 (2014).
15. Flatz, L. *et al.* Development of replication-defective lymphocytic choriomeningitis virus vectors for the induction of potent CD8+ T cell immunity. *Nat. Med.* **16,** 339–345 (2010).
16. Kandoth, C. *et al.* Mutational landscape and significance across 12 major cancer types. *Nature* **502,** 333–339 (2013).
17. Williams, R. *et al.* Preclinical models of HPV+ and HPV- HNSCC in mice: an immune clearance of HPV+ HNSCC. *Head Neck* **31,** 911–918 (2009).
18. Witt, A. *et al.* IAP antagonization promotes inflammatory destruction of vascular endothelium. *EMBO Rep.* **16,** 719–727 (2015).
19. Preynat-Seauve, O. *et al.* Tumor-infiltrating dendritic cells are potent antigen-presenting cells able to activate T cells and mediate tumor rejection. *J. Immunol.* **176,** 61–67 (2006).
20. Willimsky, G. *et al.* Virus-induced hepatocellular carcinomas cause antigen-specific local tolerance. *J. Clin. Invest.* **123,** 1032–1043 (2013).
21. Zhang, K. X. *et al.* Down-regulation of type I interferon receptor sensitizes bladder cancer cells to vesicular stomatitis virus-induced cell death. *Int. J. Cancer* **127,** 830–838 (2010).
22. Dunn, G. P., Sheehan, K. C., Old, L. J. & Schreiber, R. D. IFN unresponsiveness in LNCaP cells due to the lack of JAK1 gene expression. *Cancer Res.* **65,** 3447–3453 (2005).

23. Pauls, E. *et al.* Cell cycle control and HIV-1 susceptibility are linked by CDK6-dependent CDK2 phosphorylation of SAMHD1 in myeloid and lymphoid cells. *J. Immunol.* **193,** 1988–1997 (2014).
24. Saville, M. K. & Watson, R. J. The cell-cycle regulated transcription factor B-Myb is phosphorylated by cyclin A/Cdk2 at sites that enhance its transactivation properties. *Oncogene* **17,** 2679–2689 (1998).
25. Panda, D. *et al.* RNAi screening reveals requirement for host cell secretory pathway in infection by diverse families of negative-strand RNA viruses. *Proc. Natl Acad. Sci. USA* **108,** 19036–19041 (2011).
26. Kato, M. *et al.* Transgenic mouse model for skin malignant melanoma. *Oncogene* **17,** 1885–1888 (1998).
27. Miyawaki, S. *et al.* A new mutation, aly, that induces a generalized lack of lymph nodes accompanied by immunodeficiency in mice. *Eur. J. Immunol.* **24,** 429–434 (1994).
28. Auffray, C., Sieweke, M. H. & Geissmann, F. Blood monocytes: development, heterogeneity, and relationship with dendritic cells. *Annu. Rev. Immunol.* **27,** 669–692 (2009).
29. Han, S. J. *et al.* Internalization and TLR-dependent type I interferon production by monocytes in response to *Toxoplasma gondii*. *Immunol. Cell. Biol.* **92,** 872–881 (2014).
30. Scheu, S., Dresing, P. & Locksley, R. M. Visualization of IFNbeta production by plasmacytoid versus conventional dendritic cells under specific stimulation conditions *in vivo*. *Proc. Natl Acad. Sci. USA* **105,** 20416–20421 (2008).
31. Cao, W. *et al.* Rapid differentiation of monocytes into type I IFN-producing myeloid dendritic cells as an antiviral strategy against influenza virus infection. *J. Immunol.* **189,** 2257–2265 (2012).
32. Bugl, S. *et al.* Steady-state neutrophil homeostasis is dependent on TLR4/TRIF signaling. *Blood* **121,** 723–733 (2013).
33. Dunay, I. R., Fuchs, A. & Sibley, L. D. Inflammatory monocytes but not neutrophils are necessary to control infection with *Toxoplasma gondii* in mice. *Infect. Immun.* **78,** 1564–1570 (2010).
34. Wojtasiak, M. *et al.* Depletion of Gr-1+, but not Ly6G+, immune cells exacerbates virus replication and disease in an intranasal model of herpes simplex virus type 1 infection. *J. Gen. Virol.* **91,** 2158–2166 (2010).
35. Lang, P. A. *et al.* Hematopoietic cell-derived interferon controls viral replication and virus-induced disease. *Blood* **113,** 1045–1052 (2009).
36. Browne, E. P., Wing, B., Coleman, D. & Shenk, T. Altered cellular mRNA levels in human cytomegalovirus-infected fibroblasts: viral block to the accumulation of antiviral mRNAs. *J. Virol.* **75,** 12319–12330 (2001).
37. Albini, A. *et al.* Inhibition of angiogenesis and vascular tumor growth by interferon-producing cells: a gene therapy approach. *Am. J. Pathol.* **156,** 1381–1393 (2000).
38. Muik, A. *et al.* Re-engineering vesicular stomatitis virus to abrogate neurotoxicity, circumvent humoral immunity, and enhance oncolytic potency. *Cancer Res.* **74,** 3567–3578 (2014).
39. Chan, W. M. & McFadden, G. Oncolytic Poxviruses. *Annu. Rev. Virol.* **1,** 119–141 (2014).
40. Zeh, H. J. *et al.* First-in-man study of western reserve strain oncolytic vaccinia virus: safety, systemic spread, and antitumor activity. *Mol. Ther.* **23,** 202–214 (2015).
41. Pol, J., Kroemer, G. & Galluzzi, L. First oncolytic virus approved for melanoma immunotherapy. *Oncoimmunology* **5,** e1115641 (2016).
42. Lichty, B. D., Breitbach, C. J., Stojdl, D. F. & Bell, J. C. Going viral with cancer immunotherapy. *Nat. Rev. Cancer* **14,** 559–567 (2014).
43. LaRocca, C. J., Oliveira, A. R., Davydova, J. & Yamamoto, M. Esophageal cancer treatment using an interferon-expressing oncolytic adenovirus in combination with chemotherapy and radiation. *Mol. Ther.* **22,** S253–S253 (2014).
44. Brown, M. C. *et al.* Oncolytic polio virotherapy of cancer. *Cancer Am. Cancer Soc.* **120,** 3277–3286 (2014).
45. Huang, H. L., Xiao, T., He, L. F., Ji, H. B. & Liu, X. Y. Interferon–armed oncolytic adenovirus induces both apoptosis and necroptosis in cancer cells. *Acta Biochhem. Biophys. Sin.* **44,** 737–745 (2012).
46. Naik, S., Nace, R., Barber, G. N. & Russell, S. J. Potent systemic therapy of multiple myeloma utilizing oncolytic vesicular stomatitis virus coding for interferon-beta. *Cancer Gene Ther.* **19,** 443–450 (2012).
47. Hasegawa, Y. *et al.* Urokinase-targeted fusion by oncolytic sendai virus eradicates orthotopic glioblastomas by pronounced synergy with interferon-beta gene. *Mol. Ther.* **18,** 1778–1786 (2010).
48. Li, H., Peng, K. W., Dingli, D., Kratzke, R. A. & Russell, S. J. Oncolytic measles viruses encoding interferon beta and the thyroidal sodium iodide symporter gene for mesothelioma virotherapy. *Cancer Gene Ther.* **17,** 550–558 (2010).
49. Benencia, F. *et al.* HSV oncolytic therapy upregulates interferon-inducible chemokines and recruits immune effector cells in ovarian cancer. *Mol. Ther.* **12,** 789–802 (2005).
50. Lang, P. A. *et al.* Tissue macrophages suppress viral replication and prevent severe immunopathology in an interferon-I-dependent manner in mice. *Hepatology* **52,** 25–32 (2010).
51. Moskophidis, D. *et al.* Resistance of lymphocytic choriomeningitis virus to alpha/beta interferon and to gamma interferon. *J. Virol.* **68,** 1951–1955 (1994).
52. Recher, M. *et al.* Extralymphatic virus sanctuaries as a consequence of potent T-cell activation. *Nat. Med.* **13,** 1316–1323 (2007).
53. Stojdl, D. F. *et al.* Exploiting tumor-specific defects in the interferon pathway with a previously unknown oncolytic virus. *Nat. Med.* **6,** 821–825 (2000).
54. Wang, F. *et al.* Disruption of Erk-dependent type I interferon induction breaks the myxoma virus species barrier. *Nat. Immunol.* **5,** 1266–1274 (2004).
55. Moerdyk-Schauwecker, M. *et al.* Resistance of pancreatic cancer cells to oncolytic vesicular stomatitis virus: role of type I interferon signaling. *Virology* **436,** 221–234 (2013).
56. Zapata, J. C. & Salvato, M. S. Arenavirus variations due to host-specific adaptation. *Viruses Basel* **5,** 241–278 (2013).
57. Fischer, S. A. *et al.* Transmission of lymphocytic choriomeningitis virus by organ transplantation. *N. Engl. J. Med.* **354,** 2235–2249 (2006).
58. Hunziker, L., Ciurea, A., Recher, M., Hengartner, H. & Zinkernagel, R. M. Public versus personal serotypes of a viral quasispecies. *Proc. Natl Acad. Sci. USA* **100,** 6015–6020 (2003).
59. Ferrantini, M., Capone, I. & Belardelli, F. Interferon-alpha and cancer: mechanisms of action and new perspectives of clinical use. *Biochimie* **89,** 884–893 (2007).
60. Zhou, Y., Wang, S., Yue, B. G., Gobl, A. & Oberg, K. Effects of interferon alpha on the expression of p21cip1/waf1 and cell cycle distribution in carcinoid tumors. *Cancer Invest.* **20,** 348–356 (2002).
61. Murphy, D., Detjen, K. M., Welzel, M., Wiedenmann, B. & Rosewicz, S. Interferon-alpha delays S-phase progression in human hepatocellular carcinoma cells via inhibition of specific cyclin-dependent kinases. *Hepatology* **33,** 346–356 (2001).
62. Zhou, X., Ramachandran, S., Mann, M. & Popkin, D. L. Role of lymphocytic choriomeningitis virus (LCMV) in understanding viral immunology: past, present and future. *Viruses* **4,** 2650–2669 (2012).
63. Spranger, S., Bao, R. & Gajewski, T. F. Melanoma-intrinsic β-catenin signalling prevents anti-tumour immunity. *Nature* **523,** 231–235 (2015).
64. Reig, M. *et al.* Unexpected early tumor recurrence in patients with hepatitis C virus -related hepatocellular carcinoma undergoing interferon-free therapy: a note of caution. *J. Hepatol.* **65,** 719–726 (2016).
65. Moss, B. & Earl, P. L. in *Current Protocols in Molecular Biology* (eds Ausubel, F. M. *et al.*) pp. 16.16.11–16.16.17 (Wiley, 1991).
66. Ugurel, S. *et al.* B-RAF and N-RAS mutations are preserved during short time *in vitro* propagation and differentially impact prognosis. *PLoS ONE* **2,** e236 (2007).
67. Recher, M. & Lang, K. S. Innate (over)immunity and adaptive autoimmune disease. *Curr. Top. Microbiol. Immunol.* **305,** 89–104 (2006).

Acknowledgements

We thank Konstanze Schättel for technical support. We thank Stephan Lang (ENT Department) and his clinical colleagues for retrieving the clinical samples used in this study. We thank Bertrand Huard (University Medical Center, Geneva, Switzerland) for donating MC38-OVA and EL4-OVA cells. This study was supported by the Alexander von Humboldt Foundation (SKA-2008 to K.S.L. and SKA-2010 to P.A.L.) and the Deutsche Forschungsgemeinschaft (DFG; CRC974, CRC/TRR60, CRC/TRR36, LA1419/7-1, LA2559/5-1, RTG1949, RTG2098, SCHE692/3-1 and SCHE962/4-1), the Strategic Research Fund of the Heinrich-Heine-University Duesseldorf (to S.S.) and by the Deutsche Krebshilfe (number 107993 to M.S.). H.K. was supported by an IFORES fellowship of the Medical Faculty of the University Duisburg-Essen. National Institutes of Health (NIH, USA) Tetramer Core Facility provided the tetramers. The West German Cancer Center at University Hospital Essen is supported by an Oncology Center of Excellence grant of the Deutsche Krebshilfe (number 110534).

Author contributions

H.K. designed, planned and performed the experiments, analysed data and wrote the paper. P.S. and A.A.P. performed experiments, data analysis and writing. I.H. performed vasculature experiments, data analysis and provided reagents. A.G. and I.V. were involved in data analysis and discussion. T.B., S.N., B.H. and J.B. helped in experiments. J.C. performed bioinformatics analysis. L.F. was involved in data discussion. S.K., M.H., P.A.K., G.W., D.V.L., I.D., J.R., P.C., S.S., G.W., M.L., D.H. and D.S. provided reagents and were involved in data discussion. P.A.L. provided reagents, discussed the data and wrote the paper. S.B. initiated the study, provided reagents and discussed the data. M.S. initiated the study, provided reagents, discussed the data and wrote the paper. K.S.L. initiated, organized and designed the study, and wrote the manuscript.

Additional information

Supplementary Information accompanies this paper at http://www.nature.com/naturecommunications

Competing financial interests: The authors declare no competing financial interests.

Reprints and permission information is available online at http://npg.nature.com/reprintsandpermissions/

How to cite this article: Kalkavan, H. *et al.* Spatiotemporally restricted arenavirus replication induces immune surveillance and type I interferon-dependent tumour regression. *Nat. Commun.* **8,** 14447 doi: 10.1038/ncomms14447 (2017).

Publisher's note: Springer Nature remains neutral with regard to jurisdictional claims in published maps and institutional affiliations.

Cell Death and Differentiation (2015) 22, 164–173

www.nature.com/cdd

OPEN

Toso regulates differentiation and activation of inflammatory dendritic cells during persistence-prone virus infection

PA Lang[1,2,10], A Meryk[2,3,10], AA Pandyra[3,10], D Brenner[4,5], A Brüstle[4], HC Xu[1,3], K Merches[3,6], F Lang[6], V Khairnar[3], P Sharma[3], P Funkner[1], M Recher[7], N Shaabani[3], GS Duncan[4], V Duhan[3], B Homey[8], PS Ohashi[4], D Häussinger[1], PA Knolle[9], N Honke[3,11], TW Mak*[,4,11] and KS Lang[1,3,11]

During virus infection and autoimmune disease, inflammatory dendritic cells (iDCs) differentiate from blood monocytes and infiltrate infected tissue. Following acute infection with hepatotropic viruses, iDCs are essential for re-stimulating virus-specific CD8$^+$ T cells and therefore contribute to virus control. Here we used the lymphocytic choriomeningitis virus (LCMV) model system to identify novel signals, which influence the recruitment and activation of iDCs in the liver. We observed that intrinsic expression of Toso (Faim3, FcμR) influenced the differentiation and activation of iDCs *in vivo* and DCs *in vitro*. Lack of iDCs in Toso-deficient (*Toso*$^{-/-}$) mice reduced CD8$^+$ T-cell function in the liver and resulted in virus persistence. Furthermore, *Toso*$^{-/-}$ DCs failed to induce autoimmune diabetes in the rat insulin promoter-glycoprotein (RIP-GP) autoimmune diabetes model. In conclusion, we found that Toso has an essential role in the differentiation and maturation of iDCs, a process that is required for the control of persistence-prone virus infection.

Cell Death and Differentiation (2015) **22**, 164–173; doi:10.1038/cdd.2014.138; published online 26 September 2014

More than 500 million people worldwide suffer from chronic infections with hepatitis B or hepatitis C viruses.[1] Although both viruses are poorly cytopathic, persistence of either virus can lead to chronic liver inflammation and potentially cause liversteatosis, liver cirrhosis, end-stage liver failure or hepatocellular carcinoma. Virus-specific CD8$^+$ T cells are a major determinant governing the outcome of viral hepatitis due to their antiviral activity against virus-infected hepatocytes.[2–5] However, during prolonged infection, virus-specific CD8$^+$ T cells are exhausted, resulting in their loss of function and consequently virus persistence.[1,6] Regulators influencing CD8$^+$ T-cell function during chronic virus infection still remain ill defined.

Inflammatory dendritic cells (iDCs) can develop from a subset of monocytes recruited to the site of inflammation.[7,8] This monocyte subset is characterized by the expression of CD115$^+$/Ly6C^{hi}/CCR2$^+$.[7] iDCs express CD11c, CD11b, and Ly6C.[9–11] IDCs that exhibit tumor necrosis factor (TNF)-α production and inducible nitric oxide synthase (iNOS) were named TNF-α and iNOS producing DCs (Tip-DCs). iDCs contribute to the elimination of pathogens following bacterial infection.[12–14] During infection with influenza virus, iDCs enhance CD8$^+$ T-cell immunopathology, but have limited impact on viral replication.[11,15] According to recent observations, chronic activation of toll-like receptor 9 leads to intrahepatic myeloid-cell aggregates (iMATE).[16] These aggregates, which contain iDCs, are essential for T-cell activation and therefore participate in virus control.[16] Co-stimulatory signals from either direct cell contact or from cytokines in combination with continued antigen contact in iMATEs lead to proliferation and activation of virus-specific T cells.[16] These observations suggest that infiltration of

[1]Department of Gastroenterology, Hepatology and Infectious Diseases, Heinrich-Heine-University Düsseldorf, Universitätsstr. 1, Düsseldorf 40225, Germany; [2]Department of Molecular Medicine II, Heinrich-Heine-University Düsseldorf, Universitätsstr. 1, Düsseldorf 40225, Germany; [3]Institute of Immunology, Medical Faculty, University of Duisburg-Essen, Hufelandstr. 55, Essen 45147, Germany; [4]Campbell Family Institute for Breast Cancer Research, Princess Margaret Cancer Centre, UHN, 620 University Avenue Toronto, Toronto, ON, Canada M5G 2C1; [5]Institut für Klinische Chemie und Pathobiochemie, Klinikum rechts der Isar, Technische Universität Munich, Munich 81675, Germany; [6]Department of Physiology I, University of Tuebingen, Gmelinstr. 5, Tuebingen 72076, Germany; [7]Primary Immunodeficiency Clinic, Medical Outpatient Division and Immunodeficiency Lab, Department of Biomedicine, University Hospital Basel, Basel, Switzerland; [8]Department of Dermatology, Heinrich-Heine-University Düsseldorf, Universitätsstr. 1, Düsseldorf 40225, Germany and [9]Institute of Molecular Immunology, Technische Universität Munich, Munich 81675, Germany

*Corresponding author: TW Mak, Medical Biophysics and Immunology, The Campbell Family Institute for Breast Cancer Research at Princess Margaret Cancer Centre, 620 University Avenue, Suite 706, Toronto, Ontario, Canada M5G 2C1. Tel: 001 416 946 2234; Fax: 001 416 204 5300; E-mail: philipp.lang@gmx.net or karlsebastian.lang@uk-essen.de or tmak@uhnresearch.ca

[10]These authors share first authorship.

[11]These authors share last authorship.

Abbreviations: ALT, Alanine-amino transferase; β-ME, Beta-mercaptoethanol; BMDC, Bone marrow-derived dendritic cell; FACS, Fluorescence-activated cell sorting; GM-CSF, Granulocyte macrophage colony-stimulating factor; GP, Glycoprotein; IL-6, Interleukin-6; iDC, inflammatory dendritic cell; iNOS, inducible nitric oxide synthase; IFN-γ, Interferon-gamma; IL7Rα, Interleukin-7 receptor alpha chain; iMATE, Intrahepatic myeloid cell aggregate; LPS, Lipopolysaccharide; LCMV, Lymphocytic choriomeningitis virus; LCMV-GP, LCMV glycoprotein; LCMV-GP33, LCMV glycoprotein 33–41; MFI, Mean fluorescence intensity; MHC, Major histocompatibility complex; NF-κB, Nuclear factor 'kappa-light-chain-enhancer' of activated B cells; PD-1, Programmed cell death-1; RIP, Rat insulin promoter; PFU, Plaque-forming unit; TLR, Toll-like receptor; TNF-α, Tumor necrosis factor alpha; Tip-DCs, TNF-α and iNOS producing DCs; WT, Wild type

Received 16.12.13; revised 27.6.14; accepted 07.7.14; Edited by RA Knight; published online 26 September 2014

professional antigen-presenting cells into target organs is important for the maintenance of strong antiviral cytotoxic $CD8^+$ T-cell activity. Factors regulating iDC infiltration into the liver remain poorly understood.

Toso is a membrane protein whose extracellular domain has homology to the immunoglobulin variable (IgV) domains. The cytoplasmic region has partial homology to the FAST kinase (Fas-activated serine/threonine kinase).[17] Toso is expressed on B cells and activated T cells[17] and is over-expressed in B-cell lymphomas.[18,19] Expression of Toso can influence survival of macrophages.[20] Originally, Toso was described as an inhibitor of FAS signaling.[17,21] More recently, a role of Toso in IgM binding and TNFR signaling was also demonstrated[22–24] and consistently, Toso-deficient animals are protected from lipopolysaccharide (LPS)-induced septic shock.[24,25] Recently, we identified a role of Toso in the activation of granulocytes, monocytes, and DCs.[26–28] During infection with Listeria, the expression of Toso regulated granulocyte function.[26,27] The role of Toso in the function of monocytes and other myeloid cells still remains to be further elucidated.

In this study, we investigated the role of Toso during chronic viral infection by using the murine lymphocytic choriomeningitis virus (LCMV). We report that Toso promotes the differentiation and maturation of iDCs at virus-infected sites, which were essential for effector $CD8^+$ T-cell function and in accelerating the control of the virus. We further tested the role of Toso in the rat insulin promoter-glycoprotein (RIP-GP) autoimmune diabetes model and found that Toso was required to trigger diabetes in RIP-GP mice. Taken together, we have identified an essential role of Toso in the differentiation and maturation of iDCs, which is essential for the control of persistence-prone virus infection and triggering of autoimmune disease.

Results

LCMV infection induces iDCs in the liver. To investigate signals important for iDCs generation in the liver, we first infected wild-type (WT) mice with $2x10^6$ plaque-forming units (PFU) of LCMV strain WE. In confirmation of previous reports, we found that MHC-II^+ $CD45^+$ cells infiltrate the liver between days 4 and 6 (Figure 1a). MHC-II^+ cells expressed CD11c (Figure 1a). Some of the $CD11c^+$ cells expressed iNOS (Figure 1b). This suggests that iDCs infiltrate the liver during LCMV infection. Using flow cytometric analysis, we found that in addition to $CD8^+$ T cells, $CD11b^+$ myeloid cells also infiltrated the liver following LCMV infection. Most of those cells expressed Ly6C, and a subpopulation expressed CD11c (Figure 1c). Quantification of the fluorescence-activated cell sorting (FACS) data showed that on day 6, a time point when $CD8^+$ T cells infiltrate the liver, iDCs also infiltrated the liver (Figure 1d). Furthermore, inflammatory signals derived by $CD8^+$ T cells were responsible for infiltration of iDCs because lack of $CD8^+$ T cells limited recruitment of iDCs (Figure 1d). Taken together, these data suggest that inflammatory signals in the liver recruit and activate $CD11c^+$ cells during LCMV infection.

Toso is necessary for the development of iDCs in the liver. Next, we explored whether Toso influences the recruitment and differentiation of $CD11c^+$ cells. We infected WT mice and *Toso*$^{-/-}$ mice with 2×10^6 PFU of LCMV-WE and analyzed the livers 6 days later. The infected hepatocytes in WT animals were surrounded by T cells ($CD90.2^+$) and iDCs (Figure 2a). *Toso*$^{-/-}$ mice showed similar numbers of infected hepatocytes and $CD8^+$ T cells (Figure 2a). In contrast to WT mice however, numbers of $CD11c^+$ iDCs were limited in *Toso*$^{-/-}$ mice (Figure 2a). Using flow cytometric analysis we observed that iDCs were reduced in liver tissue of *Toso*$^{-/-}$ mice when compared with WT animals (Figures 2b and c), whereas $CD8^+$ T cells on day 6 were comparable between WT and *Toso*$^{-/-}$ mice (Figure 2c). Toso was previously shown to influence signaling of IgM and CD95.[17,23,24] To explore whether either of the signal was responsible for the lack of iDCs observed in the liver of *Toso*$^{-/-}$ mice, we analyzed mice that were deficient in soluble IgM (sIgM$^{-/-}$ mice) and Fas (*Fas*$^{lpr/lpr}$ mice). We did not observe reduced numbers of iDCs in sIgM$^{-/-}$ or *Fas*$^{lpr/lpr}$ mice (Supplementary Figure 1), suggesting that Toso influenced iDC generation independently of both signals. Taken together, these data indicate that iDCs infiltrate LCMV-infected liver tissue and this is dependent on the expression of the membrane protein Toso.

Intrinsic Toso expression regulates the differentiation of iDCs. Next, we wondered whether cell intrinsic expression of Toso was critical for iDC infiltration into liver tissue. We generated mixed bone marrow chimeras by lethally irradiating recipient WT mice followed by reconstitution with either WT, *Toso*$^{-/-}$, or a 1 : 1 mixture of WT and *Toso*$^{-/-}$ bone marrow. Cells derived from WT bone marrow were identified using the CD45.1 congenic marker. Cells derived from *Toso*$^{-/-}$ bone marrow were identified with CD45.2. Fifty days after bone marrow transplantation, mice were infected with 2×10^5 PFU of LCMV. On day 6 following infection, the number of iDCs of WT or *Toso*$^{-/-}$ origin in liver tissue was determined. As expected, iDCs in mice that received WT bone marrow were all of CD45.1 origin, whereas iDCs in mice which received *Toso*$^{-/-}$ bone marrow were all of CD45.2 origin (Figure 3a). Numbers of iDCs were reduced in mice reconstituted with *Toso*$^{-/-}$ bone marrow when compared with mice reconstituted with WT bone marrow (Figure 3b). Mixed bone marrow chimeras, which received a 1 : 1 ratio of WT and *Toso*$^{-/-}$ bone marrow, showed a reduced proportion of iDCs of *Toso*$^{-/-}$ (CD45.2) origin (Figures 3a and b). This was not due to a difference in hematopoietic cell development as no difference was observed in numbers of blood monocytes of WT (CD45.1) or *Toso*$^{-/-}$ (CD45.2) origin (Figure 3c). These data indicate that cell intrinsic Toso expression is critical for infiltration and differentiation of iDCs into the target tissue during LCMV infection.

Toso is critical for maturation of functional DCs *in vitro*. Next, we determined whether our *in vivo* phenotype was reproducible *in vitro*. We treated bone marrow cells with granulocyte macrophage colony-stimulating factor (GM-CSF) and measured expression of Ly6C and CD11c 6 days later. We found that cultures from WT cells showed a

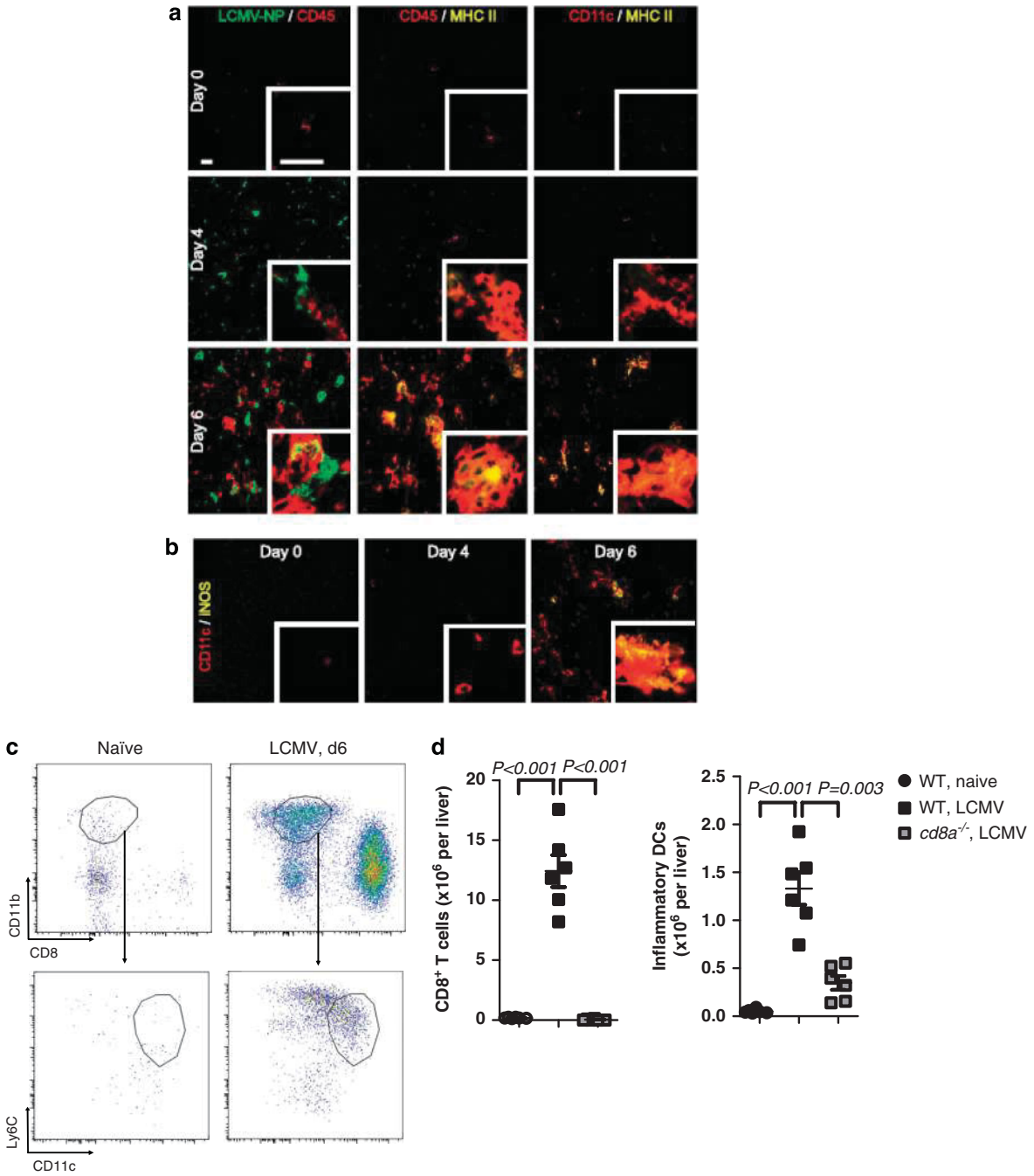

Figure 1 LCMV infection induces iDCs in the liver. C57BL/6 mice were infected with 2×10^6 PFU of LCMV-WE on day 0. (**a**) After 0, 4 and 6 days, the livers were removed and analyzed using histology for expression of LCMV-NP, the pan leukocyte marker CD45, MHC-II and CD11c (one representative of $n = 5$ is shown). (**b**) On day 0, 4 and 6, livers were analyzed using histology for expression of CD11c and iNOS (one representative of $n = 5$ is shown). (**c**) Livers from uninfected (naive) mice and day 6 infected mice were digested and cell suspensions were stained for CD8, CD11b, Ly6C and CD11c. Top panel: Dot plots show expression of CD11b and CD8. Lower panel: expression of Ly6C and CD11c for cells gated on CD11b. Gate indicates iDCs. One of three representative dot plots is shown. (**d**) Livers from uninfected (naive) WT mice and day 6 infected WT and *CD8a*$^{-/-}$ mice were digested and cell suspension was stained for CD8, CD11b, Ly6C and CD11c. The Graph shows the number of CD8$^+$ T cells and iDCs (CD11b$^+$ Ly6C$^+$ CD11c$^+$, $n = 6$). Scale bars, 25 μm (main image and inset)

significantly higher percentage of CD11c$^+$ cells when compared with bone marrow cultures from *Toso*$^{-/-}$ mice (Figures 4a and b). We did not detect a significant difference in total numbers of WT and *Toso*$^{-/-}$ CD11c$^+$ cells/well on our day 6 DC cultures, although there is a trend of higher numbers of CD11c$^+$ WT cells (Figure 4b). Co-staining revealed that the Ly6C-positive cells were Gr1$^+$ CD11b$^+$ CD80$^-$ cells (data not shown). To test the effect of Toso on the activation of DCs, we generated bone marrow DCs *in vitro* and activated them 9 days later with LPS. In WT mice we found that DCs expressed CD80 and CD86 and produced interleukin-6 (IL-6) after LPS challenge, whereas *Toso*$^{-/-}$

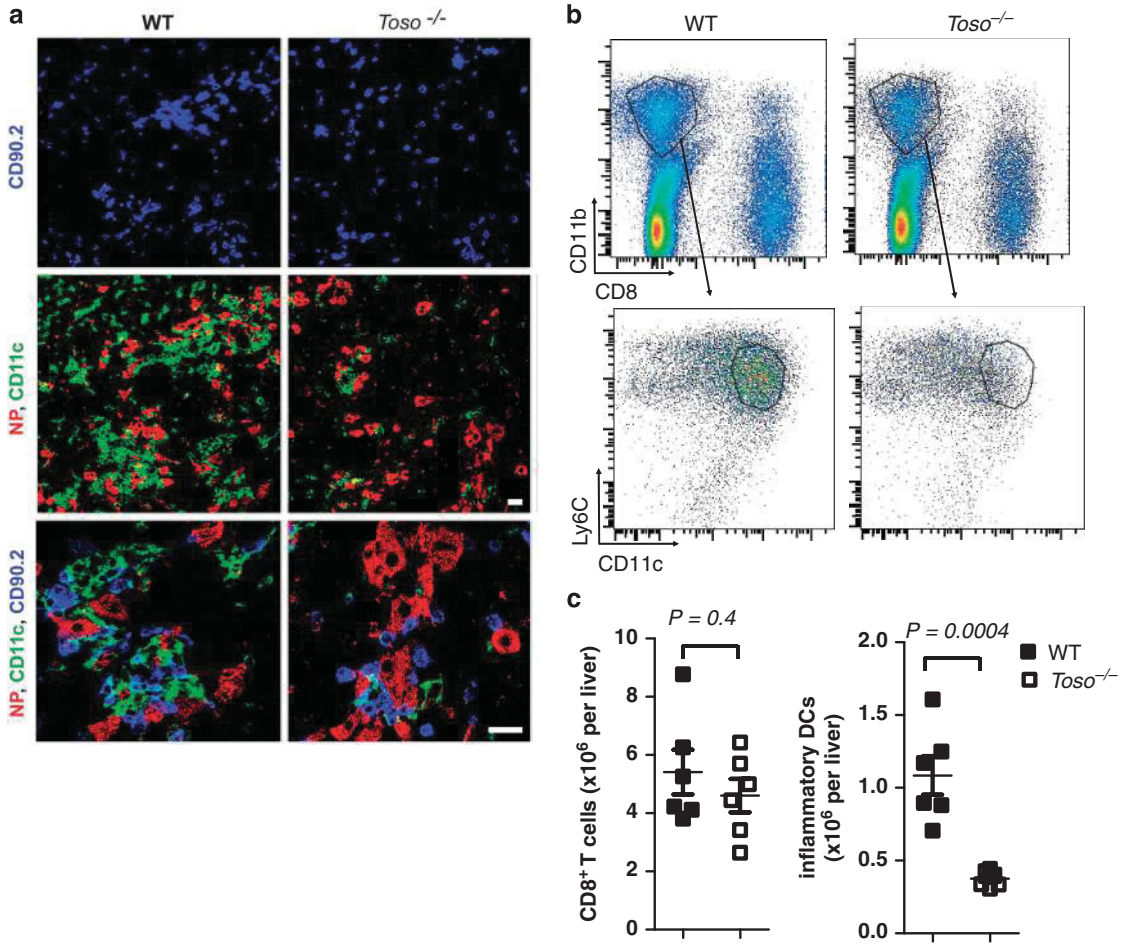

Figure 2 Toso is necessary for development of iDCs in the liver. *Toso*$^{-/-}$ mice and corresponding WT control mice were infected with 2×10^6 PFU of LCMV-WE. (**a**) On day 6, livers were analyzed for T cells (CD90.2), dendritic cells (CD11c$^+$) and virus-infected cells (NP$^+$) by immunofluorescence (one representative slide of $n = 6$ is shown). Scale bars, 20 μm. **(b** and **c)** On day 6, livers were examined for CD8$^+$ T cells and iDCs (CD11b$^+$ Ly6C$^+$ CD11c$^+$). Dot plots show expression of CD11b and CD8 (top panel), and expression of Ly6C and CD11c for cells gated on CD11b (lower panel). Statistical analysis of total CD8$^+$ T cells and inflammatory DCs (CD11b$^+$ Ly6C$^+$ CD11c$^+$) is shown (**c**), $n = 6$, pooled from two independent experiments)

DCs displayed limited expression of CD80 and CD86 and limited production of IL-6 (Figures 4c and d). To validate the capacity of *Toso*$^{-/-}$ DCs to activate CD8$^+$ T cells and induce co-stimulatory signals *in vivo*, we injected *in vitro*-generated bone marrow-derived dendritic cells of WT and *Toso*$^{-/-}$ mice into RIP-GP animals after pulsing with the LCMV peptides (GP33, GP276, and GP61).[29] Induction of diabetes in this model depends on the induction of auto-reactive CD8$^+$ T cells, which infiltrate the pancreas.[30–32] WT DCs induced auto-reactive CD8$^+$ T cells and mice developed diabetes (Figure 4e). In contrast, *Toso*$^{-/-}$ DCs could not induce diabetes in RIP-GP mice (Figure 4e). Next, we wanted to gain insights into the mechanism of reduced activation of *Toso*$^{-/-}$ DCs. Previously, we identified that Toso can influence nuclear factor 'kappa-light-chain-enhancer' of activated B cells (NF-κB) signaling.[26] Indeed, we found that after activation with LPS, *Toso*$^{-/-}$ DCs showed reduced phosphorylation of NF-κB p65 (Figure 4f), whereas phosphorylation of p38 and ERK was not affected by the absence of Toso (Figure 4f). In conclusion, we found that the absence of Toso on DCs resulted in reduced activation of DCs, an effect that was correlated with reduced phosphorylation of NF-κB.

Toso influences function of CD8$^+$ T cells in the liver. To further validate whether the lack of iDCs in *Toso*$^{-/-}$ mice results in attenuated CD8$^+$ T-cell responses, we utilized the P14 mouse that expresses a transgenic T-cell receptor recognizing the LCMV epitope GP33.[33] P14 TCR transgenic splenocytes expressing the congenic marker (CD45.1) were injected intravenously into naive CD45.2$^+$ WT and *Toso*$^{-/-}$ recipients. Recipient mice were infected with LCMV, and the donor and host CD8$^+$ T-cell response was monitored. Till day 6, the expansion of donor (CD45.1 positive) T cells was similar between WT and *Toso*$^{-/-}$ mice (Figure 5a). As expected, the numbers of iDCs in the liver were reduced in *Toso*$^{-/-}$ mice (Figure 5a). This strengthens our data that Toso has intrinsic functions in iDCs. Adoptively transferred virus-specific CD8$^+$ T cells exhibited significantly reduced interferon-gamma (IFN-γ) production when transferred into *Toso*$^{-/-}$ recipients (Figure 5b). This indicates that reduced numbers and function of iDCs in *Toso*$^{-/-}$ recipient mice have

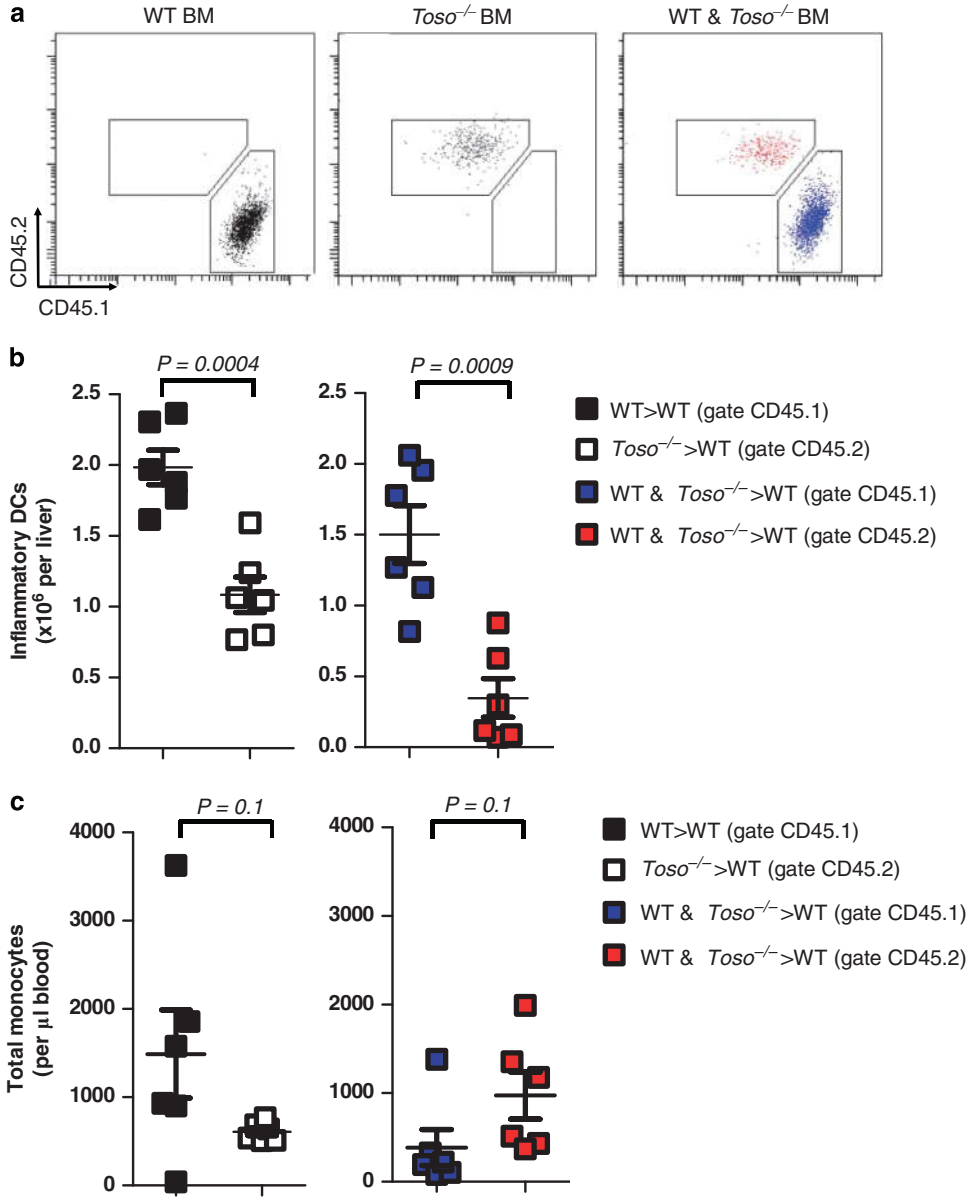

Figure 3 Intrinsic Toso expression regulates iDCs differentiation. CD45.2$^+$ WT mice were irradiated and reconstituted with bone marrow from either CD45.1$^+$ WT mice, CD45.2$^+$ *Toso*$^{-/-}$ mice or with a 1 : 1 mixture of WT and *Toso*$^{-/-}$ bone marrow. Fifty days after bone marrow transplantation, mice were infected with 2x10^5 PFU of LCMV (**a**) representative FACS plots showing expression of CD45.2 and CD45.1 on iDCs (Ly6C$^+$ CD11c$^+$ cells) in the liver ($n = 6$). (**b**) The total number of inflammatory DCs from the liver derived from CD45.1$^+$ WT bone marrow and CD45.2$^+$ *Toso*$^{-/-}$ bone marrow is shown from WT > WT chimeras (black), *Toso*$^{-/-}$ > WT chimeras (white), and WT & *Toso*$^{-/-}$ > WT chimeras (gate CD45.1 = blue; gate CD45.2 = red) ($n = 6$, pooled from two independent experiments). (**c**) The total number of monocytes (Ly6C^{hi} CD11b$^+$) present per μl of blood derived from CD45.1$^+$ WT bone marrow and CD45.2$^+$ *Toso*$^{-/-}$ bone marrow is shown from WT > WT chimeras (black), *Toso*$^{-/-}$ > WT chimeras (white) and WT and *Toso*$^{-/-}$ > WT chimeras (gate CD45.1 = blue; gate CD45.2 = red) ($n = 6$, pooled from two independent experiments)

an impact on CD8$^+$ T-cell function in the liver. To analyze the direct impact of DCs on CD8$^+$ T cells in the liver, we performed adoptive transfer experiments of WT and *Toso*$^{-/-}$ DCs into WT and *Toso*$^{-/-}$ mice. On day 6, we analyzed frequencies of virus-specific CD8$^+$ T cells in the liver. Transfer of WT DCs enhanced the frequency of LCMV glycoprotein 33–41 (LCMV-GP33)-specific CD8$^+$ T cells in WT mice (Figure 5c). In contrast,WT mice transferred with *Toso*$^{-/-}$ DCs showed reduced frequencies of LCMV-GP33-specific CD8$^+$ T cells (Figure 5c). Similarly, *Toso*$^{-/-}$ mice showed increased LCMV-GP33-specific CD8$^+$ T cells when transferred with WT DCs (Figure 5c). Transfer of *Toso*$^{-/-}$ DCs resulted in limited increase of LCMV-GP33-specific CD8$^+$ T cells (Figure 5c). Collectively, these data demonstrate that lack of Toso in DCs rather than in T cells influences CD8$^+$ T-cell function in the liver.

Toso deficiency alters CD8$^+$ T-cell-dependent virus control and immunopathology. To investigate the impact of Toso on the course of virus-induced hepatitis, virus

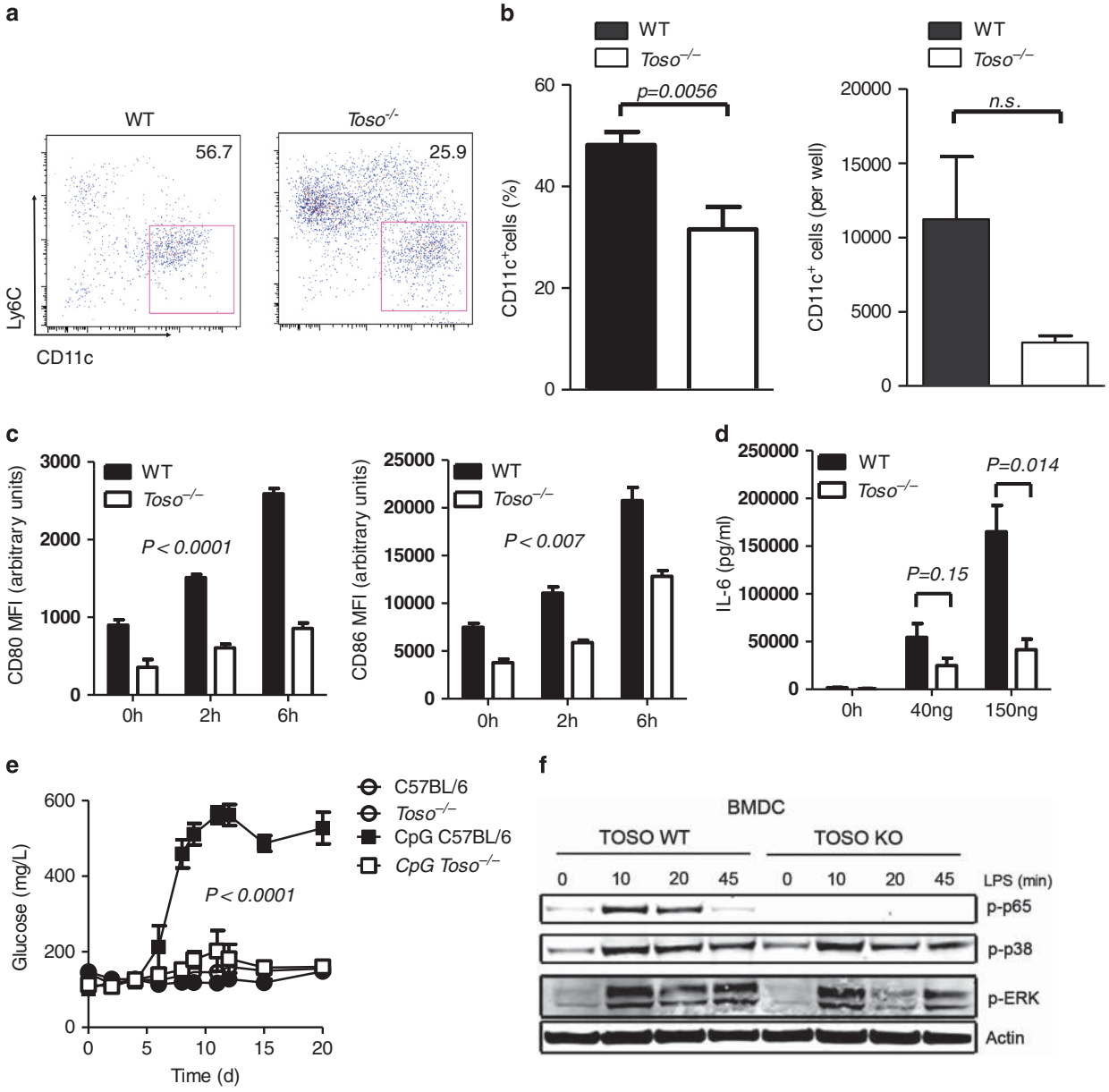

Figure 4 Toso is critical for maturation of functional dendritic cells. (**a** and **b**) Bone marrow cells from *Toso*$^{-/-}$and corresponding WT control mice were cultured in the presence of 40 ng/ml GM-CSF. Numbers of CD11c^{+} cells were analyzed on day 6. Representative FACS plot (**a**) and quantification of CD11c^{+} cells in percentage of living cells ($n=8$) and absolute numbers of CD11c^{+} cells per well (**b**, $n=4$–6) are shown. (**c** and **d**) DCs were generated from WT and *Toso*$^{-/-}$bone marrows. On day 9, DCs were stimulated with LPS. The MFI of CD80 and CD86 was analyzed on cells gated for CD11c at the indicated time points (**c**, $n=6$). Interleukin-6 was analyzed in the supernatant following 20 h stimulation with the indicated concentrations of LPS (**d**, a representative of two independent experiments is shown with three technical replicates). (**e**) WT or *Toso*$^{-/-}$dendritic cells were generated from bone marrow cells cultured with 400 ng/ml GM-CSF. Ten days later, dendritic cells were incubated with GP33, GP276 and GP61 with or without addition of CpG (5 μM) and injected into RIP-GP mice. Induction of diabetes was analyzed ($n=6$). (**f**) Western blot of p-p65, p-p38, p-ERK and actin in bone marrow-derived dendritic cells isolated from WT and *Toso*$^{-/-}$ mice without or with stimulation with 50 ng/ml LPS at the indicated time points (one of two experiments is shown)

control, and the systemic antiviral T-cell response, we infected WT and *Toso*$^{-/-}$ mice with 2×10^{6} PFU LCMV-WE. On day 6, we phenotyped CD8^{+} T cells in the spleen and liver. WT CD8^{+} T cells of LCMV-infected mice showed expression of programmed cell death-1 (PD-1), CXCR3 and reduced expression of interleukin-7 receptor alpha chain (IL7Rα) when compared with CD8^{+} T cells of naive mice (Figure 6a). This suggests strong T-cell activation in WT animals.[34] In contrast, CD8^{+} T cells in the spleen of *Toso*$^{-/-}$ mice showed reduced expression of PD-1, CXCR3 and higher expression of IL7Rα (Figure 6a), suggesting reduced activation of CD8^{+} T cells in *Toso*$^{-/-}$ mice. Accordingly, *Toso*$^{-/-}$ mice showed reduced numbers of virus-specific CD8^{+} T cells after day 6 when compared with WT animals (Figure 6b). This indicates that iDCs contribute to continuous activation and expansion of antiviral T cells. Consequently, *Toso*$^{-/-}$ mice failed to clear virus from blood, whereas WT mice eliminated LCMV from circulating blood 3 weeks after infection (Figure 6c). Next, we assessed liver cell damage by measuring the alanine-amino transferase (ALT) activity in the

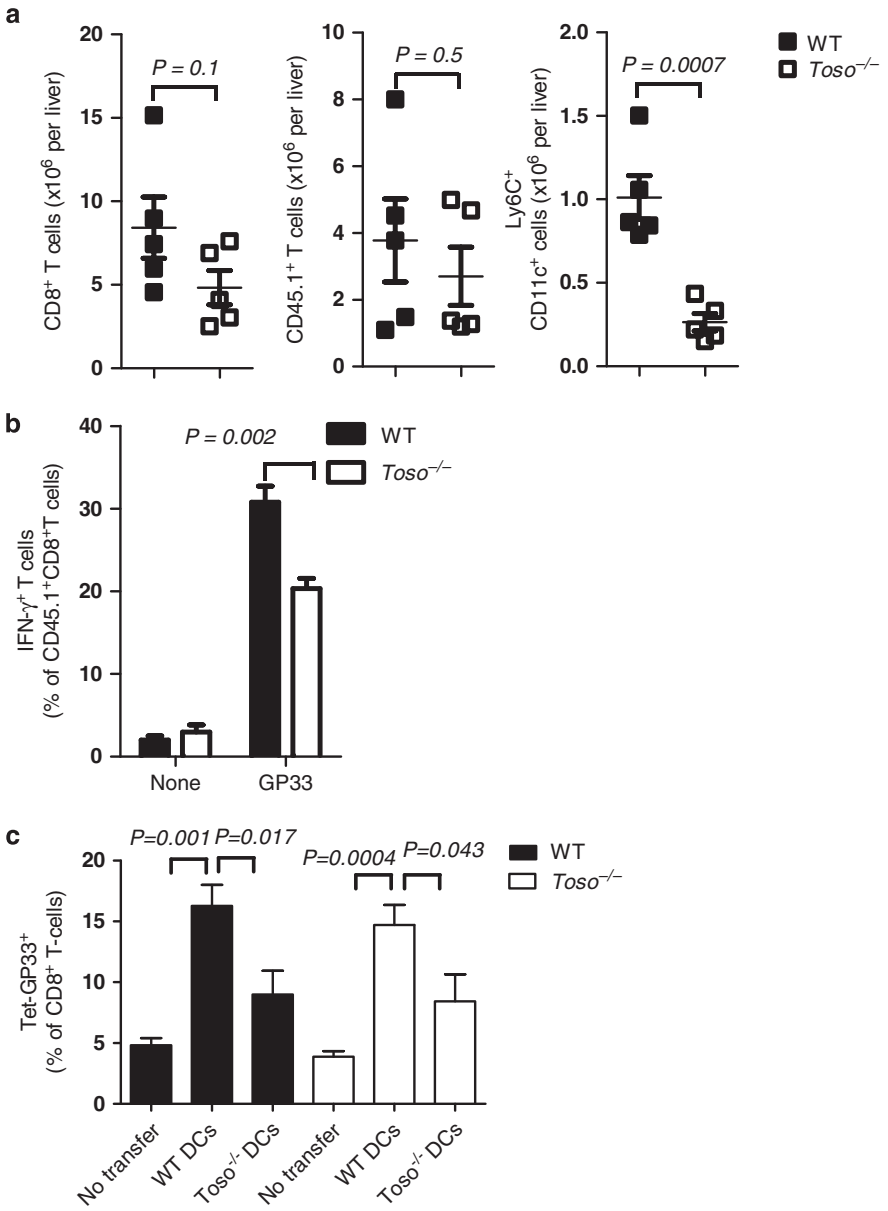

Figure 5 Toso influences function of CD8$^+$ T cells in the liver. 10^4 splenocytes from an LCMV-specific T-cell receptor transgenic mouse (P14 mouse expressing CD45.1) were injected intravenously into CD45.2$^+$ WT and *Toso*$^{-/-}$ recipient mice on day -1. On day 0, recipient mice were infected with 2 x 10^6 PFU of LCMV-WE. (**a**) On day 6, following infection livers were analyzed for host CD8$^+$ T cells, donor T cells (CD45.1$^+$) and iDCs (Ly6C$^+$CD11c$^+$) ($n=5$, pooled from two independent experiments). (**b**) Spleen lymphocytes were re-stimulated with LCMV-derived GP33 peptide and IFN-γ produced by donor TCR transgenic CD8$^+$ CD45.1$^+$ cells was analyzed by intracellular staining (**c**), $n=5$, pooled from two independent experiments). (**c**) WT and *Toso*$^{-/-}$ mice were infected with 2 x 10^6 PFU of LCMV-WE. On day 3, WT and *Toso*$^{-/-}$ DCs (derived from the bone marrow) which were infected with LCMV 24 h earlier were transferred into infected mice. On day 6, frequencies of virus-specific CD8$^+$ T cells were analyzed in the liver by GP33 tetramer staining ($n=5$–9)

serum of LCMV-infected WT and *Toso*$^{-/-}$ mice. Consistent with the reduced T-cell function, virus-induced liver cell damage was reduced in Toso-deficient mice (Figure 6d). We speculated that the reduction in liver cell damage was due to limited T-cell function. To gain further insights we used the LCMV strain Docile, which also persists in WT mice. During infection, antiviral CD8$^+$ T cells were again reduced in *Toso*$^{-/-}$ mice when compared with WT animals (Figure 6e). Nevertheless, LCMV established a persistent infection in WT and *Toso*$^{-/-}$ mice (Figure 6f). Consistently, the reduced CD8$^+$ T-cell response corresponded to lower ALT levels in Toso-deficient mice when compared with WT controls (Figure 6g). Taken together, these data indicate that Toso promotes long-term *in vivo* CD8$^+$ T-cell function and virus persistence.

CD8$^+$ T cells can be activated during bacterial infection in *Toso*$^{-/-}$ mice. DCs are needed for the generation of almost any CD8$^+$ T-cell response. In contrast, iDCs in the liver impact the CD8$^+$ T-cell response only under very specific conditions. Next, we analyzed the impact of Toso during subcutaneous bacterial infection. We infected WT and *Toso*$^{-/-}$

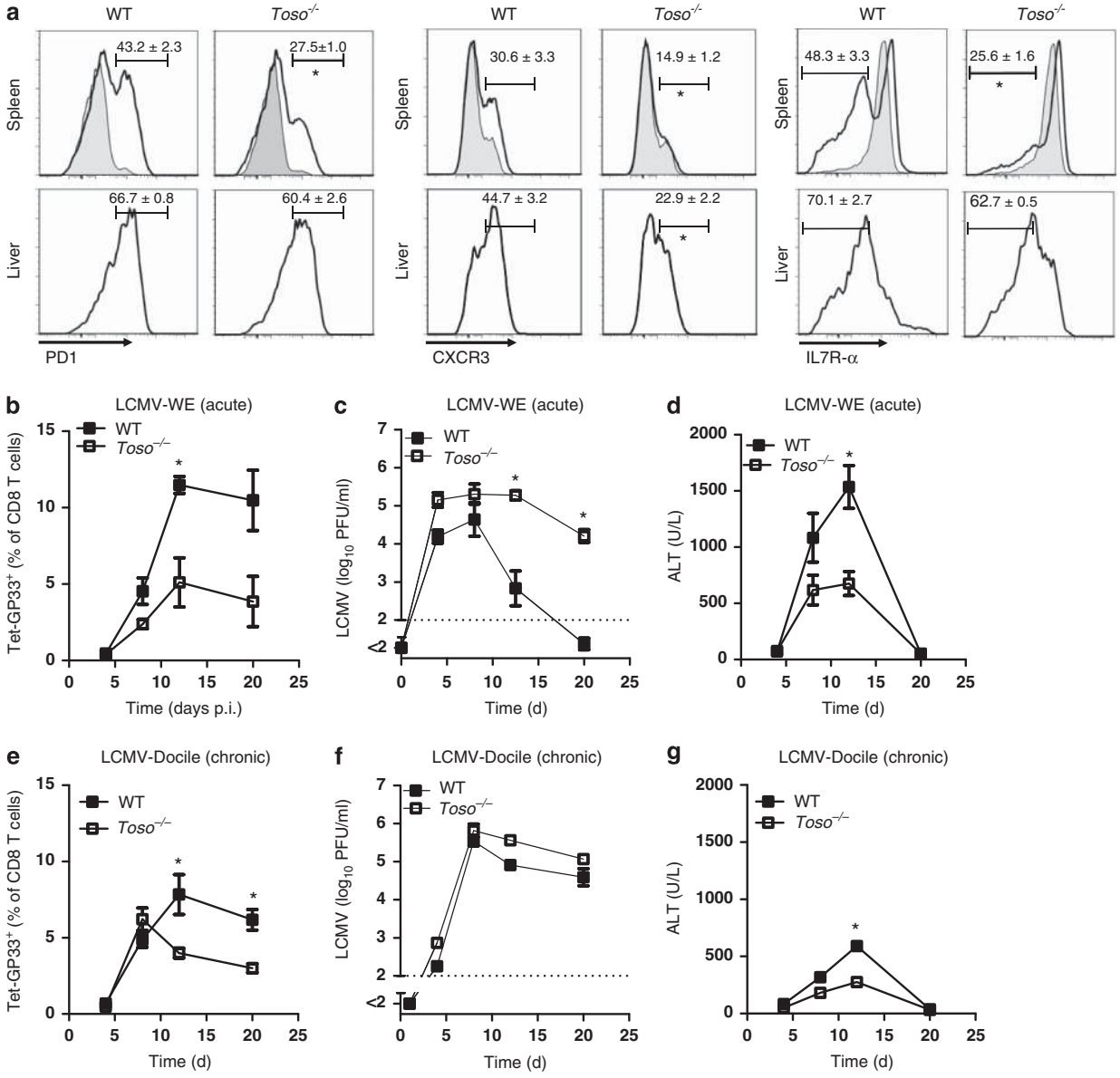

Figure 6 Toso deficiency alters CD8$^+$ T-cell-dependent virus control and immunopathology. (**a–c**) *Toso*$^{-/-}$ mice or WT mice were infected with 2×10^6 PFU of LCMV-WE. The CD8$^+$ T cells in the spleen and liver were analyzed by flow cytometry using the markers PD-1, CXCR3 and IL7R-α. Black line shows expression in CD8$^+$ T cells of virus-infected WT and *Toso*$^{-/-}$ mice. Gray histograms show expression in CD8$^+$ T cells of naive WT mice (**a**, $n = 3$–6). Virus-specific CD8$^+$ T cells were analyzed in the blood by GP33 tetramer staining (**b**, $n = 3$–4). Titers of infectious virus were analyzed in the serum of LCMV-WE-infected mice (**c**, $n = 4$–8, $^*P < 0.05$). At the indicated time points, serum ALT activity was analyzed (**d**, $n = 3$–8, $^*P < 0.05$). (**e–g**) WT or *Toso*$^{-/-}$ mice were infected with 2x10^6 PFU of LCMV-Docile. Virus-specific CD8$^+$ T cells were analyzed in the blood by GP33 tetramer staining (**e**, $n = 4$). Titers of infectious virus were analyzed over time in the serum of WT or *Toso*$^{-/-}$ mice (**f**, $n = 3$–4). At the indicated time points, serum ALT activity was analyzed (**g**, $n = 3$–4, $^*P < 0.05$)

mice subcutaneously with Listeria-GP33. Under these conditions, *Toso*$^{-/-}$ mice generated a functional CD8$^+$ T-cell response (Supplementary Figure 2) suggesting a specific role for Toso on the immune response during LCMV infection.

Discussion

In this study, we report a novel role of Toso in promoting effective immune responses during chronic virus infection using the well-defined LCMV model system. Infection of *Toso*$^{-/-}$mice with LCMV led to reduced effector CD8$^+$ T-cell function, resulting in delayed virus clearance. This did not result from an inherent defect in CD8$^+$ T cells in the absence of Toso, but rather correlated with the impaired functionality of *Toso*$^{-/-}$ iDCs within infected liver and spleen.

iDCs in WT animals expressed high levels of CD11c, MHC-II and CD80. Some of these cells additionally expressed iNOS and TNF-α (also called Tip-DCs). CCR2 is essential for the exit of monocytes from the bone marrow into circulating blood[15,35] and thus is likely to impact iDC development. However, while CCR2 is important for release of mature monocytes from bone marrow, Toso appears to play a role in the differentiation of these cells after their entry into infected tissues. The differentiation of iDCs in lungs of influenza-

infected mice has also been described.[11] iDCs during influenza infection may also contribute to the development of fully functional effector CD8$^+$ T cells.[15] Although the absence of Toso may be expected to be disadvantageous for the host following infection with a cytopathic virus-like influenza, impaired function of Toso during infection with non-cytopathic viruses such as LCMV and hepatitis viruses may be beneficial for the host by preventing potentially damaging immunopathology.[1,36] Interestingly, the presence or absence of virally induced pathology following infection with persistent low cytopathic viruses such as HIV, Hepatitis B and Hepatitis C virus,[1] and with cytopathic viruses such as severe acute respiratory syndrome [37,38] and H5N1 influenza[39] can differ between individuals, and the underlying cause for such differential outcomes remains unclear. We speculate that differences in expression or function of Toso may contribute to the inter-individual variability of disease outcome following viral infections.

Toso$^{-/-}$mice infected with LCMV exhibited reductions in CD8$^+$ T-cell activation as determined by decreased IFN-γ production. It remains unclear which signals contribute to the different functions of CD8$^+$ T cells in *Toso*$^{-/-}$mice. PD-1 is known to promote T-cell exhaustion, whereas IL7R provides essential survival signals to T cells.[40] Thus, changes in the expression of these molecules on T cells or the ligands on antigen-presenting cells in *Toso*$^{-/-}$mice may alter the ability of these cells to survive during chronic infection.[41–44] However, in the absence of Toso, the generation of memory T cells was impaired, suggesting that Toso, in promoting DC–T-cell interactions, impacts the generation and maintenance of effector CD8$^+$ T cells. In humans, chronic virus infection enhances PD-1 expression and correlates with virus persistence.[44,45] Based on those findings and our own observations, we hypothesize that Toso, in addition to PD-1, may modulate T-cell effector function.

The molecular mechanisms affected by Toso signaling in DCs still remain elusive. While we identified NF-κB as an important downstream transcription factor affected by Toso expression, the upstream signaling remains unknown. Recently, Toso was discovered to be a receptor for IgM[23] and while there is good evidence that IgM can activate Toso,[46,47] we also observed IgM-independent effects of Toso. Indeed, Toso has been described as influencing very diverse signaling events.[17,20,21,24,48] In view of the diverse signaling pathways affected by Toso, we speculate that Toso might interfere with several pathways eventually converging on the downstream transcription factor NF-*k*B.

In conclusion, we have shown that Toso expression promotes functional maturation and activation of iDCs within virus-infected tissue. Impaired DC maturation resulted in impaired expansion and effector function of CD8$^+$ T cells, increased viral replication and reduced immunopathology.

Materials and Methods

Virus, bacteria and mice. *Toso*$^{-/-}$mice were used as previously described.[26] sIgM$^{-/-}$ mice, lacking soluble IgM and *Fas*$^{lpr/lpr}$ mice, lacking FAS signaling, were kept on C57BL/6 background. P14 mice that express LCMV-GP33-specific T-cell receptor as a transgene were used. For adoptive transfer experiments, mice congenic for CD45 (CD45.1) were used to distinguish between transferred cells and endogenous (CD45.2) cells. All experiments were performed in single ventilated cages. Animal experiments were carried out with authorization of the Veterinäramt of Nordrhein Westfalen, Germany and in accordance with the German law for animal protection and in accordance to the institutional guidelines at the Ontario Cancer Institute. LCMV strain WE was originally obtained from F. Lehmann-Grube (Heinrich Pette Institute, Hamburg, Germany) and was propagated in L929 cells. Virus titers were measured using focus-forming assays as previously described.[49] Mice were infected with 2×10^6 PFUs LCMV-WE. For bacterial infections, recombinant Listeria expressing the LCMV-GP33 epitope was used. This recombinant strain of Listeria is highly attenuated compared with WT Listeria strains. For experiments with mixed chimeras, C57BL/6 mice were irradiated with 10.5 Gy. The next day, mice were reconstituted with either WT (CD45.1) bone marrow, *Toso*$^{-/-}$(CD45.2) bone marrow or with a 1 : 1 mixture of WT (CD45.1) and *Toso*$^{-/-}$(CD45.2) bone marrow. After 50 days, mice were infected with LCMV and analyzed 6 days post-infection.

DC cultures. To generate conventional DCs, we isolated bone marrow taken from femurs and tibias of mice. Following erythrocyte elimination, we cultured bone marrow cells in very low endotoxin Dulbecco's modified Eagle medium supplemented with 10% fetal calf serum and 0.1% β-mercaptoethanol (β-ME) in the presence of GM-CSF. On day 3 of differentiation, an equal volume of growth medium was added. Growth medium was exchanged on day 6 of differentiation, and differentiation status was checked by FACS. On day 9 of differentiation, cells were harvested for use in stimulation experiments with LPS and for immunization of RIP-GP mice.

Histology. Histological analysis was performed on snap-frozen or formalin-fixed tissue as previously described[31,32] using anti-LCMV-NP antibody generated in-house (clone VL4, clone KL53). Antibodies against CD11b, CD11c, CD90.2 and F4/80 were purchased from eBiosciences (San Diego, CA, USA). Anti-iNOS antibody was purchased from AnaSpec (Fremont, CA, USA).

ALT. ALT levels were measured using a serum multiple biochemical analyzer (Ektachem DTSCII, Johnson & Johnson Inc., Rochester, NY, USA).

Western blot and ELISA. Proteins were isolated with trizol and solubilized with 10 M urea/50 mM DTT. Protein lysates were normalized for total protein (Bio-Rad). Proteins were analyzed by electrophoresis under denaturating conditions using 4–20% SDS Clear-PAGE and blotted onto nitrocellulose membranes (Whatman, Buckinghamshire, UK). The membranes were stained with antibodies against p-p65, p-p38, p-ERK and actin (Cell Signaling, Danvers, MA, USA). IL-6 in the serum of cultured DCs was detected using the mouse IL-6 Elisa kit (eBiosciences).

Flow cytometric analysis. Tetramers were kindly proved by the NIH. Surface and intracellular FACS staining was performed as previously described.[31] For liver FACS the upper right liver lobe (lobus, representing 20% of the total liver) was digested with Liberase, DNAse (Roche, Basel, Switzerland) for 30 min at 37 °C and then smashed. Spleens were smashed without digestion. Anti-CD8a (BD Biosciences, San Jose, CA, USA), anti-PD1, anti-CXCR3, anti-IL-7 Rα, anti-CD11c, anti-CD11b, anti-Ly6C, anti-CD80, anti-CD86, anti-MHC-II (eBioscience) were used. For quantification of total cell numbers in the liver and spleen, calibrating beads were added to the cell suspensions and total numbers calculated back accordingly.

Statistical analysis. Data are expressed as mean ± S.E.M. Statistically significant differences between two different groups were analyzed using Student's *t*-test. Analyses with several groups were tested using a one-way ANOVA with post-testing according to Bonferroni or Dunnett. Statistically significant differences between treatment groups in experiments involving more than one analysis time point were calculated using two-way ANOVA (repeated measurements). *P*-values <0.05 were considered statistically significant.

Conflict of Interest

The authors declare no conflict of interest.

Acknowledgements. This study was supported by the Alexander von Humboldt Foundation (SKA2008 to KSL and SKA2010 to PAL). Furthermore, this study was supported by the German Research Council (TRR60, CRC974, LA2558-3-5/1, LA1419/5-1). This work was also supported by CIHR. DB was supported by a postdoctoral fellowship from the German Research Foundation (DFG).

1. Rehermann B, Nascimbeni M. Immunology of hepatitis B virus and hepatitis C virus infection. *Nat Rev Immunol* 2005; **5**: 215–229.
2. Sobao Y, Tomiyama H, Sugi K, Tokunaga M, Ueno T, Saito S *et al.* The role of hepatitis B virus-specific memory CD8 T cells in the control of viral replication. *J Hepatol* 2002; **36**: 105–115.
3. Thimme R, Oldach D, Chang KM, Steiger C, Ray SC, Chisari FV *et al.* Determinants of viral clearance and persistence during acute hepatitis C virus infection. *J Exp Med* 2001; **194**: 1395–1406.
4. Rehermann B, Fowler P, Sidney J, Person J, Redeker A, Brown M *et al.* The cytotoxic T lymphocyte response to multiple hepatitis B virus polymerase epitopes during and after acute viral hepatitis. *J Exp Med* 1995; **181**: 1047–1058.
5. Ferrari C, Penna A, Bertoletti A, Valli A, Antoni AD, Giuberti T *et al.* Cellular immune response to hepatitis B virus-encoded antigens in acute and chronic hepatitis B virus infection. *J Immunol* 1990; **145**: 3442–3449.
6. Recher M, Lang KS, Navarini A, Hunziker L, Lang PA, Fink K *et al.* Extralymphatic virus sanctuaries as a consequence of potent T-cell activation. *Nat Med* 2007; **13**: 1316–1323.
7. Geissmann F, Jung S, Littman DR. Blood monocytes consist of two principal subsets with distinct migratory properties. *Immunity* 2003; **19**: 71–82.
8. Auffray C, Sieweke MH, Geissmann F. Blood monocytes: development, heterogeneity, and relationship with dendritic cells. *Annu Rev Immunol* 2009; **27**: 669–692.
9. Nakano H, Lin KL, Yanagita M, Charbonneau C, Cook DN, Kakiuchi T *et al.* Blood-derived inflammatory dendritic cells in lymph nodes stimulate acute T helper type 1 immune responses. *Nat Immunol* 2009; **10**: 394–402.
10. Bosschaerts T, Guilliams M, Stijlemans B, Morias Y, Engel D, Tacke F *et al.* Tip-DC development during parasitic infection is regulated by IL-10 and requires CCL2/CCR2, IFN-gamma and MyD88 signaling. *PLoS Pathog* **6**: e1001045.
11. Aldridge JR Jr., Moseley CE, Boltz DA, Negovetich NJ, Reynolds C, Franks J *et al.* TNF/iNOS-producing dendritic cells are the necessary evil of lethal influenza virus infection. *Proc Natl Acad Sci USA* 2009; **106**: 5306–5311.
12. Serbina NV, Salazar-Mather TP, Biron CA, Kuziel WA, Pamer EG. TNF/iNOS-producing dendritic cells mediate innate immune defense against bacterial infection. *Immunity* 2003; **19**: 59–70.
13. Serbina NV, Jia T, Hohl TM, Pamer EG. Monocyte-mediated defense against microbial pathogens. *Annu Rev Immunol* 2008; **26**: 421–452.
14. Peters W, Scott HM, Chambers HF, Flynn JL, Charo IF, Ernst JD *et al.* Chemokine receptor 2 serves an early and essential role in resistance to *Mycobacterium tuberculosis*. *Proc Natl Acad Sci USA* 2001; **98**: 7958–7963.
15. Pamer EG. Tipping the balance in favor of protective immunity during influenza virus infection. *Proc Natl Acad Sci USA* 2009; **106**: 4961–4962.
16. Huang LR, Wohlleber D, Reisinger F, Jenne CN, Cheng RL, Abdullah Z *et al.* Intrahepatic myeloid-cell aggregates enable local proliferation of CD8(+) T cells and successful immunotherapy against chronic viral liver infection. *Nat Immunol* 2013; **14**: 574–583.
17. Hitoshi Y, Lorens J, Kitada SI, Fisher J, LaBarge M, Ring HZ *et al.* Toso, a cell surface, specific regulator of Fas-induced apoptosis in T cells. *Immunity* 1998; **8**: 461–471.
18. Pallasch CP, Schulz A, Kutsch N, Schwamb J, Hagist S, Kashkar H *et al.* Overexpression of TOSO in CLL is triggered by B-cell receptor signaling and associated with progressive disease. *Blood* 2008; **112**: 4213–4219.
19. Proto-Siqueira R, Panepucci RA, Careta FP, Lee A, Clear A, Morris K *et al.* SAGE analysis demonstrates increased expression of TOSO contributing to Fas-mediated resistance in CLL. *Blood* 2008; **112**: 394–397.
20. Sigruener A, Buechler C, Bared SM, Grandl M, Aslanidis C, Ugocsai P *et al.* E-LDL upregulates TOSO expression and enhances the survival of human macrophages. *Biochem Biophys Res Commun* 2007; **359**: 723–728.
21. Song Y, Jacob CO. The mouse cell surface protein TOSO regulates Fas/Fas ligand-induced apoptosis through its binding to Fas-associated death domain. *J Biol Chem* 2005; **280**: 9618–9626.
22. Shima H, Takatsu H, Fukuda S, Ohmae M, Hase K, Kubagawa H *et al.* Identification of TOSO/FAIM3 as an Fc receptor for IgM. *Int Immunol* **22**: 149–156.
23. Kubagawa H, Oka S, Kubagawa Y, Torii I, Takayama E, Kang DW *et al.* Identity of the elusive IgM Fc receptor (FcmuR) in humans. *J Exp Med* 2009; **206**: 2779–2793.
24. Nguyen XH, Lang PA, Lang KS, Adam D, Fattakhova G, Föger N *et al.* Toso regulates the balance between apoptotic and nonapoptotic death receptor signaling by facilitating RIP1 ubiquitination. *Blood* 2011; **118**: 598–608.
25. Nguyen X, Lang PA, Lang KS, Adam D, Fattakhova G, Föger N *et al.* Toso regulates death receptor-induced apoptosis by facilitating RIP1 ubiquitination. *Blood* 2010; **118**(3): 598–608.
26. Lang KS, Lang PA, Meryk A, Pandyra AA, Boucher LM, Pozdeev VI *et al.* Involvement of Toso in activation of monocytes, macrophages, and granulocytes. *Proc Natl Acad Sci USA* 2013; **110**: 2593–2598.
27. Lang KS, Lang PA, Meryk A, Pandyra AA, Merches K, Lee KH *et al.* Reply to Honjo et al.: Functional relevant expression of Toso on granulocytes. *Proc Natl Acad Sci USA* 2013; **110**: E2542–E2543.
28. Brenner D, Brüstle A, Lin GH, Lang PA, Duncan GS, Knobbe-Thomsen CB *et al.* Toso controls encephalitogenic immune responses by dendritic cells and regulatory T cells. *Proc Natl Acad Sci USA* 2014; **111**: 1060–1065.
29. Ohashi PS, Oehen S, Buerki K, Pircher H, Ohashi CT, Odermatt B *et al.* Ablation of "tolerance" and induction of diabetes by virus infection in viral antigen transgenic mice. *Cell* 1991; **65**: 305–317.
30. Lang KS, Recher M, Junt T, Navarini AA, Harris NL, Freigang S *et al.* Toll-like receptor engagement converts T-cell autoreactivity into overt autoimmune disease. *Nat Med* 2005; **11**: 138–145.
31. Honke N *et al.* Usp18 driven enforced viral replication in dendritic cells contributes to break of immunological tolerance in autoimmune diabetes. *PLoS pathog* 2013; **9**: e1003650.
32. Honke N, Shaabani N, Cadeddu G, Sorg UR, Zhang DE, Trilling M *et al.* Enforced viral replication activates adaptive immunity and is essential for the control of a cytopathic virus. *Nat Immunol* 2012; **13**: 51–57.
33. Ohashi PS, Pircher H, Mak TW, Bürki K, Zinkernagel RM, Hengartner H *et al.* Ontogeny and selection of the T cell repertoire in transgenic mice. *Semin Immunol* 1989; **1**: 95–104.
34. Cui W, Kaech SM. Generation of effector CD8 + T cells and their conversion to memory T cells. *Immunol Rev* 2010; **236**: 151–166.
35. Kuziel WA, Morgan SJ, Dawson TC, Griffin S, Smithies O, Ley K *et al.* Severe reduction in leukocyte adhesion and monocyte extravasation in mice deficient in CC chemokine receptor 2. *Proc Natl Acad Sci USA* 1997; **94**: 12053–12058.
36. Woltman AM, Boonstra A, Janssen HL. Dendritic cells in chronic viral hepatitis B and C: victims or guardian angels? *Gut* **59**: 115–125.
37. Kuba K, Imai Y, Rao S, Gao H, Guo F, Guan B *et al.* A crucial role of angiotensin converting enzyme 2 (ACE2) in SARS coronavirus-induced lung injury. *Nat Med* 2005; **11**: 875–879.
38. Frieman M, Heise M, Baric R. SARS coronavirus and innate immunity. *Virus Res* 2008; **133**: 101–112.
39. Peiris JS, Cheung CY, Leung CY, Nicholls JM. Innate immune responses to influenza A H5N1: friend or foe? *Trends Immunol* 2009; **30**: 574–584.
40. Lang PA, Recher M, Haussinger D, Lang KS. Genes determining the course of virus persistence in the liver: lessons from murine infection with lymphocytic choriomeningitis virus. *Cell Physiol Biochem* 2010; **26**: 263–272.
41. Barber DL, Wherry EJ, Masopust D, Zhu B, Allison JP, Sharpe AH *et al.* Restoring function in exhausted CD8 T cells during chronic viral infection. *Nature* 2006; **439**: 682–687.
42. Lang KS, Recher M, Navarini AA, Harris NL, Löhning M, Junt T *et al.* Inverse correlation between IL-7 receptor expression and CD8 T cell exhaustion during persistent antigen stimulation. *Eur J Immunol* 2005; **35**: 738–745.
43. Wherry EJ, Barber DL, Kaech SM, Blattman JN, Ahmed R. Antigen-independent memory CD8 T cells do not develop during chronic viral infection. *Proc Natl Acad Sci USA* 2004; **101**: 16004–16009.
44. Day CL, Kaufmann DE, Kiepiela P, Brown JA, Moodley ES, Reddy S *et al.* PD-1 expression on HIV-specific T cells is associated with T-cell exhaustion and disease progression. *Nature* 2006; **443**: 350–354.
45. Radziewicz H, Hanson HL, Ahmed R, Grakoui A. Unraveling the role of PD-1/PD-L interactions in persistent hepatotropic infections: potential for therapeutic application? *Gastroenterology* 2008; **134**: 2168–2171.
46. Shima H, Takatsu H, Fukuda S, Ohmae M, Hase K, Kubagawa H *et al.* Identification of TOSO/FAIM3 as an Fc receptor for IgM. *Int Immunol* 2010; **22**: 149–156.
47. Vire B, David A, Wiestner A. TOSO, the Fcmicro receptor, is highly expressed on chronic lymphocytic leukemia B cells, internalizes upon IgM binding, shuttles to the lysosome, and is downregulated in response to TLR activation. *J Immunol* 2011; **187**: 4040–4050.
48. Nguyen XH, Fattakhova G, Lang PA, Lang KS, Adam D, Föger N *et al.* Antiapoptotic function of Toso (Faim3) in death receptor signaling. *Blood* **119**: 1790–1791 2012.
49. Lang KS, Recher M, Navarini AA, Freigang S, Harris NL, van den Broek M *et al.* Requirement for neutralizing antibodies to control bone marrow transplantation-associated persistent viral infection and to reduce immunopathology. *J Immunol* 2005; **175**: 5524–5531.

Supplementary Information accompanies this paper on Cell Death and Differentiation website (http://www.nature.com/cdd)

Involvement of Toso in activation of monocytes, macrophages, and granulocytes

Karl S. Lang[a,b,c,1], Philipp A. Lang[a,b,1], Andreas Meryk[b,c,1], Aleksandra A. Pandyra[a,c,1], Louis-Martin Boucher[a], Vitaly I. Pozdeev[b], Michael W. Tusche[a], Joachim R. Göthert[d], Jillian Haight[a], Andrew Wakeham[a], Annick J. You-Ten[a], David R. McIlwain[a,b], Katja Merches[c,e], Vishal Khairnar[c], Mike Recher[f,g], Garry P. Nolan[h], Yasumichi Hitoshi[i], Pauline Funkner[b], Alexander A. Navarini[j,k], Admar Verschoor[l], Namir Shaabani[c], Nadine Honke[b,c], Linda Z. Penn[a], Pamela S. Ohashi[a], Dieter Häussinger[b], Kyeong-Hee Lee[m,2], and Tak W. Mak[a,2,3]

[a]Campbell Family Institute for Breast Cancer Research, Ontario Cancer Institute, University Health Network, Toronto, ON, Canada M5G 2C1; [b]Department of Gastroenterology, Hepatology and Infectious Diseases, University of Düsseldorf, 40225 Düsseldorf, Germany; [c]Institute of Immunology, University Hospital, University Duisburg-Essen, 45147 Essen, Germany; [d]Department of Hematology, West German Cancer Center, University Hospital of Essen, 45147 Essen, Germany; [e]Department of Physiology 1, University of Tübingen, Gmelinstr. 5, D-72076 Tübingen, Germany; [f]Division of Immunology, Children's Hospital, Harvard Medical School, Boston, MA; [g]Primary Immunodeficiency Clinic, Medical Outpatient Division and Immunobiology Laboratory, Department of Biomedicine, University Hospital Basel, Basel, Switzerland; [h]Department of Microbiology and Immunology, Stanford University, Stanford, CA 94305; [i]Rigel Inc., South San Francisco, CA; [j]Department of Dermatology, University Hospital of Zurich, Zurich, Switzerland; [k]Division of Genetics and Molecular Medicine, St. John's Institute of Dermatology, Guy's Hospital, King's College, London, United Kingdom; [l]Institute for Medical Microbiology, Immunology and Hygiene, Technische Universität München, D-81675 Munich, Germany; and [m]Division of Molecular Immunology, Research Center Borstel, Leibniz Center for Medicine and Biosciences, 23845 Borstel, Germany

Contributed by Tak W. Mak, December 20, 2012 (sent for review November 15, 2012)

Rapid activation of immune responses is necessary for antibacterial defense, but excessive immune activation can result in life-threatening septic shock. Understanding how these processes are balanced may provide novel therapeutic potential in treating inflammatory disease. Fc receptors are crucial for innate immune activation. However, the role of the putative Fc receptor for IgM, known as Toso/Faim3, has to this point been unclear. In this study, we generated Toso-deficient mice and used them to uncover a critical regulatory function of Toso in innate immune activation. Development of innate immune cells was intact in the absence of Toso, but Toso-deficient neutrophils exhibited more reactive oxygen species production and reduced phagocytosis of pathogens compared with controls. Cytokine production was also decreased in *Toso*$^{-/-}$ mice compared with WT animals, rendering them resistant to septic shock induced by lipopolysaccharide. However, *Toso*$^{-/-}$ mice also displayed limited cytokine production after infection with the bacterium *Listeria monocytogenes* that was correlated with elevated presence of *Listeria* throughout the body. Accordingly, *Toso*$^{-/-}$ mice succumbed to infections of *L. monocytogenes*, whereas WT mice successfully eliminated the infection. Taken together, our data reveal Toso to be a unique regulator of innate immune responses during bacterial infection and septic shock.

sepsis | ROS | LPS

During systemic bacterial infection, bacteria have to be controlled within the first few hours to days to guarantee survival. Macrophages, monocytes, and granulocytes are major contributors to antibacterial immune defense. Each of these cell types contributes to control of infection through phagocytosis of bacteria, production of antibacterial substances, and generation of cytokines, which recruit additional immune cells. Antibacterial immune responses can cause substantial collateral damage to tissue, and therefore immune effector functions have to be well controlled. How the innate immune system manages to restrict activation of effector cells largely to the sites of bacterial infection is still under intensive investigation.

Toso is a plasma membrane protein that contains an extracellular region with homology to the Ig variable (IgV) domains and a cytoplasmic region with partial homology to Fas-activated serine/threonine kinase (FAST kinase) (1). Toso was first identified as a molecule expressed on activated T cells capable of protecting T cells from programmed cell death (1). Toso is additionally expressed on B cells, overexpressed in B-cell lymphomas (2, 3), and is important for macrophage homeostasis (4). Mechanistically, Toso was originally described to influence Fas signaling (1, 5). We previously reported that TNF-induced apoptosis is enhanced in the absence of Toso (6, 7). Other work has shown that Toso can act as an Fc receptor for IgM (8, 9) and is important for the phagocytosis of IgM-coated targets (10). However, the physiological relevance of the diverse functions attributed to Toso remains to be verified.

In this study, we analyzed how Toso influences innate immune activation during bacterial infection in vitro and in vivo. We generated gene-targeted Toso-null (*Toso*$^{-/-}$) mutant mice and found that phagocytosis of pathogenic bacteria into both granulocytes and monocytes is influenced by IgM and Toso. In vivo, the lack of Toso reduced antibacterial cytokines, resulting in enhanced tolerance toward LPS-induced septic shock. However, *Toso*$^{-/-}$ mice were found to succumb to infection with *Listeria monocytogenes* more readily than WT controls.

Results

Toso Is Expressed on Granulocytes and Monocytes. To study the physiological role of Toso, we first generated Toso-deficient mice as described in *Experimental Procedures* and Fig. S1. We then analyzed Toso expression on bone marrow–derived granulocytes from WT and *Toso*$^{-/-}$ animals using a Toso-specific antibody (7). Immature (Ly6G^{med}) and mature (Ly6G^{hi}) granulocytes from WT bone marrow exhibited expression of Toso (Fig. 1*A*). Next we analyzed expression of spleen-derived monocytes. Monocytes showed clear expression of Toso (Fig. 1*B*). These findings indicate that Toso is present on innate immune cells such as monocytes and granulocytes.

Toso Does Not Influence Differentiation of Granulocytes and Monocytes. To determine whether Toso is important for the generation of myeloid cells, differentiation of granulocytes and monocytes from myeloid precursors was analyzed in WT and *Toso*$^{-/-}$ mice (Fig. 2*A*). Pre-GM and GMP cells were comparable between WT and

Author contributions: K.S.L., P.A.L., A.M., A.A.P., L.-M.B., P.S.O., K.-H.L., and T.W.M. designed research; K.S.L., P.A.L., A.M., A.A.P., L.-M.B., V.I.P., M.W.T., J.R.G., K.M., V.K., N.H., P.S.O., and K.-H.L. performed research; L.-M.B. contributed new reagents/analytic tools; K.S.L., P.A.L., A.M., A.A.P., V.I.P., M.W.T., J.R.G., J.H., A.W., A.J.Y.-T., D.R.M., K.M., V.K., M.R., G.P.N., Y.H., P.F., A.A.N., A.V., N.S., N.H., L.Z.P., P.S.O., D.H., K.-H.L., and T.W.M. analyzed data; and K.S.L., P.A.L., A.A.P., D.R.M., K.-H.L., and T.W.M. wrote the paper.

The authors declare no conflict of interest.

Freely available online through the PNAS open access option.

[1]K.S.L., P.A.L., A.M., and A.A.P. contributed equally to this work.

[2]K.-H.L. and T.W.M. contributed equally to this work.

[3]To whom correspondence should be addressed. E-mail: tmak@uhnres.utoronto.ca.

This article contains supporting information online at www.pnas.org/lookup/suppl/doi:10.1073/pnas.1222264110/-/DCSupplemental.

IMMUNOLOGY

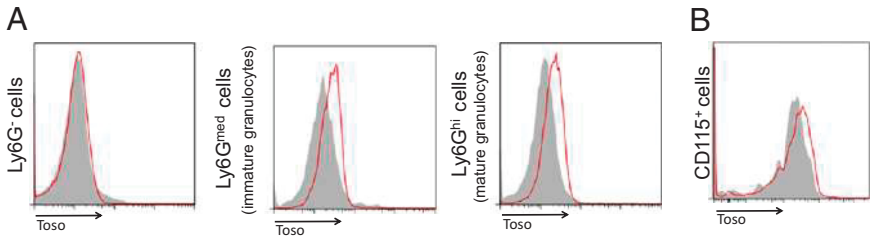

Fig. 1. Toso is expressed on granulocytes and monocytes. (*A*) Bone marrow cells from WT and *Toso*$^{-/-}$ mice were immunostained with anti-Ly6G (high expressing cells = mature granulocytes, medium expressing cells = immature granulocytes) plus rat anti-mouse Toso antibody. Red shows staining for WT cells; gray area shows staining of *Toso*$^{-/-}$ cells. One of two experiments is shown. (*B*) Splenocytes from WT and *Toso*$^{-/-}$ mice were stained with anti-CD115 (monocytes) plus rat anti-mouse Toso antibody (red). Red shows staining for WT cells; gray area shows staining of *Toso*$^{-/-}$ cells. One of two experiments is shown.

Toso$^{-/-}$ mice (Fig. 2 *B* and *C*). Monocytes and immature and mature granulocytes were also present in similar numbers in WT and *Toso*$^{-/-}$ mice (Fig. 2 *D* and *E*), suggesting that differentiation of granulocytes and monocytes was not dramatically impaired in the absence of Toso.

Lack of Toso Enhances Reactive Oxygen Species Production in Granulocytes. Next, the function of Toso in mature granulocytes was investigated by stimulation with *N*-formyl-methionine-leucine-phenylalanine (fMLP). fMLP engages the formyl peptide receptor (encoded by the *Fpr1 gene*) on granulocytes, mimicking pathogen contact (11, 12). About 10% of WT granulocytes produced reactive oxygen species (ROS) and degranulated following fMLP treatment (Fig. 3 *A* and *B*). In contrast, treatment with fMLP activated 50% of *Toso*$^{-/-}$ granulocytes, suggesting that the activation threshold to produce ROS is reduced in Toso-deficient granulocytes (Fig. 3 *A* and *B*). Even without fMLP treatment *Toso*$^{-/-}$ granulocytes also showed enhanced release of ROS compared with WT granulocytes (3.5 ± 0.6% vs. 1.4 ± 0.3%; $P = 0.003$). This phenotype could be reproduced using an independent strain of Toso KO mice (*Toso*$^{del/del}$; Fig. S2). Treatment with either LPS or GM-CSF, two stimuli known to prime granulocytes (13, 14), in combination with fMLP showed similarly enhanced ROS production in Toso-deficient granulocytes. Cellular stress (such as heat or cold shock) can also activate primed granulocytes (15) and represents a source of stimulation thought to contribute significantly to (auto)inflammatory diseases (16–18). To determine whether *Toso*$^{-/-}$ granulocytes were unusually prone to such activation, we incubated WT and *Toso*$^{-/-}$ granulocytes for 30 min at a range of temperatures and measured numbers of degranulating neutrophils. Temperature reduction from 37 °C to 14 °C induced degranulation in about 30% of *Toso*$^{-/-}$ granulocytes but in only a negligible percentage of WT granulocytes (Fig. 3*D*).

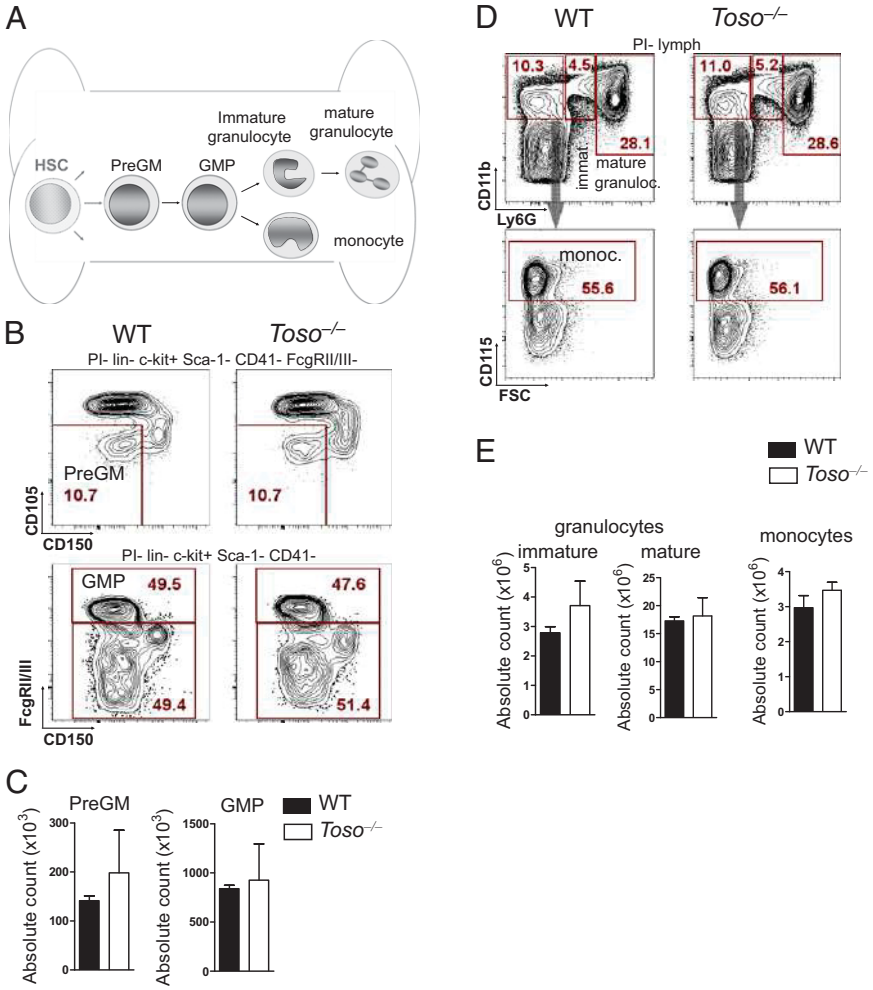

Fig. 2. Toso does not influence granulomonopoiesis in the bone marrow. (*A*) Scheme of granulocytes and monocyte development in bone marrow. (*B* and *C*) Flow cytometric analysis of early granulomonocytic progenitor compartments (PreGM and GMP) of WT mice and *Toso*$^{-/-}$ mice by staining for CD150, CD105, FcgRII/III, lineage markers, c-kit, Sca-1, and CD41. Original FACS contour plots (*B*) and quantification of progenitor compartments (*C*, $n = 3$) are shown. One of two experiments is shown. (*D* and *E*) Flow cytometric analysis of WT mice and *Toso*$^{-/-}$ mice stained for CD11b, Ly6G, CD115, and lymphoid markers (lymph). Original FACS contour plots (*D*) and quantification of different granulo- and monocytic subsets (*E*, $n = 3$) are shown. One of two experiments is shown.

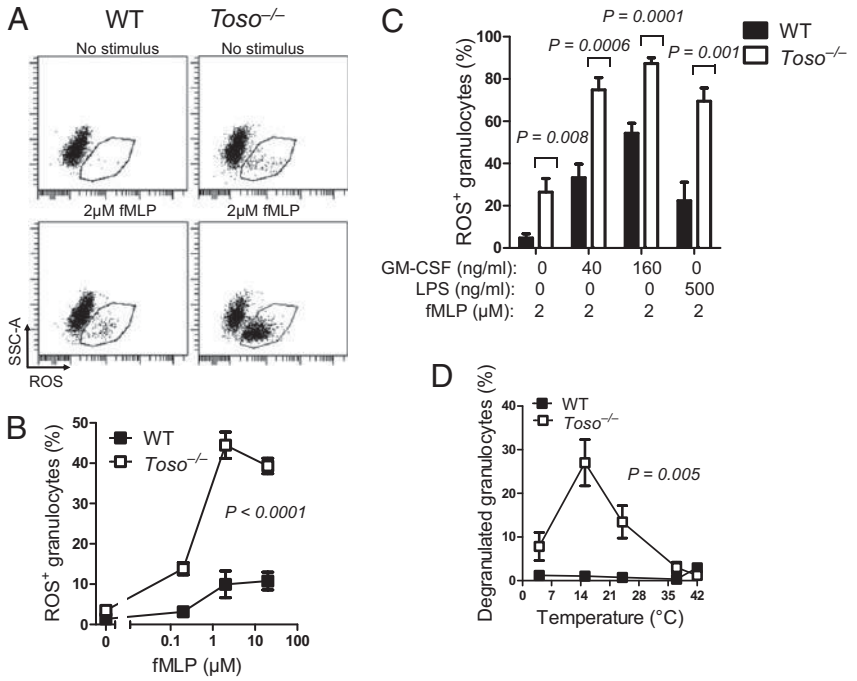

Fig. 3. Lack of Toso enhances ROS production in granulocytes. (*A* and *B*) Blood cells from WT or *Toso*$^{-/-}$ mice were incubated with or without the indicated concentrations of fMLP for 30 min at 37 °C, and granulocyte activation was assessed by measuring ROS production (dihydro-rhodamine staining) and degranulation (side-scatter) as described in *Experimental Procedures*. (*Left*) Representative dot plot of cells gated on total granulocytes (*A*). The mean percentage ± SEM of total granulocytes that was activated at each fMLP concentration (*B*, $n = 6$). (*C*) Blood cells from WT and *Toso*$^{-/-}$ mice ($n = 6$/group) were primed by incubation for 30 min with 40 ng/mL GM-CSF supernatant or 500 ng/mL LPS, and activated by stimulation with 2 μM fMLP for 15 min. The percentage of activated granulocytes was determined as for *A*. (*D*) Blood cells from WT and *Toso*$^{-/-}$ mice ($n = 6$/group) were incubated at the indicated temperatures for 30 min. The percentage of granulocytes that had degranulated was measured using flow cytometric side scatter as described in *Experimental Procedures*. Results shown are the mean percentage of degranulated cells ± SEM.

These findings indicated that the absence of Toso triggered enhanced ROS production in granulocytes.

Toso Influences Phagocytosis of Granulocytes and Monocytes. Next we analyzed whether Toso is involved in the phagocytosis of bacteria. Toso is described as an Fc receptor for IgM, which is internalized after IgM binding (8–10). To determine whether Toso and/or IgM are important for triggering granulocyte-mediated phagocytosis of *Listeria*, we incubated samples of peripheral blood from WT, *Toso*$^{-/-}$, or sIgM$^{-/-}$ mice with carboxyfluorescein succinimidyl ester (CFSE)-labeled *Listeria monocytogenes* and used flow cytometry to evaluate *Listeria* binding by Ly6G-positive granulocytes. WT granulocytes showed greater binding of *Listeria* than either *Toso*$^{-/-}$ or sIgM$^{-/-}$ granulocytes (Fig. 4*A*). Although a significant proportion of *Listeria* could still bind to granulocytes in the absence of Toso, confocal microscopy confirmed that reduced binding of CFSE-positive *Listeria* was also correlated with reduced *Listeria* uptake in Toso deficiency (Fig. S3). Next, we further investigated the mechanism of reduced *Listeria* binding to *Toso*$^{-/-}$ granulocytes by incubating CFSE-labeled *Listeria* with granulocytes isolated from WT or *Toso*$^{-/-}$ mice in the presence of serum obtained on day 3 postinfection from *Listeria*-infected WT or sIgM$^{-/-}$ mice. Binding of *Listeria* by *Toso*$^{-/-}$ granulocytes was reduced compared with WT controls under normal serum conditions, but not in the absence of serum IgM (Fig. 4*B*). Similar to granulocytes, Toso-deficient monocytes also showed reduced binding of *Listeria* (Fig. 4*C*). These data suggest that Toso is integrally involved in the IgM-mediated attachment of *Listeria*. Absence of Toso led to reduced phagocytosis of *Listeria* in *Toso*$^{-/-}$ granulocytes.

Toso Deficiency Leads to Reduced NF-κB Phosphorylation and Cytokine Production. We previously demonstrated that Toso limits signaling induced by the proinflammatory cytokine TNF-α (7). Limited signaling was mainly linked to defects in NF-κB activation. Because Toso-deficient granulocytes showed enhanced ROS production and granulocytes and monocytes exhibited defective phagocytosis, we wondered whether toll like receptor (TLR)-induced cytokine production might also be impaired. Indeed, LPS-stimulated *Toso*$^{-/-}$ macrophages exhibited delayed NF-κB activation after LPS stimulation compared with WT macrophages (Fig. 5).

Lack of Toso Reduces the LPS Response In Vivo. Next we analyzed cytokine production in WT and *Toso*$^{-/-}$ mice during treatment with LPS. We found that systemic injection of LPS led to reduced IL-6 and TNF-α production in *Toso*$^{-/-}$ mice relative to controls (Fig. 6 *A* and *B*). In line with this, *Toso*$^{-/-}$ mice survived LPS treatment, whereas WT mice died (Fig. 6*C*). Those data show that, although ROS production was enhanced in *Toso*$^{-/-}$ mice, the cytokine response during LPS challenge was functionally limited.

Impaired Control of *Listeria* in Toso-Deficient Mice. Our data showed that lack of Toso correlated with enhanced ROS production but

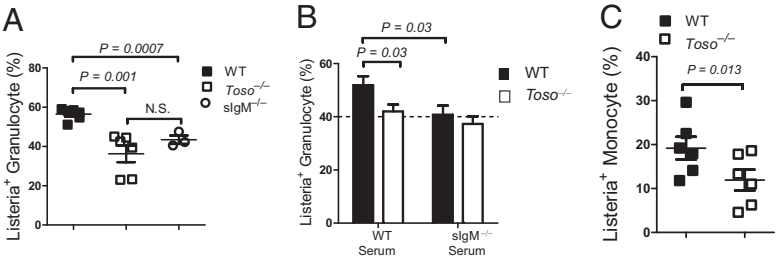

Fig. 4. Toso influences phagocytosis of granulocytes and monocytes. (*A*) Peripheral blood was incubated for 60 min with 10^6 CFU of CFSE-labeled *Listeria* and CSFE-positive granulocytes were analyzed by flow cytometry. Data points are values for individual mice ($n = 3$–6/group). (*B*) Blood leukocytes from WT or *Toso*$^{-/-}$ mice were washed three times to remove IgM. Granulocytes were then incubated for 60 min with CFSE-labeled *Listeria* plus serum from WT or sIgM$^{-/-}$ mice that had been infected with *Listeria* 3 d prior. *Listeria* uptake by granulocytes was analyzed. Horizontal line, mean for IgM independent *Listeria* uptake. Results are the mean ± SEM ($n = 10$). (*C*) Peripheral blood was incubated for 60 min with 10^6 CFU of CFSE-labeled *Listeria*, and CSFE-positive monocytes were analyzed by flow cytometry. Data points are values for individual mice ($n = 6$/group).

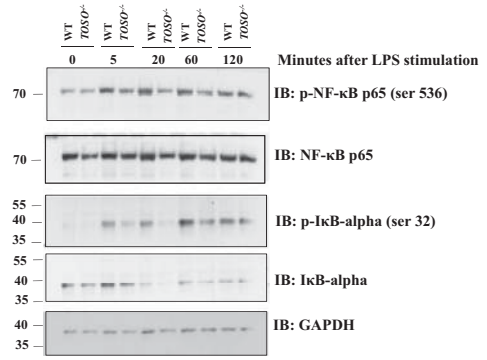

Fig. 5. Toso deficiency leads to reduced NF-κB phosphorylation, Bone marrow–derived macrophages were generated from WT and *Toso*$^{-/-}$ bone marrow. Cells were challenged with LPS (100 ng/mL). NF-κB activation was analyzed after different time points. One of three similar experiments is shown.

reduced cytokine production and phagocytosis. To determine the impact of those deficiencies on the control of bacterial infection, we infected WT and *Toso*$^{-/-}$ mice with *L. monocytogenes*. Consistent with our in vitro results, peripheral blood granulocytes obtained from *Toso*$^{-/-}$ mice on day 2 after systemic *Listeria* inoculation (1×10^4 CFUs) showed elevated ROS production compared with granulocytes from infected WT mice (Fig. 7*A*). This observation correlated with the increased release of myeloperoxidase (MPO) protein into the serum of infected *Toso*$^{-/-}$ mice compared with infected WT animals (Fig. 7*B*). There were no obvious differences in the number of granulocytes in infected organs (Fig. 7*C*). However, the number of bacteria was enhanced within the granulomas compared with WT mice (Fig. 7*C*). Reduced bacterial control in the presence of granulocytes suggested that infiltration of granulocytes into target tissues was not defective in the absence of Toso, but likely that these granulocytes displayed reduced effector function within the tissues. Consistently, cytokine production was reduced in *Toso*$^{-/-}$ mice compared with WT mice after *L. monocytogenes* infection compared with WT animals (Fig. 7*D*). Three days after infection, higher *Listeria* titers were found in *Toso*$^{-/-}$ spleen, liver, and brain tissue compared with the WT tissue (Fig. 7*E*). As a result, *Toso*$^{-/-}$ mice rapidly succumbed to a dose of *Listeria* that was generally lethal to only 20% of WT mice (Fig. 7*F*), indicating that Toso is essential for effective control of *Listeria* in vivo. Taken together, the absence of Toso resulted in limited cytokine production after *L. monocytogenes* infection and death of infected *Toso*$^{-/-}$ mice.

Discussion

In this study, we demonstrated that Toso regulates ROS production, cytokine production, and phagocytosis. A previous report established that the presence of Toso on T cells rendered them less sensitive to Fas-induced cell death (1), and we have recently shown that Toso overexpression reduces apoptotic signaling induced by TNF-α treatment (6, 7). In addition, we found here that Toso is involved in IgM-dependent phagocytosis and that the lack of Toso reduces cytokine responses after LPS treatment. The latter effect correlated with reduced NF-κB phosphorylation. Taking those effects together, we suggest that Toso is probably involved in several signaling pathways. From our findings, we conclude two functions of Toso: (*i*) Toso can act as an FcR that can bind to IgM-coated pathogens, triggering phagocytosis; and (*ii*) Toso regulates surface signals that drive antipathogenic signaling. Such dual functions have been previously described for other granulocyte receptors, including α_M-integrin (CD11b). CD11b not only acts as receptor for several ligands (ICAM-1, iC3b, collagen, fibrinogen) (19) but also negatively regulates TLR signaling (20–22). The mechanism of phagocytosis probably involves small GTPases and actin polymerization (23); however, how these are linked to Toso remains to be studied.

We found that the susceptibility of Toso-deficient mice to bacterial infection correlated with reduced phagocytic capacity and enhanced ROS production. Even without any additional stimulation, ROS were detectable in Toso-deficient granulocytes. Together those data suggest that fMLP signaling was probably not affected specifically by Toso. More likely, Toso expression generally enhances the activation threshold of granulocytes. From our data, we would interpret that the absence of this mechanism in Toso deficiency would result in activation of granulocytes without any additional stimulus. Recently, Cole et al. showed that ROS production enhanced the spread of *Listeria* between cells (24), hastening mouse death. In line with that, depletion of monocytes rather than depletion of granulocytes enhanced susceptibility to *Listeria* infection in mice (25). These studies, and the data described here, underscore that enhanced ROS production of granulocytes likely has an overall negative impact in the control of *Listeria*. How early and enhanced ROS production can negatively impact *Listeria* infection remains largely unexplained. We found that deficiency of Toso led to enhanced bacterial titers in the spleen, liver, and brain. Using histology, we also found enhanced *Listeria* numbers within granulomas. As the granulomas did not show an obvious difference in size between WT and *Toso*$^{-/-}$ mice, we suggest that homing to the site of infection was not altered between WT and *Toso*$^{-/-}$ mice. Instead, it was likely the effector function within the infected tissue, which was defective in the absence of Toso.

We found that, *Toso*$^{-/-}$ granulocytes were still able to uptake *Listeria*, albeit at a reduced level. Because *Toso*$^{-/-}$ was nevertheless more susceptible to *Listeria* infection, it is unclear whether additional mechanisms besides *Listeria* uptake are also defective in the absence of Toso. As activation of innate immune cells can partially depend on the phagocytosis of pathogenic pattern molecules, we postulate that Toso is not only directly affecting innate immune cell effector functions, but perhaps more importantly is regulating the immune activation, which strongly impacts pathogen control. Indeed, using LPS treatment, we found that Toso influences cytokine induction during this model of sterile immune activation.

Enhanced ROS production and deficient cytokine response in parallel to reduced phagocytosis are likely the reason for the rapid death of Toso-deficient mice during *Listeria* infection (26, 27). Theoretically, enhanced ROS levels could also lead to death of mice due to collateral damage to tissue (28). However, because we saw significantly enhanced bacterial titers in the brains of

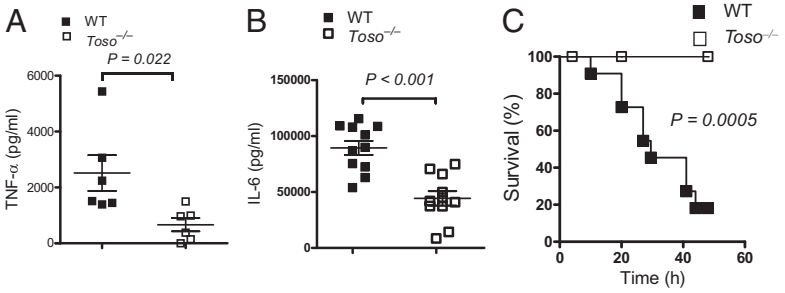

Fig. 6. Lack of Toso reduces the LPS response in vivo. WT and *Toso*$^{-/-}$ mice were injected intraperitoneally at a dose of 25 mg/kg. (*A*) TNF-α was analyzed after 4 h ($n = 6$). (*B*) IL-6 was analyzed after 2 h ($n = 11$). (*C*) Survival was monitored ($n = 11$).

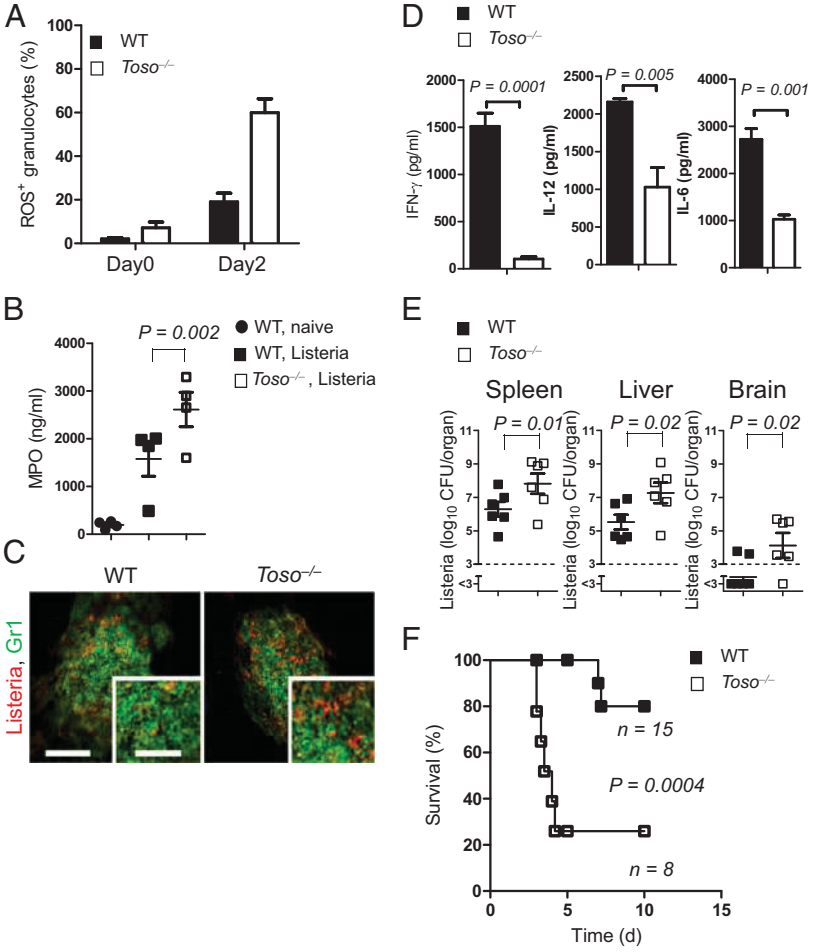

Fig. 7. Impaired control of *Listeria* in Toso-deficient mice. WT and *Toso*$^{-/-}$ mice were infected with 1×10^4 CFU *Listeria* or 1×10^5 CFU *Listeria* for *B*. (*A*) ROS production on the indicated days postinfection by granulocytes from peripheral blood of WT and *Toso*$^{-/-}$ mice ($n = 4$–5). (*B*) Levels of MPO protein in the plasma of uninfected WT mice and at 6 h postinfection in the plasma ($n = 4$/group). (*C*) *Listeria* and granulocyte infiltration was analyzed in the liver on day 3. One of three representative slides is shown. (Scale bar = 50 μm; Scale bar inset, 25 μm.) (*D*) IFN-γ, IL-12, and IL-6 concentrations were analyzed in the serum at different time points ($n = 4$). (*E*) *Listeria* titers on day 3–4 postinfection in spleen, liver, and brain of WT and *Toso*$^{-/-}$ mice ($n = 6$/group). (*F*) Kaplan-Meier survival curves for WT ($n = 15$) and *Toso*$^{-/-}$ ($n = 8$) mice.

Toso-deficient mice and because we could rescue *Listeria* susceptibility of Toso-deficient mice with transfer of WT granulocytes (Fig. S4), we would rather speculate that bacterial burden was the reason for the hastened death of Toso-deficient mice.

Although the main function of granulocytes is the early control of pathogens, hyperactivation of these cells is a hallmark of autoinflammatory disorders such as periodic fever syndromes and autoimmune diseases such as rheumatoid arthritis, vasculitis, and autoinflammatory lung injury (18, 29–31). The reasons for these instances of inappropriate granulocyte activation are not known (16, 17). In particular, vasculitis is associated with enhanced granulocyte activation and/or autoantibodies directed against granulocytic components (31, 32). Consistent with this disease, Toso-deficient animals exhibit autoantibody formation (33). Future studies will examine the exciting possibility that Toso also influences granulocyte activation in human inflammatory diseases.

In conclusion, we demonstrated that Toso is a regulator of granulocyte activation. Toso thus plays a key role in the coordination of granulocyte phagocytosis, ROS production, and degranulation and is critical for the normal control of bacterial infection in mice.

Experimental Procedures

Mice. Genomic DNA fragments containing the *Toso* gene were isolated from a mouse genomic DNA library (129J/Ola; J. Rossant, SickKids Hospital, University of Toronto, Toronto, Canada) using a mouse full-length *Toso* cDNA as a probe. The KO construct was assembled using two PCR-generated fragments: a 6.5-kb fragment found within an intron located in the 5′ leader sequence of the gene and a 0.65-kb fragment downstream of the last methionine. Both fragments were inserted on either side of a neomycin (*neo*) expression cassette, such that homologous recombination caused the replacement of almost all of the *Toso* coding region by *neo* (Fig. S1*A*). An artificial EcoRI site was added to reduce the WT 6-kb EcoRI fragment to a 2.3-kb size when probed on a Southern blot with a flanking probe. The KO construct was electroporated into D3 embryonic stem (ES) cells, and a clone demonstrating homologous recombination was injected into E3.5 C57/BL6 blastocysts, which were implanted in pseudopregnant ICR mice. The chimeric progeny were bred until germ-line transmission was achieved, and heterozygotes bearing the KO allele were intercrossed to generate homozygous progeny. Deletion of *Toso* was confirmed by PCR and RT-PCR analyses of various tissues (Fig. S1 *B*–*D*). *Toso*$^{-/-}$ mice were backcrossed into the C57BL/6 background for more than nine generations before use in experiments. *Toso*$^{del/del}$ mice, an independent line of Toso KO mice on the C57BL/6 background, have been previously described (7). sIgM$^{-/-}$ mice were also maintained on the C57BL/6 genetic background. All experiments were performed in single ventilated cages. Animal experiments were carried out in Germany and Canada under the authorization of the Veterinäramt of Duesseldorf and in accordance with German laws for animal protection and according to institutional guidelines at the Ontario Cancer Institute of the University Health Network.

***Listeria* Infection and In Vitro Phagocytosis.** *L. monocytogenes* (ATCC strain 43251) bacteria were the kind gift of Klaus Pfeffer (Institute of Medical Microbiology and Hospital Hygiene, Heinrich-Heine-University Duesseldorf, Duesseldorf, Germany) and were maintained in heart infusion agar as previously described (34). If not otherwise indicated, mice were infected i.v. with 2×10^4 CFU of *Listeria*. For CFSE labeling, 10^9 CFUs *Listeria* were incubated for 10 min with 50 μM CSFE (Invitrogen) in 10 mL PBS. After two washes in PBS/10% (vol/vol) FCS and an additional three washes in medium, CSFE-labeled *Listeria* were incubated for indicated time points with granulocytes in antibiotic-free, FCS-free medium.

Granulocyte Activation and FACS. Stimuli for granulocyte activation were fMLP (Sigma Aldrich), LPS (Sigma), and GM-CSF (self-made from GM-CSF–producing cells [X63O]). For granulocyte activation studies, mouse peripheral blood was incubated with DMEM/2% FCS containing fMLP plus anti-Gr1,

anti-CD11b antibody (eBiosciences) and dihydro-rhodamine (Alexis). For priming studies, granulocytes were pretreated for 30 min with cytokines followed by 15-min activation with fMLP. Granulocytes, which produced enhanced levels of ROS and showed degranulation in SSC-A, were considered activated granulocytes. Toso expression was analyzed by an anti-Toso antibody generated previously in the laboratory of K.-H.L. Absolute counts of bone marrow cells were determined on a Z2 cell counter (Beckman Coulter). FACS analysis was performed on a LSRII flow cytometer (Becton Dickinson) after staining with fluorochrome-conjugated antibodies (Becton Dickinson, eBioscience, Biolegend) as previously described (35, 36). Toso expression was analyzed by a monoclonal antibody against murine Toso (clone B68) that was generated in the laboratory of K.-H.L. (7).

Bone Marrow–Derived Macrophages. Bone marrow cells were treated with macrophage colony-stimulating factor (M-CSF) derived from L929 cells in very low endotoxin DMEM 10% FCS. After 8–10 d, cells were used for experiments.

LPS Treatment. WT and Toso-deficient animals were injected i.p. with a 25-mg/kg dose of LPS (026:B6; Sigma).

Myeloperoxidase. Levels of myeloperoxidase protein in serum were quantified by ELISA (Hycult Biotech) according to the manufacturer's instructions.

Quantitative RT-PCR. RNA extraction and cDNA synthesis were performed using Trifast (peqlab) and the QuantiTec Rev. Transcription Kit (Qiagen) according to the manufacturers' instructions. Analysis of specific gene expression was performed using Toso (Faim3) kits (Applied Biosystems or Qiagen). The mRNA expression levels of all target genes were normalized against GAPDH or 18sRNA.

Temperature Shock Experiment. Mouse peripheral blood (10 μL) was incubated with 100 μL DMEM/2% FCS plus anti-Gr1 and anti-CD11b for 30 min either at 4 °C, 15 °C, 24 °C, 37 °C, or 42 °C. Degranulated granulocytes were determined by SSC-A.

Immunoblotting. Bone marrow–derived macrophages were seeded in six-well tissue-culture plates and treated as indicated. Cells were washed with PBS and lysed using 1.1% SDS, 11% glycerol, and 0.1 M Tris, pH 6.8, with 10% β-mercaptoethanol. Blots were probed with anti–phospho-NF-κB p65 (Ser536), anti–phospho-IκBα (Ser32), anti-IκBα, anti-GAPDH (Cell Signaling), and anti–NF-κB p65 (Santa Cruz).

Histology. Histological analyses were performed on snap-frozen tissues as previously described (34). Slides were stained for anti–Gr1-FITC (eBiosciences) and rabbit anti-*Listeria* (Abcam), followed by staining with anti-rabbit phycoerythrin (Jackson Laboratories).

ELISAs. Supernatant or serum cytokine levels were detected using the IL-6 (eBioscience), TNFα (eBioscience), and INFγ (eBioscience) detection kits.

Statistical Analyses. Where appropriate, data are expressed as the mean ± SEM. Statistically significant differences between two groups were analyzed using the unpaired Student *t* test. Analyses of multiple groups were performed using one-way ANOVA in conjunction with the Bonferroni or Dunnett test. Statistically significant differences between experimental groups over multiple time points were calculated using two-way ANOVA (repeated measurements). $P < 0.05$ was considered statistically significant.

ACKNOWLEDGMENTS. We thank Alisha Elford for technical support and Mary Saunders for scientific editing. K.S.L. and P.A.L. were funded by the Alexander von Humboldt Foundation (SKA2008 and SKA2010). This study was supported by the German research foundation (DFG) with projects: CRC974, TTR60, LA2558/3-1, and LA1419/5-1. M.R. was supported by Swiss National Science Foundation Grant PASMP3-127678/1. In addition, this work was supported by a grant from the Canadian Institutes of Health Research [Funding Reference Number 79434 (to P.S.O.)] and the research also funded in part by the Ontario Ministry of Health and Long Term Care. P.S.O. holds a Canada Research Chair in Autoimmunity and Tumor Immunity.

1. Hitoshi Y, et al. (1998) Toso, a cell surface, specific regulator of Fas-induced apoptosis in T cells. *Immunity* 8(4):461–471.
2. Pallasch CP, et al. (2008) Overexpression of TOSO in CLL is triggered by B-cell receptor signaling and associated with progressive disease. *Blood* 112(10):4213–4219.
3. Proto-Siqueira R, et al. (2008) SAGE analysis demonstrates increased expression of TOSO contributing to Fas-mediated resistance in CLL. *Blood* 112(2):394–397.
4. Sigruener A, et al. (2007) E-LDL upregulates TOSO expression and enhances the survival of human macrophages. *Biochem Biophys Res Commun* 359(3):723–728.
5. Song Y, Jacob CO (2005) The mouse cell surface protein TOSO regulates Fas/Fas ligand-induced apoptosis through its binding to Fas-associated death domain. *J Biol Chem* 280(10):9618–9626.
6. Nguyen XH, et al. (2012) Antiapoptotic function of Toso (Faim3) in death receptor signaling. *Blood* 119(7):1790–1791.
7. Nguyen XH, et al. (2011) Toso regulates the balance between apoptotic and non-apoptotic death receptor signaling by facilitating RIP1 ubiquitination. *Blood* 118(3): 598–608.
8. Shima H, et al. (2010) Identification of TOSO/FAIM3 as an Fc receptor for IgM. *Int Immunol* 22(3):149–156.
9. Kubagawa H, et al. (2009) Identity of the elusive IgM Fc receptor (FcmuR) in humans. *J Exp Med* 206(12):2779–2793.
10. Vire B, David A, Wiestner A (2011) TOSO, the Fcmicro receptor, is highly expressed on chronic lymphocytic leukemia B cells, internalizes upon IgM binding, shuttles to the lysosome, and is downregulated in response to TLR activation. *J Immunol* 187(8):4040–4050.
11. Selvatici R, Falzarano S, Mollica A, Spisani S (2006) Signal transduction pathways triggered by selective formylpeptide analogues in human neutrophils. *Eur J Pharmacol* 534(1–3):1–11.
12. Graves V, et al. (1992) Simultaneous mobilization of Mac-1 (CD11b/CD18) and formyl peptide chemoattractant receptors in human neutrophils. *Blood* 80(3):776–787.
13. Guthrie LA, McPhail LC, Henson PM, Johnston RB, Jr. (1984) Priming of neutrophils for enhanced release of oxygen metabolites by bacterial lipopolysaccharide. Evidence for increased activity of the superoxide-producing enzyme. *J Exp Med* 160(6):1656–1671.
14. Dahinden CA, Zingg J, Maly FE, de Weck AL (1988) Leukotriene production in human neutrophils primed by recombinant human granulocyte/macrophage colony-stimulating factor and stimulated with the complement component C5A and FMLP as second signals. *J Exp Med* 167(4):1281–1295.
15. Werz O, Bürkert E, Samuelsson B, Rådmark O, Steinhilber D (2002) Activation of 5-lipoxygenase by cell stress is calcium independent in human polymorphonuclear leukocytes. *Blood* 99(3):1044–1052.
16. Nathan C (2006) Neutrophils and immunity: Challenges and opportunities. *Nat Rev Immunol* 6(3):173–182.
17. Cascão R, Rosário HS, Fonseca JE (2009) Neutrophils: Warriors and commanders in immune mediated inflammatory diseases. *Acta Reumatol Port* 34(2B):313–326.
18. Mayadas TN, Tsokos GC, Tsuboi N (2009) Mechanisms of immune complex-mediated neutrophil recruitment and tissue injury. *Circulation* 120(20):2012–2024.
19. Ross GD (2002) Role of the lectin domain of Mac-1/CR3 (CD11b/CD18) in regulating intercellular adhesion. *Immunol Res* 25(3):219–227.
20. Han C, et al. (2010) Integrin CD11b negatively regulates TLR-triggered inflammatory responses by activating Syk and promoting degradation of MyD88 and TRIF via Cbl-b. *Nat Immunol* 11(8):734–742.
21. Means TK, Luster AD (2010) Integrins limit the Toll. *Nat Immunol* 11(8):691–693.
22. Mócsai A, et al. (2006) Integrin signaling in neutrophils and macrophages uses adaptors containing immunoreceptor tyrosine-based activation motifs. *Nat Immunol* 7(12):1326–1333.
23. Castellano F, Chavrier P, Caron E (2001) Actin dynamics during phagocytosis. *Semin Immunol* 13(6):347–355.
24. Cole C, Thomas S, Filak H, Henson PM, Lenz LL (2012) Nitric oxide increases susceptibility of Toll-like receptor-activated macrophages to spreading Listeria monocytogenes. *Immunity* 36(5):807–820.
25. Shi C, et al. (2011) Ly6G+ neutrophils are dispensable for defense against systemic Listeria monocytogenes infection. *J Immunol* 187(10):5293–5298.
26. Pfeffer K, et al. (1993) Mice deficient for the 55 kd tumor necrosis factor receptor are resistant to endotoxic shock, yet succumb to L. monocytogenes infection. *Cell* 73(3): 457–467.
27. McIlwain DR, et al. (2012) iRhom2 regulation of TACE controls TNF-mediated protection against Listeria and responses to LPS. *Science* 335(6065):229–232.
28. Tsuboi N, Asano K, Lauterbach M, Mayadas TN (2008) Human neutrophil Fcgamma receptors initiate and play specialized nonredundant roles in antibody-mediated inflammatory diseases. *Immunity* 28(6):833–846.
29. Hirahashi J, et al. (2009) Mac-1 (CD11b/CD18) links inflammation and thrombosis after glomerular injury. *Circulation* 120(13):1255–1265.
30. Witko-Sarsat V, Rieu P, Descamps-Latscha B, Lesavre P, Halbwachs-Mecarelli L (2000) Neutrophils: Molecules, functions and pathophysiological aspects. *Lab Invest* 80(5): 617–653.
31. Kain R, Firmin DA, Rees AJ (2010) Pathogenesis of small vessel vasculitis associated with autoantibodies to neutrophil cytoplasmic antigens: New insights from animal models. *Curr Opin Rheumatol* 22(1):15–20.
32. Pagnoux C, Guilpain P, Guillevin L (2007) Churg-Strauss syndrome. *Curr Opin Rheumatol* 19(1):25–32.
33. Ouchida R, et al. (2012) Critical role of the IgM Fc receptor in IgM homeostasis, B-cell survival, and humoral immune responses. *Proc Natl Acad Sci USA* 109(40): E2699–E2706.
34. Navarini AA, et al. (2006) Increased susceptibility to bacterial superinfection as a consequence of innate antiviral responses. *Proc Natl Acad Sci USA* 103(42):15535–15539.
35. Sprussel A, et al. (2012) Lysine-specific demethylase 1 restricts hematopoietic progenitor proliferation and is essential for terminal differentiation. *Leukemia* 26(9): 2039–2051.
36. Pronk CJ, et al. (2007) Elucidation of the phenotypic, functional, and molecular topography of a myeloerythroid progenitor cell hierarchy. *Cell Stem Cell* 1(4):428–442.

Published in final edited form as:

Sci Signal. ; 8(401): ra109. doi:10.1126/scisignal.aac5356.

Deletions in the cytoplasmic domain of iRhom1 and iRhom2 promote shedding of the TNF receptor by the protease ADAM17

Sathish K. Maney[1,*], **David R. McIlwain**[1,2,*], **Robin Polz**[1,*], **Aleksandra A. Pandyra**[3,*], **Balamurugan Sundaram**[1], **Dorit Wolff**[1], **Kazuhito Ohishi**[4], **Thorsten Maretzky**[5], **Matthew A. Brooke**[6], **Astrid Evers**[5], **Ananda A. Jaguva Vasudevan**[1], **Nima Aghaeepour**[2], **Jürgen Scheller**[7], **Carsten Münk**[1], **Dieter Häussinger**[1], **Tak W. Mak**[8], **Garry P. Nolan**[2], **David P. Kelsell**[6], **Carl P. Blobel**[4,9], **Karl S. Lang**[3,†], **Philipp A. Lang**[1,10,†,‡]

[1]Department of Gastroenterology, Hepatology and Infectious Diseases, Medical Faculty, University Hospital, Heinrich Heine University Düsseldorf, Moorenstrasse 5, 40225 Düsseldorf, Germany.

[2]Baxter Laboratory in Stem Cell Biology, Department of Microbiology and Immunology, Stanford University, Stanford, CA 94305, USA.

[3]Institute of Immunology, Medical Faculty, University of Duisburg-Essen, Hufelandstrasse 55, Essen 45147, Germany.

[4]Department of Pathology, Graduate School of Medicine, Osaka University, 2-2 Yamadaoka, Suita, Osaka 565-0871, Japan.

[5]Arthritis and Tissue Degeneration Program, Hospital for Special Surgery, New York, NY 10021, USA.

[6]Centre for Cell Biology and Cutaneous Research, Blizard Institute, Barts and The London School of Medicine and Dentistry, Queen Mary University of London, 4 Newark Street, London E1 2AT, UK.

[7]Institute of Biochemistry and Molecular Biology II, Medical Faculty, Heinrich Heine University Düsseldorf, 40225 Düsseldorf, Germany.

[8]Campell Family Institute for Breast Cancer Research, Ontario Cancer Institute, University Health Network, 620 University Avenue, Toronto, Ontario M5G 2C1, Canada.

[9]Departments of Medicine and of Physiology, Biophysics and Systems Biology, Weill Medical College of Cornell University, New York, NY 10021, USA.

[10]Department of Molecular Medicine II, Medical Faculty, Heinrich Heine University Düsseldorf, Universitätsstrasse 1, 40225 Düsseldorf, Germany.

[‡]Corresponding author. philipp.lang@med.uni-duesseldorf.de.

[*]These authors contributed equally to this work.

[†]These authors contributed equally to this work.

Author contributions:

S.K.M., D.R.M., and P.A.L. designed the study. S.K.M., R.P., B.S., A.A.P., D.W., T.M., A.E., K.O., M.A.B., and P.A.L. performed the experiments. J.S., D.H., C.P.B., A.A.J.V., C.M., T.W.M., K.S.L., D.P.K., N.A., and G.P.N. provided the materials and discussed the data. S.K.M., D.R.M., A.A.P., J.S., D.H., C.P.B., A.A.J.V., C.M., T.W.M., K.S.L., D.P.K., N.A., G.P.N., and P.A.L. contributed to drafting the manuscript.

Competing interests: The authors declare that they have no competing interests.

Abstract

The protease ADAM17 (a disintegrin and metalloproteinase 17) catalyzes the shedding of various transmembrane proteins from the surface of cells, including tumor necrosis factor (TNF) and its receptors. Liberation of TNF receptors (TNFRs) from cell surfaces can dampen the cellular response to TNF, a cytokine that is critical in the innate immune response and promotes programmed cell death but can also promote sepsis. Catalytically inactive members of the rhomboid family of proteases, iRhom1 and iRhom2, mediate the intracellular transport and maturation of ADAM17. Using a genetic screen, we found that the presence of either iRhom1 or iRhom2 lacking part of their extended amino-terminal cytoplasmic domain (herein referred to as ΔN) increases ADAM17 activity, TNFR shedding, and resistance to TNF-induced cell death in fibrosarcoma cells. Inhibitors of ADAM17, but not of other ADAM family members, prevented the effects of iRhom-ΔN expression. iRhom1 and iRhom2 were functionally redundant, suggesting a conserved role for the iRhom amino termini. Cells from patients with a dominantly inherited cancer susceptibility syndrome called tylosis with esophageal cancer (TOC) have amino-terminal mutations in iRhom2. Keratinocytes from TOC patients exhibited increased TNFR1 shedding compared with cells from healthy donors. Our results explain how loss of the amino terminus in iRhom1 and iRhom2 impairs TNF signaling, despite enhancing ADAM17 activity, and may explain how mutations in the amino-terminal region contribute to the cancer predisposition syndrome TOC.

INTRODUCTION

A disintegrin and metalloproteinase 17 (ADAM17) [also known as TNFα converting enzyme (TACE)] is a membrane-anchored metalloproteinase, capable of processing a wide array of cell surface/membrane proteins, and is a central regulator of epidermal growth factor receptor (EGFR) and tumor necrosis factor receptor (TNFR) signaling pathways, which control cell proliferation, survival, oncogenesis, and immunity (1). TNF is liberated from its membrane anchor by ADAM17 to produce a soluble proinflammatory cytokine (2–4). However, ADAM17 can also modulate responses to this cytokine by catalyzing shedding of TNF-binding receptors p55 (TNFR1) and p75 (TNFR2) (5, 6). TNFR1 signaling is a key component of innate immunity, host defense, and septic shock (7, 8), yet TNFR1 engagement can also induce cell death through signaling leading to activation of caspase-8 (9).

ADAM17 is controlled by catalytically inactive members of the rhomboid protease family: iRhom1 and iRhom2. These integral membrane proteins promote the maturation and transport of ADAM17 to the cell surface (10–13). Absence of iRhom2 abolishes ADAM17 activity in immune cells thereby blocking TNF secretion, resulting in susceptibility toward bacterial infections but resistance to septic shock and rheumatoid arthritis (11–14). In nonhematopoietic cells, ADAM17 appears to be controlled by a combination of iRhom2 and iRhom1 (10). The essential role of iRhoms in regulating the function of ADAM17 is highlighted by recent iRhom1 and iRhom2 double knockout studies demonstrating fully impaired ADAM17 maturation across all tissues examined (15) and striking similarity between *iRhom1*$^{-/-}$ *iRhom2*$^{-/-}$ mice and ADAM17-deficient mice (15). However, much

remains to be learned about how iRhoms accomplish their regulation of ADAM17 and what features of iRhoms are important for their function.

Reports have identified familial dominantly acting mutations in the N-terminal cytoplasmic tail of iRhom2 (also known as RHBDF2 in humans) as causative for a rare syndrome named tylosis with esophageal cancer (TOC), which is characterized by palmoplantar keratoderma and up to 95% lifetime risk of malignancy of the esophagus (16, 17). These TOC-associated mutations in iRhom2 are associated with an increase in the maturation and activity of ADAM17 in patient-derived epidermal keratinocytes, resulting in significantly up-regulated shedding of ADAM17 substrates, including EGF family growth factors and proinflammatory cytokines (18, 19). Furthermore, studies of two separate spontaneous mouse mutants (*Cub* and *Uncv*) reveal hair and skin abnormalities also associated with deletions in the N terminus of iRhom2 (11–14, 20). Although the immediate consequences of these murine mutations are not entirely clear, especially in the case of *cub* mice, all studies in both humans and mice suggest phenotypes involving misregulation of ADAM17 substrates and offer a clue that the N-terminal domain of iRhom2 may be important for controlling its activity (21).

Our initial identification of a connection between iRhom2 and ADAM17 involved a cyclic packaging rescue (CPR) screen for TNF resistance, which identified a version of iRhom2 with a truncated N terminus (12). Here, we report a separate TNF resistance CPR screen, which identified two versions of iRhom1, both also missing parts of their N termini. To gain more insight into how iRhoms operate, we examined the ability of truncated and full-length iRhoms to regulate ADAM17 activity in a well-defined cellular context. We observed a high degree of functional overlap for iRhom1 and iRhom2 and demonstrate that deletion of parts of the cytoplasmic N terminus of iRhom2 or iRhom1 results in specific enhancement of ADAM17 activity, TNFR shedding, and resistance to TNF-induced cell death. Our results support the link of N-terminal iRhom mutants with constitutive activity of ADAM17.

RESULTS

Truncation of iRhom2 or iRhom1 cytoplasmic domains triggers resistance against TNF-induced cell death

L-929 murine fibrosarcoma cells are highly sensitive to TNF-induced cell death through engagement of their cognate cell surface receptors (22–24). Complementary DNAs (cDNAs) capable of conferring resistance to L-929 cell killing by TNF were identified from a mouse 3T3 cell–derived cDNA library through enrichment in a CPR screen (25). Three different cDNAs were isolated after six successive rounds of infection, cell killing, and rescue of viral particles from surviving cells (Fig. 1A). Sequencing revealed the identity of these hits as c-FLIP, an established negative regulator of TNF-induced cell death (26), along with two cDNAs corresponding to nucleotides 249 to 2571 and 618 to 2571 of native iRhom1 (the latter referred to henceforth as iRhom1-ΔN) (Fig. 1B and fig. S1A). The similarity of this result to the identification of an N-terminally truncated version of iRhom2 we previously reported using a separate CPR screen (12) and recent literature concerning mutations in the N terminus of iRhom2 (20, 21, 27) led us to investigate whether there was a selective

advantage for removal of part of the extended cytoplasmic N terminus, a hallmark feature of iRhoms (28).

Full-length and ΔN truncated iRhom proteins were detected at predicted molecular weights, and in similar abundance, in cells stably overexpressing tagged iRhom constructs (Fig. 1C). We first compared the ability of cells overexpressing either full-length wild-type iRhom2, iRhom2-ΔN, or vector control to withstand exposure to recombinant TNF (Fig. 1D). We observed only a slight reduction in cell death assessed by annexin Vand 7-AAD staining for cells expressing wild-type iRhom2, whereas iRhom2-ΔN cells had markedly lower levels of annexin V, 7-AAD–positive cells (Fig. 1D). We found similar effects when comparing cells expressing wild-type iRhom1 versus iRhom1-ΔN, which were also strongly resistant to TNF cytotoxicity (Fig. 1E). Next, we confirmed these observations using a separate assay to measure cells remaining adherent after 48 hours of TNF treatment. Consistently, we observed a slight protection against TNF-mediated cell death in wild-type iRhom2–expressing cells, but major protection was triggered by iRhom2-ΔN (fig. S1B). Moreover, iRhom1-ΔN–expressing cells were also protected against TNF-induced cell death compared to wild-type iRhom1 (fig. S1C). Cells expressing full-length and ΔN-iRhoms retained a similar capacity to undergo cell death resulting from other stimuli, such as staurosporine (fig. S1D). These data indicate that deletion of part of the cytoplasmic domain of either iRhom1 or iRhom2 confers a selective advantage over their full-length counterparts in TNF resistance.

Truncated iRhoms curb TNFR signaling through release of TNFRs

We next investigated the mechanism by which iRhom2-ΔN confers resistance toward TNF-induced cytotoxicity by examining the status of signaling downstream of the TNFRs. TNFR engagement in L-929 cells results in activation of both cell survival and cell death signaling pathways, causing activation of cell survival–associated nuclear factor κB (NF-κB) and cleavage of cell death–associated poly(adenosine diphosphate–ribose) polymerase (PARP) (29–32). When we examined PARP levels by immunoblot, we detected cleaved PARP in TNF-treated control cells (Fig. 2A). However, PARP cleavage was reduced in cells expressing wild-type iRhom2 and was not detected in cells expressing iRhom2-ΔN (Fig. 2A). Next, we looked for hallmarks of TNF-mediated NF-κB activation (33) and detected inhibitor of κB-α (IκB-α) phosphorylation and degradation as well as Ser^{536} phosphorylation of p65 in vector and wild-type iRhom2–expressing cells but not in iRhom2-ΔN–expressing cells (Fig. 2B). These findings indicate that TNFR signaling was blocked by iRhom2-ΔN upstream of both survival and death signaling branches (9).

To test whether surface TNFR abundance itself was affected by different iRhom2 isoforms, we used flow cytometry to measure TNFR abundance on the surface of L-929 cells transduced with vector, wild-type iRhom2, or iRhom2-ΔN. TNFR1 and TNFR2 abundance was highly reduced on cells expressing iRhom2-ΔN or iRhom1-ΔN compared to cells expressing vector or either wild-type iRhom (Fig. 2, C and D). When we measured the concentration of soluble TNFRs in conditioned media from these cultures, we observed greater concentrations of soluble TNFR1 and TNFR2 in conditioned media from cells expressing iRhom2-ΔN or iRhom1-ΔN than in those from control cells or cells expressing

either wild-type iRhom (Fig. 2, E and F). These effects were not associated with either decreased *TNFR* transcript expression (fig. S2, A and B) or large differences in total cellular abundance of TNFRs (fig. S2, C to E).

Together, the data indicate that the blockade in TNFR signaling after ΔN-iRhom expression was caused by reduced surface abundance and enhanced shedding of TNFRs. Previous work suggested that shedding of TNFRs was responsible for iRhom2-mediated resistance toward TNF by blocking TNFR signaling (11, 12). We now show that this shedding mechanism is true not only for truncated iRhom2 but also for truncated iRhom1. Furthermore, we confirm that TNFR signaling is blocked by ΔN-iRhom expression by showing that both downstream cell survival and cell death signaling responses are impaired in these cells.

iRhom-regulated TNFR shedding depends on ADAM17

TNFRs are cleaved from the cell surface by membrane proteases such as ADAM17 (fig. S3A) (5, 6). To investigate whether increased TNFR shedding into the supernatant of iRhom-ΔN–expressing cells was dependent on metalloproteinases in L-929 cells, we investigated shedding in the presence of several ADAM family inhibitors. Increased release of TNFRs into the supernatant of iRhom2-ΔN–expressing cells relative to control or wild-type iRhom2 was blocked by the broad-spectrum metalloproteinase inhibitor marimastat (Fig. 3A). Furthermore, shedding induced by iRhom2-ΔN or iRhom1-ΔN was unaffected by an ADAM10-selective inhibitor, GI254023X (GI) (34), but was abolished by an inhibitor of both ADAM10 and ADAM17, GW280264X (GW) (Fig. 3, B and C). Consistently, culturing iRhom2-ΔN–expressing cells with marimastat restored the ability of recombinant TNF to trigger cell death to a similar extent as that observed in cells expressing wild-type iRhom2 (Fig. 3D). TNF itself had little effect on TNFR shedding (fig. S3, B and C).

To firmly establish that ΔN-iRhoms exert their effects through ADAM17, we stably expressed either a scrambled control or one of two ADAM17-specific short hairpin RNA (shRNAs) (Fig. 4A) in L-929 cells transduced with vector, wild-type iRhom2, and iRhom2-ΔN. Surface TNFR1 and TNFR2 abundance was reduced in cells expressing iRhom2-ΔN or iRhom1-ΔN relative to wild-type or vector-transduced controls; however, these effects were rescued by ADAM17 silencing (Fig. 4B and fig. S4, A and B), suggesting that truncated iRhoms enhance ADAM17-dependent shedding. Next, we examined whether ADAM17 silencing would disrupt the survival advantage of ΔN-iRhoms against TNF. As expected, knocking down ADAM17 abolished the survival advantage caused by expression of ΔN-iRhoms conferred in response to TNF (Fig. 4, C and D). Together, the data indicate that TNFR shedding and TNF resistance phenotypes associated with expression of N-terminally truncated iRhoms can be blocked by knockdown or inhibition of ADAM17, establishing ADAM17 as a mechanism through which iRhoms mediate their effects on TNF signaling, at least in the cell context studied.

Truncation of the cytoplasmatic tail results in enhanced presence of iRhom2 at the cell surface

We next asked how wild-type iRhoms and their ΔN counterparts might differentially affect ADAM17 activity. Binding of iRhom2 to ADAM17 is thought to be important for ADAM17

maturation and activation (11–13). When we pulled down either wild-type or truncated iRhom2, we detected ADAM17 in both immunoprecipitated lysates (Fig. 5A). Reciprocally, when ADAM17 was pulled down, both wild-type iRhom2 and iRhom2-ΔN were detected (Fig. 5A). Similar data were obtained in wild-type iRhom1– and iRhom1-ΔN–expressing cells (fig. S5A). These data indicated that both isoforms of iRhom1 and iRhom2 are capable of binding ADAM17, consistent with previous reports (12, 35).

When we enriched for cell surface proteins, we noticed that a larger proportion of iRhom2-ΔN was present in surface fractions versus intracellular fractions and relative to wild-type iRhom2 (Fig. 5B). These findings were further confirmed by T7 surface antibody staining and flow cytometry, where the MFI for iRhom2-ΔN was significantly higher than that for wild-type iRhom2 (Fig. 5C). Consistently, immunofluorescence of tagged iRhom2 revealed greater staining intensity for iRhom2-ΔN versus wild-type iRhom2 on formalin-fixed cells, differences which were not apparent after 1% Triton permeabilization (Fig. 5D). Furthermore, in permeabilized cells, subcellular localization of both wild-type iRhoms and ΔN-iRhoms in the proximity of Golgi marker GM130 (fig. S5B) was consistent with previous reports (12, 36). Increased surface localization of iRhom2-ΔN compared with wild-type iRhom2 persisted after ADAM17 knockdown and in ADAM17 knockout fibroblasts (Fig. 5, E and F) (4), indicating that ADAM17 is not strictly required for iRhom2-ΔN trafficking.

Truncated and wild-type iRhom2 did not exhibit significantly different rates of protein degradation after inhibition of protein synthesis with cycloheximide, as measured by immunoblotting (fig. S5C). This argues against a role for differential protein stability affecting iRhom2 surface abundance. Increased surface abundance of iRhom2-ΔN is also unlikely to be the result of greater RNA expression because transcript abundance was comparable between iRhom2-ΔN and wild-type iRhom2 (fig. S5D). We detected mature ADAM17 on the cell surface of cells expressing vector, wild-type iRhom2, or iRhom2-ΔN (fig. S5E). However, a puzzling overall reduction in the total quantity of mature ADAM17 was observed in immunoblots of cells expressing iRhom-ΔN (Fig. 5A and fig. S5, A and E), an effect that was prevented by marimastat treatment (fig. S5F). These data indicate that ΔN-iRhoms are capable of binding to ADAM17 in a similar manner to that of wild-type iRhoms and that the specific effects of iRhom2-ΔN may be related to its enhanced abundance at the cell surface.

N-terminal iRhom mutations increase constitutive activity of ADAM17

ADAM17 can be rapidly activated in response to stimuli including phorbol 12-myristate 13-acetate (PMA) (37, 38). We therefore wondered whether the effects of ΔN-iRhoms might influence the rapid activation of ADAM17. When we stimulated L-929 cells with PMA, we observed an expected increase in TNFR1 and TNFR2 shedding from cells expressing either vector or wild-type iRhom2 (fig. S6A). In contrast, we did not detect PMA-induced TNFR shedding from cells expressing iRhom2-ΔN (fig. S6A), and the amount of TNFRs in the stimulated cells expressing iRhom2-ΔN was not increased when compared to cells expressing wild-type iRhom2 (fig. S6A). In all cases, PMA-stimulated TNFR shedding was blocked by marimastat (fig. S6A) or GW, which both inhibit ADAM17, but not by the

ADAM10-selective inhibitor GI (Fig. 6A). Furthermore, similar data using cells expressing iRhom1-ΔN or wild-type iRhom1 indicated that both truncated iRhoms may induce a constitutively active TNFR shedding state, resembling PMA-stimulated shedding state in control cells (Fig. 6B).

To investigate these effects in a different cellular context, we coexpressed wild-type or truncated iRhom2 or as control an unrelated cytoplasmic protein MAD2 (mitotic arrest deficient 2) along with the iRhom2-selective AP-tagged ADAM17 substrate KitL2 in *iRhom2*$^{-/-}$ iMEFs (10, 12). To improve the detection of potential differences in shedding, we took advantage of the reversible nature of ADAM17 inhibition with marimastat to block shedding overnight, enabling uncleaved substrate to accumulate, and then observed constitutive shedding immediately after washout of the inhibitor. Compared to control cells, only cells expressing iRhom2-ΔN exposed overnight to marimastat exhibited greatly enhanced shedding of KitL2 (Fig. 6C). In a separate experiment, we used an irreversible inhibitor of ADAM17 [diphenylamine carboxylate (DPC)], which selectively binds to active ADAM17. Thus, if ADAM17 is not activated while cells are exposed to DPC, ADAM17 can be fully activated after the inhibitor has been removed; however, if ADAM17 is activated in the presence of DPC, ADAM17 will not be able to recover activity after the inhibitor is removed (37). Incubation of cells expressing iRhom2-ΔN with DPC for as little as 30 min prevented the increased KitL2 shedding even after the inhibitor was removed, whereas cells expressing wild-type iRhom2 required overnight exposure to DPC to exhibit ADAM17 inactivation (fig. S6B). These data suggest that ADAM17 is constitutively in a more active state in the iRhom2-ΔN setting.

Dominantly acting familial mutations in the N-terminal cytoplasmatic tail of iRhom2 cause a cancer susceptibility disorder called TOC (16, 17). These mutations increase constitutive ADAM17 activity in keratinocytes (18). Compared to overexpression of wild-type murine iRhom2 in iRhom1 and iRhom2 double knockout iMEFs, expression of a construct bearing mouse homologs of two causative iRhom2$^{I156T/P159L}$ TOC mutations caused increased constitutive TGF-α shedding (Fig. 6D). Finally, we examined human immortalized keratinocyte cell lines TYLK1 and TYLK2 derived from TOC patients bearing heterozygous mutation in iRHOM2$^{(I186T/WT)}$ (16, 17) and control keratinocyte cell lines (K17). Significantly higher amounts of constitutive TNFR1 shedding into culture supernatants were detected from cells generated from TOC patients compared to cells derived from healthy controls (Fig. 6E), shedding that could be blocked by the ADAM17 inhibitor TMI-005. These data are consistent with enhanced ADAM17-dependent shedding of amphiregulin, TGF-α, and heparin-binding EGF-like growth factor that is observed in TOC patient–derived keratinocytes (18). These results indicate that ADAM17 activity is enhanced by N-terminal iRhom mutations and may provide an explanation for why cells that have ΔN-iRhom proteins have a selective advantage over their wild-type counterparts in promoting resistance to TNF-induced cell death.

DISCUSSION

Here, we have identified a high degree of functional overlap for iRhom1 and iRhom2 in controlling the activity of ADAM17. Starting from unbiased genetic screens, we have

established that deletion of part of the cytoplasmic N terminus of either iRhom1 or iRhom2 results in a gain of function by promoting constitutive ADAM17-dependent shedding of TNFRs from L-929 cells, thereby blocking downstream signaling and protecting cells from TNF-induced cytotoxicity. We demonstrate that iRhom1- and iRhom2-dependent effects are conserved for at least two endogenous ADAM17 substrates (TNFR1 and TNFR2), and using gene silencing shows these effects to be specific to ADAM17.

Little is known about how the iRhoms are functionally controlled. Our results suggest that the extended cytoplasmic N-terminal domain is of conserved importance for the actions of both iRhom1 and iRhom2. Dominant inherited human N-terminal mutations in iRhom2 result in overgrowth of epithelial tissues and predisposition to esophageal cancer (39). Our results involving dominant N-terminal mutated mouse iRhoms and enhanced TNFR shedding from TOC patient–derived keratinocytes suggest that these human mutations could similarly result in greater or constitutive ADAM17 activity. This could result in direct consequences for neoplasia, such as overproduction of EGFR ligands, strongly implicated in cancer (40) and previously observed in TOC keratinocytes (18), or shedding of TNFRs as an evasion mechanism for tumor cells to escape cell death induced by TNF. Increased abundance of ADAM17 is also known to be associated with breast, ovarian, kidney, colon, and prostate cancers (41).

Recent studies involving two separate spontaneous mouse mutants with deletions in the N terminus of iRhom2 describe hair and skin abnormalities in these animals (20, 21, 27, 42). Discerning the consequences of these mutations has not been entirely straightforward; Hosur *et al.* report enhanced stability of mutant iRhom2 in *cub* mice and elevated secretion of ADAM17 substrate amphiregulin, observations not corroborated by Siggs *et al.* (20) in the same mice. Mice bearing a separate *Uncv* allele display aberrancies in hair follicles, which may be connected to misregulation of ADAM17 substrates. In the case of both *cub* and *Uncv*, expression of mutant alleles results in an apparent decrease in mature ADAM17 by Western blotting (20, 27). Paradoxically, we also see an apparent reduction in mature ADAM17 by immunoblot after expression of ΔN-iRhoms, despite strong evidence of enhanced ADAM17 activity. Because this effect could be reversed by inhibiting ADAM17 with marimastat, we hypothesize that the apparent reduction of mature ADAM17 may be an artifact of activation-associated autocatalytic degradation of ADAM17 known to occur when it is strongly activated, such as by high concentration of PMA (43). Rapid inhibition of ADAM17 activity with DPC in iRhom2-ΔN–expressing cells provides further evidence for enhanced constitutive ADAM17 activity in this context.

Aside from the mouse and human mutations listed above, the in vivo relevance of alternative iRhom1 or iRhom2 isoforms has not yet been described. However, expression of C-terminally tagged iRhom2 and iRhom1 frequently results in lower–molecular weight bands, which could correspond to posttranslationally processed iRhoms lacking N-terminal regions (11, 44). Whether these versions exist for endogenous proteins, and whether they represent activated iRhom states, warrants investigation in future studies, including the generation of high-quality antibodies. Similar to our results, a previous study involving expression of human iRhom1 (44) (then referred to as $p100^{hRho}$) in the fly wing identified a phenotype for an N-terminally truncated but not full-length version of the protein. Because iRhom1 has

been previously suggested to play a role in human cancer (45, 46), and considering functional overlap, we have identified between N-terminal mutations in iRhom1 and iRhom2 the potential existence of human mutations in iRhom1, and their contributions to cancer warrants further study.

MATERIALS AND METHODS

CPR screening

L-929 selector cell line was established by transfection of expression plasmids coding for mCAT1 (murine cationic amino acid transporter, mediating ecotropic retrovirus infection) and hCAR (human coxsackie-virus and adenovirus receptor), and selected for high infectivity to green fluorescent protein–expressing ecotropic retrovirus and human adenovirus and high susceptibility to TNF. CPR was carried out as described previously (25). The Phoenix ecotropic packaging cell line was transfected with retroviral mouse 3T3 cell cDNA library by using calcium phosphate coprecipitation. Retroviral supernatants were obtained 2 days after transduction and used to transduce the selector cells. Two days after retrovirus transduction, cells were cultured with TNF (2 ng/ml) for 24 hours. Surviving cells were allowed to recover from TNF stress and expanded in culture for 3 days, and then infected with adenoviruses expressing gag-pol and env (amounts of adenoviruses were determined empirically). Rescued retroviruses were harvested 2 days after adenovirus infection and used to transduce new batches of selector cells. Genomic DNA was extracted from a fraction of the surviving cells at each round of screening. A portion of cDNA inserts were amplified by PCR using primers 5′-AGCCCTCACTCCTTCTCTAG-3′ and 5′-ACCTACAGGTGGGGTCTTTCATTCCC-3′ and sequenced.

Generation and maintenance of cells expressing iRhom isoforms

Constructs of wild-type iRhom1 and iRhom1-ΔN, and wild-type iRhom2 and iRhom2-ΔN were constructed using a three-step ligation. The 5′ and 3′ portions were amplified, and restricted middle portion was ligated into modified version of pMSCVpuro (Clontech) containing a C-terminal T7 tag vector. Retrovirus encoding wild-type iRhom1 and iRhom1-ΔN, wild-type iRhom2 and iRhom2-ΔN, and empty pMSCVpuro alone (BD Biosciences) was produced in Phoenix ecotropic packaging cells and used to infect L-929 cells. Stable L-929 cells were generated through selection using puromycin (10 μg/ml). Unless otherwise indicated, cells were cultured in Dulbecco's modified Eagle's medium (DMEM) supplemented with 2 μM of L-glutamine, 0.1 U of penicillin, streptomycin (0.1 μg/ml), antibiotics, and 10% fetal calf serum (FCS).

MEFs were isolated from E13.5 wild type, ADAM17$^{-/-}$(4), iR2$^{-/-}$ iR1$^{-/-}$, and iR1/2$^{-/-}$ (10, 12, 15) embryos to generate primary MEFs for immortalization. Briefly, head and viscera were removed, and the remaining tissues were subjected to trypsin treatment for 15 min at 37°C. Cells were collected and immortalized by transducing the plasmid expressing SV40 large Tantigen maintained in DMEM supplemented with anti-biotics and 10% FCS.

Immunofluorescence

Intracellular immunofluorescence staining was performed in L-929 cells stably expressing T7-iRhom2, T7–iRhom2-ΔN, T7-iRhom1, T7–iRhom1-ΔN, and control vector, grown on glass coverslips, fixed with 4% formalin, and were permeabilized with 1% Triton X-100. All iRhom versions were detected using a T7 tag rabbit primary monoclonal antibody (mAb) at 1:300 (Abcam) and donkey anti-rabbit Cy3-labeled secondary Ab (Jackson ImmunoResearch). The Golgi marker GM130 (BD eBioscience) was recognized with a donkey anti-mouse Cy2-labeled secondary Ab (Jackson ImmunoResearch). Surface immunofluorescence staining of T7-iRhom2 and T7–iRhom2-ΔN cells was performed after fixation with 4% formalin. iRhom versions were detected using a T7 tag rabbit mAb at 1:300 (Abcam) and donkey anti-rabbit Cy3-labeled secondary Ab (Jackson ImmunoResearch). Slides were stained with phalloidin-FITC (Sigma) and Hoechst 34580 (Invitrogen). Images were captured using confocal microscopy (Zeiss ELYRA).

Stable knockdown of ADAM17

Lentiviral particles were generated by calcium phosphate transfection of subconfluent (50 to 60%) 293TV cells with 10 μg of shRNA (OriGene) and 5 μg each of pMDG1.vsvg, pRSV-Rev, and pMDLg/pRRE constructs. Lentiviral particles were collected 24 and 48 hours later, filtered through a 0.45-μm filter, and stored at −80°C. Parental L-929 cells were infected with lentiviral particles containing the indicated shRNAs, and cells were selected with puromycin selection (48 hours; 5 μg/ml).

ELISA detection of TNF and TNFR shedding

To analyze the TNFR shedding in L-929 cells overexpressing T7-iRhom2, T7–iRhom2-ΔN, T7-iRhom1, T7–iRhom1-ΔN, and control vector, cells were seeded (1×10^5) in 24-well plates. After 24 hours, supernatant was harvested and subjected to enzyme-linked immunosorbent assay (ELISA; DuoSet ELISA, R&D Systems), which was performed according to the manufacturer's instructions. Cells were co-incubated with marimastat (20 μM; BB 2516, Tocris Bioscience) for 6 hours. For the treatment with GI or GW (Sigma), culture medium was removed, and the cells were washed with phosphate-buffered saline (PBS). Fresh FCS-free DMEM containing 3 μM of the inhibitors was added to the cells, and the TNFR shedding was analyzed after 6 hours.

Similarly, for TNFR shedding from TOC patient–derived keratinocytes, 2×10^5 cells per cell line were seeded into 24-well tissue culture plates. After 24 and 48 hours, supernatant was harvested and used for ELISA, performed according to the manufacturer's instructions (as above). To enable blockade of ADAM17, cells were co-incubated with ADAM17 inhibitor TMI-005 (500 nM) or vehicle (DMSO). This medium was then collected after either 24 or 48 hours, and the concentration of TNFR therein was measured by ELISA. All experiments were carried out in triplicate.

Ectodomain shedding assay for AP-tagged KitL2

iRhom2-deficient fibroblasts were transfected with iRhom and AP-tagged KitL2 constructs using lipofectamine 2000 as previously described (47). Twenty-four hours after transfection, cells were incubated with marimastat (a gift from O. Ouerfelli, Sloan-Kettering Institute,

New York, NY) or DPC-333/BMS-561392 (a gift from R. Waltermire, Bristol-Myers Squibb, New Brunswick, NJ) overnight or as indicated, followed by three brief washes. Constitutive shedding was measured after 2 hours of subsequent incubation. Quantification of AP activity culture supernatant and cell lysate was performed by colorimetric assays as previously described (47).

Viability assay

L-929 cells (1×10^5) overexpressing T7-iRhom2, T7–iRhom2-ΔN, T7-iRhom1, T7–iRhom1-ΔN, and control vector were seeded in 24-well plates. Same conditions were used for ADAM17 shRNA–treated cells. Cells were incubated with recombinant mouse TNF (R&D Systems), with or without 20 μM BB 2516 (Tocris Bioscience). Viability was determined at indicated time points using annexin V–7-AAD exclusion (eBioscience) by flow cytometry (48).

Clonogenic assay

L-929 cells (1×10^5) overexpressing T7-iRhom2, T7–iRhom2-ΔN, T7-iRhom1, T7–iRhom1-ΔN, and control vector were seeded in 24-well plates. Cells were treated with recombinant mouse TNF (R&D Systems) at the indicated concentrations. After 48 hours, cells were washed and stained with crystal violet at room temperature for 1 hour. The remaining crystal violet was dissolved with methanol after analysis.

Reverse transcription PCR

RNA was extracted using RNeasy Kit (Qiagen). mRNA expression of wild-type iRhom1 and iRhom1-ΔN, and wild-type iRhom2 and iRhom2-ΔN was performed by reverse transcription PCR (Bio-Rad). For the analysis, the expression of the entire target mRNA was normalized to β-actin or GAPDH expression. Gene expression values were then calculated on the $\Delta\Delta C_t$ method. Relative quantities (RQ) were determined with the equation $RQ = 2^{-\Delta\Delta Ct}$.

Cell surface protein isolation

Surface proteins from L-929 cells over expressing T7-iRhom2, T7–iRhom2-ΔN, or control vector were isolated using the sulfo-NHS-SS-biotin–based Cell Surface Protein Isolation Kit (Pierce) according to the manufacturer's instructions, after addition of 20 μM BB 2516 (Tocris Bioscience) and 1,10-phenanthroline (Sigma) to the lysis and wash buffers. Cell surface fractions were compared to column flow-through (intracellular fractions) by immunoblotting.

Flow cytometry

Single-cell suspensions from cultured cells were stained for 20 min at 4°C with T7 antibody in PBS containing 1% FCS and 5 mM EDTA. Staining for annexin Vand 7-AAD (eBioscience) was performed in solution containing 5mMCa^{2+}. Staining with TNFR1- and TNFR2-biotin antibodies (eBioscience) was performed in PBS containing 1% FCS and 5 mM EDTA for 1 hour at room temperature, followed by wash and incubation with phycoerythrin-Cy7–coupled streptavidin-labeled antibody (eBioscience) for 30 min at 4°C.

Immunoprecipitation and immunoblotting

Briefly, cells were lysed in PBS containing 1% Triton X-100 (PBS-T; Sigma), EDTA-free protease inhibitor cocktail (Roche), PhosSTOP (1 tablet/10 ml), and the inhibitors BB 2516 (20 μM; Tocris Bioscience) and 1,10-phenanthroline (10 mM; Sigma). The pulldown was performed using mouse mAbs recognizing the T7 tag or ADAM17 antibody (Abcam). To analyze the PARP cleavage, the cells were exposed to 2.5 ng of recombinant mouse TNF (R&D Systems) for indicated time points. Phospho-p65 or phospho–IκB-α activation was determined by harvesting cells from 60-mm dishes after treatment with 2.5 ng of recombinant mouse TNF for indicated time points. After lysis, the samples were used for immunoblotting using phospho-p65 and phospho–IκB-α antibodies (Cell Signaling).

Stability assay

L-929 cells (1×10^5) overexpressing T7-iRhom2, T7–iRhom2-ΔN, or control vector were seeded in 24-well plates. Cells were incubated with cycloheximide (100 μg/ml; Sigma) for indicated time points. After fixing cells using 4% formalin (Sigma) in PBS at room temperature for 40 min, cells were washed two times with and resuspended in PBS-T for 15 min at room temperature in the dark. After additional wash and suspension in PBS containing 1% FCS and 5 mM EDTA, cells were stained with a T7 antibody (eBioscience) on ice for 30 min, followed by measurement using flow cytometry.

Statistical analysis

Data are expressed as means ± SEM or SD. Statistical significance between two groups was analyzed using the Mann-Whitney *U* test. For experiments involving analysis of multiple time points, two-way analysis of variance (ANOVA) with an additional Bonferroni posttest was used. *P* values <0.05 were considered statistically significant. In all the experiments, *n* indicates the number of independent experiments performed.

Supplementary Material

Refer to Web version on PubMed Central for supplementary material.

Acknowledgments:

We are grateful for the technical assistance of E. Bäcker. We thank O. Ouerfelli (Sloan-Kettering Institute, New York, NY) and R. Waltermire (Bristol-Myers Squibb, New Brunswick, NJ) for the gifts of marimastat and DPC-333/BMS-561392, respectively.

Funding: This study was supported by the Alexander von Humboldt Foundation (SKA2010), the Medical Research Council (MR/L010402/1) and Cancer Research UK (C7570/A19107 to D.P.K.), the German Research Council (SFB974, LA2558/3-1, LA2558/5-1, TRR60, LA1419/5-1, and EV 206/1-1), the Forschungskommission of the Heinrich Heine University, the Canadian Institutes of Health Research Fellowship (201210MFE-289576-150035 to D.R.M.), and the NIH (GM64750 to C.P.B.). J.S. is supported by the German Research Council (SCHE907/3-1). G.P.N. is supported by grants from the NIH (U19 AI057229, U54CA149145, N01-HV-00242, 1U19AI100627, 5R01AI07372405, R01CA184968, 1 R33 CA183654, R33 CA183692, HHSF223201210194C, 41000411217, and 7500108142) and the U.S. Department of Defense (OC110674 and 11491122).

REFERENCES AND NOTES

1. Blobel CP, ADAMs: Key components in EGFR signalling and development. Nat. Rev. Mol. Cell Biol 6, 32–43 (2005). [PubMed: 15688065]

2. Moss ML, Jin S-L, Milla ME, Bickett DM, Burkhart W, Carter HL, Chen W-J,Clay WC, Didsbury JR, Hassler D, Hoffman CR, Kost TA, Lambert MH,Leesnitzer MA, McCauley P, McGeehan G, Mitchell J, Moyer M, Pahel G, Rocque W,Overton LK, Schoenen F, Seaton T, Su J-L, Warner J, Willard D, Becherer JD, Cloning of a disintegrin metalloproteinase that processes precursor tumour-necrosis factor-α. Nature 385, 733–736 (1997). [PubMed: 9034191]
3. Black RA, Rauch CT, Kozlosky CJ, Peschon JJ, Slack JL, Wolfson MF,Castner BJ, Stocking KL, Reddy P, Srinivasan S, Nelson N, Boiani N, Schooley KA,Gerhart M, Davis R, Fitzner JN, Johnson RS, Paxton RJ, March CJ, Cerretti DP, A metalloproteinase disintegrin that releases tumour-necrosis factor-α from cells. Nature 385, 729–733 (1997). [PubMed: 9034190]
4. Horiuchi K, Kimura T, Miyamoto T, Takaishi H, Okada Y, Toyama Y, Blobel CP, Cutting edge: TNF-a-converting enzyme (TACE/ADAM17) inactivation in mouse myeloid cells prevents lethality from endotoxin shock. J. Immunol 179, 2686–2689 (2007). [PubMed: 17709479]
5. Peschon JJ, Slack JL, Reddy P, Stocking KL, Sunnarborg SW, Lee DC,Russell WE, Castner BJ, Johnson RS, Fitzner JN, Boyce RW, Nelson N,Kozlosky CJ, Wolfson MF, Rauch CT, Cerretti DP, Paxton RJ, March CJ,Black RA, An essential role for ectodomain shedding in mammalian development. Science 282, 1281–1284 (1998). [PubMed: 9812885]
6. Reddy P, Slack JL, Davis R, Cerretti DP, Kozlosky CJ, Blanton RA, Shows D,Peschon JJ, Black RA, Functional analysis of the domain structure of tumor necrosis factor-α converting enzyme. J. Biol. Chem 275, 14608–14614 (2000). [PubMed: 10799547]
7. Pfeffer K, Matsuyama T, Kündig TM, Wakeham A, Kishihara K, Shahinian A,Wiegmann K, Ohashi PS, Krönke M, Mak TW, Mice deficient for the 55 kd tumor necrosis factor receptor are resistant to endotoxic shock, yet succumb to L. monocytogenes infection. Cell 73, 457–467 (1993). [PubMed: 8387893]
8. Rothe J, Lesslauer W, Lötscher H, Lang Y, Koebel P, Köntgen F, Althage A,Zinkernagel R, Steinmetz M, Bluethmann H, Mice lacking the tumour necrosis factor receptor 1 are resistant to TNF-mediated toxicity but highly susceptible to infection by *Listeria* monocytogenes. Nature 364, 798–802 (1993). [PubMed: 8395024]
9. Micheau O, Tschopp J, Induction of TNF receptor I-mediated apoptosis via two sequential signaling complexes. Cell 114, 181–190 (2003). [PubMed: 12887920]
10. Maretzky T, McIlwain DR, Issuree PDA, Li X, Malapeira J, Amin S, Lang PA,Mak TW, Blobel CP, iRhom2 controls the substrate selectivity of stimulated ADAM17-dependent ectodomain shedding. Proc. Natl. Acad. Sci. U.S.A 110, 11433–11438 (2013). [PubMed: 23801765]
11. Adrain C, Zettl M, Christova Y, Taylor N, Freeman M, Tumor necrosis factor signaling requires iRhom2 to promote trafficking and activation of TACE. Science 335, 225–228 (2012). [PubMed: 22246777]
12. McIlwain DR, Lang PA, Maretzky T, Hamada K, Ohishi K, Maney SK, Berger T,Murthy A, Duncan G, Xu HC, Lang KS, Häussinger D, Wakeham A, Itie-Youten A,Khokha R, Ohashi PS, Blobel CP, Mak TW, iRhom2 regulation of TACE controls TNF-mediated protection against *Listeria* and responses to LPS. Science 335, 229–232 (2012). [PubMed: 22246778]
13. Siggs OM, Xiao N, Wang Y, Shi H, Tomisato W, Li X, Xia Y, Beutler B, iRhom2 is required for the secretion of mouse TNFα. Blood 119, 5769–5771 (2012). [PubMed: 22550345]
14. Issuree PDA, Maretzky T, McIlwain DR, Monette S, Qing X, Lang PA,Swendeman SL, Park-Min K-H, Binder N, Kalliolias GD, Yarilina A, Horiuchi K,Ivashkiv LB, Mak TW, Salmon JE, Blobel CP, iRHOM2 is a critical pathogenic mediator of inflammatory arthritis. J. Clin. Invest 123, 928–932 (2013). [PubMed: 23348744]
15. Xue L, Maretzky T, Weskamp G, Monette S, Qing X, Issureea PDA, Crawford HC,McIlwain DR, Mak TW, Salmon JE, Blobel CP, iRhoms 1 and 2 are essential upstream regulators of ADAM17-dependent EGFR signaling. Proc. Natl. Acad. Sci. U.S.A 112, 6080–6085 (2015). [PubMed: 25918388]
16. Blaydon DC, Etheridge SL, Risk JM, Hennies H-C, Gay LJ, Carroll R, Plagnol V,McRonald FE, Stevens HP, Spurr NK, Bishop DT, Ellis A, Jankowski J, Field JK,Leigh IM, South AP, Kelsell DP, *RHBDF2* mutations are associated with tylosis, a familial esophageal cancer syndrome. Am. J. Hum. Genet 90, 340–346 (2012). [PubMed: 22265016]

17. Saarinen S, Vahteristo P, Lehtonen R, Aittomäki K, Launonen V, Kiviluoto T,Aaltonen LA, Analysis of a Finnish family confirms *RHBDF2* mutations as the underlying factor in tylosis with esophageal cancer. Fam. Cancer 11, 525–528 (2012). [PubMed: 22638770]
18. Brooke MA, Etheridge SL, Kaplan N, Simpson C, O'Toole EA, Ishida-Yamamoto A,Marches O, Getsios S, Kelsell DP, iRHOM2-dependent regulation of ADAM17 in cutaneous disease and epidermal barrier function. Hum. Mol. Genet 23, 4064–4076 (2014). [PubMed: 24643277]
19. Etheridge SL, Brooke MA, Kelsell DP, Blaydon DC, Rhomboid proteins: A role in keratinocyte proliferation and cancer. Cell Tissue Res. 351, 301–307 (2013). [PubMed: 23263464]
20. Siggs OM, Grieve A, Xu H, Bambrough P, Christova Y, Freeman M, Genetic interaction implicates iRhom2 in the regulation of EGF receptor signalling in mice. Biol. Open 3, 1151–1157 (2014). [PubMed: 25395669]
21. Hosur V, Johnson KR, Burzenski LM, Stearns TM, Maser RS, Shultz LD, *Rhbdf2* mutations increase its protein stability and drive EGFR hyperactivation through enhanced secretion of amphiregulin. Proc. Natl. Acad. Sci. U.S.A 111, E2200–E2209 (2014). [PubMed: 24825892]
22. Vercammen D, Beyaert R, Denecker G, Goossens V, Van Loo G, Declercq W,Grooten J, Fiers W, Vandenabeele P, Inhibition of caspases increases the sensitivity of L929 cells to necrosis mediated by tumor necrosis factor. J. Exp. Med 187, 1477–1485 (1998). [PubMed: 9565639]
23. Tsujimoto M, Yip YK, Vilcek J, Tumor necrosis factor: Specific binding and internalization in sensitive and resistant cells. Proc. Natl. Acad. Sci. U.S.A 82, 7626–7630 (1985). [PubMed: 2999773]
24. Vanlangenakker N, Bertrand MJM, Bogaert P, Vandenabeele P, Vanden Berghe T, TNF-induced necroptosis in L929 cells is tightly regulated by multiple TNFR1 complex I and II members. Cell Death Dis. 2, e230 (2011). [PubMed: 22089168]
25. Bhattacharya D, Logue EC, Bakkour S, DeGregori J, Sha WC, Identification of gene function by cyclical packaging rescue of retroviral cDNA libraries. Proc. Natl. Acad. Sci. U.S.A 99, 8838–8843 (2002). [PubMed: 12084928]
26. Irmler M, Thome M, Hahne M, Schneider P, Hofmann K, Steiner V, Bodmer J-L,Schröter M, Burns K, Mattmann C, Rimoldi D, French LE, Tschopp J, Inhibition of death receptor signals by cellular FLIP. Nature 388, 190–195 (1997). [PubMed: 9217161]
27. Liu B, Xu Y, Li WL, Zeng L, Proteomic analysis of differentially expressed skin proteins in *iRhom2*^{Uncv} mice. BMB Rep. 48, 19–24 (2015). [PubMed: 24667173]
28. Adrain C, Freeman M, New lives for old: Evolution of pseudoenzyme function illustrated by iRhoms. Nat. Rev. Mol. Cell Biol 13, 489–498 (2012). [PubMed: 22781900]
29. Azijli K, Weyhenmeyer B, Peters GJ, de Jong S, Kruyt FAE, Non-canonical kinase signaling by the death ligand TRAIL in cancer cells: Discord in the death receptor family. Cell Death Differ. 20, 858–868 (2013). [PubMed: 23579241]
30. Kearney CJ, Cullen SP, Tynan GA, Henry CM, Clancy D, Lavelle EC,Martin SJ, Necroptosis suppresses inflammation via termination of TNF- or LPS-induced cytokine and chemokine production. Cell Death Differ 22, 1313–1327 (2015). [PubMed: 25613374]
31. McIlwain DR, Berger T, Mak TW, Caspase functions in cell death and disease. Cold Spring Harb. Perspect. Biol 5, a008656 (2013). [PubMed: 23545416]
32. Strelow A, Bernardo K, Adam-Klages S, Linke T, Sandhoff K, Krönke M, Adam D, Overexpression of acid ceramidase protects from tumor necrosis factor–induced cell death. J. Exp. Med 192, 601–612 (2000). [PubMed: 10974027]
33. Legler DF, Micheau O, Doucey M-A, Tschopp J, Bron C, Recruitment of TNF receptor 1 to lipid rafts is essential for TNFα-mediated NF-κB activation. Immunity 18, 655–664 (2003). [PubMed: 12753742]
34. Hundhausen C, Misztela D, Berkhout TA, Broadway N, Saftig P, Reiss K, Hartmann D,Fahrenholz F, Postina R, Matthews V, Kallen K-J, Rose-John S, Ludwig A, The disintegrin-like metalloproteinase ADAM10 is involved in constitutive cleavage of CX3CL1 (fractalkine) and regulates CX3CL1-mediated cell-cell adhesion. Blood 102, 1186–1195 (2003). [PubMed: 12714508]

35. Christova Y, Adrain C, Bambrough P, Ibrahim A, Freeman M, Mammalian iRhoms have distinct physiological functions including an essential role in TACE regulation. EMBO Rep. 14, 884–890 (2013). [PubMed: 23969955]
36. Zettl M, Adrain C, Strisovsky K, Lastun V, Freeman M, Rhomboid family pseudo-proteases use the ER quality control machinery to regulate intercellular signaling. Cell 145, 79–91 (2011). [PubMed: 21439629]
37. Le Gall SM, Maretzky T, Issuree PDA, Niu X-D, Reiss K, Saftig P, Khokha R,Lundell D, Blobel CP, ADAM17 is regulated by a rapid and reversible mechanism that controls access to its catalytic site. J. Cell Sci 123, 3913–3922 (2010). [PubMed: 20980382]
38. Maretzky T, Evers A, Zhou W, Swendeman SL, Wong P-M, Rafii S, Reiss K,Blobel CP, Migration of growth factor-stimulated epithelial and endothelial cells depends on EGFR transactivation by ADAM17. Nat. Commun 2, 229 (2011). [PubMed: 21407195]
39. Nitoiu D, Etheridge SL, Kelsell DP, Insights into desmosome biology from inherited human skin disease and cardiocutaneous syndromes. Cell Commun. Adhes 21, 129–140 (2014). [PubMed: 24738885]
40. Hirsch FR, Varella-Garcia M, Cappuzzo F, Predictive value of EGFR and HER2 overexpression in advanced non-small-cell lung cancer. Oncogene 28, S32–S37 (2009). [PubMed: 19680294]
41. Mochizuki S, Okada Y, ADAMs in cancer cell proliferation and progression. Cancer Sci. 98, 621–628 (2007). [PubMed: 17355265]
42. Leilei Y, Bing L, Yang L, Shaoxia W, Yuan X, Dongping W, Huahu Y, Shichen S,Guangzhou Z, Ruiyun P, Lin Z, Wenlong L, iRhom2 mutation leads to aberrant hair follicle differentiation in mice. PLOS One 9, e115114 (2014). [PubMed: 25546423]
43. Doedens JR, Black RA, Stimulation-induced down-regulation of tumor necrosis factor-α converting enzyme. J. Biol. Chem 275, 14598–14607 (2000). [PubMed: 10799546]
44. Nakagawa T, Guichard A, Castro CP, Xiao Y, Rizen M, Zhang H-Z, Hu D, Bang A,Helms J, Bier E, Derynck R, Characterization of a human rhomboid homolog, p100^{hRho}/RHBDF1, which interacts with TGF-α family ligands. Dev. Dyn 233, 1315–1331 (2005). [PubMed: 15965977]
45. Zou H, Thomas SM, Yan Z-W, Grandis JR, Vogt A, Li L-Y, Human rhomboid family-1 gene *RHBDF1* participates in GPCR-mediated transactivation of EGFR growth signals in head and neck squamous cancer cells. FASEB J. 23, 425–432 (2009). [PubMed: 18832597]
46. Yan Z, Zou H, Tian F, Grandis JR, Mixson AJ, Lu PY, Li L-Y, Human rhomboid family-1 gene silencing causes apoptosis or autophagy to epithelial cancer cells and inhibits xenograft tumor growth. Mol. Cancer Ther 7, 1355–1364 (2008). [PubMed: 18524845]
47. Maretzky T, Zhou W, Huang X-Y, Blobel CP, A transforming Src mutant increases the bioavailability of EGFR ligands via stimulation of the cell-surface metalloproteinase ADAM17. Oncogene 30, 611–618 (2011). [PubMed: 20871631]
48. Grusdat M, McIlwain DR, Xu HC, Pozdeev VI, Knievel J, Crome SQ,Robert-Tissot C, Dress RJ, Pandyra AA, Speiser DE, Lang E, Maney SK,Elford AR, Hamilton SR, Scheu S, Pfeffer K, Bode J, Mittrücker H-W, Lohoff M,Huber M, Häussinger D, Ohashi PS, Mak TW, Lang KS, Lang PA, IRF4 and BATF are critical for CD8^{+} T-cell function following infection with LCMV. Cell Death Differ. 21, 1050–1060 (2014). [PubMed: 24531538]

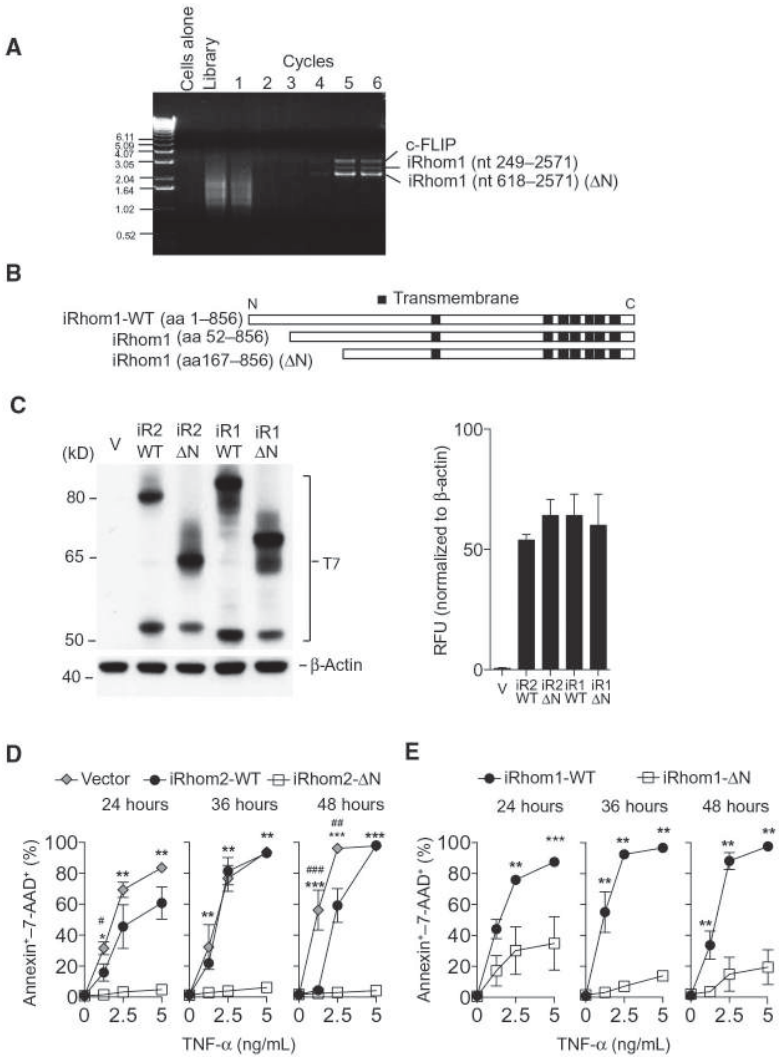

Fig. 1. N truncated iRhom1-ΔN confers TNF resistance as identified by CPR screening.

(**A**) Polymerase chain reaction (PCR) results from each round in the CPR screen (see Materials and Methods) showing enrichment for c-FLIP and two short versions of iRhom1 in TNF-resistant cells. (**B**) Systematic representation of wild-type (WT) and short versions of iRhom1 identified by CPR relative to their predicted transmembrane domain structures. (**C**) Immunoblotting and densitometry for T7 in lysates from L-929 cells expressing a control vector, T7-tagged WT or ΔN-iRhom1 (iR1) or iRhom2 (iR2) ($n = 3$). (**D** and **E**) Cell death, assessed by annexin V binding and 7-AAD staining using flow cytometry, in 1×10^5 L-929 cells transfected as indicated and treated with recombinant TNF for up to 48 hours ($n \geq 5$). Data are means ± SEM from the number of experiments (n) indicated; $^{*}P < 0.05$, $^{**}P < 0.01$, $^{***}P < 0.001$ against ΔN; $^{\#}P < 0.05$, $^{\#\#}P < 0.01$ against vector. nt, nucleotide; aa, amino acid.

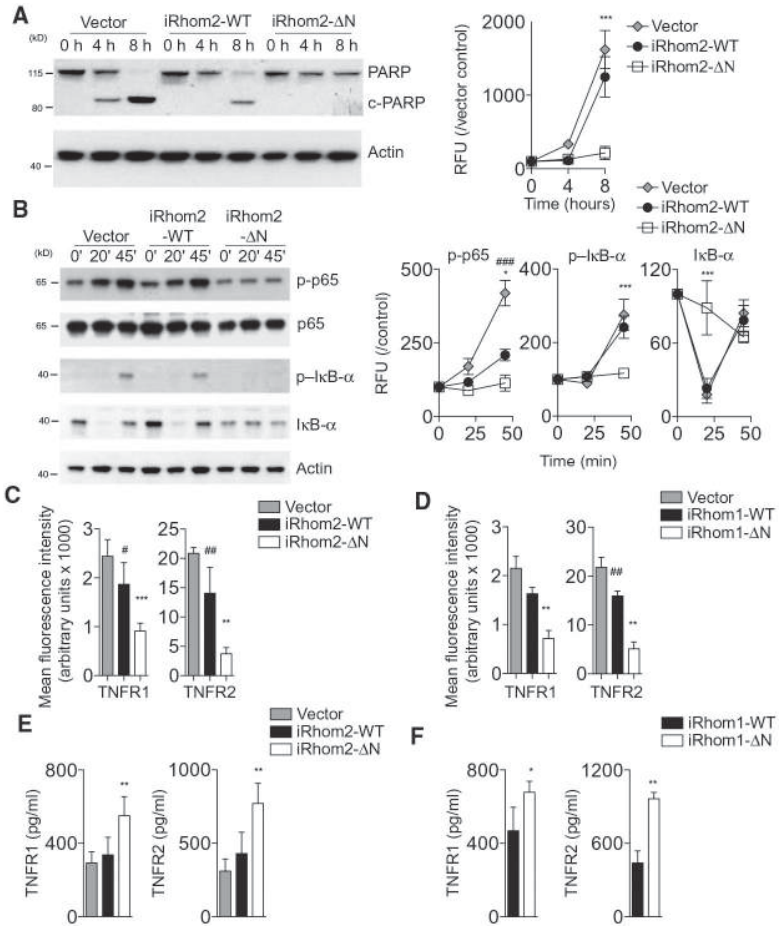

Fig. 2. iRhom2-ΔN induces TNFR shedding.

(**A** and **B**) Immunoblotting and densitometry for PARP (A) or total and phosphorylated NF-κB pathway proteins (B) in lysates from L-929 cells overexpressing a vector control, iRhom2-WT, or iRhom2-ΔN and exposed to recombinant TNF (2.5 ng/ml) for up to 8 hours (A) or 45 min (B) ($n = 3$, normalized to control and actin). (**C** and **D**) Flow cytometry analysis of TNFR1 and TNFR2 surface abundance on L-929 cells overexpressing WT or truncated iRhom2 (C) or iRhom1 (D) ($n = 5$ or 6, respectively). (**E** and **F**) Amount of TNFR1 and TNFR2 in supernatants from 1×10^5 L-929 cells expressing WT or truncated iRhom2 (E) or iRhom1 (F) ($n = 5$). Data are means ± SEM from the number of experiments (n) indicated; $^{*}P < 0.05$, $^{**}P < 0.01$, $^{***}P < 0.001$ against ΔN; $^{\#}P < 0.05$, $^{\#\#}P < 0.01$, $^{\#\#\#}P < 0.001$ against vector. RFU, relative fluorescence units.

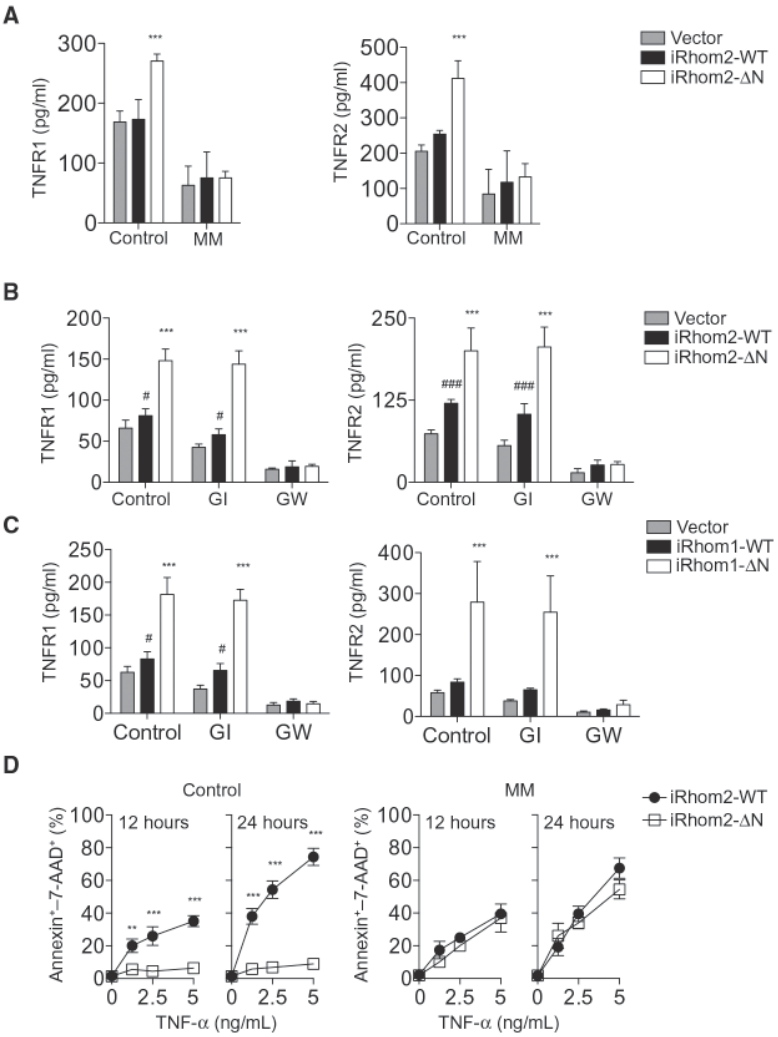

Fig. 3. Effects of ΔN-iRhoms can be blocked by ADAM17 inhibitors.

(**A** and **B**) Abundance of TNFR1 and TNFR2 in the culture supernatants from 1×10^5 L-929 cells expressing WT or truncated iRhom2 cultured in presence or absence of marimastat (MM; 20 μM) (A) or GI or GW (each 3 μM) (B) for 6 hours ($n = 5$ or 6, respectively). (**C**) As in (B) in 1×10^5 L-929 cells expressing WT or truncated iRhom1. (**D**) Cell death as a percentage of annexin–7-AAD$^+$ cells in cultures ($n = 3$) of 1×10^5 L-929 cells expressing WT or truncated iRhom2 treated with recombinant TNF in the presence or absence of marimastat (20 μM). Data are means ± SEM from the number of experiments (n) indicated; $^{**}P < 0.01$, $^{***}P < 0.001$ against WT; $^{\#}P < 0.05$, $^{\#\#\#}P < 0.001$ against vector.

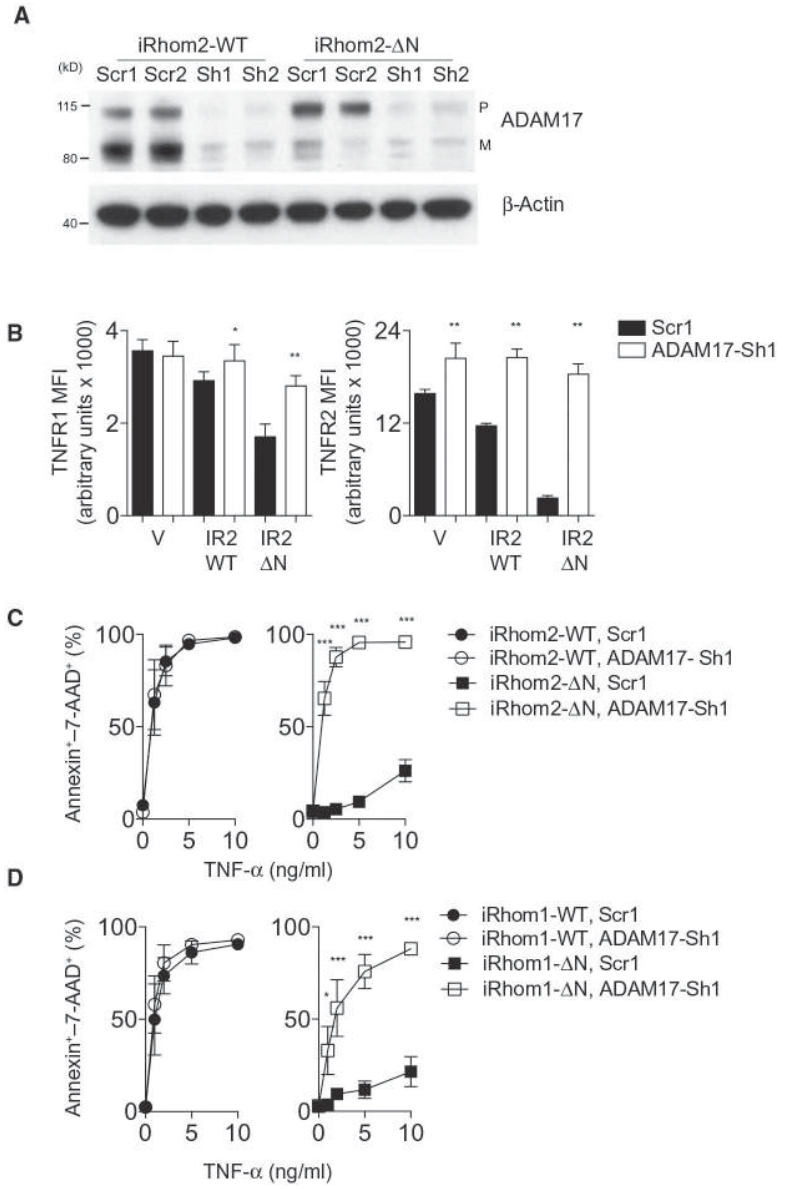

Fig. 4. Stable knockdown of ADAM17 prevents increased TNFR shedding and resistance to TNF.

(**A**) Immunoblot for pro (P) and mature (M) ADAM17 in lysates from L-929 cells expressing full-length and ΔN-iRhom2 transfected with either a scrambled control (Scr1) or an *ADAM17*-targeted shRNA (ADAM17-Sh1). Blot is representative of three experiments. (**B**) Surface abundance of TNFR1 and TNFR2 as determined by flow cytometry on L-929 cells expressing a vector control, full-length (WT) iRhom2 or iRhom2-ΔN in the presence of either control or ADAM17 shRNA ($n = 6$). (**C** and **D**) Cell death as a proportion of annexin–7-AAD$^+$ cells in cultures of 1×10^5 L-929 cells stably expressing full-length or ΔN-iRhom2 (C) or iRhom1 (D) and either scrambled or ADAM17 shRNA treated with recombinant TNF for 48 hours ($n = 4$ or 6, respectively). Data are means ± SEM from the number of experiments (n) indicated; *$P < 0.05$, ***$P < 0.001$. MFI, mean fluorescence intensity.

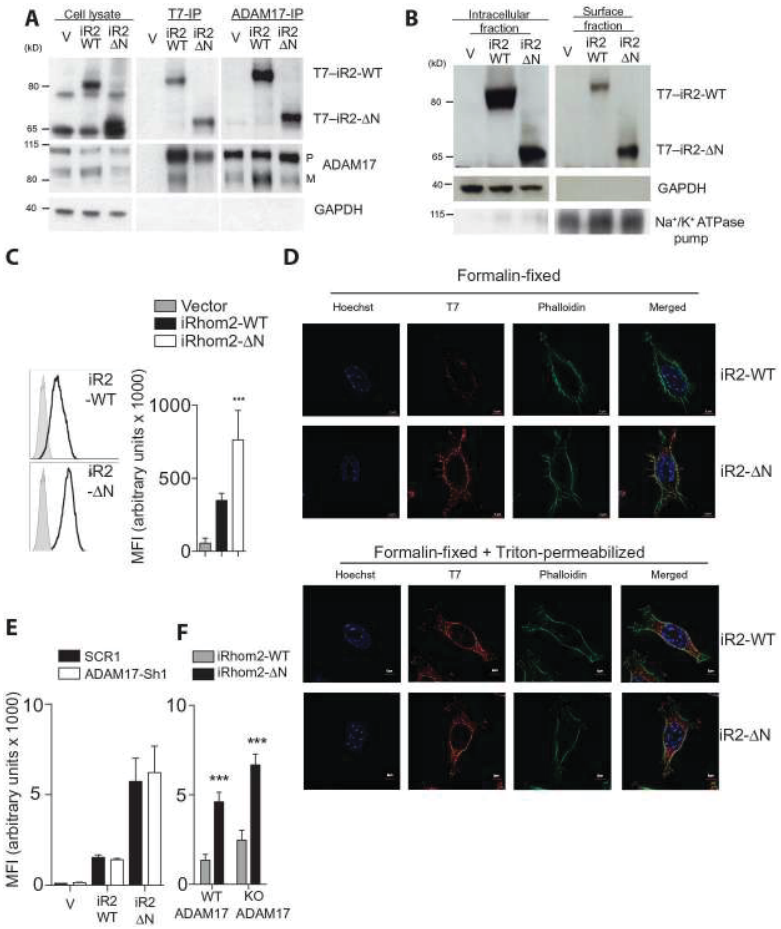

Fig.5. Truncation of the cytoplasmatic tail results in increased surface expression of iRhom2.

(**A**) Immunoprecipitation (IP) for T7 or ADAM17 followed by immunoblotting for the same in lysates from L-929 cells stably expressing T7-tagged WT or truncated iRhom2. Blot is representative of three experiments. (**B**) Immunoblotting for iRhom2 using a T7 antibody in intracellular and cell surface fractions from L-929 cells stably expressing WT or truncated iRhom2. Blot is representative of three experiments. (**C**) Surface abundance of iRhom2, determined using an antibody against T7, on stably transfected L-929 cells ($n = 8$). (**D**) Immunocytochemistry for iRhom2 using T7 antibodies (Cy3), phalloidin–fluorescein isothiocyanate (FITC), and Hoechst staining in stably transfected L-929 cells, fixed, and/or permeabilized as indicated ($n \geq 3$ experiments). (**E** and **F**) Flow cytometry analysis of MFI of the surface abundance of iRhom2 on unpermeabilized stably transfected L-929 cells expressing either scrambled or ADAM17 shRNA ($n \geq 4$ experiments) (E) or immortalized WT or *Adam17* knockout (KO) mouse embryonic fibroblasts (MEFs) ($n = 12$ experiments) (F). Data are means ± SEM from the number of experiments (n) indicated; $^{***}P < 0.001$. GAPDH, glyceraldehyde-3-phosphate dehydrogenase. Na^+/K^+ ATPase, Na^+- and K^+-dependent adenosine triphosphatase.

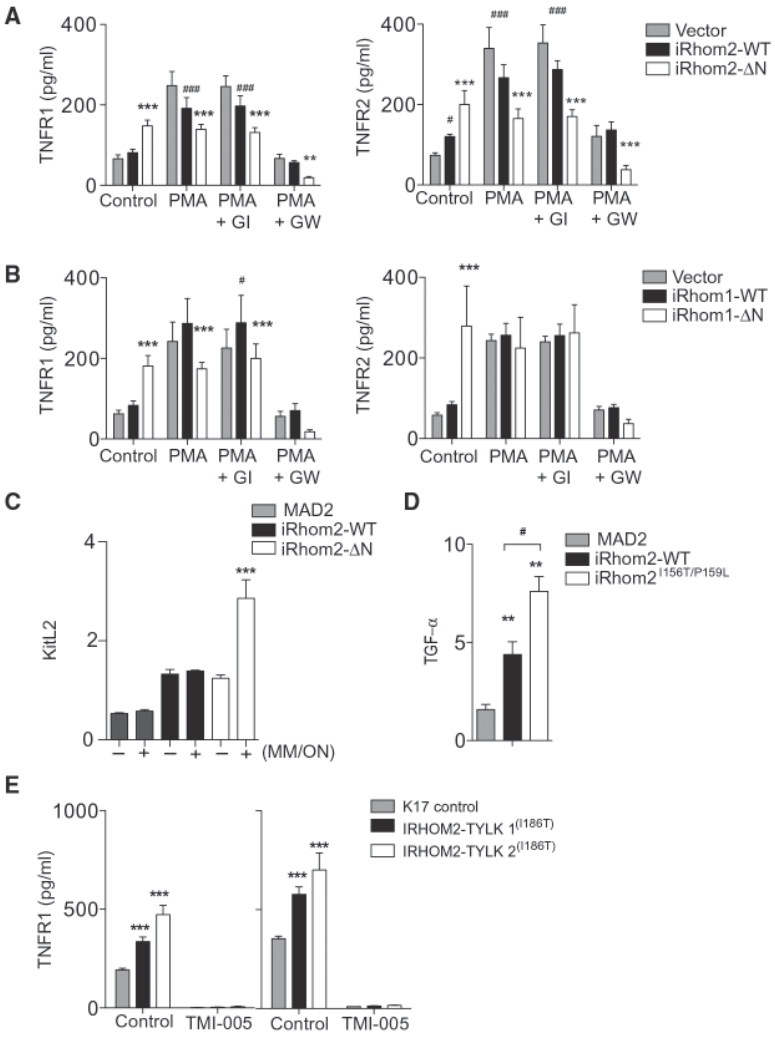

Fig. 6. N-terminal mutations in iRhom2 trigger constitutive activity of ADAM17.

(**A** and **B**) TNFR1 and TNFR2 in conditioned media of 1×10^5 L-929 cells expressing WT or ΔN-iRhom2 (A) or iRhom1 (B) cultured with PMA (100 ng/ml) in the presence (where indicated) of GI or GW (3 μM each) ($n = 6$). (**C**) KitL2 shedding in immortalized MEFs (iMEFs) genetically lacking iRhom2 transfected with alkaline phosphatase (AP)–tagged KitL2 along with MAD2 (control), iRhom2-WT, or iRhom2-ΔN, and (where indicated, +) preincubated with marimastat overnight (MM/ON), followed by washout of the inhibitor ($n = 3$). (**D**) Transforming growth factor–α (TGF-α) shedding from iMEFs genetically lacking iRhom1 and iRhom2 and transfected with AP-tagged TGF-α along with MAD2 (control), murine WT iRhom2, or iRhom2$^{I156T/P159L}$ ($n \geq 5$). (**E**) Concentration of soluble TNFR1 in supernatants from 2×10^5 keratinocytes from either healthy donors (K17 cells) or tylosis patients who have mutations in IRHOM2$^{(I186T/WT)}$ [TYLK1 and TYLK2 treated with vehicle (dimethyl sulfoxide; DMSO) or TMI-005 ADAM17 inhibitor for 24 (left) or 48 (right) hours]. Data are means ± SEM from the number of experiments (n) indicated; *$P <$

0.05, $^{**}P < 0.01$, $^{***}P < 0.001$ against WT (A and B) or MAD2 (D and E); $^{\#}P < 0.05$ against vector (A and B) or mutant construct (D and E).